

ÉCOLE DOCTORALE des Sciences de la Vie et de la Santé
UMR_S INSERM 1109

Immuno-Rhumatologie Moléculaire

THÈSE présentée par :
Alev YILMAZ

soutenue le : **30 septembre 2021**

pour obtenir le grade de : **Docteur de l'Université de Strasbourg**

Discipline : Sciences de la Vie et de la Santé

Spécialité : Aspects moléculaires et cellulaires de la Biologie

**Impact of Tenascin-C on anti-tumor immunity
in a breast tumor progression model**

THÈSE dirigée par :

Dr OREND Gertraud

DR, HDR, Université de Strasbourg, France

RAPPORTEURS :

Dr ROUSSELLE Patricia

DR, HDR, Université Claude Bernard Lyon 1, France

Dr HAGEDORN Martin

MCU, HDR Université de Bordeaux, France

Examinateur interne :

Dr. BOUCHER Philippe

PR, HDR Université de Strasbourg, France

“Education is the most powerful weapon which you can use to change the world “

Nelson Mandela (1918-2013)

Babaanneme, meleklerin en güzeli.

Acknowledgements

Throughout my thesis I have been surrounded by many people without whom I would never have succeeded to get this far, and I would like to take here the opportunity to express them my gratitude.

I would like to thank Patricia Rousselle, Martin Hagedorn and Philippe Boucher, for having accepted to be part of my thesis committee and thereby to accompany me during the last step of this intense journey.

Gertraud, I would like to thank you for these last 4 years and for all I learned from you. Never I saw such a passion for science, never I saw such a tenacity. Thanks for all the discussions we had. I experienced doubts, self-questioning and I realize that I am stronger now. It was not an easy journey but you always found the right words to pick me up when I stumbled and lose my balance.

Je souhaite remercier également Hélène Burckel, Nathalie Salomé, Frédéric Gros et Fabien Alpy d'avoir accepté de faire partie de mon comité de suivi de thèse, de m'avoir écouté et guidé.

A toutes les personnes de mon équipe, je tiens à vous dire à quel point votre présence et votre aide m'ont été précieuses. Plus que des collègues vous avez été mes compagnons de voyage et les nombreuses péripéties que nous avons vécues ensemble sont des souvenirs impérissables. Merci de m'avoir soutenu, d'avoir partagé les moments de joie et de détresse, et de m'avoir aidé par votre expérience à surmonter les obstacles. Selven, merci d'avoir été là à mes débuts, tu as été un exemple pour moi et je t'en suis reconnaissante. William, merci de m'avoir pris sous ton aile et de m'avoir guidé. Thomas, merci pour la complicité que l'on a partagé, j'ai trouvé en toi un ami sur qui je peux compter. Chérine, merci pour toutes les émotions que tu m'as fait vivre, beaucoup de larmes de joies et parfois de tristesse partagées, merci pour ton soutien quotidien. Nathalie, merci pour toute ton aide et tes conseils. Tes paroles m'ont permis de gagner en confiance et ta bienveillance m'a plus d'une

fois émue. Marine, ma protégée, je suis heureuse que nos chemins se soient croisées et persuadée que l'avenir nous permettra de nous retrouver. Fanny, merci de prendre soin de toute cette petite équipe par ta bienveillance, merci pour ton aide technique et pour tous les à-côtés que je n'ai pas besoin de citer ! Gilles, merci pour ta bonne humeur et ton altruisme. Isabelle, merci pour ta sagesse, ton optimisme et ta sensibilité. Aurore, toi qui nous mets dans le droit chemin lorsque l'on s'égare, merci pour toute ton aide. Magalie, merci pour ton soutien durant cette dernière année. Merci à toutes les autres personnes de notre unité, Olivier, Grégory, Annabel, Laetitia, Linda et toutes celles que j'oublie de citer.

Mon aventure n'aurait pas été la même sans vous tous.

Maman, papa, merci de m'avoir permis de suivre la voie que je souhaitais et de n'avoir jamais douté de moi, de mes valeurs et de mes capacités. Merci d'avoir éclairé mon chemin, de m'avoir appris à distinguer le bien du mal et de n'avoir jamais lâché ma main. Je suis fière d'être votre fille et j'espère que vous êtes fiers de moi. Duygu, mon cookie, tu as toujours étais là pour moi, et si j'ai réussi aujourd'hui c'est parce que tu m'as montré la voie. Tu es celle que j'admire, celle sur qui je peux toujours compter et celle qui me pousse à être meilleure. Can, merci d'avoir toujours cru en moi et de m'avoir soutenu quels que soient mes choix. Tu es celui qui me fait grandir en m'apprenant à remettre en question le monde qui m'entoure. Ben, toi qui apaises mon cœur en me prouvant tous les jours que je suis dans le tien, tu es celui grâce à qui je ne regrette rien de cette aventure. Merci pour tout le bonheur que tu me procures au quotidien.

Vous êtes le centre de mon univers et l'amour que je vous porte ne peut être égalé.

Déclaration sur l'honneur

Declaration of Honour

J'affirme être informé que le plagiat est une faute grave susceptible de mener à des sanctions administratives et disciplinaires pouvant aller jusqu'au renvoi de l'Université de Strasbourg et possible de poursuites devant les tribunaux de la République Française.

Je suis conscient(e) que l'absence de citation claire et transparente d'une source empruntée à un tiers (texte, idée, raisonnement ou autre création) est constitutive de plagiat.

Au vu de ce qui précède, j'atteste sur l'honneur que le travail décrit dans mon manuscrit de thèse est un travail original et que je n'ai pas eu recours au plagiat ou à toute autre forme de fraude.

I affirm that I am aware that plagiarism is a serious misconduct that may lead to administrative and disciplinary sanctions up to dismissal from the University of Strasbourg and liable to prosecution in the courts of the French Republic.

I am aware that the absence of a clear and transparent citation of a source borrowed from a third party (text, idea, reasoning or other creation) is constitutive of plagiarism.

In view of the foregoing, I hereby certify that the work described in my thesis manuscript is original work and that I have not resorted to plagiarism or any other form of fraud.

Nom : YILMAZ

Prénom : Alev

Ecole doctorale : Ecole Doctorale des Sciences de la Vie et de la Santé

Laboratoire : INSERM U1109

Date : 01.10.2021

Table of content

Abbreviations	1
List of Figures	5
Thesis summary in French	7
Introduction	17
1. Breast cancer	17
1.1 Incidence and mortality	17
1.2 Breast cancer classification	17
1.2.1 Histological classification	17
1.2.2 Histological grading	18
1.2.3 Tumor-Node-Metastasis staging	18
1.2.4 Molecular classification	19
1.3 Local and systemic breast cancer treatment strategies	20
1.3.1 Locoregional therapies	20
1.3.1.1 Breast surgery.....	20
1.3.1.2 Radiotherapy	21
1.3.2 Systemic therapies	21
1.3.2.1 Chemotherapy	21
1.3.2.2 Hormonal therapy	22
1.3.2.3 Targeted therapy	23
1.3.2.4 Immune checkpoint therapy	24
2. Tumor Microenvironment	25
2.1 Cellular components of the tumor microenvironment	26
2.1.1 Cancer cells.....	26
2.1.2 Cancer stem cells.....	28
2.1.3 Cancer associated fibroblasts.....	28
2.1.4 Endothelial cells and pericytes.....	29
2.1.5 Immune cells	30
2.1.6 Adipocytes.....	31
2.2 Soluble factors	31
2.3 The extracellular matrix (ECM)	32
2.3.1 ECM architecture and components.....	32

2.3.2 ECM alterations and roles in the TME	33
3. Tenascin-C (TNC)	33
3.1 Structure and expression of TNC.....	33
3.2 Physiological roles of TNC.....	35
3.3 TNC in cancer	36
3.3.1 TNC expression in cancer and clinical significance.....	36
3.3.2 Source of TNC in the TME	37
3.3.2.1 TNC derived from cancer-associated stroma	37
3.3.2.2 TNC derived from cancer cells.....	38
3.3.3 Pathological roles of TNC in cancer.....	38
3.3.3.1 Impact on angiogenesis.....	38
3.3.3.2 Impact on cell proliferation.....	39
3.3.3.3 Impact on cell migration and invasion	39
3.3.3.4 Impact on epithelial-to-mesenchymal transition	40
3.3.3.5 Impact on stemness properties.....	41
3.3.3.6 Impact on immunosurveillance	41
4. Cancer immunity.....	41
4.1 Cancer immunosurveillance.....	41
4.2 Cancer immunoediting	43
4.3 Impact of the TME on key immune effector and regulatory cells.....	46
4.3.1 Impact of the TME on key players of innate immunity.....	46
4.3.2 Impact of the TME on key players of adaptive immunity	48
4.4 Cancer immune contexture.....	50
4.5 Immunomodulatory functions of TNC	51
5. Natural killer group 2 member (NKG2D)/NKG2DL ligand axis	53
5.1 NKG2D receptor and its ligands in mouse and in human.....	53
5.1.1 NKG2D receptor	53
5.1.1.1 NKG2D receptor complex.....	53
5.1.1.2 DAP10-dependent signaling pathways.....	55
5.1.1.3 DAP12-dependent signaling pathways.....	55
5.1.1.4 NKG2D expression pattern in mouse and in human	56
5.1.1.4.1 NKG2D and NK cells.....	57
5.1.1.4.2 NKG2D and T cells	57
5.1.1.4.3 NKG2D and macrophages.....	58

5.1.2 NKG2D ligands	58
5.1.2.1 Diversity of NKG2D ligands in mouse and in human.....	58
5.1.2.2 NKG2DL regulation	58
5.1.2.2.1 Transcriptional regulation of NKG2DL.....	59
5.1.2.2.2 Post-transcriptional regulation	59
5.1.2.2.3 Post-translational regulation.....	60
5.1.2.2.3.1 Release of soluble NKG2DLs	60
5.1.2.2.3.2 Internalization of NKG2DLs.....	61
5.2 NKG2D/NKG2DL-mediated immune surveillance in cancer	61
5.3 Down-modulation of NKG2D in tumor immunity.....	62
5.4 NKG2D/NKG2DL-mediated immune escape	62
5.5 NKG2D/NKG2DL as a target in cancer therapy.....	63
5.5.1 Targeting the down-regulation of NKG2DL expression.....	64
5.5.2 Targeting NKG2DL with engineered T cells	64
5.5.3 Targeting NKG2D using bispecific proteins	65
5.5.4 Cross-talk between immune checkpoint therapy and NKG2D/NKG2DL activation	65
Thesis Objectives	67
Results	69
I. Published paper: Tenascin-C immobilizes infiltrating T lymphocytes through CXCL12 promoting breast cancer progression	69
Abstract	69
Introduction	69
Results and Figures	70
Discussion	84
Material and methods	85
References	88
Expanded view figures	91
Appendix figures S1-6	101
II. Unpublished results: TNC impacts tumor onset and NKG2DL expression in the NT193 model	117
1.1 Introduction	117
1.2 Results.....	119
1.3 Material and methods	134
1.4 Tables.....	139
1.5 Supplemental figure	141

Discussion and Perspectives.....	143
I. Published paper: Tenascin-C immobilizes infiltrating T lymphocytes through CXCL12 promoting breast cancer progression	144
II. Unpublished results: TNC impacts tumor onset and NKG2DL expression in the NT193 model	152
Summary	160
References.....	161
Appendix I: Tenascin-C increases lung metastasis by impacting blood vessel invasions	182
Appendix II: Impact of tenascin-C on radiotherapy in a novel syngeneic oral squamous cell carcinoma model with spontaneous dissemination to the lymph nodes	206

Abbreviations

ADAM	A Disintegrin And Metalloprotease
ALDH1	Aldehyde Dehydrogenase 1
AMD	AMD3100
ATM	Ataxia Telangiectasia Mutated
ATR	Ataxia Telangiectasia and Rad3 related
APC	Antigen Presenting Cells
αSMA	alpha-Smooth Muscle Actin
AUF1	AU-rich element RNA-binding Factor 1
BCSCs	Breast Cancer Stem Cells
BVI	Blood Vessel Invasion
CAA	Cancer Associated Adipocyte
CAF	Cancer Associated Fibroblast
CAR	Chimeric Antigen Receptor
CD3ζ	Zêta-chain of CD3
Chk	Checkpoint Kinase
CK8/18	Cytokeratines-8/-18
Cl.casp3	Cleaved caspase 3
CM	Conditioned Medium
COL	Collagen
CSC	Cancer Stem Cells
CTL	Cytotoxic T lymphocyte
CTLA-4	Cytotoxic T-Lymphocyte-associated Antigen-4
CXCL	C-X-C motif chemokine
CXCR	C-X-C chemokine receptor
DAMP	Damage/Danger Associated Molecular Pattern molecule
DAP	DNAX-Activating Protein
DAPI	Di Aminido Phenyl Indol
DC	Dendritic Cell
DDR	DNA Damage Response
DKK1	Dickkopf-1
DMEM	Dulbecco's Modified Eagle's Medium
DMSO	Dimethyl Sulfoxide
DNA	Deoxyribonucleic Acid
E-cad	E-cadherin
ECM	Extracellular Matrix
EDTA	Ethylenediaminetetraacetic Acid
EGF	Epidermal Growth Factor
EMT	Epithelial-to-Mesenchymal Transition
ET	Endothelin
ER	Estrogen Receptor
ERK	Extracellular signal-Regulated Kinases

FAP	Fibroblast Activation Protein
FBG	Fibrinogen Globe
FBS	Fetal Bovine Serum
FN	Fibronectin
FNIII	Fibronectin type-III
FSP1	Fibroblast-Specific Protein 1
FVB	Friend leukemia Virus B
Grb2	Growth factor receptor-bound protein 2
Gzmb	Granzyme B
H60	Histocompatibility antigen 60
HCMV	Human Cytomegalovirus
HER2	Human Epidermal growth Factor
HIF1 α	Hypoxia-Inducible Factor 1-alpha
HR	Hazard Ratio
Hscore	Histological score
ICT	Immune Checkpoint therapy
IDC	Invasive Ductal Carcinoma
IF	Immunofluorescence
IFN	Interferon
IL	Interleukin
ILC	Invasive Lobular Carcinoma
ip	intraperitoneal
ITAM	Immune receptor Tyrosine-based Activation Motif
iv	intravenous
JNK	Jun N-terminal Kinase
KD	Knockdown
Klrk1	Killer cell lectin-like receptor subfamily K, member 1
KO	Knockout
LEC	Lymphatic Endothelial Cells
LPS	Lipopolysaccharide
LT	Lymphocyte T
MEC	Matrix Extracellulaire
MET	Mesenchymal-to-Epithelial Transition
MFS	Metastasis Free Survival
MHC	Major Histocompatibility Complex
MIC	MHC class I chain-related protein
miR	microRNAs
MMP	Matrix Metalloproteinase
MMTV	Mouse Mammary Tumor Virus
MULT1	Murine UL16-binding protein-like transcript 1
NF- κ B	Nuclear Factor Kappa-light-chain-enhancer of activated B cells
NGS	Normal Goat Serum
NK	Natural Killer
NKG2D	Natural Killer Group 2 member D

NKG2DL	Natural Killer Group 2 member D Ligand
NKT	Natural Killer T cell
OS	Overall Survival
PD-1	Programmed Death-1
PDGF- α	Platelet-Derived Growth Factor alpha
PD-L1	Programmed Death-Ligand 1
PI3K	Phosphatidylinositol 3-Kinase
PLC- γ 2	Phospholipase C gamma 2
PM	Parenchymal Metastasis
PR	Progesterone Receptor
Rae-1	Retinoic acid early transcript 1
RIPA	Radioimmunoprecipitation assay
RNA	Ribonucleic Acid
RNA seq	RNA sequencing
RT-qPCR	Real time quantitative PCR
scFv	Single chain variable fragment
shRNA	Short hairpin RNA
shTNC	TNC knockdown
shNKG2DL	NKG2DL knockdown
SDF-1	Stromal cell-Derived Factor 1
SLP-76	Src homology 2 domain-containing leukocyte phosphoprotein of 76 kDa
TACS	Tumor-Associated Collagen Signature
TAM	Tumor Associated Macrophage
TCR	T Cell Receptor
TGF β	Transforming Growth Factor beta
Th	T helper
TIL	Tumor Infiltrating T Lymphocyte
TLR4	Toll Like Receptor-4
TMA	Tissue Microarray
TME	Tumor Microenvironment
TMT	Tumor Matrix Tracks
TN	Triple Negative
TNC	Tenascin-C
TNF	Tumor Necrosis Ractor
TNM	Tumor Node Metastasis
Treg	Regulatory T cells
ULBPs	UL16-binding proteins
UTR	Untranslated Region
VEGF	Vascular Endothelial Growth Factor
Vim	Vimentin
WB	Western Blot
WT	Wild-type
ZAP70	Zeta-chain-associated Protein of 70 kDa

List of figures

Figure 1. Histological grade of breast cancer

Table 1. Staging of breast cancer based on the TNM classification

Figure 2. Role of CTLA-4 and PD-1 in immunoregulation and monoclonal antibodies (mAbs) used in immunotherapy.

Figure 3. Composition of the tumor microenvironment

Figure 4. The hallmarks of cancer

Figure 5. Structure of TNC and potential binding partners

Figure 6. The Cancer-Immunity cycle

Figure 7. The cancer immunoediting concept

Figure 8. Differentiation of naïve CD4+ T cell in helper T cell subsets is determined by cytokines

Figure 9. NKG2D receptor complex and its ligands in human and mouse

Figure 10. NKG2D-DAP10 and NKG2D-DAP12 mediated signal transduction

Thesis summary in French

Introduction

Le cancer du sein demeure une maladie mortelle malgré un diagnostic plus précoce et le développement de nouvelles stratégies thérapeutiques. Cette forte mortalité peut s'expliquer par la capacité des cellules tumorales à échapper à la surveillance immunitaire et disséminer dans des organes à distance de la tumeur primaire afin de former des métastases, entraînant ainsi une diminution de l'efficacité des traitements (Minn et al., 2005). Il est désormais clairement démontré que la progression tumorale n'est pas seulement dépendante des caractéristiques intrinsèques des cellules cancéreuses mais que ces dernières résident dans un écosystème complexe appelé le microenvironnement tumoral (MET) qui joue un rôle crucial dans cette progression tumorale et le développement de métastases (Balkwill et al., 2012; Joyce and Pollard, 2009). Le MET est composé de plusieurs types cellulaires distincts tels que les cellules endothéliales, les fibroblastes associés au cancer et les cellules immunitaires. Outre la composante cellulaire, le MET contient également des facteurs solubles et des molécules de la matrice extracellulaire (MEC).

La MEC est un réseau complexe de protéines qui fournit non seulement des repères architecturaux et un échafaudage physique aux cellules environnantes, mais qui joue également un rôle actif en interagissant avec ces cellules par le biais de récepteurs (Hynes and Naba, 2012). La MEC présente dans les tissus sains est fortement altérée lors de phénomènes pathologiques tels que le cancer et diffère non seulement dans sa composition mais également dans les fonctions qu'elle exerce et son impact sur les autres composants du MET. Dans un contexte tumoral, les informations biochimiques induites par ces interactions déclenchent des voies de signalisations permettant de moduler le fonctionnement des cellules tumorales, stromales et immunitaires, impactant ainsi des processus tels que la survie, la prolifération et l'invasion des cellules cancéreuses (Brassart-Pasco et al., 2020 ; Frantz et al., 2010).

La ténascine-C (TNC), molécule de la MEC, est l'une des protéines dont l'expression est altérée dans un contexte tumoral. En effet, présente dans de nombreux tissus durant le développement embryonnaire, la TNC n'est exprimée que très faiblement dans les tissus sains adultes. Cependant elle se retrouve fortement exprimée dans certaines pathologies et notamment dans de nombreux types de cancers (Midwood et al., 2011, Midwood et al., 2016). D'autre part, son expression élevée est associée à une diminution de la survie sans métastases et à un faible taux de survie globale des patients notamment dans le cas du cancer du sein (Oskarsson et al., 2011; Lowy and Oskarsson, 2015). De nombreuses études sur divers modèles tumoraux ont permis de montrer l'impact de la TNC sur les cellules cancéreuses (Yoshida et al., 2015 ; Huang et al., 2001). Ainsi, il a été montré que la TNC favorise la prolifération, la survie et la migration des cellules cancéreuses, ainsi que l'angiogenèse associée au développement tumoral (Saupe et al., 2013). Par ailleurs, certaines études ont mis en évidence le rôle important de la TNC dans la modulation de l'immunité anti-tumorale (Jachetti et al., 2015 ; Parekh et al., 2005 ; Deligne et al., 2020).

L'immunité anti-tumorale fait intervenir de nombreux types de cellules immunitaires ayant des rôles distincts permettant d'entraver la progression tumorale, et l'infiltration des cellules immunitaires effectrices au sein de la niche tumorale est primordiale pour mener à bien leurs fonctions (Fridman et al., 2012). Plusieurs études ont montré que dans un contexte tumoral la TNC peut affecter l'immunité innée et l'immunité adaptative favorisant ainsi la progression tumorale. Une étude réalisée sur un modèle murin de cancer du sein spontané a par exemple montré que la TNC est capable d'empêcher l'infiltration des monocytes et des macrophages au sein de la niche tumorale (Talts et al., 1999). Il a d'autre part été observé dans des modèles de cancer de la prostate et de cancer du poumon que la TNC diminue la prolifération et l'activation des lymphocytes T ainsi que la production de cytokines, altérant ainsi la réponse anti-tumorale médiée par les lymphocytes T (Parekh et al., 2005 ; Jachetti et al., 2015). L'immunité anti-tumorale est notamment médiée par des récepteurs présents sur les cellules immunitaires permettant à ces dernières de reconnaître des ligands exprimés à la surface des cellules cancéreuses conduisant à l'activation des cellules immunitaires effectrices et à la destruction des cellules cancéreuses. C'est notamment le cas du Natural killer group 2 member D (NKG2D) qui reconnaît les ligands NKG2D (NKG2DL) exprimés à la surface des cellules cancéreuses et induit

des voies de signalisation permettant l'activation de cellules immunitaires spécifiques et la production de cytokines, renforçant ainsi la surveillance immunitaire anti-tumorale (Diefenbach et al., 2001). Cependant, certaines cellules cancéreuses sont capables par différents mécanismes d'échapper à la surveillance immunitaire et il apparaît ainsi essentiel de mieux comprendre l'impact de la MEC et plus particulièrement de la TNC sur l'immunité anti-tumorale afin de développer des stratégies thérapeutiques pour contrecarrer l'échappement immunitaire.

Objectifs

Mon projet de thèse avait pour but d'étudier l'impact de la TNC sur l'immunité anti-tumorale. Pour cela, j'ai utilisé deux modèles murins préalablement établis dans le laboratoire. Le premier est le modèle MMTV-NeuNT qui est un modèle génétique de cancer du sein ErbB2-dépendant permettant d'obtenir des tumeurs multifocales ainsi que le développement de métastases pulmonaires au bout de 9 mois de développement (Muller et al. 1988). Le second modèle est un modèle de greffe orthotopique syngénique basé sur la lignée cellulaire cancéreuse NT193 générée à partir d'une tumeur mammaire MMTV-NeuNT. Ce modèle de greffe permet le développement d'une tumeur primaire ainsi que de métastases pulmonaires en moins de 3 mois après la greffe. Pour pouvoir étudier distinctement le rôle de la TNC stromale et de la TNC tumorale, ces deux modèles ont été manipulés afin de moduler l'expression de la TNC dans les cellules NT193 (shcontrol (shC) et shTNC) ainsi que dans les souris hôtes (TNC wildtype (WT) et TNC knockout (TNCKO)).

Les deux principaux objectifs de ma thèse étaient :

1. Etudier les effets de la TNC sur l'infiltrat immunitaire et l'impact sur la progression tumorale
2. Etudier l'impact de la TNC sur l'axe NKG2D/NKG2DL

Résultats

1. Etudier les effets de la TNC sur l'infiltrat immunitaire et l'impact sur la progression tumorale

Afin d'étudier l'impact de la TNC sur l'immunité anti-tumorale, nous avons réalisé une analyse génomique sur des tumeurs isolées de souris MMTV-NeuNT WT ou TNCKO. Cette analyse a révélé plus de 2000 gènes dérégulés entre les tumeurs des deux génotypes, parmi lesquels 136 sont des gènes associés à l'immunité. Ayant trouvé de telles différences entre les deux génotypes quant aux gènes associés à l'immunité, nous avons voulu étudier l'infiltration immunitaire dans un contexte tumoral. Pour cela nous avons utilisé le modèle de greffe orthotopique en établissant deux groupes d'étude distincts, ceci en injectant des cellules NT193 ayant une expression réduite de la TNC (NT193 shTNC) dans des hôtes KO pour la TNC (groupe nommé TNCKO/shTNC), et des cellules NT193 exprimant la TNC (NT193 shC) dans des souris WT pour la TNC (groupe nommé WT/shC). Une analyse comparative de l'infiltrat immunitaire présent dans le tissu cancéreux de ces deux groupes a été réalisé par immunomarquage de diverses cellules immunitaires telles que les leucocytes CD45⁺, les lymphocytes T (LT) CD4⁺, les LT CD8⁺ et les cellules dendritiques/myéloïdes CD11⁺. Aucune différence n'a été observée en termes d'abondance ou de localisation concernant les cellules CD4⁺, CD45⁺ et CD11⁺. En ce qui concerne les LT CD8, leur abondance s'est avérée ne pas différer entre les deux groupes contrairement à leur localisation. En effet, alors que dans le groupe TNCKO/shTNC les LT CD8 sont retrouvées au sein de la niche de cellules tumorales, dans le groupe WT/shC elles résident majoritairement dans le stroma sans atteindre les cellules tumorales. De plus, en quantifiant l'apoptose des cellules tumorales dans les deux groupes, nous avons pu montrer que l'infiltration des LT CD8 dans le groupe TNCKO/shTNC entraîne une augmentation du nombre de cellules tumorales en apoptose. Ces résultats démontrent que la TNC modifie la localisation des LT CD8 dans notre modèle de greffe NT193 impactant ainsi leur fonction.

Afin de comprendre le mécanisme sous-jacent à ce phénomène de séquestration des cellules T CD8 dans le stroma par la TNC, nous nous sommes basés sur une

analyse transcriptomique réalisée sur des tumeurs WT/shC et KO/shTNC. Cette analyse a notamment permis d'identifier la molécule CXCL12 comme étant significativement dérégulée en l'absence de TNC. Cette chimiokine étant décrite pour sa capacité à induire le chimiotactisme des LT CD8 (Okabe et al., 2005), nous avons décidé d'étudier le lien potentiel entre l'induction de CXCL12 par la TNC et la rétention des LT CD8 dans le stroma en présence de TNC dans nos deux modèles d'étude MMTV-NeuNT et NT193. Nous avons ainsi pu montrer par des analyses *in vitro* et *in vivo* que la présence de TNC augmente l'expression de CXCL12 dans nos deux modèles. De plus, afin de comprendre par quelle voie de signalisation la TNC induit CXCL12, nous avons mesuré son expression dans les cellules NT193 après utilisation d'inhibiteurs de voies de signalisation distinctes dont celui du TGF β , des intégrines $\alpha 4\beta 1$ et $\alpha 9\beta 1$, et du TLR4. Nous avons ainsi pu observer qu'en inhibant la voie du TLR4, l'expression de CXCL12 induite par la TNC est réduite, suggérant que la TNC régule l'expression de CXCL12 par l'activation du TLR4 (connu par ailleurs comme interagissant avec la TNC).

Par la suite, afin de savoir si CXCL12 est le principal chimioattractant par lequel la TNC immobilise les LT CD8, nous avons étudié la capacité de rétention cellulaire de la TNC en utilisant des chambres de migration. Pour cela, la face inférieure de l'insert a été recouverte d'une couche de TNC, et un milieu riche en CXCL12, ou en CCL21 (chimiokine utilisée en comparaison) a été déposé dans la chambre inférieure. Nous avons ainsi pu observer un nombre plus important de cellules adhérant à la couche de TNC en présence de CXCL12 qu'en présence de CCL21. De plus, en réalisant ces expériences en présence de l'AMD3100, un inhibiteur de CXCR4 qui est le récepteur de CXCL12, les effets liés au CXCL12 décrits précédemment sont abolis, confirmant ainsi que la rétention des LT CD8 par la TNC est dépendante de l'axe de signalisation CXCL12/CXCR4.

Enfin, afin d'étudier si l'effet de l'inhibition de CXCR4 sur l'infiltration des LT CD8 observé *in vitro* est également retrouvé *in vivo*, nous avons utilisé notre modèle de greffe WT/shC. Deux semaines après avoir greffé des cellules NT193 shC dans des hôtes WT, les souris ont reçu une injection péri-tumorale quotidienne d'AMD3100 durant 5 semaines. L'analyse des tumeurs provenant de ces souris a montré une diminution du poids de la tumeur chez les souris traitées à l'AMD3100 comparées au

groupe contrôle traité au PBS, concordant avec l'augmentation observée d'apoptose ainsi qu'une augmentation de la quantité de LT CD8 présents dans la niche de cellules tumorales. Ces résultats montrent que l'effet de la TNC sur la rétention des LT CD8 dans le stroma tumoral est régulé par l'axe de signalisation CXCL12/CXCR4.

Afin d'étudier la pertinence des résultats observés dans nos modèles murins chez l'homme, nous avons analysé des tissus cancéreux mammaires de patients nous permettant ainsi de montrer que l'infiltration des LT CD8 dans la niche tumorale est diminuée chez les patients présentant une expression élevée de TNC comparés aux patients présentant une faible expression de TNC. D'autre part, l'analyse de la survie globale (OS) ainsi que de la survie sans métastases (MFS) des patients d'une cohorte établie de patients atteints de cancer du sein a permis de montrer que les patients présentant une infiltration élevée de LT CD8 ainsi qu'une expression élevée de TNC ont des OS et MFS significativement diminués comparés aux patients présentant une infiltration élevée de LT CD8 et une faible expression de TNC. Ces données obtenues chez des patients atteints de cancer du sein confirment donc la pertinence des résultats que nous avons obtenus dans nos modèles murins.

2. Etudier l'impact de la TNC sur l'axe NKG2D/NKG2DL

L'utilisation du modèle NT193 nous a permis de montrer que la TNC dérivée des cellules stromales et des cellules tumorales joue un rôle dans le développement tumoral. En effet, un rejet partiel voire total de la tumeur a été observé dans la seule condition où les cellules NT193 greffées ainsi que les hôtes expriment la TNC (WT/shC). Aucun rejet tumoral n'a été observé lorsque l'expression de la TNC stromale ou tumorale est diminuée (TNCKO/shC et WT/shTNC). Ces résultats suggèrent que la TNC a un impact sur le développement tumoral et que seule l'expression combinée de la TNC stromale et tumorale donne lieu à un rejet tumoral. La lignée NT193 est composée de cellules épithéliales et de cellules mésenchymateuses. Nous avons émis l'hypothèse que le phénotype des cellules composant la lignée NT193 peut avoir un impact sur la tumorigénèse. Afin de caractériser ces deux types cellulaires nous avons établi à partir des NT193 deux lignées cellulaires distinctes, l'une épithéliale (nommée E), l'autre mésenchymateuse (nommée M). Afin de caractériser ces deux lignées nous avons réalisé une analyse

transcriptomique qui nous a permis d'observer la présence de plus de 12000 gènes dont l'expression est significativement différente entre la lignée E et la lignée M, avec notamment des gènes associés à l'adhésion et à la migration cellulaire, à l'apoptose et à la transition épithélio-mésenchymateuse. Nous avons également pu montrer grâce à des tests fonctionnels que les cellules M présentent une capacité de prolifération et de migration supérieure aux cellules E, ainsi qu'une forte expression de la TNC comparée à celle des cellules E. Ces résultats suggèrent la possibilité que ces deux types cellulaires présentent des propriétés tumorigéniques distinctes.

Afin d'étudier le comportement de ces deux types cellulaires *in vivo*, nous avons greffé séparément les cellules E et les cellules M dans des souris FVB. Nous avons ainsi pu observer que l'ensemble des souris greffées avec les cellules E développent une tumeur mammaire dans les 6 semaines suivant la greffe alors qu'aucune des souris greffées avec les cellules M ne développe de tumeur jusqu'à la fin de l'expérience fixée à 6 semaines post greffe. Afin de comprendre le destin des cellules M *in vivo* nous avons analysé les glandes mammaires ainsi que les poumons des souris greffées avec ces cellules M. Nous avons ainsi pu observer par immunomarquage des glandes mammaires que les cellules cancéreuses M sont visibles dans le tissu sous forme de clusters de cellules même si aucune tumeur palpable ne s'est développée. De plus, en analysant l'expression du marqueur de cellules cancéreuses *ErbB2* dans les poumons nous avons pu observer une plus forte expression de ce marqueur dans les poumons de souris greffées avec les cellules M que dans les poumons des souris greffées avec les cellules E, suggérant une dissémination des cellules M aux poumons malgré l'absence de tumeur primaire palpable.

Afin de comprendre pourquoi les cellules M ne forment pas de tumeur primaire *in vivo*, nous avons étudié de manière plus approfondie les résultats de notre séquençage réalisé sur les cellules E et M afin de cibler les gènes pouvant potentiellement être impliqués dans ce phénomène de rejet. Nous avons ainsi pu observer que les cellules M expriment fortement des ligands NKG2D (NKG2DL) comparées aux cellules E, ligands qui permettent aux cellules immunitaires disposant de récepteurs NKG2D de reconnaître les cellules cancéreuses et de les détruire, et nous avons confirmé au niveau protéique les différences d'expression de ces ligands entre les cellules M et les cellules E.

La TNC possède de nombreuses fonctions pouvant avoir un impact sur la réponse immunitaire et plusieurs études ont montré ses rôles immuno-suppressifs. Cependant, il a également été montré dans un modèle d'inflammation chronique (Midwood et al., 2009) ainsi que plus récemment dans un modèle tumoral (Spenlé et al., 2020), que la TNC peut dans certains cas être reconnue par le système immunitaire comme une molécule associée au danger (DAMP) et de ce fait déclencher l'action du système immunitaire.

Notre hypothèse est que la TNC que nous avons montré comme étant fortement exprimée dans les cellules M, pourrait jouer un rôle dans l'axe NKG2D/NKG2DL et permettre au système immunitaire de reconnaître les cellules M et de les détruire, les empêchant ainsi de former une tumeur palpable. Certaines cellules M pourraient néanmoins échapper à la surveillance immunitaire menant ainsi à l'état d'équilibre observé au niveau du site de greffe au sein duquel les cellules M résident en cluster mais ne forment pas de tumeur, et grâce à leurs propriétés invasives certaines cellules M pourraient disséminer jusqu'aux poumons.

Pour tester cette hypothèse, nous avons tout d'abord comparé l'expression des NKG2DL dans les cellules tumorales M exprimant la TNC (MshC) ou ayant une expression réduite de la TNC (MshTNC). Nous avons ainsi pu montrer que la présence de TNC induit une augmentation des ligands NKG2D. Par la suite, afin de savoir si la forte expression de TNC dans les cellules M est le principal obstacle au développement d'une tumeur primaire, nous avons greffé les cellules tumorales MshC et MshTNC dans la glande mammaire de souris FVB. Nous avons ainsi pu observer le développement d'une tumeur primaire chez l'ensemble des souris greffées avec les cellules MshTNC et ce au bout de 2 semaines post greffe. Ce résultat confirme donc l'implication de la TNC dans le rejet des cellules tumorales M. De manière intéressante nous avons par la suite observé le rejet de 50% des tumeurs dérivées des cellules MshTNC. De plus, l'expérience ayant été prolongé jusqu'à 90 jours post greffe (versus 42 jours pour la précédente expérience de greffe des cellules MshC) nous avons pu observer le développement d'une tumeur primaire dérivée des cellules MshC à partir de 50 jours post greffe avec 60% des souris présentant une tumeur primaire à la fin de notre expérience (90 jours post greffe). Ces résultats suggèrent que la présence de TNC retarde le développement de la

tumeur dérivée des cellules M et pourrait potentiellement faire intervenir l'immunité anti-tumorale.

Afin de tester la seconde partie de notre hypothèse concernant l'implication de l'axe NKG2D/NKG2DL dans le rejet des cellules tumorales M, nous avons établi une nouvelle lignée de cellules M n'exprimant que très faiblement les NKG2DL (shNKG2DL). Nos premiers résultats montrent que l'expression de la TNC est drastiquement diminuée dans les cellules M 3-shNKG2DL suggérant une interdépendance entre l'expression de la TNC et des NKG2DL. Ces cellules ont ensuite été greffées dans la glande mammaire de souris FVB, cependant aucune souris greffées n'a développé de tumeurs mammaires jusqu'à la fin de l'expérience fixée à 90 jours post greffe. Les résultats sont actuellement en cours d'étude et une analyse approfondie nous permettra d'orienter nos futures expériences pour comprendre ce phénomène de rejet.

Conclusion

Plusieurs études ont montré que la ténascine-C est capable de moduler l'immunité anti-tumorale en impactant la fonction et la localisation de divers types de cellules immunitaires tels que les macrophages et les lymphocytes T. Grâce à nos modèles MMTV-NeuNT et NT193, nous avons pu montrer que la TNC joue un rôle important dans le développement tumoral. Ainsi, la TNC empêche une action efficace de la réponse anti-tumorale en séquestrant les LT CD8 dans les réseaux de matrice, ceci en faisant intervenir la voie de signalisation CXCL12/CXCR4. Nous avons pu observer que cette séquestration a un impact direct sur la progression tumorale et que son inhibition permet au LT CD8 d'infiltrer la niche tumorale pour tuer les cellules cancéreuses permettant ainsi une diminution du développement tumoral. D'autre part, nos résultats non publiés suggèrent que la TNC a un lien avec l'axe NKG2D/NKG2DL dont l'impact sur le développement tumoral reste à établir. En effet, les résultats préliminaires sur notre nouvelle lignée cellulaire M 3-shNKG2DL suggèrent une corrélation entre une expression des NKG2DL et une forte expression de TNC. Les futurs résultats de ce projet pourraient être déterminants dans la compréhension de ce potentiel lien, des mécanismes sous-jacents ainsi que de l'impact sur le développement tumoral.

Introduction

1. Breast cancer

1.1 Incidence and mortality

Cancer is a major public health problem with an estimated 19.3 million of new cancer cases, and one of the main causes of mortality worldwide, with nearly 10 million deaths in 2020 (Sung et al., 2021; Ferlay et al., 2020). Among the most common cancers in 2020, breast cancer is at the first place with an incidence of 2.26 million cases, and the fifth most common causes of cancer death with 685 000 deaths after lung, colorectal, prostate and stomach cancer (Ferlay et al., 2020). The overall 5-year relative survival rate is around 90% for breast cancer, but this percentage is highly variable depending on breast cancer subtypes.

1.2 Breast cancer classification

Breast cancer is a heterogeneous disorder comprising many subtypes that display distinct pathological features and clinical implications (Yersal and Barutca, 2014). Therefore, a consensus classification is needed to stratify patients for suitable treatment strategy. The current classification system state that I will briefly describe below includes histological classification and grade, tumor, node and metastasis staging (TNM), and status of hormone receptors and Human epidermal growth factor receptor 2 (HER2) (Tsang and Tse, 2020; Al-Thoubaity, 2019).

1.2.1 Histological classification

Histopathological classification is based on several criteria among which cell type characteristics, immunohistochemical profile and extracellular secretion, allowing to distinguish two major classes, namely invasive ductal carcinoma (IDC) that represents around 80% of all invasive cancers, and invasive lobular carcinoma (ILC) representing around 10% of all invasive cancer (Tsang and Tse, 2020; Al-Thoubaity, 2019; Viale, 2012).

1.2.2 Histological grading

Histological grading determines the differentiation state of tumor cells and distinguishes 3 grades that represent the “aggressive potential” of the tumor (Viale, 2012; Rakha et al., 2010) (Figure 1). The first grade (Grade 1), namely “low grade” has the best prognosis and concerns a well differentiated phenotype. Cancer cell proliferation is slow and the cells look similar to normal breast epithelial cells. The “intermediate grade” (Grade 2) cancers are moderately differentiated and the proliferation of cancer cells are faster than normal. The “high grade” (Grade 3) cancers are poorly differentiated and have the worst prognosis with a rapid growth of cancer cells that present abnormal phenotypes.

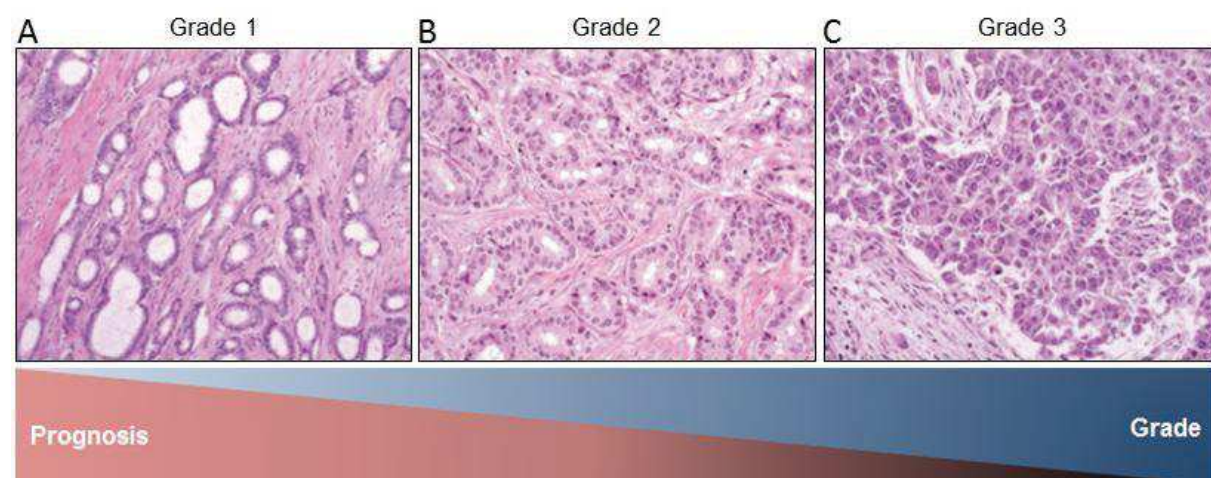


Figure 1. Histological grade of breast cancer (adapted from Rakha et al., 2010). **(A)** Grade 1 represents a well-differentiated tumor displaying high homology to normal breast tissue histology with glandular/tubular differentiation, low nuclear pleomorphism and low mitotic count. **(B)** Grade 2 represents a moderately differentiated tumor with an increased nuclear pleomorphism and mitotic count, and less glandular/tubular differentiation. **(C)** Grade 3 represents a poorly differentiated tumor with no tubule formation, and a high nuclear pleomorphism and mitotic count.

1.2.3 Tumor-Node-Metastasis staging

The TNM staging aims to stratify cancers according to the primary tumor features (T), the regional lymph node status (N) and the presence or absence of distant metastasis (M) (Cséni et al., 2018). The letter “T” is followed by a number from 0 to 4 describing the size and location of the tumor, and the higher the number is, the

bigger the tumor. The “N” is followed by a number from 0 to 3 depending on the spread of the cancer to the lymph nodes and how far from the primary tumor are the affected lymph nodes. The “M” is followed by either 0 or 1 depending whether the tumor has spread to other tissues. Based on this TNM staging breast cancer is classified in four stages (Table 1).

Overall Stage	T category	N category	M category
Stage 0	Tis	N0	M0
Stage I	T1	N0	M0
Stage IIA	T0	N1	M0
	T1	N1	M0
	T2	N0	M0
Stage IIB	T2	N1	M0
	T3	N0	M0
Stage IIIA	T0	N2	M0
	T1	N2	M0
	T2	N2	M0
	T3	N1	M0
	T3	N2	M0
Stage IIIB	T4	Any N	M0
Stage IIIC	Any T	N3	M0
Stage IV	Any T	Any N	M1

Table 1: Staging of breast cancer based on the TNM classification (from Alfonse et al., 2014). Abbreviation: Tis, in-situ carcinomas

1.2.4 Molecular classification

With the development of gene expression profiling using cDNA microarray technology and immunohistochemistry, it is now possible to classify breast tumors into four clinically relevant molecular subtypes based on similarities in gene expression profiles (Tsang and Tse, 2020; Gomes do Nascimento and Otoni, 2020): Luminal A, Luminal B, HER2-enriched and Triple Negative (TN). These four subtypes can be distinguished by their estrogen receptor (ER), progesterone receptor (PR) and HER2 receptor expression. In addition to these receptor status, the expression of Ki67 (a cell proliferation marker) is usually assessed by immunohistochemistry to assess tumor's aggressiveness (Fragomeni et al., 2019). The most common

molecular type is Luminal A tumors that are defined as ER and/or PR positive and HER2-negative, with low expression of Ki67. Luminal A tumors have the best prognosis with a slow growth. Luminal B tumors are considered as more aggressive with a faster growth and are defined as ER-positive and/or PR-positive, HER2 positive or negative with a high expression of Ki67. HER2-enriched subtype characterizes tumors that are both ER and PR negative and HER2 positive with a high Ki67 expression. These tumors grow faster than luminal tumors. Triple-negative tumors, that are considered having the worst prognosis, are defined as negative for both hormone receptors and HER2 with a high Ki67 expression.

Using one of these classification strategies alone might not be sufficient to precisely stratify patients and predict clinical outcomes. Therefore it is crucial to combine several criteria to choose the most efficient therapeutic strategy for breast cancer patients.

1.3 Local and systemic breast cancer treatment strategies

The choice of therapeutic strategy to treat breast cancer depends on the previously described criteria, patient age and overall health status. Over the last three decades, the increasing knowledge on breast cancer along with medical technical progress have allowed the development of new therapeutic approaches involving locoregional and systemic therapies.

1.3.1 Locoregional therapies

1.3.1.1 Breast surgery

At the time of diagnosis, more than 90% of breast cancers are not metastatic (Waks and Winer, 2019). In this case, the aim is to eradicate the primary tumor and prevent recurrence. The current approaches are either mastectomy (less and less required) or a conserving surgery with excision combined to radiation. These two approaches have the same cure rates with equivalent relapse-free and overall survival (Fisher et al., 2002). However, for most breast cancer patients, surgery is combined with radiotherapy and/or systemic therapy.

1.3.1.2 Radiotherapy

Radiotherapy consists of delivering high-energy rays such as X-rays to kill cancer cells. In most cases radiotherapy is used post-surgery to kill the remaining cancer cells in early breast cancer patients with lymph node involvement. It has been shown that radiotherapy post-surgery improves the locoregional disease-free and the overall disease-free survival (He et al., 2015). There are two main types of radiotherapy currently used in clinic. The first one is the external beam radiation that is the most common radiotherapy strategy used for breast cancer patients (Chand-Fouché et al., 2016). This technique consists of using an external machine to deliver the radiations on the area affected by the cancer. The second technique is called brachytherapy, also known as internal radiation. This technique is also used after having tumor surgery and consists of placing for a short time a radioactive device in the area where the tumor has been removed.

1.3.2 Systemic therapies

Systemic therapy can be used as first-line therapy but can also be used either before surgery (neoadjuvant) to reduce tumor burden, or after surgery (adjuvant) in case the biopsy post-surgery reveals an increased level of the biomarkers used to evaluate the risk of recurrence, or as both neoadjuvant and adjuvant (Maughan et al., 2010).

1.3.2.1 Chemotherapy

Chemotherapy consists of delivering chemical agents intravenously or orally to kill cancer cells and is based on the ability of these chemical agents to interfere with cell cycle progression. This strategy enables to target not only the cancer cells remaining in the primary tumor bed after surgery and radiotherapy, but also the invasive tumors and distant metastasis that cannot be targeted with locoregional therapies. Indeed, chemotherapy can be given as neoadjuvant or adjuvant but can also be used as the main treatment in the case of advanced or metastatic breast cancer (Maughan et al., 2010). Chemotherapy is mostly recommended for patients presenting high risk of breast cancer recurrence and the decision to use this treatment is based on the benefit/risk balance for the patient. There is a plethora of chemotherapy drugs classified depending on their mode of action. These drugs affect cancer cells at

different points in the cell cycle and thus combining drugs is the most effective treatment strategy. The most commonly used combination to treat breast cancer includes molecules from the anthracycline and taxane families (Hassan et al., 2010). Anthracycline molecules act by preventing religation of topoisomerase II-induced double-stranded DNA breaks by intercalating with DNA and forming anthracycline-DNA-topoisomerase II ternary complexes. DNA damage cannot be repaired and thereby leads to the initiation of programmed cell death. Taxane molecules are mitotic inhibitors that act by inhibiting microtubule depolymerization needed for cell division, thus blocking the cell cycle progression. There are also several other drug families such as alkylating agents and antimetabolites, showing thus the wide range of possible combinations (Hassan et al., 2010). Although chemotherapy was shown to decrease significantly breast cancer recurrence, it can also damage healthy cells and cause short-term side effects that usually disappear with time (such as hair and weight loss, tiredness etc.), but also sometimes long-term side effects that remain lifelong (such as infertility, neuropathy etc.) (Partridge et al., 2001).

1.3.2.2 Hormonal therapy

Hormonal therapy, also called endocrine therapy, consists of either blocking the production of hormones or interfering with hormone effects on breast cancer cells. Hormonal therapy is used for hormone receptor-positive breast cancers (ER+ and/or PR+) and can be used as adjuvant/neoadjuvant for early-stage breast cancer and also in advanced or metastatic breast cancer. Several strategies are currently available in hormonal therapy, such as blocking ovarian function (in woman breast cancer patients), blocking estrogen production and blocking the effect of estrogens on cancer cells (Drăgănescu and Carmocan, 2017). Ovarian function can be stopped by ovarian ablation (surgery or radiation therapy) or by medication. Another option is to reduce estrogen production by targeting aromatase enzyme that catalyzes the last steps of estrogen biosynthesis. Aromatase inhibitors are only used in women who have undergone menopause because too much aromatase is produced in premenopausal women to be effectively blocked by these inhibitors. The third option is to block the effect of estrogens by using competitive inhibitors of estrogen such as tamoxifen that prevent estrogens from binding to its receptor. Hormonal therapy can

lead to several side effects such as tiredness, joint and muscle pain, but also to more severe side effects such as cataract and osteoporosis (Burstein and Griggs, 2010).

1.3.2.3 Targeted therapy

Targeted therapy consists in targeting specific cancer associated molecules expressed on cancer cells or in modulating their microenvironment to block signaling pathways responsible for their proliferation, survival and spread. This strategy enables to reduce the possible adverse effects on healthy cells. Targeted therapy comprises several strategies such as the use of monoclonal antibodies for targeting molecules located outside the cells, or the use of small molecules that can penetrate into the cells to target molecules within the cells (Lee et al., 2018). Moreover, immunotherapeutic cancer vaccines have been developed for targeting specific tumor-associated antigens through T cell stimulation. Another strategy is the gene therapy that consists in introducing genetic material leading to either the correction or the destruction of the cells harboring genetic aberrations. There is a wide range of molecules currently used in targeted therapy. One of the most widely used strategy targeting tumor cells and considered currently as the most efficient one consists in the inhibition of HER2 which is overexpressed in 25% of breast cancers by using the recombinant antibody trastuzumab (Herceptin) (Masoud and Pagès, 2017). This molecule inhibits signaling pathways triggered by HER2 and involved in cancer cell proliferation and survival. However, resistance and tumor relapse can develop and therefore more information is needed how to treat this cancer subtype. Another strategy is to inhibit the phosphatidylinositol 3-kinase (PI3K)/AKT/mTor signaling pathway that is known to regulate multiple cellular processes involved in the promotion of tumor cell growth, survival and spread (Vivanco and Sawyers, 2002). Other than targeting directly cancer cells, it is also possible to target molecules within the tumor microenvironment (TME) involved in the promotion of cancer progression. One relevant target is the vascular endothelial growth factor (VEGF) that promotes angiogenesis. Indeed, knowing that new blood vessel formation supplies nutrients and oxygen to cancer cells, targeting angiogenesis promoters is a relevant therapeutic target and several drugs directed against VEGF such as bevacizumab, sunitinib and sorafenib have shown promising outcomes in triple-negative and advanced or metastatic breast cancers (Ju et al., 2018). Another strategy used in

targeted therapy is to potentiate immune system responses by targeting immune suppressor molecules expressed on tumor cells. This is the so-called immune checkpoint therapy (see below).

1.3.2.4 Immune checkpoint therapy

Under normal conditions, checkpoint proteins enable to maintain a balanced activation of the immune system by preventing the excessive activation of T cells. These molecules expressed on the cell surface bind receptors expressed on T cells and this binding switches off the activity of T cells (Ju et al., 2018). However, cancer cells can overexpress immune checkpoint regulating molecules and can block T cells, evading thereby immune surveillance. The immune checkpoint therapy consists in using inhibitors that can block the activity of immune checkpoint molecules and thus enhance T cell activation. The main molecules currently used in immune checkpoint therapy are programmed death-1 (PD-1), programmed death-ligand 1 (PD-L1) and cytotoxic T-lymphocyte-associated antigen-4 (CTLA-4) inhibitors (Ju et al., 2018; Rotte, 2019; Sharma and Allison, 2015) (Figure 2). Binding of PDL-1 that is overexpressed on tumor cells to PD-1 expressed on T cells inhibits downstream signaling within the T cell and leads to a reduced expression of transcription factors that are associated with effector T cell functions. This binding can be prevented by using monoclonal antibodies targeting either PD1 such as pembrolizumab, or PDL1 such as atezolizumab. T cell activation not only requires the binding of T-cell receptor to antigen presented by major histocompatibility complex (MHC) proteins but also a co-stimulatory signal through the binding of the receptor CD28 expressed on T cells to CD80 and CD86 ligands present on antigen-presenting cells (Rotte, 2019; Darvin et al., 2018). CTLA-4 is a receptor found on activated T cell and regulatory T (T_{reg}) cell surface and acts by competing the CD28 receptor. Indeed, CTLA-4 can bind CD80 and CD86 with higher affinity and avidity than CD28 preventing the second activation signal for T cells, thus downregulating T cell activation. Blocking the binding of CTLA-4 to CD80 and CD86 by using monoclonal antibodies such as ipilimumab boosts the immune response against cancer cells (Sharma and Allison, 2015).

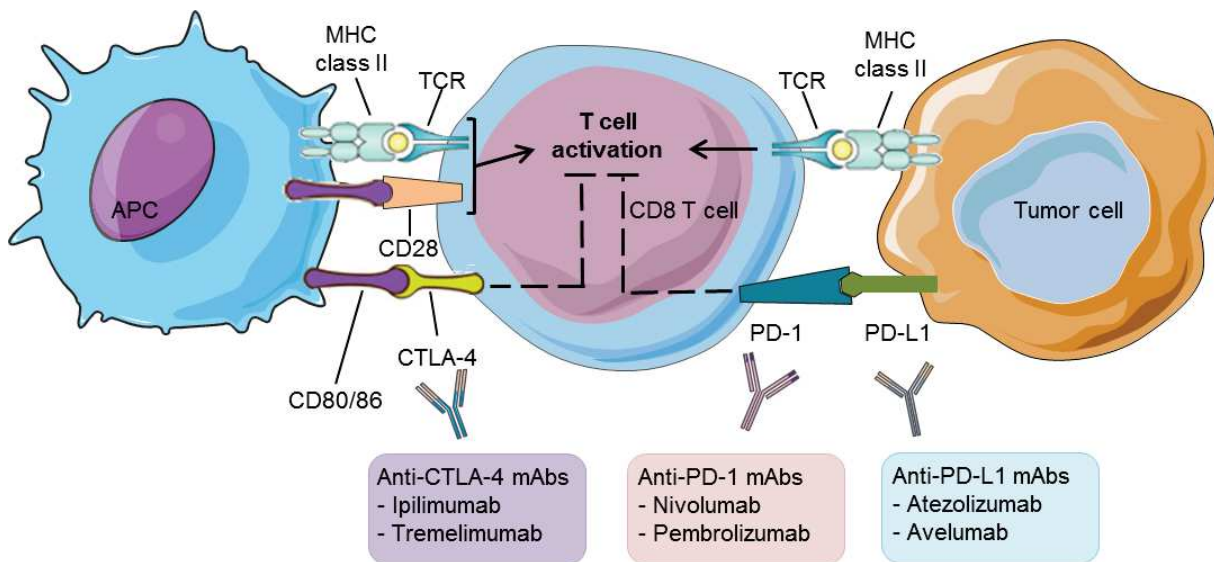


Figure 2. Role of CTLA-4 and PD-1 in immunoregulation and monoclonal antibodies (mAbs) used in immunotherapy. T-cell activation requires binding of the T-cell receptor (TCR) to the antigen in association with major histocompatibility complex (MHC), and binding of CD28 costimulatory receptor on the T-cell surface with CD80/86 ligand on the antigen-presenting cell (APC). CTLA-4 receptor binds CD80/86 with higher affinity than CD28 thereby downregulating T-cell activation. Anti-CTLA-4 mAbs inhibit the binding of CTLA-4 to CD80/86 thus restoring T-cell activation. PD-L1 ligand expressed on tumor cells binds PD-1 receptor on T cell inducing an inhibitory signal to T cells. Anti-PD-1 and anti-PD-L1 mAbs block this interaction leading to tumor-specific T-cell reactivation.

2. Tumor microenvironment

The non-exhaustive panel of therapeutic strategies described above clearly shows that cancer treatments do not only aim to target cancer cells themselves but also components of the tumor microenvironment (TME), highlighting the importance of the TME in cancer progression. Indeed, over the last two decades it has been well demonstrated that the TME plays a crucial role in cancer progression, and that understanding the roles of not only each component of the TME but also their interactions is fundamental to develop efficient therapeutic strategies. The TME encompasses different cellular components but also soluble growth factors and extracellular matrix, and the interplay between malignant cells and their microenvironment can promote tumor initiation, progression and metastases development, impacting thereby patient prognosis (Balkwill et al., 2012; Joyce and Pollard, 2009) (Figure 3).

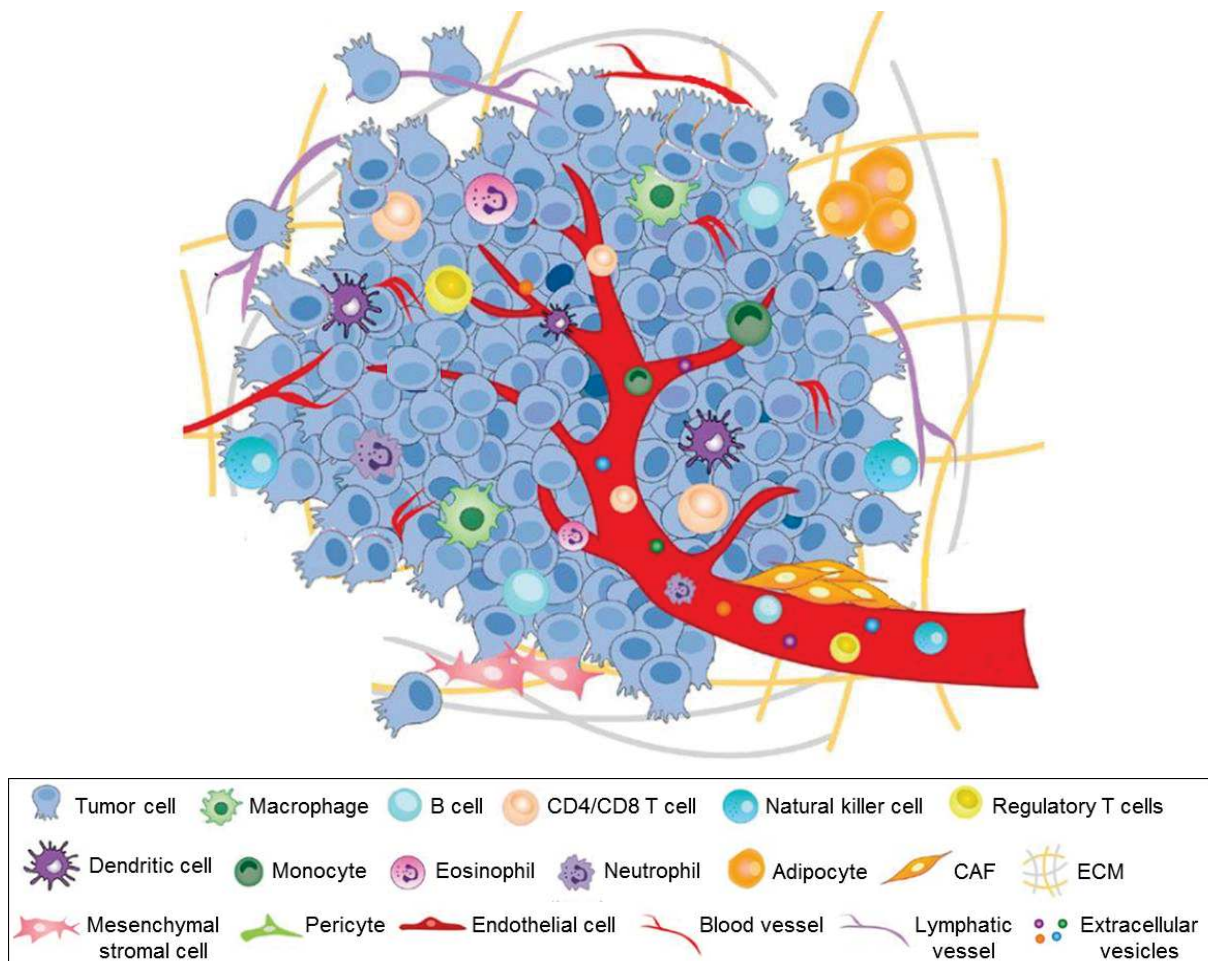


Figure 3. Composition of the tumor microenvironment (adapted from Bejarano et al., 2021). The tumor microenvironment is composed of numerous cell types and secreted factors. Cellular components of the TME include tumor cells, immune cells such as T and B lymphocytes, dendritic cells, tumor-associated macrophages, natural killer cells, neutrophils and eosinophils; stromal cells such as cancer-associated fibroblasts (CAF), mesenchymal stromal cells, endothelial cells and pericytes, and tissue-specific cell types such as adipocytes. These cells secrete extracellular matrix (ECM) components, cytokines, growth factors and extracellular vesicles. Blood and lymphatic vessels form the vascular network within the TME. Each of these components can contribute to cancer progression.

2.1 Cellular components of tumor microenvironment

2.1.1 Cancer cells

A tumor is composed by tumor cells that arise from a progressive transformation of normal cells into malignant cells displaying specific properties classified and named

as the hallmarks of cancer (Hanahan and Weinberg, 2011) (Figure 4). These transformations occur in response to genetic alterations in oncogenes and tumor suppressor genes enabling the accumulation of pro-tumoral properties. These properties are notably described in the well-known paper from Hanahan and Weinberg (2011) that highlights the 10 hallmarks of cancer which are: evading growth suppressors, avoiding immune destruction, enabling replicative immortality, inducing tumor-promoting inflammation, activating invasion and metastasis, inducing angiogenesis, resisting cell death, deregulating cellular energetics in favor of malignant cell proliferation, sustaining proliferative signaling and the presence of genome instability and mutations. Later, the importance of TME has been pointed out showing that cancer cells do not support alone tumor progression but corrupt their microenvironment establishing a tumor bed, and that all the hallmarks of cancer involve the contribution of the TME (Hanahan and Coussens, 2012). Besides these features common for all cancer cells, some breast cancer cells display specific molecular alterations that are used as biomarkers for breast cancer classification such as an overexpression of the receptors for estrogen, progesterone and HER2.

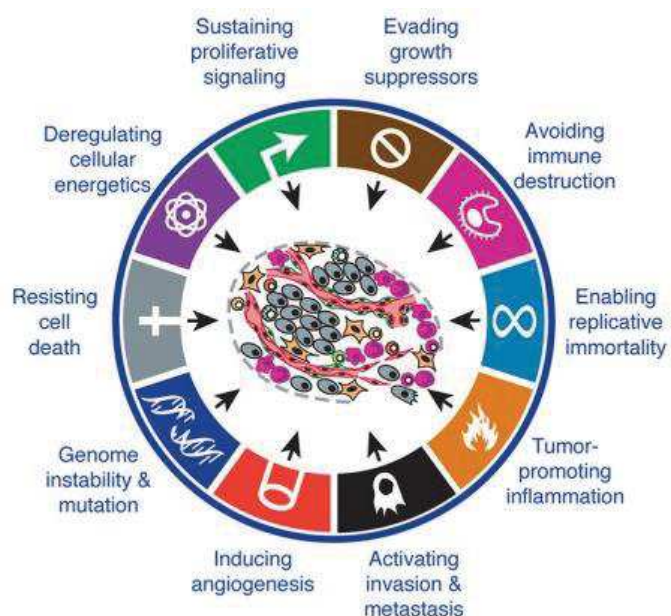


Figure 4. The hallmarks of cancer (adapted from Hanahan and Weinberg, 2011). The hallmarks of cancer involve not only intrinsic characteristics of the malignant cells but also contributions of the tumor microenvironment through interactions of tumor cells with other TME components such as immune cells.

2.1.2 Cancer stem cells

Cancer stem cells are a small population of cancer cells within tumor that show self-renewal and differentiation properties. Breast cancer stem cells (BCSCs) have been shown to exhibit the expression of specific molecular signatures including CD44⁺/CD24⁻, CD133⁺ and Aldehyde dehydrogenase 1^{high} (ALDH1^{high}) (Butti et al., 2018). Moreover, several signaling pathways have been identified as being involved in their stemness such as Notch, Wnt and Hedgehog (Takebe et al., 2015). BCSCs have also the ability to promote the formation of new blood vessels by differentiating into endothelial cells, a process called vasculogenic mimicry, and by secreting proangiogenic factors such as VEGF and the stromal cell-derived factor 1 (SDF-1 or CXCL12). Among their multiple properties one can also cite their resistance to anoikis which is a programmed cell death occurring upon loss of attachment to the extracellular matrix (ECM) in anchorage-dependent cells (Kim et al., 2012). These properties enable BCSCs to promote metastasis formation. Another important and challenging BCSCs property is their resistance to chemo- and radiotherapy. Indeed, BCSCs were shown to present an altered/higher expression of DNA repair enzymes and DNA repair checkpoint proteins enabling them to repair DNA damage caused by chemo- and radiotherapy (Wang, 2015). BCSCs also display resistance to a broad spectrum of molecules used in therapy such as cisplatin and anti-estrogen drugs (Butti et al., 2018). Altogether, these examples of BCSC properties highlight their crucial role in tumor progression, metastasis development and anti-cancer treatment resistance. Therefore, targeting BCSCs is relevant to treat breast cancer patients, and several treatment strategies targeting BCSCs markers, self-renewal pathways, and BCSCs drug resistance properties are currently under study.

Apart from malignant cells, the TME is composed of several other cell types playing different roles that can support tumor progression and metastasis development.

2.1.3 Cancer associated fibroblasts

Cancer associated fibroblast (CAF) is a group of activated fibroblasts found in the TME and represents the most abundant component of the tumor stroma (Balkwill et al., 2012). CAFs have no specific biomarkers but can be distinguished from resident fibroblasts and other mesenchymal cells by the combined expression of several

biomarkers including mesenchymal markers such as vimentin, alpha-smooth muscle actin (αSMA), fibroblast activation protein (FAP), fibroblast-specific protein 1 (FSP1) and platelet-derived growth factor alpha (PDGF-α) (Ping et al., 2021). The origin of CAFs in the TME remains unclear and several hypotheses have been pointed out. It was for instance suggested that cancer cells can activate normal resident fibroblasts into CAFs by the delivering of transforming growth factor beta (TGFβ) through exosomes (Goulet et al., 2018). Some studies showed that CAFs are derived from endothelial cells by undergoing an endothelial-to-mesenchymal transition. Apart from these two explanations other studies showed that CAFs can originate from bone marrow-derived mesenchymal stem cells, adipocytes, pericytes, hematopoietic stem cells and stellate cells invading into the tumor tissue (Ping et al., 2021). These multiple origins may explain the diversity of CAFs functions. Indeed, CAFs have several functions that support tumor progression such as matrix deposition and remodeling, modulation of immune responses and angiogenesis promotion. CAFs act also as a reservoir of growth factors, chemokines and pro-inflammatory factors that support tumor progression and metastasis development (Orimo et al., 2005). It has been for example shown that CAFs secrete CXCL12 that promotes tumor cell migration and angiogenesis. Moreover, CAFs are able to produce matrix metalloproteinases (MMPs) such as MMP9 that leads to ECM remodeling thereby promoting cancer cell invasion.

2.1.4 Endothelial cells and pericytes

Angiogenesis is considered as a hallmark of cancer and was shown to support and promote tumor progression by supplying nutrients and oxygen to cancer cells (Hanahan and Weinberg, 2011). The rapid proliferation of cancer cells moves the center of the tumor more and more away from blood vessel, causing thereby hypoxia. Hypoxia leads to the increase of VEGF and other angiogenic factors that stimulate new blood vessel formation by recruiting notably endothelial cells and pericytes that form the boundaries of capillaries (Farc and Cristea, 2020). Unlike the blood vessels found in healthy tissues, the tumor vasculature is abnormal with disorganized and leaky vessels that impact also its function such as increasing interstitial fluid pressure, reducing blood flow and impairing drug distribution. Pericytes provide structural support to blood vessels, however the new vessels formed in tumor context

present few pericytes promoting the impairment of blood vessel integrity (Balkwill et al., 2012). The TME also contains lymphatic endothelial cells (LEC) forming lymphatic vessels that represent an alternative route for cancer cell dissemination. In a primary tumor, lymphangiogenesis is driven by VEGF-C and VEGF-D which also promote metastasis (Ma et al., 2018).

2.1.5 Immune cells

Immune cells are a major component of the TME and all immune cell types may be found within the TME. Indeed, the TME can comprise innate and adaptive immune cells including macrophages, dendritic cells, natural killer cells, mastocytes, and B and T lymphocytes (Farc and Cristea, 2020).. I will give here a few examples of immune cell functions in the TME. One of the cell types from the innate immune system found in the TME are the tumor associated macrophages (TAMs) that were shown to be associated with advanced tumor progression and metastasis, and to correlate with poor prognosis in several cancers such as breast, prostate and ovarian cancers (Pollard, 2004). TAMs can promote cancer cell invasion and proliferation through the production of molecules involved in inflammation such as tumor necrosis factor (TNF)- α and interleukin (IL)-1 β . TAMs are also able to potentiate tissue remodeling by secreting MMPs and epidermal growth factor (EGF), and to facilitate tumor cell proliferation, migration and survival by the secretion of growth factors and cytokines (Condeelis and Pollard, 2006). Another example is dendritic cells (DCs) that are considered as the most efficient antigen-presenting cells (Gabrilovich et al., 2012). The presence of DCs correlates with a good prognosis in several cancers but in some cases the immune suppressive mechanisms of the TME can affect the function of DCs. Indeed, it was shown that some growth factors such as TGF β 1 and VEGFA secreted in the TME can impair DC functions, thereby compromising anti-tumor immune responses (Gabrilovich et al., 2012; Hargadon et al., 2016). Another major immune cell type found in the TME, this time from the adaptive immune system, is T lymphocytes. There are two major groups of mature T cells, namely the CD8 cytotoxic T cells and the CD4 helper T cells comprising each several subtypes. T lymphocytes are known to have both tumor-suppressive and tumor-promoting effects depending on the T cell subtype and on the context (Balkwill et al., 2012). CD8 T cells are one of the most potent effectors of the antitumor immune response

and high numbers of CD8 T cells and CD4 T helper 1 cells are associated with a good prognosis in several cancers (Fridman et al., 2012). On the contrary, the presence of high numbers of T_{reg} cells (a subtype of CD4 T cells) correlated with poor prognosis in many cancer types. These examples show that the immune landscape within the TME is crucial and can alter the prognosis of cancer patients. The impact of the immune cells in the TME on tumor progression and its therapeutic implications will be addressed in more detail in section 4. of this manuscript.

2.1.6 Adipocytes

White adipocyte tissue represents 90% of normal breast tissue and it was shown that in the tumor context cancer-associated adipocytes (CAAs) can interact with breast tumor cells impacting tumor progression (Birbrair, 2020). CAAs are able to secrete a wide range of factors such as metabolites, hormones, enzymes and cytokines (called adipokines) triggering cancer cell proliferation, migration and invasion. For instance, CAAs are able to promote angiogenesis through VEGFA expression which triggers cancer cell proliferation and invasion. Several studies also showed that adipocytes can promote metastasis in breast cancer patients through the release of cytokines such as IL6, IL8 and IL10 (Chu et al., 2019). Another adipokine found in the TME is leptin that can bind the leptin receptor present on breast cancer cells which induces their proliferation (Birbrair, 2020).

2.2 Soluble factors

The TME is composed of a plethora of soluble factors derived from several families playing important roles in tumor progression such as growth factors, hormones, cytokines and enzymes, and several of them have been aforementioned. To briefly summarize, these soluble factors can be secreted by immune cells but also by other stromal cells present in the TME and by cancer cells themselves and impact cancer progression in multiple ways. Indeed, it was shown that soluble factors can promote angiogenesis, tumor cell migration, proliferation, invasion and metastasis development, and can also have immune suppressive effects (Joyce and Pollard, 2009; Farc and Cristea, 2021). Moreover, the presence and abundance of specific soluble factors in the TME can be a determinant of therapeutic efficacy.

2.3 The extracellular matrix (ECM)

2.3.1 ECM architecture and components

The ECM is a complex three-dimensional meshwork of highly cross-linked fibrous proteins and non-fibrous proteoglycans that provides not only a physical scaffold for the cells but also has a dynamic role by affecting cell behavior (Hynes and Naba, 2012). The ECM is composed of two biochemically and morphologically distinct entities: the basement membrane organized as thin meshes which separate the epithelium from the adjacent stroma, and the interstitial matrix organized as loose fibril-like structure that interconnects cells in the stroma and the stroma with the basement membrane (Theocharis et al., 2016). The repertoire of ECM proteins (plus ECM associated molecules such as soluble factors and matrix remodeling enzymes) is termed the “matrisome”. Analysis of human and mouse genomes enabled to define a robust list of proteins found in the ECM of mammals. This list was called the “core” matrisome and is composed of around 300 proteins comprising collagen, proteoglycans, and glycoproteins (Hynes and Naba, 2012). Briefly, collagens are the most abundant structural proteins of the ECM and provide tensile strength to all forms of ECMs. Proteoglycans are found interspersed among the collagen fibrils and have several functions such as to withstand compressional forces by providing hydration through the binding of water. They can also bind cations such as calcium and many growth factors secreted into the ECM. Last but not least, the matrisome contains glycoproteins that have a plethora of functions regulating cell adhesion, migration, proliferation and survival (Mouw et al., 2014). Among these glycoproteins one can cite laminins, fibronectin, and tenascins. These molecules act also as reservoir for bioactive molecules through their capacity to sequester and release growth factors and cytokines thereby impacting the microenvironment and cell behavior (Yue, 2015). The interaction between the ECM and the cells is mediated by cell surface receptors including integrins and syndecans that upon ligation trigger intracellular signaling pathways (Theocharis et al., 2016; Yue, 2015).

Although fundamentally, some molecules are found in the ECM of all tissues, each tissue has a specific ECM composition. The ECM is constantly undergoing remodeling and its composition and organization impact cellular processes such as growth, migration, and differentiation.

2.3.2 ECM alterations and roles in the TME

Importantly in the TME, the ECM proteome that is part of the cancer matrisome, is highly altered compared to those in healthy tissues and some of its components can be used as prognostic biomarkers (Brassart-Pasco et al., 2020). The stiffness of tumors is strongly higher than the surrounding normal tissue and this is due to an excessive deposition of structural components such as collagens and elastin fibers (Frantz et al., 2010). Indeed, the ECM in the TME is mainly secreted by CAFs that were shown to produce more ECM molecules than normal fibroblasts. After the excessive deposition of elastin and collagens, these molecules are cross-linked by transglutaminase and lysyl oxidase generating thereby larger and more rigid fibrils that stiffen the ECM and facilitate cancer cell migration (Brassart-Pasco et al., 2020; Frantz et al., 2010). Several components of the TME such as tumor cells and CAFs are also able to secrete proteases such as MMPs that degrade the ECM and release growth factors such as VEGF and TGF- β , promoting thereby tumor cell migration, proliferation and survival. The degradation of ECM macromolecules by proteases leads also to the release of small ECM fragments into the circulation and the levels of these fragments in the serum of cancer patients can be used as biomarkers (Brassart-Pasco et al., 2020). For instance, the levels of type VI collagen $\alpha 1$ and $\alpha 3$ chain fragments appeared to be higher in the serum of breast cancer patients compared to healthy patients. Moreover, high expression of fibronectin by cancer cells has been correlated with poor overall survival in invasive breast cancer patients (Bae et al., 2013). Similarly, high expression of tenascin-C (TNC) was shown to be associated with poor overall survival and poor metastasis-free survival in breast cancer patients (Oskarsson et al., 2011).

3. Tenascin-C (TNC)

3.1 Structure and expression of TNC

TNC is a large hexameric extracellular glycoprotein belonging to the tenascin family that includes also tenascin-R, -W and -X (Chiquet-Ehrismann and Tucker, 2011). Each TNC monomer is composed of four domains with distinct functions: an N-terminal assembly domain, followed by 14.5 EGF-like repeats, 17 fibronectin type-III (FNIII) domains with 8 constant and up to 9 alternatively spliced domains, and a C-

terminal fibrinogen-like globular (FBG) domain (Midwood et al., 2016) (Figure 5). The heptad repeats within the N-terminal assembly domain mediates the trimerization of the molecule and then two trimers assemble during TNC secretion to form the hexameric form named hexabrachion. Each domain of TNC can interact with several molecules such as cell surface receptors like integrins, growth factors but also other ECM molecules like fibronectin (Orend and Chiquet-Ehrismann, 2006). This wide range of partners confers to TNC a plethora of functions that will be discussed later.

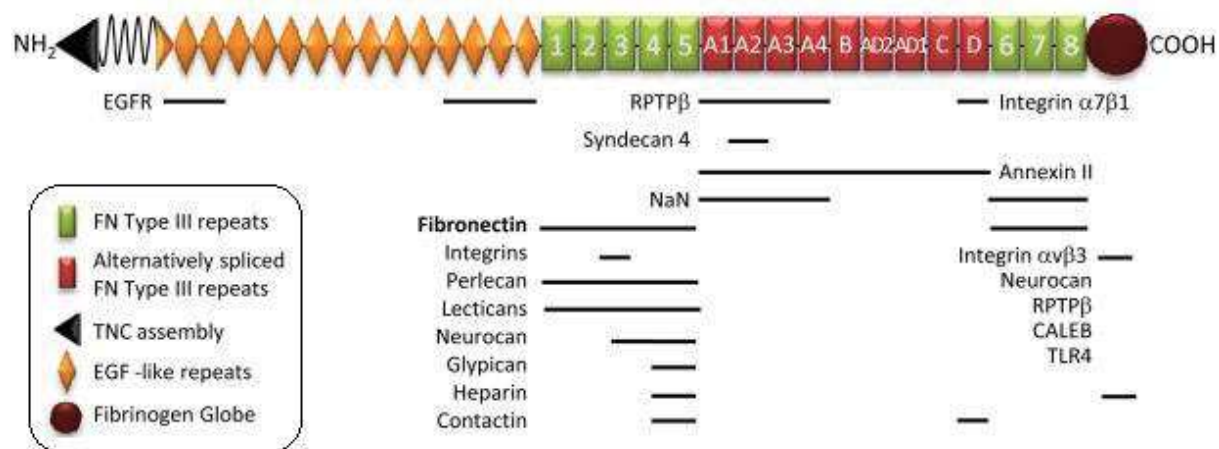


Figure 5. Structure of TNC and potential binding partners (adapted from Van Obberghen-Schilling et al., 2011). Each monomer of TNC is composed of an oligomerization domain, epidermal growth factor-like repeats (EGF-L), fibronectin type-III (FNIII) repeats and a fibrinogen like domain. Binding sites for interacting molecules are indicated.

TNC is expressed in several different structures during embryonic development. Indeed, in developing tissues TNC was reported to be expressed for instance around motile cells, in the central nervous system, in dense connective tissue such as cartilage, tendons, and bone as well as in branching morphogenesis (Midwood et al., 2016). However, in adult tissues TNC expression is restricted to a few places namely tendons, stem cell niches and reticular fibers in lymphoid organs. Furthermore, TNC can also be expressed *de novo* under some “stressed” and pathological conditions such as wound healing, chronic inflammation, cardiovascular disease and cancer (Midwood et al., 2011).

TNC expression can be triggered by several molecules notably by cytokines such as TNF- α and interferon (IFN)- γ , interleukins such as IL-1 and IL-4, and growth factors such as TGF- β and EGF (Midwood and Orend, 2009). Moreover, it was shown that mechanical stress, hypoxia and reactive oxygen species can also trigger TNC expression. Several signaling pathways were also shown to induce TNC expression such as Notch, Wnt/ β -catenin and PI3K/Akt signaling pathways. Furthermore, some transcription factors were reported to induce TNC expression by binding its promoter such as c-Jun, NF κ B and Sox4 (Orend and Chiquet-Ehrismann, 2006; Midwood and Orend, 2009). Unlike the multitude of molecules able to induce TNC expression, only few mechanisms are negative regulators of TNC expression. One can cite the microRNA-335, the transcription factor GATA and some anti-inflammatory corticosteroids that were shown to downregulate TNC expression (Chiquet-Ehrismann and Chiquet, 2003; Tavazoie et al., 2008).

3.2 Physiological roles of TNC

As described before, TNC is mostly expressed during embryogenesis and tissue development. Yet, the physiological roles of TNC remained elusive for a long time after its discovery because the first studies of TNC knockout (KO) mice in the early 90s were described as showing no abnormalities (Saga et al., 1992; Forsberg et al., 1996). These results were intriguing knowing that the TNC sequence is highly phylogenetically conserved. It took a few years more to show that even though mice KO for TNC are outwardly normal, they display an abnormal behavior (Mackie and Tucker, 1999). Indeed, several behavioral experiments showed a hyperactivity and “fearless” behavior in those mice that could increase their exposition to life-threatening situations or to predation, explaining potentially the conservation of TNC sequence through vertebrate evolution. It was later shown that TNC plays a major role in the development and the organization of the nervous system. TNC KO mice were for instance reported to present a reduced proliferation and an accelerated maturation of oligodendrocyte precursors (Chiquet-Ehrismann and Tucker, 2011; Mackie and Tucker, 1999; Chiquet-Ehrismann et al., 2014). Thanks to the TNCKO mouse models, more and more studies showed the different roles of TNC besides to its impact on nervous system development and organization. One can for instance cite the abnormal branching morphogenesis such as abnormal prostate development,

abnormal stem cell niches and abnormal responses to injury (Chiquet-Ehrismann et al., 2014). Concerning the latter one, TNC was described for having a role in the three overlapping phases following tissue injury, namely inflammation, tissue rebuilding and tissue remodeling (Midwood and Orend, 2009). TNC expression is rapidly induced after tissue injury and detected to be concentrated in areas of high immune cell infiltration during the acute inflammation phase. It has been suggested that in this context, TNC can stimulate the migration and activation of lymphocytes (Midwood and Orend, 2009; Chiquet-Ehrismann et al., 2014). During tissue rebuilding and tissue remodeling, TNC was reported to stimulate ECM synthesis and assembly, and cell migration and survival involving keratinocytes that facilitate tissue repair (Midwood and Orend, 2009). Altogether, these examples show that TNC has different roles that are cell-type-, tissue- and context-dependent.

3.3 TNC in cancer

TNC was reported as being expressed under some pathological conditions such as cancer, and its expression has significant functional consequences, as well as an impact on cancer patient prognosis.

3.3.1 TNC expression in cancer and clinical significance

Diverse types of cancers were reported to express TNC and its expression has been associated with key clinical parameters, such as relapse-free and overall patient survival (Lowy and Oskarsson, 2015). In breast cancer, TNC is highly expressed at the invasive front of the primary tumor as well as at the metastatic site (Oskarsson et al., 2011; Jahkola et al., 1996; Ishihara et al., 1995). Moreover, TNC expression was correlated with invasive cases of breast cancer and associated with an aggressiveness of pulmonary metastasis leading to poor metastasis-free and poor overall survival of breast cancer patients (Oskarsson et al., 2011). TNC expression levels are also used as a predictive marker for the malignant potential of breast cancer cells (Goepel et al., 2000). For lung cancer and melanoma too, the highest TNC expression was observed in the advanced/invasive cases (Lowy and Oskarsson, 2015). In head and neck cancer TNC expression was associated with early metastatic recurrence and poor overall survival (Juhász et al., 2000). Among other cancer types displaying high TNC expression one can cite glioblastoma and

colorectal cancer. Whereas in several cancers including breast cancer, the stratification of cancers depending on TNC levels above and below the median showed a worsened clinical outcome for patient with TNC levels above the median (Ishihara et al. 1995), also TNC levels below the median can be considered as high in comparison to normal tissue that is essentially devoid of TNC. As soon as TNC is increased it can promote tumor metastasis as seen in osteosarcoma and glioblastoma involving a different mechanism as seen in tumors with very high TNC levels. In particular, TNC induced cell rounding through integrin $\alpha 9\beta 1$, inhibiting YAP signaling thereby promoting amoeboid migration and lung metastasis (Sun et al., 2018).

3.3.2 Sources of TNC in the TME

In many cancers, TNC expression is heterogeneously distributed in tumor nodules and metastasis, and the highest expression of TNC is found being associated with the invasive front (Orend and Chiquet-Ehrismann, 2006; Lowy and Oskarsson, 2015; Oskarsson et al., 2011; Jahkola et al., 1996). This heterogeneous distribution suggests that TNC has distinct sources in the TME. Indeed, studies showed that both cancer-associated stroma and tumor cells themselves can express TNC and a combined high expression by both cellular sources correlated with shortest patient survival (Ishihara et al., 1995).

3.3.2.1 TNC derived from cancer-associated stroma

A prominent source of TNC in the TME is the stromal cells. Indeed, a study showed the importance of the stroma as a source of TNC by orthotopically grafting 4T1 breast cancer cells into mice WT or KO for TNC. The authors observed less metastatic nodules in TNCKO mice (O'Connell et al., 2011). In this study, the authors also reported that the main producers of TNC within the stroma are the activated fibroblasts and that TNC produced by these stromal cells are important for metastatic dissemination. Another source of TNC within the stroma is the activated endothelial cells and it was reported that while resting endothelial cells do not express TNC, its expression is highly induced during tumor-associated angiogenesis (Zagzag et al., 1996).

3.3.2.2 TNC derived from cancer cells

Beside TNC derived from cancer-associated stromal cells, TNC can also be expressed by cancer cells. Indeed, several *in situ* hybridization and immunohistochemical analyses showed that TNC is expressed by cancer cells in different types of tumors such as breast cancer, oral squamous cell carcinoma and melanoma (Oskarsson et al., 2011; Yoshida et al., 1997; Hindermann et al., 1999; Shao et al., 2015). Importantly, by analyzing various breast cancer cases expressing either stromal TNC or cancer cell-derived TNC or both, Ishihara and colleagues (1995) showed that both sources of TNC impact patient outcome (Ishihara et al., 1995). Indeed, the group of patients displaying both stromal and cancer cell-derived TNC exhibited increased frequency of lymph node metastasis and correlated with worsened survival. Another study used short hairpin RNAs (shRNAs) against TNC to downregulate TNC expression in breast cancer cells before injecting them either into the mammary fat pad or directly to the lungs via the tail vein. Thus, the authors observed that TNC deficiency in tumor cells impaired lung metastasis development (Oskarsson et al., 2011).

3.3.3 Pathological roles of TNC in cancer

3.3.3.1 Impact on angiogenesis

As previously discussed (section 2.1.4), tumor associated angiogenesis is a crucial event promoting tumor progression since it supplies nutrients and oxygen for cancer cell proliferation and survival. The role of TNC in tumor associated angiogenesis was addressed by several studies. For instance, Saupe and colleagues (2013) used an immune-competent transgenic mouse model of endocrine pancreatic cancer where the mice were engineered to express different TNC levels. The authors thereby showed that TNC expression promotes the angiogenic switch (Saupe et al., 2013). As a potential mechanism that could explain this impact, the authors showed that TNC induces Wnt signaling by downregulating its inhibitor Dickkopf-1 (DKK1), thus leading to pro-angiogenesis signaling. Indeed, Wnt signaling pathway is known for being a crucial pathway driving angiogenesis (Dejana, 2010). In this study, TNC expression was correlated with highly aberrant vessel phenotype (irregularly shaped, wider, discontinued and leaky) (Saupe et al., 2013). Another study on human gliomas

reported that TNC expression correlates with the degree of tumor neovascularization (Herold-Mende et al., 2002). Several mechanisms other than the Wnt pathway have been suggested to mediate TNC-dependent tumor angiogenesis presumably in a tumor and context dependent manner. By injecting human melanoma cells into mice WT or KO for TNC, Tanaka and colleagues (2004) observed more abundant blood vessels in WT mice that correlated with increased VEGFA levels in the blood circulation, suggesting a regulation of VEGFA by TNC (Tanaka et al., 2004).

3.3.3.2 Impact on cell proliferation

TNC has a context- and cell type-dependent impact on proliferation. Several studies showed that TNC stimulates the proliferation of many different tumor cell lines such as breast cancer, pancreatic cancer and laryngeal cancer cell lines (Yoshida et al., 2015; Yoshida et al., 1999; Paron et al., 2011, Huang et al., 2001). Moreover, it was reported that TNC staining in cancer tissues often co-localized with cells positively stained for the proliferating cell marker Ki-67 (Orend and Chiquet-Ehrismann, 2006). One of the possible underlying mechanisms that have been highlighted is the ability of TNC to compete syndecan-4-binding to fibronectin. This binding impairs thereby the co-receptor function of syndecan-4 in integrin signaling and notably the syndecan-4/integrin $\alpha 5\beta 1$ -mediated cell proliferation (Orend and Chiquet-Ehrismann, 2006; Yoshida et al., 2015; Huang et al., 2001). In normal anchorage-dependent fibroblasts TNC has been reported to cause cell cycle arrest and subsequent cell proliferation (Orend et al., 2003).

3.3.3.3 Impact on cell migration and invasion

TNC was reported to be strongly implicated in mediating the migratory and invasive behavior of cancer cells. Indeed, it was shown by performing *in vitro* assays such as wound healing and chemotactic transwell migration on several cancer cell types that the presence of TNC (as soluble factor or as coating molecule) stimulates the migration and invasion of cancer cells. This was shown for instance in human glioma cells where TNC was reported to stimulate fibronectin-mediated cell migration (Deryugina and Bourdon, 1996) and to enhance glioblastoma invasion (Hirata et al., 2009). One of the underlying mechanisms proposed in the glioma context is that TNC triggers MMP12 that can degrade ECM components stimulating thus cancer cell

migration and invasion (Sarkar et al., 2006). In pancreatic cancer, the enhanced migration and invasion behavior of cancer cells in presence of TNC was linked to the JNK/c-Jun signaling (Cai et al., 2017). In breast cancer, the down-regulation of TNC impaired breast cancer cell migration and invasion (Wawrzyniak et al., 2020). Several mechanisms have been proposed to explain the impact of TNC on these properties. Among them one can cite the ability of TNC to increase MMPs that have been reported to play an important role in cell migration and invasion (Nabeshima et al., 2002). Indeed, co-stimulation of human breast cancer cells with TGF- β and TNC enhanced MMP-9 expression and increased cancer cell invasion (Ilunga et al., 2004). A further study showed that TNC stimulates cancer cell migration and invasion involving MMP-13 (Hancox et al., 2009). Another mechanism is the induction of the epithelial-to-mesenchymal transition process. Indeed, TNC was shown to induce the epithelial-to-mesenchymal transition (EMT) which can confer migratory and invasive properties to cancer cells (more detail in section 3.3.3.4) (Orend and Chiquet-Ehrismann, 2006).

3.3.3.4 Impact on epithelial-to-mesenchymal transition

The EMT is a process during which epithelial cells undergo several changes in their shape and properties and gain a mesenchymal phenotype. EMT is a process having crucial roles during embryogenesis and development, and was also reported to play important roles in tumor progression through several mechanisms such as providing migratory, invasive and stemness properties to cancer cells (Thiery et al., 2009). TNC was found to be co-expressed with EMT markers such as vimentin and was described to induce EMT in many cancers involving several distinct pathways. For instance, TNC induced EMT-like changes in MCF-7 breast cancer cells involving binding to $\alpha v\beta 6$ and $\alpha v\beta 1$ integrins (Katoh et al., 2013). In colorectal cancer, TNC expression was associated with an EMT signature and was reported to impact colorectal cancer patient prognosis (Takahashi et al., 2013; Yang et al., 2018). In pancreatic cancer, TNC was shown to trigger EMT through JNK/c-Jun signaling (Cai et al., 2017). Another important inducer of EMT is TGF β signaling and our previous work showed that TNC promotes breast cancer lung metastasis by impacting blood vessel invasions through TGF β -induced EMT (see appendix I, (Sun et al., 2019)).

3.3.3.5 Impact on survival and stemness properties

As described before (section 2.1.2), cancer stem cells (CSC) are a small population of cancer cells within a tumor that show self-renewal and differentiation properties. These cells are crucial in tumor progression and metastasis development, and most likely cause cancer relapse. TNC was reported to be involved in the promotion of cancer stemness properties in several cancers. This is for instance the case in esophageal squamous cell carcinoma where TNC enhanced cancer stemness properties through the Akt/HIF1 α axis (Yang et al., 2019). TNC triggers also signaling known to be involved in stemness such as Wnt and Notch pathways in breast cancer, and Hedgehog in colorectal cancer (Takebe et al., 2011; Takebe et al., 2015; Yang et al., 2020). One of the CSC properties is an enhanced survival and TNC was indeed shown to promote cancer cell survival by inducing resistance to apoptosis in pancreatic cancer cells through the activation of Erk/NF- κ B pathway (Shi et al., 2015). Moreover, the EMT process have been well described as providing stem cell properties to cancer cells and as described above (section 3.3.3.4) TNC is a known inducer of EMT (Polyak and Weinberg, 2009; Orend and Chiquet-Ehrismann, 2006). Another CSC property is their resistance to anti-cancer treatment such as chemo- and radiotherapy. In this context, TNC was for instance shown to inhibit chemosensitivity of glioma cells to paclitaxel (a chemotherapy drug used in clinic) through the activation of the PI3K/AKT signaling pathway (Zhang et al., 2021).

3.3.3.6 Impact on immunosurveillance

The impact of TNC on immunity is addressed in section 4.5 of this manuscript.

4. Cancer immunity

4.1 Cancer immunosurveillance

The first assumption of cancer immunity concept emerged more than a century ago, when Paul Ehrlich postulated that the proliferation of aberrant cells can be restrained for not becoming unusually common by what he called the “organism’s positive mechanisms” (Ehrlich, 1909). It took several decades before two scientists, Burnet and Thomas revisited Ehrlich’s postulate and formulated the immune surveillance

theory (Burnet, 1970). Thomas hypothesized the existence of a mechanism protecting against neoplastic diseases in complex long-lived organisms. Burnet postulated that tumor cells display neo-antigens on their surface that can be recognized and killed by the immune system (Dunn et al., 2004a). Over the following decades these postulates, several studies enabled the validation of the immune surveillance concept (Dunn et al., 2002).

Nowadays, the genetic instability and mutations occurring in malignant cells are well established as being part of the hallmarks of cancer (Hanahan and Weinberg, 2011). Indeed, oncogenesis is accompanied by the accumulation of mutations that induce neo-expression of antigens at the surface of cancer cells, rendering them recognizable by the immune system. In 2013, Chen and Mellman described a series of sequential events by which the anti-cancer immune responses mediate an effective killing of cancer cells, named the cancer-immunity cycle (Chen and Mellman, 2013) (Figure 6). The first step of the cycle is the release of neo-antigens expressed on cancer cells as a result of genomic instability and mutations. After their release, these antigens are captured by professional antigen presenting cells (APCs), mainly dendritic cells, which then migrate to lymph nodes to present the antigens to CD8 T cells. This leads to the priming and the activation of the effector T cells that then migrate through the blood vessels to reach the tumor site and infiltrate the tumor stroma where they recognize the tumor cells. The recognition of tumor cells by effector T cells is mediated through the interaction of the T cell receptor (TCR) with the tumor antigens. This leads to T cell-mediated cytotoxic responses through the secretion of cytokines and enzymes (such as perforin and granzyme B) that kill tumor cells. Also, the destruction of cancer cells leads to the release of new tumor antigens perpetuating the cancer-immunity cycle (Chen and Mellman, 2013; Pio et al., 2019).

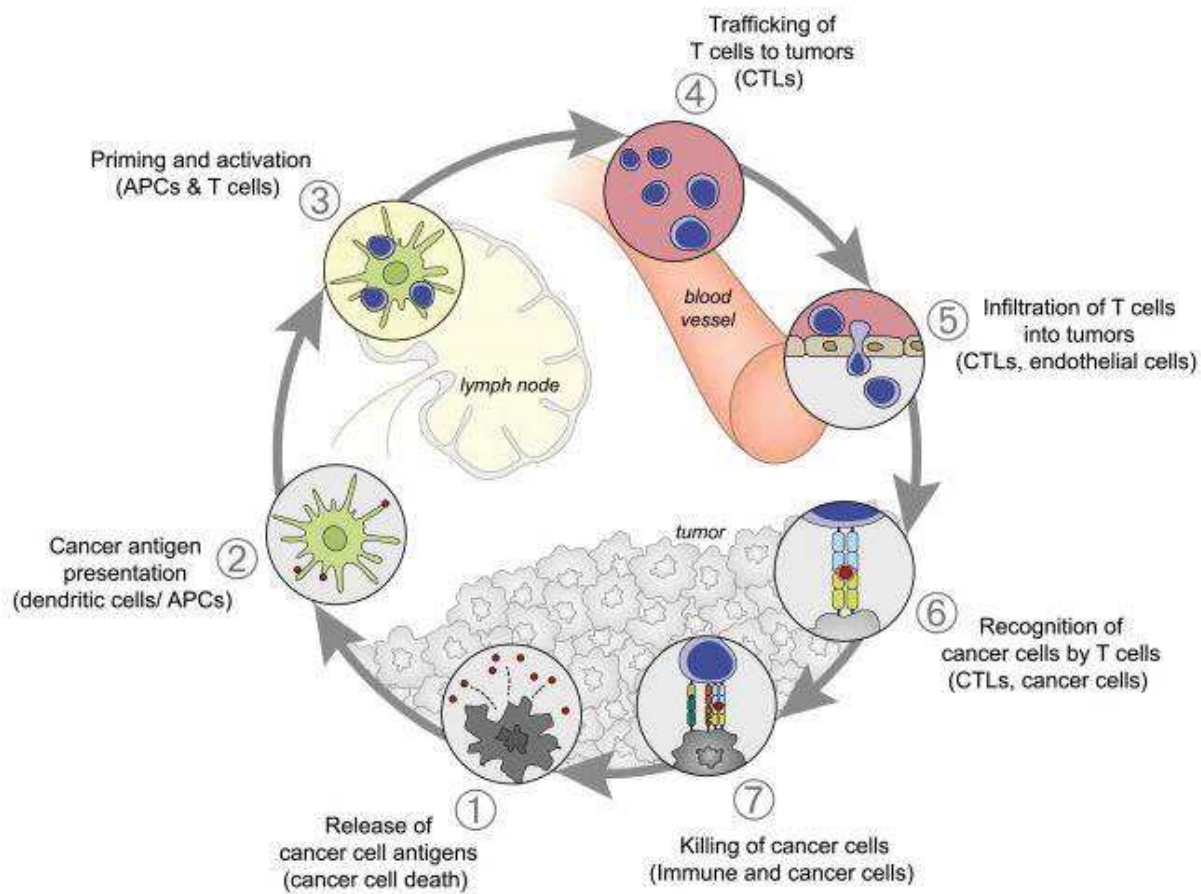


Figure 6. The Cancer-Immunity cycle (from Chen and Mellman, 2013). The cancer-immunity cycle is divided into seven major steps described above. Briefly, tumor cells release tumor associated antigens that are captured by APCs and then presented to T cells for priming. The activated T cells migrate through the blood vessel towards the tumor nest, infiltrate the tumor and kill the tumor cells. Abbreviations: APC, antigen presenting cells; CTLs, cytotoxic T lymphocytes.

4.2 Cancer immunoediting

A complex relationship exists between the immune system and cancer. The cancer immune surveillance process described above depicts only one part of this relationship as it is obvious that tumor cells evade immune surveillance. In 2002 Dunn and Schreiber proposed a more accurate concept to describe the roles of the immune system in cancer that they named “cancer immunoediting” (Dunn et al., 2004b). This concept is based on the postulate that the immune system is able not only to eliminate tumors but also to modulate the immunogenicity of cancer cells (Dunn et al., 2004b). This theory was supported by several studies such as the one

from Shankaran and colleagues (2001) showing that tumors developing in immunocompetent hosts are less immunogenic than those developing in immunodeficient hosts (Shankaran et al., 2001). This observation suggests that the immune system can promote the development of tumor cells able to escape from the immune system. The cancer immunoediting process comprises three distinct phases: elimination, equilibrium, and escape (Dunn et al., 2004a; Dunn et al., 2004b) (Figure 7). The elimination phase corresponds to the classical concept of cancer immune surveillance where the immune system successfully eradicates the proliferating cancer cells involving both innate and adaptive immune responses. However, some tumor cells survive the elimination phase and enter in the equilibrium phase. During this phase tumor cells and adaptive immunity coexist in a dynamic equilibrium where lymphocytes and some cytokines such as IFNy and IL-12 exert a selection pressure on cancer cells. The selection pressure is able to restrain but not to fully eradicate all tumor cells, thus leading to cancer cells carrying mutations providing them increased resistance to the immune attack. Thus, the malignant cells evolve to a less immunogenic phenotype. In the last phase, namely the escape phase, tumor cells having survived eradication by the immune system expand in an uncontrolled manner. Several mechanisms have been described for being involved in the tumor escape. One can for instance cite the neo expression of immune modulatory molecules on the tumor cell surface such as PD-L1 that once bound to its receptor PD-1 expressed on effector T cells negatively regulates their activity (Labani-Motlagh et al., 2020). Tumor cells are also able to establish a pro-tumorigenic microenvironment by secreting immune suppressive molecules such as IL-10 and TGF β and to increase their resistance to apoptosis (Spenle et al., 2020).

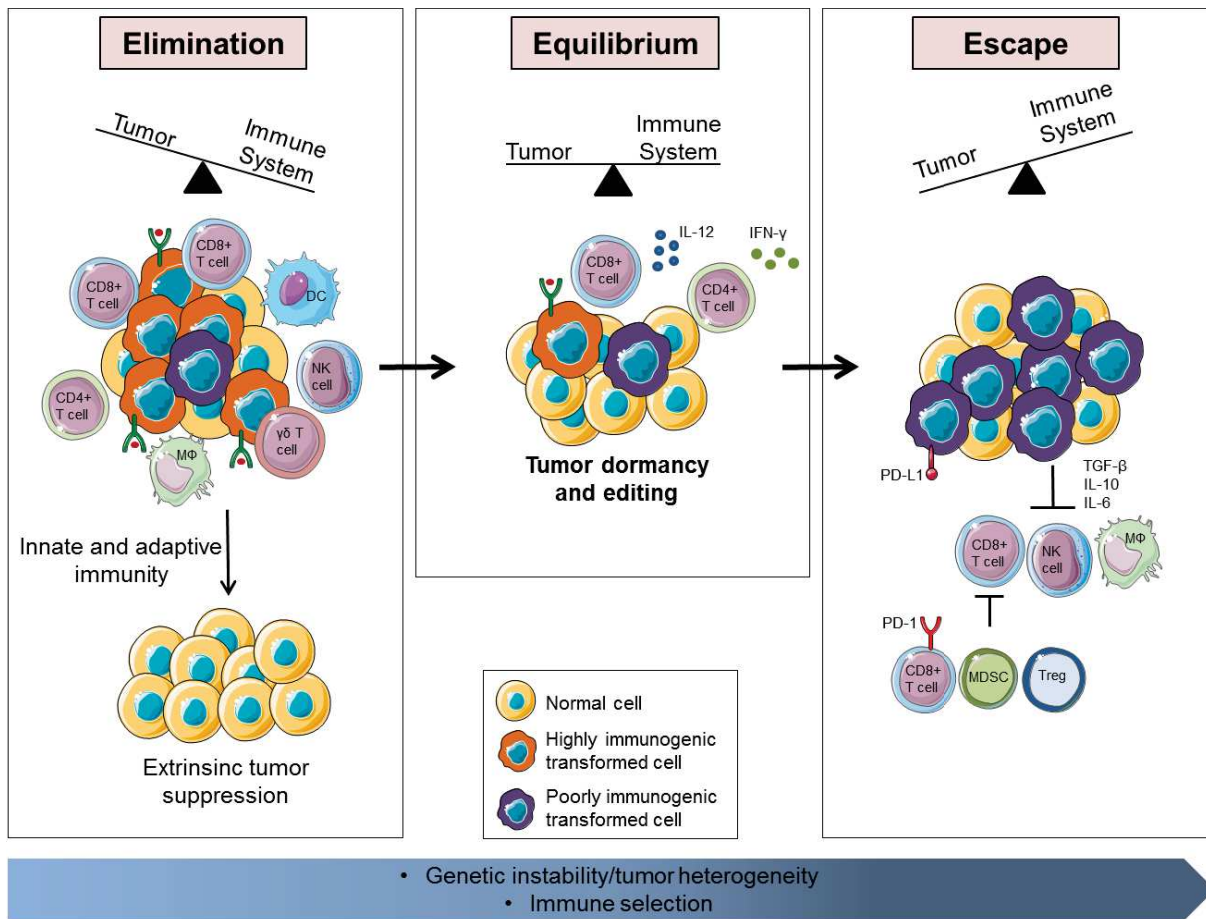


Figure 7. The cancer immunoediting concept (inspired by Schreiber, Old, and Smyth, 2011). At early stages of tumorigenesis, malignant cells express distinct tumor-specific markers that generate “danger” signals recognized by the immune system leading to the initiation of the cancer immunoediting process. During the first phase of elimination the innate and adaptive immune system eradicate malignant cells. However, if this process is not successful the tumor cells may enter the equilibrium phase where malignant cells can undergo tumor dormancy and editing. T-cells, IL-12 and IFN-γ are required to maintain this state of functional dormancy. Only adaptive immunity intervenes during the equilibrium phase. Constant immune selection pressure during this phase leads to the emergence of tumor cell variants that are no longer recognized by the adaptive immunity (loss of tumor-associated antigens or defective antigen processing or presentation). These tumor cells may then enter the escape phase where the immune system can no longer block their outgrowth, thereby leading to tumor progression. Abbreviations: MΦ, macrophage; MDSC, Myeloid-derived suppressor cell.

4.3 Impact of the TME on key immune effector and regulatory cells

4.3.1 Impact of the TME on key players of innate immunity

The three main immune effector cells from innate immunity found in the TME are TAMs, DCs and natural killer (NK) cells.

TAMs are described to have a dual and opposite context-dependent role. Indeed, they are associated with both anti-tumor and pro-tumor responses and are classified into two major distinct subgroups according to the responses they induce, namely the M1 phenotype and the M2 phenotype (Gonzalez et al., 2018). Remarkably, TAMs display the ability to adapt and switch between the M1 and M2 phenotype, depending on the signals received from the TME (Biswas and Mantovani, 2010). M1 macrophages are referred as being pro-inflammatory and during the first steps of carcinogenesis anti-tumor macrophages usually display an M1-like polarization. These macrophages are able to secrete pro-inflammatory cytokines such as IL-1, IL-12, IL-23 and TNF- α (Noy and Pollard, 2014; Mantovani et al., 2017). They are also able to produce cytotoxic mediators such as oxidative and nitrogen radicals, and to trigger Type 1 helper T cell (Th1) responses. Unlike the M1 macrophages, M2 macrophages are anti-inflammatory and are described to have an immune suppressive role. As the tumor progresses, the signals within the TME trigger the switch from an M1 to an M2-like polarization. Several factors are involved in the switch from M1 to M2, such as the production of IL-4 and IL-13 that promote Type 2 helper T cell (Th2) responses (Noy and Pollard, 2014; Mantovani et al., 2017; Biswas and Mantovani, 2010). These M2 macrophages were shown to have several roles in promoting tumor progression such as by stimulating angiogenesis, promoting cancer cell proliferation, migration and invasion, and inducing immune suppression of anti-tumor effector immune cells. The impact of M2 macrophages is mediated through different mechanisms. One can for instance cite the secretion of immune suppressive cytokines such as IL-10 and TGF β leading to the impairment of T cell activity and DC maturation. M2 macrophages are also able to secrete growth factors such as EGF and VEGF that promote cancer cell proliferation and angiogenesis, respectively. Several studies showed that high density of TAMs correlates with poor prognosis and reduced overall survival (Gonzalez et al., 2018; Zhang et al., 2012).

DCs are a heterogeneous family of immune cells that are known for being the most potent APCs of the immune system (Gonzalez et al., 2018). Indeed, they play a crucial role ensuring the link between the innate and the adaptive immunity by uptaking, processing and presenting antigens, including tumor antigens, to T cells (Wylie et al., 2019). Although DCs are involved in generating cancer immune surveillance, the TME can impact their anti-tumor functions. Indeed, these cells can be subjected to suppressive mechanisms leading to the impairment of their antigen presenting function or impacting their activation/maturation (Wylie et al., 2019; Ma et al., 2013). The functions of DCs can be negatively regulated by several factors present in the TME such as IL-6, IL-10, VEGF and TGF- β (Ma et al., 2013; Fu and Jiang, 2018). For instance, IL-6 was shown to impair the maturation and migration of DCs and can induce tolerogenic phenotypes of DCs that have immune suppressive functions such as the activation of T_{reg} cells. IL-10 is produced by several cell types in the TME such as cancer cells and TAMs, and was shown to impair DC maturation and ability in antigen presentation and priming of T cells. VEGF and TGF- β were reported to impair the differentiation and maturation of DCs, suppressing thereby their capacity to initiate anti-tumor immune responses. Several studies reported an altered maturation of DCs and a decreased antigen presenting function of DCs in breast cancer patients (Gabrilovich et al., 1997; Satthaporn et al., 2004).

NK cells are also key players of the innate immunity and are characterized by their ability to directly eliminate cancer cells without any previous sensitization. NK cell function is mediated by receptors expressed on their surface that are able to recognize molecules expressed on “abnormal cells” (stressed, infected or malignant cells) activating thereby NK cell killing functions (Vivier et al., 2008). Among those activating receptors one can cite the Natural killer group 2 member D (NKG2D) receptor that will be described in more detail in the section 5. of this manuscript. In the TME, several factors are positive regulators of NK cell functions. This is for instance the case of IL-2, IL-12, IL-15, IL-18 and IFN- γ produced mainly by Th1 cells and DCs and that were reported to activate and potentiate the cytotoxic activity of NK cells (Konjević et al., 2019). However, the TME can also have immunosuppressive effect on these cells decreasing thereby their efficacy. Indeed, several factors produced by different TME components including tumor cells, TAMs and Th2 cells can prevent NK cell activation through IL-6, IL-10 and TGF- β (Konjević et al., 2019;

Stojanovic et al., 2013). These factors can impair NK cell effector function by downmodulating NK cell activating receptors either directly or indirectly by antagonizing the effect of stimulatory cytokines. Several studies showed that in solid tumors such as breast, gastric, lung and colorectal cancer, NK cell infiltration is associated with improved overall survival (Nersesian et al., 2021; Ascierto et al., 2013). Also in breast cancer, poor infiltration of NK cells was suggested to be predictive for chemotherapy treatment failure (Garcia-Chagollan et al., 2018).

4.3.2 Impact on key players from adaptive immunity

T lymphocytes are key effectors of adaptive immunity and play a crucial role during cancer progression. T cells are composed of many subtypes that can have either inflammatory or ant-inflammatory effects, depending on the immunological context and the signals from the TME. The two major T lymphocyte subtypes are CD8 cytotoxic T lymphocytes (CTLs) and CD4 T helper cells.

Naïve CD8 T cells are activated into CTLs upon APCs-mediated tumor antigen presentation. CTLs are known to be the most potent effector cells of the anti-tumor immunity and high levels of CTL infiltration was shown to be associated with good prognosis and higher response to chemotherapy in breast cancer patients (Ono et al., 2011). CTL infiltration into the TME and the tumor nest is dependent of chemokines abundant in the TME. For instance, tumors displaying high amounts of CCL5 (released by tumor cells) and of CXCL9 (released by APCs) were shown to be highly infiltrated by CTLs and to have a better response to checkpoint blockade inhibition therapy (Dangaj et al., 2019). The killing action of CTLs is engaged upon activation of the TCR and is mediated through the secretion of perforin, granzyme B and other cytokines triggering cancer cell apoptosis (Labani-Motlagh et al., 2020). However, CTLs have to overcome several challenges for being able to infiltrate the tumor nest and exert their antitumor effector function. For instance, cancer cells are able to evade CTL-mediated killing by several mechanisms including the downregulation of MHC protein expression on their surface or the upregulation of anti-apoptotic molecules. CTLs killing activity can also be downmodulated by the upregulation of inhibitory checkpoint receptor present on their surface such as CTLA-4 and PD1 (Sharma and Allison, 2015). Moreover, the ECM is able to act as a

physical barrier and to modulate the infiltration of CTLs into the tumor nest, but the underlying mechanisms were not fully understood (Cohen and Blasberg, 2017).

Naïve CD4⁺ T helper cells can differentiate into different cell subsets upon APCs-mediated tumor antigen presentation. The main subtypes of Th cells include Th1, Th2, Th17 and T_{regs}. Their differentiation is determined by the cytokines present in the priming environment (Figure 8).

Briefly, Th1 responses are mediated through IL-2, IL-12 and IFN γ and promote CTL activation. Moreover, IFN γ secretion is also able to stimulate the upregulation of MHC and to inhibit tumor-associated angiogenesis, thereby impairing tumor growth (Labani-Motlagh et al., 2020). On the opposite, Th2-mediated responses can promote tumor growth by secreting immunosuppressive cytokines such as IL-13 and TGF β . Th17 cells have a controversial role in tumor immunity and were found to display a dual role that is context- and cancer type-dependent. For instance, high Th17 cell infiltration into the tumor was correlated with poor prognosis in colon and pancreatic cancer patients while in ovarian cancer patients it was associated with better survival (Bailey et al., 2014). This could be explained by the fact that Th17-derived cytokines can stimulate Th1 responses promoting thereby antitumor immunity, but can also secrete pro-inflammatory cytokines and promote tumor-associated angiogenesis. Moreover, Th17 cells are able to convert into T_{reg} cells that have immune suppressive properties. Thus, Th17 cells can have either regulatory or inflammatory properties depending on the stimuli they encounter. Here again the TME plays a crucial role since the cytokines present in the TME determine the effector or the regulatory functions of Th17 cells. For instance, the presence of cytokines such as IL-23, IL-6 and IL-12 will favor the effector function of Th17 cells whereas TGF β and IL-2 cytokines will favor the regulatory function of Th17 cells (Bailey et al., 2014). Finally, T_{reg} were shown to have multiple functions in the immune tolerance preventing autoimmunity. Indeed, T_{reg} cells are for instance able to inhibit the activity of immune effector cells and to favor the polarization of M1 macrophages into M2 macrophages. In the tumor context, high T_{reg} cell infiltration was associated with poor overall survival of breast cancer patients with invasive tumors (Bates et al., 2006).

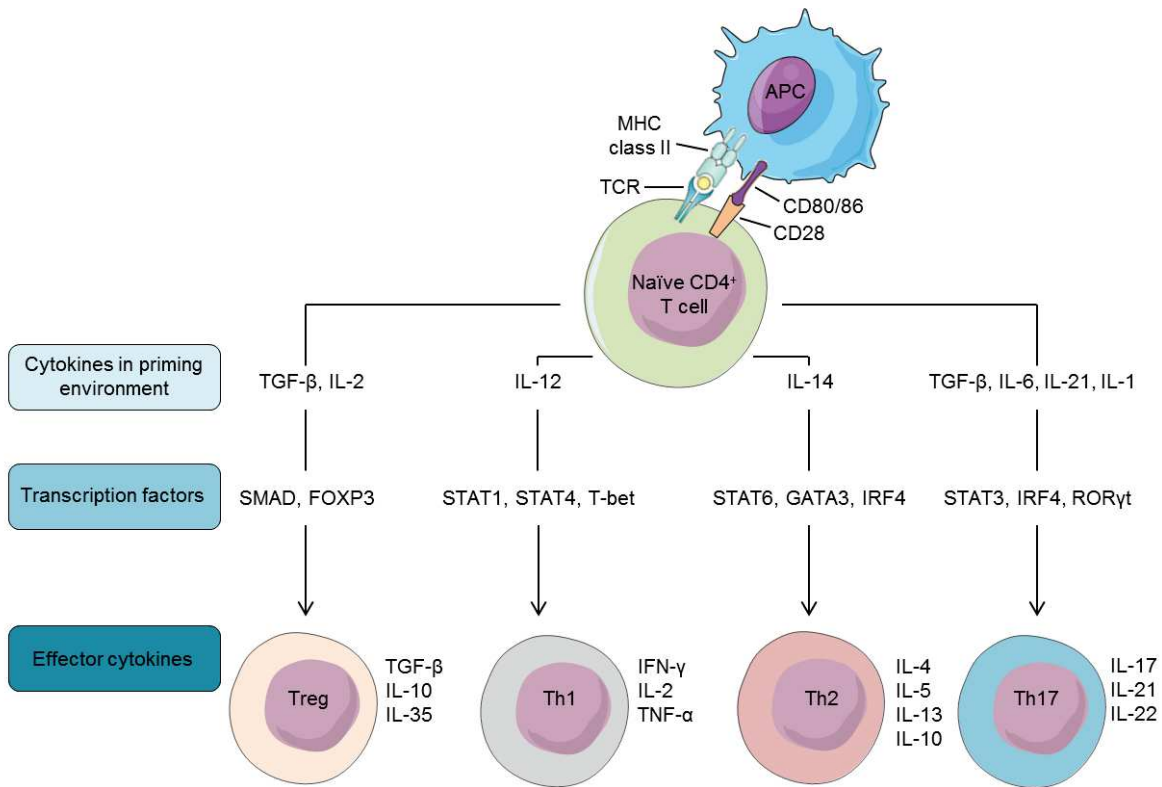


Figure 8. Differentiation of naïve CD4+ T cell in helper T cell subsets is determined by cytokines. The cytokines present in the priming environment determine the fate of naïve CD4+ T cell by triggering the activation of transcription factors within the cell. Once programmed, these cells secret the effector cytokines.

4.4 Cancer immune contexture

Over the last two decades, increasing evidences showed the impact of cancer patient's immune system on clinical outcome and highlighted the crucial importance to identify TME composition for predicting responses to cancer treatment. In situ analyses have allowed to study the TME in more detail in cancer tissue and notably identified the composition, localization, density and the functional state of different immune cell populations in the TME that can be very different from patient to patient. Fridman and colleagues (2012) termed this information the "immune contexture" (Fridman et al., 2012). The importance of immune cell composition and density in the TME on cancer progression and clinical outcome was already discussed in different sections of this manuscript. In addition, the localization of immune cells also plays a crucial role. Indeed, immune cells are not randomly distributed but are located in

specific areas and can be found either in the core of the tumor, in the invasive front, in the stroma surrounding tumor bed or in the adjacent tertiary lymphoid structures (Fridman et al., 2012). Importantly, in many cancers the levels of lymphocyte infiltration in the tumor nest was shown to correlate with clinical outcome. Indeed, high infiltration of CD8 cytotoxic T cells and memory T cells was associated with good clinical outcome in many cancers such as breast, ovarian, colorectal and lung cancers. Also, high levels of Th1 in the core and at the invasive front of the tumor were identified as a good prognostic factor with longer overall survival. The localization of other T cell types has not such a clear-cut impact on clinical outcome (Bruni et al., 2020). For instance, the infiltration of T_{reg} cells has been suggested to correlate with reduced survival in many cancers such as breast and ovarian cancer whereas no impact was found on other cancer types such as brain cancer (Fridman et al., 2012; Curiel et al., 2004). Concerning NK cells, several studies showed that NK cell infiltration is associated with improved overall survival in many solid cancers such as breast cancer (Nersesian et al., 2021). The immune contexture is not only useful to predict cancer clinical outcome but also to predict anti-cancer treatment response. Indeed, it was shown that a strong immune cell component is associated with good response to chemotherapy in breast cancer and that a high lymphocyte infiltration is correlated with a higher response rate to neoadjuvant therapy (Fridman et al., 2012).

4.5 Immunomodulatory functions of TNC

TNC was described to have several context-dependent immune modulatory functions and to regulate both innate and adaptive immunity. For instance, many studies showed that TNC expression is highly induced under inflammation and that TNC itself enhances inflammatory responses where TNC can act as a danger associated molecular pattern (DAMP) molecule (Marzeda and Midwood, 2018; Midwood et al., 2009). In this context, TNC was shown to activate toll-like receptor-4 (TLR4) signaling stimulating thereby the secretion of pro-inflammatory cytokines such as IL-6, IL-8 and TNF- α by fibroblasts and macrophages (Marzeda and Midwood, 2018; Midwood et al., 2009). Also, it was shown that the KO of TNC in mice results in a rapid resolution of the acute inflammation observed in rheumatoid arthritis preventing the chronic inflammation stage (Midwood et al., 2009). In addition to TLR4, TNC was

shown to drive inflammatory responses through its interaction with integrins and notably the integrin $\alpha 9\beta 1$. For instance in arthritis, TNC was reported to bind $\alpha 9\beta 1$ thereby inducing the expression of pro-inflammatory chemokines such as CCL2, CCL4 and CXCL5 (Kanayama et al., 2009). TNC is also involved in the pathogenesis of bronchial asthma by impacting lymphocyte trafficking and T cell activation. Indeed, Nakahara and colleagues (2006) reported that mice lacking TNC expression (TNCKO) have a reduced Th2 cell response known to play a crucial role in asthma pathogenesis through the secretion of cytokines such as IL-5 and IL-4, and thereby are protected from experimentally induced asthma (Nakahara et al., 2006; Busse and Lemanske, 2001). Several other studies showed that TNC is involved in autoimmune diseases. For instance, TNC aggravates autoimmune myocarditis through the activation of dendritic cells generating autoreactive T cells, and TNCKO mice display lower Th17 cell infiltration to the heart compared to WT mice (Machino-Ohtsuka et al., 2014). The underlying mechanism proposed in this context is that TNC is able to stimulate DCs triggering the production of IL-6 that is a key cytokine mediating the differentiation of naïve CD4 T cells into Th17 T cells.

In the tumor context too, TNC expression was shown to play a crucial role in the modulation of innate and adaptive immunity. It was for example reported that TNC impairs the infiltration of monocytes and macrophages into the tumor nest in a mouse model with spontaneous SV40 T antigen induced mammary cancer (Talts et al., 1999). In lung cancer, TNC impacts tumor-infiltrating lymphocytes by inhibiting their proliferation and the secretion of IFNy (Parekh et al., 2005). A similar observation was done in a prostate cancer model where TNC impairs the activation and proliferation of T cells, and the production of cytokines (Jachetti et al., 2015). More recently, Deligne and colleagues (2020) showed by using a novel syngeneic breast cancer grafting model that tumor cell-derived TNC modulates the TAM phenotype involving TLR4 activation (Deligne et al., 2020). High tumor-derived TNC was shown to trigger the polarization of TAMs toward an immune-suppressive M2 phenotype promoting thereby tumor growth and metastasis. In this same study the authors showed that macrophages associated with high tumor-derived TNC are less efficient at driving T-cell proliferation but more efficient in the generation of Th17 T cells compared to TNC low conditions. In a 4NQO-induced oral squamous cell carcinoma (OSCC) model with WT or TNCKO levels TNC orchestrates an immune suppressive

TME (Spenle et al., 2020). In this study the authors showed that TNC induces expression of CCL21 in lymphatic endothelial cells and increases abundance of fibroblast reticular cells (FRC) another source of CCL21 thus increasing CCL21. Moreover, TNC binds CCL21 and generate an adhesive substratum for DCs that are immobilized in the tumor stroma. This caused less infiltration of DCs into the local lymph nodes and activation of cytotoxic T lymphocytes altogether reducing tumor cell killing. TNC also increases the abundance of Treg. This phenotype was largely dependent on CCR7 as CCR7 inhibition restored anti-tumor immunity.

Altogether, these studies support the crucial role played by TNC in modulating both innate and adaptive immunity system in different contexts.

5. Natural killer group 2 member D (NKG2D)/ NKG2D ligand axis

Responses by the immune system comprise receptors expressed on immune effector cells that can detect molecules expressed by “abnormal/aberrant” cells such as virus-infected, stressed, or transformed cells. This detection leads to the activation of complex signaling pathways within the immune cells enabling the immune cells to kill the “abnormal” cells. NKG2D is a major regulator of immune responsiveness where the NKG2D/NKG2D ligand (NKG2DL) axis is the target of several studies showing its role and importance in anti-tumor immunity.

5.1 NKG2D receptor and its ligands in mouse and in human

5.1.1 NKG2D receptor

5.1.1.1 NKG2D receptor complex

NKG2D is encoded by the Killer cell lectin-like receptor subfamily K member 1 gene (*Klrk1*) localized on chromosome 12 in human and chromosome 6 in mouse. The NKG2D receptor is a dimeric, type II lectin-like transmembrane activating receptor that is mostly expressed on cytotoxic immune cells (Wensveen et al., 2018). The intracellular part of this receptor is very short and does not have any known signaling properties. In human cytotoxic immune cells, NKG2D signaling is mediated through the non-covalent association of each NKG2D molecule with a cytoplasmic DAP10 (DNAX-activating protein of 10 kDa) adaptor protein, forming a hexameric NKG2D-

DAP10 transmembraneous receptor complex (Figure 9). In murine cytotoxic cells NKG2D associates with DAP12 in addition to the DAP10 (Eagle and Trowsdale, 2007). In mouse cells, two NKG2D isoforms were identified as the result of alternative splicing of the *Klrk1* transcript: a short form named NKG2D-S, and a long form named NKG2D-L differing by 13 amino acids at their N-terminus. While the NKG2D-S isoform can associate with both DAP10 and DAP12, the NKG2D-L isoform can only form a complex with DAP10. The selection of adaptor molecule association is dependent on the cell type carrying NKG2D as well as on the NKG2D isoform. The two adaptor molecules DAP10 and DAP12 are then able to initiate distinct signaling pathways (Upshaw and Leibson, 2006).

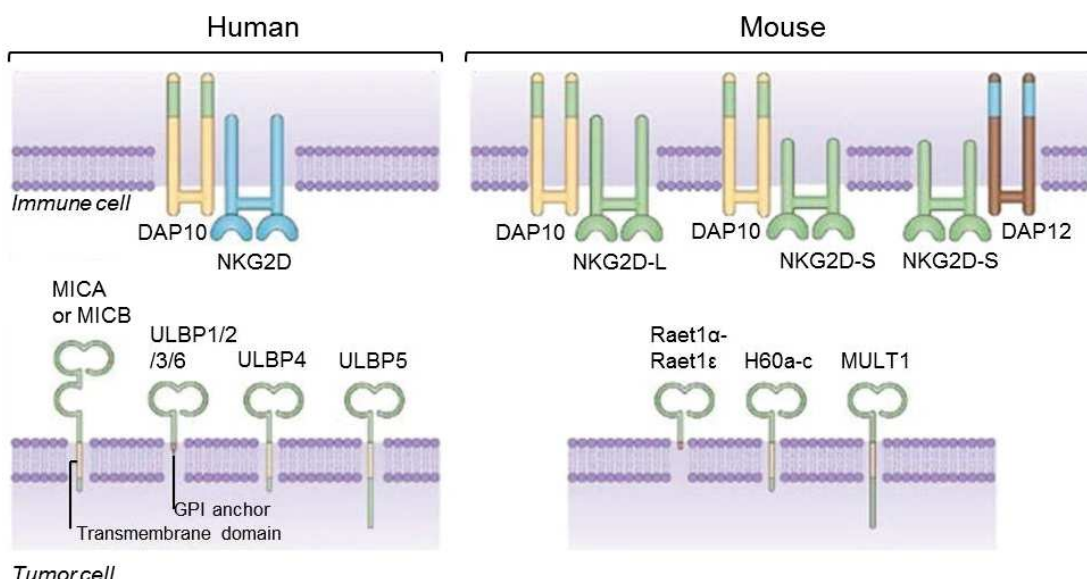


Figure 9. NKG2D receptor complex and its ligands in human and mouse (adapted from Eagle et al., 2007). In human, NKG2D signaling activity is mediated through the association with the adaptor protein DAP10. NKG2D and DAP10 assemble as a hexameric complex in the cell membrane. In mouse, cell-type specific alternative splicing of NKG2D results in two isoforms, a long form (NKG2D-L) and a short form (NKG2D-S). NKG2D-L associates exclusively with DAP10 whereas NKG2D-S can associate with DAP10 or DAP12. In human, the NKG2D ligands (NKG2DL) are classified in two families, the MHC class I chain-related protein A (MICA) and MICB, and the UL16-binding proteins (ULBPs) composed of 6 members (ULBP1-6). In mice, NKG2DL are classified in 3 families, the Retinoic acid early transcript 1 (Raet1) with 5 members, the histocompatibility antigen 60 (H60) family comprising three members and the murine UL16-binding protein-like transcript 1 (MULT1). All ligands have MHC-class-I-related $\alpha 1\alpha 2$ domains and MICA and MICB have an additional $\alpha 3$ domain.

5.1.1.2 DAP10-dependent signaling pathways

The cytoplasmic domain of DAP10 contains a costimulatory tyrosine-based signaling motif YXXM (Thyrosine-X-X-Methionine) that is phosphorylated by Src family kinase upon NKG2D stimulation (Figure 10a). The phosphorylated hexameric NKG2D-DAP10 complex can then potentially bind several adaptor proteins and trigger distinct downstream cascades (Kwon and Kim, 2012). On one side, this phosphorylation recruits the p85 subunit of PI3K that triggers the phosphorylation of several downstream molecules finally causing ERK phosphorylation, leading to cytokine release and cytotoxicity (Wensveen et al., 2018; Upshaw and Leibson, 2006; Kwon and Kim, 2012). The phosphorylation of PI3K can also activate Akt phosphorylation, leading to cell survival-related pathways, and also stimulate calcium release that is crucial for the exocytosis of lytic granules and cytokine production (Kwon and Kim, 2012). On the other hand, DAP10 phosphorylation can lead to the recruitment of the growth factor receptor-bound protein 2 (Grb2) which is a small adaptor protein that then binds Vav1. This Grb2/Vav1 complex triggers not only the activation of PI3K but also the phosphorylation of Vav1, phospholipase C Gamma 2 (PLC- γ 2) and Src homology 2 domain-containing leukocyte phosphoprotein of 76 kDa (SLP-76). This pathway finally triggers cytotoxicity and calcium release.

5.1.1.3 DAP12-dependent signaling pathways

DAP12 signals through an immune receptor tyrosine-based activation motif (ITAM) that is phosphorylated by Src kinases upon NKG2D stimulation (Wensveen et al., 2018) (Figure 10b). This phosphorylation leads to the recruitment and the binding of Syk and zeta-chain-associated protein 70 kDa (ZAP70) tyrosine kinases. This complex then triggers PLC- γ 2 phosphorylation resulting in cytokine production and cytotoxicity (Kwon and Kim, 2012).

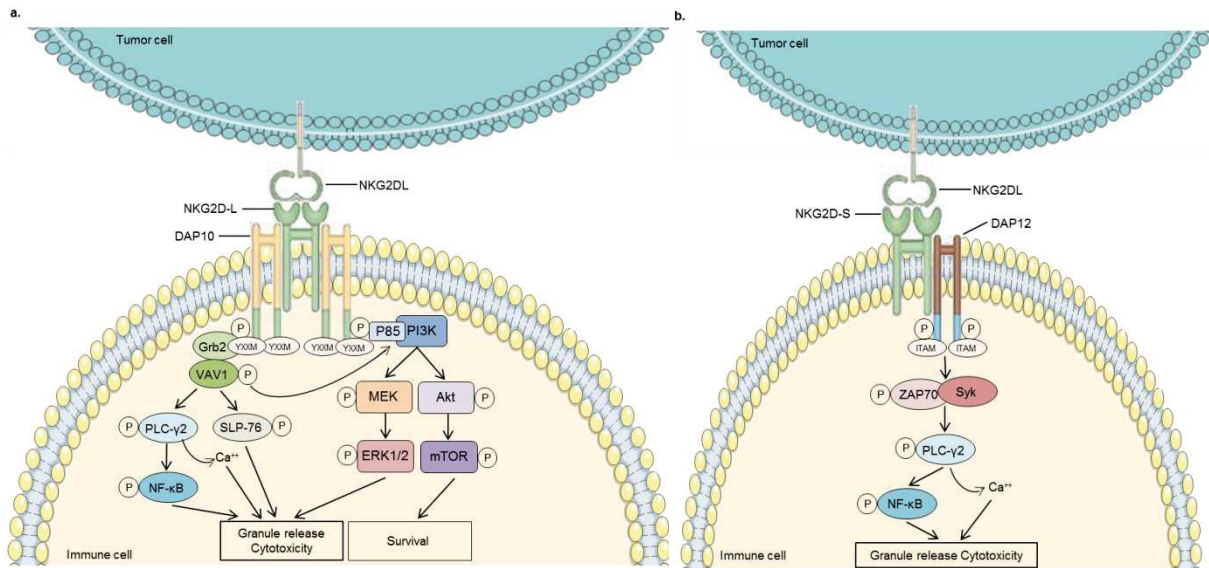


Figure 10. NKG2D-DAP10 and NKG2D-DAP12 mediated signal transduction. **a.** Binding of NKG2D-L with NKG2D ligand (NKG2DL) triggers the phosphorylation of the costimulatory tyrosine-based signaling motif (YXXM) of DAP10. The phosphorylated hexameric NKG2D-L-DAP10 complex can then bind the p85 subunit of PI3K and trigger the phosphorylation of several downstream molecules finally causing ERK phosphorylation, leading to cytokine release and cytotoxicity. PI3K phosphorylation can also activate Akt/mTOR pathway leading to cell survival. The active NKG2D-L-DAP10 complex can also recruit the growth factor receptor-bound protein 2 (Grb2) and Vav1. This Grb2/Vav1 complex can trigger the activation of PI3K pathway but also the phosphorylation of phospholipase C Gamma 2 (PLC- γ 2) and Src homology 2 domain-containing leukocyte phosphoprotein of 76 kDa (SLP-76). This pathway triggers cytotoxicity and calcium release. **b.** Binding of NKG2D-S with NKG2DL triggers the phosphorylation of the tyrosine-based activation motif (ITAM) of DAP12. This phosphorylation recruits Syk and zeta-chain-associated protein 70 kDa (ZAP70) tyrosine kinases and this complex then triggers PLC- γ 2 phosphorylation resulting in granule release and cytotoxicity.

5.1.1.4 NKG2D expression pattern in mouse and in human

Effector cells of both innate and adaptive immune responses express NKG2D. In human, NKG2D is expressed on NK cells, NK T cells (NKT), CD8 T cells and subsets of $\gamma\delta$ T cells (Raulet, 2003; Zhang et al., 2015). In mice, NKG2D expression is found on NK cells, CD8 T cells, activated NKT cells, $\gamma\delta$ T cells and activated macrophages (Upshaw and Leibson, 2006; Diefenbach et al., 2000). In mice, NKG2D expression on CD8 T cells is induced only after activation, whereas in human NKG2D is expressed also by naïve CD8 T cells. While in physiological conditions CD4 T cells

do not express NKG2D in human nor in mice, its expression can be induced in some pathological conditions under cellular stress such as in autoimmune diseases and cancer (Eagle and Trowsdale, 2007).

5.1.1.4.1 NKG2D and NK cells

NK cells are important effectors of innate immunity and play a crucial role in the early cytolytic defense by recognizing and killing infected, stressed or oncogenic cells. NKG2D expression is relatively low on NK cell precursors but this expression increases over time and remains high on mature NK cells (Wensveen et al., 2018). In mice in which both NKG2D isoforms are expressed NKG2D-S isoform expression gets strongly increased after NK cell activation, whereas NKG2D-L isoform expression is decreased. Several studies showed that NKG2D stimulation is sufficient to activate NK cells in both human and mice triggering proliferation and cytokine production such as IFN γ and TNF α (Upshaw and Leibson, 2006; Diefenbach et al., 2000; Diefenbach et al., 2003).

5.1.1.4.2 NKG2D and T cells

In human, NKG2D is expressed on both naïve and activated CD8 T cells whereas in mice NKG2D of both isoforms expression occurs only after CD8 T cell activation. Unlike in NK cells, NKG2D signaling alone is not sufficient to mediate activation of CD8 T cells. Indeed, for being functional, CD8 T cells require the simultaneous activation of the TCR. NKG2D serves thereby as co-stimulatory receptor for these cells, triggering several effects such as cell survival, proliferation, release of cytolytic granules and cytokine production such as IFN γ , TNF α and IL-2 (Wensveen et al., 2018; Prajapati et al., 2018). Moreover, it was shown that NKG2D is involved in the differentiation of CD8 T cells into memory CD8 T-cells and that the absence of NKG2D leads to a reduced capacity to form these memory cells (Wensveen et al., 2013; Soderquest et al., 2011). NKG2D serves also as a co-stimulatory receptor for $\gamma\delta$ T cells and CD4 T cells but is not sufficient alone to trigger the function of these cells.

5.1.1.4.3 NKG2D and macrophages

Macrophages have also a crucial role as immune system effectors and can recognize a large variety of pathogen-associated molecules thanks to their pattern recognition receptors such as Toll-like receptors. In mice, NKG2D is expressed on activated macrophages and NKG2D stimulation is sufficient to trigger certain macrophage effector functions (Jamieson et al. 2002). Indeed, it was shown that this stimulation leads to the production of TNF α and nitric oxide (Diefenbach et al., 2000). Several studies showed the existence of a crosstalk between macrophages and NK cells that plays an important role in antitumor responses (Nedvetzki et al., 2007; Zhou et al., 2012). Indeed, NK cells can for example recognize NKG2D expressed on lipopolysaccharide (LPS)-activated macrophages thus triggering NK cell proliferation and cytokine secretion.

5.1.2 NKG2D ligands

5.1.2.1 Diversity of NKG2D ligands in mouse and in human

While the NKG2D receptor was shown to be evolutionary highly conserved and shows no polymorphism, the diversity of NKG2DL is remarkable and shows a high degree of polymorphism (Carapito and Bahram, 2015). In human, NKG2DL are classified in two families, the MHC class I chain-related protein A (MICA) and B (MICB) and the human cytomegalovirus (HCMV) UL16-binding proteins (ULBPs) that contains six members (ULBP1-6) (Zafirova et al., 2011; Molfetta et al., 2017) (Figure 9). In mice, three families of NKG2DL have been identified, namely the Retinoic acid early transcript 1 (Raet-1) family containing five members (Raet-1 α , Raet-1 β , Raet-1 γ , Raet-1 δ , Raet-1 ϵ) that are orthologs of the human ULBPs, the histocompatibility antigen 60 (H60) family comprising three members (H60a, H60b, H60c) and the murine UL16-binding protein-like transcript 1 (MULT1) that is the unique member of this third family (Zhang et al., 2015).

5.1.2.2 NKG2DL regulation

NKG2DL are rarely expressed on healthy tissues but are induced in response to stress stimuli such as viral infection, heat shock or oncogenic transformation. The

balanced expression of NKG2DL is crucial to avoid detrimental consequences such as autoimmune responses. Indeed, several studies showed that the aberrant expression of NKG2DL is associated with autoimmune diseases, such as rheumatoid arthritis and coeliac disease (Stojanovic et al., 2018). Therefore, the expression of NKG2DL is tightly controlled and regulation appears to be exerted at different levels that I will briefly describe and exemplify.

5.1.2.2.1 Transcriptional regulation of NKG2DL

At transcription level, NKG2DL regulation involves a multitude of transcription factors, which can also explain the heterogeneous expression of NKG2DL in different cell types. A variety of different cell stress can trigger activation of the DNA damage response (DDR) signaling pathway involving Ataxia telangiectasia mutated (ATM) and Ataxia telangiectasia and Rad3 related (ATR) kinases (Zingoni et al., 2018; Duan et al., 2019). These kinases regulate downstream processes such as the activation of the checkpoint kinases (Chk) Chk1 and Chk2 and the induction of tumor suppressor p53 that binds to the p53 response element on the ULBP1/2 promotor inducing their transcription. ATM/ATR-dependent downstream mechanisms are also able to induce the expression of NF- κ B and E2F1 transcription factors leading to the transcription of Raet-1 family members in mouse, and MICA/B in human. On the other hand, NKG2DL expression can also be downregulated at transcriptional level involving for example DNA methylation and deacetylation, as it was shown that demethylating agents and histone deacetylase inhibitors are able to induce MICA/B and ULBPs (Duan et al., 2019; Kato et al., 2007). Unlike transcriptional regulatory mechanisms that are common to several distinct NKG2DL, some other mechanisms target the regulation of selective NKG2DL. As an example, different mechanisms were shown to selectively repress the expression of MICA notably in some cancers. Among those mechanisms one can cite the transcription factor STAT3 that was shown to directly interact with the MICA promoter triggering the inhibition of its transcription in multiple myeloma cells and colon cancer cells (Zingoni et al., 2018; Bedel et al., 2011).

5.1.2.2.2 Post-transcriptional regulation

NKG2DL expression is also regulated at post-transcriptional level. One of the mechanisms involves AU-rich element RNA-binding factor 1 (AUF1) molecules that

are known to mediate RNA degradation. Indeed, the activation of EGFR in response to some type of stress leads to the exclusion of AUF1 molecules from the cell nucleus, thus enabling NKG2DL mRNA stabilization (Vantourout et al., 2014). On the other hand, NKG2DL can also be downregulated at post-transcriptional level involving microRNAs (miRNAs). These miRNAs are noncoding small RNA molecules that exert their function by binding the 3'-untranslated region (UTR) of the NKG2DL promoter thus either inhibiting the translation or destabilizing the targeted mRNAs. This occurs notably in some cancers such as human melanoma, breast cancer and glioma. Indeed, several miRNAs are able to downregulate NKG2DL expression, including miR34a and miR34c, miR-519a-3p, and miR-93, that were shown to downregulate ULBP2 in human melanoma, ULBP2 and MICA in breast cancer cells, and ULBP3 and MICA/B in glioma cells respectively (Zingoni et al., 2018; Duan et al., 2019). In addition, splicing is another mechanism that generates soluble forms of some NKG2DL thereby impacting its expression on the cell surface.

5.1.2.2.3 Post-translational regulation

Mechanisms involved in the regulation of NKG2DL at protein level are multiple. Some of them comprise proteolytic cleavage and secretion in context of exosomes whereas others involve NKG2DL internalization associated or not with proteasomal degradation.

5.1.2.2.3.1 Release of soluble NKG2DLs

The proteolytic cleavage of NKG2DL is dependent on two protease families, MMPs and *A Disintegrin And Metalloproteases* (ADAMs) families. Several ADAMs and MMPs have been shown in the tumor context to mediate shedding of NKG2DL from the cell surface through their proteolytic function resulting in the release of soluble NKG2DL (Duan et al., 2019). As an example, ADAM10 and ADAM17 were shown to mediate the release of ULBP2 from the surface of human glioblastoma cells, whereas MMP2 was involved in the shedding of MICA in renal carcinoma cells. In the mouse, MMPs are able to cleave the MULT1 ligand (Raulet et al., 2014). Other factors are also involved in the regulation of NKG2DL cell surface expression. The release of MICA/B was for example shown to be inhibited by the activation of nitric oxide and to be increased by hypoxia. Moreover, the polymorphisms of MICA/B have also an

impact on the level of shedding. Indeed, it was shown that the polymorphisms lead to conformational changes and these changes affect the accessibility of proteolytic molecules such as ADAMs. In addition, NKG2DL can be excreted in exosomes (nanovesicles formed in multivesicular endosomes and released by fusion with the plasma membrane) thereby reducing NKG2DL expression on the cell surface (Clayton et al., 2008). For example, MICA was shown to be secreted by exosomes in prostate cancer cells (Duan et al., 2019; Raulet et al., 2014).

5.1.2.2.3.2 Internalization of NKG2DLs

Another post-translational regulation of NKG2DLs involves their internalization that in certain cases is associated with their proteasomal degradation as it was described for the human ULBP1 (Fernandez-Messina et al., 2016). This regulation of ULBP1 expression by protein turnover and therefore its brief residence at the cell surface may contribute to a fine tuning of immune responses. On the other hand, immature MICA was shown to be intracellularly retained in the endoplasmic reticulum thereby resulting in limited amounts of MICA at the cell surface in human melanomas (Fuentes et al., 2008).

5.2 NKG2D/NKG2DL-mediated immune surveillance in cancer

The NKG2D/NKG2DL axis plays a crucial role in anti-tumor surveillance and has an impact on tumor initiation and progression. *In vitro* experiments on both human and mouse cancer cells demonstrated that the expression of NKG2DL significantly enhances tumor cell sensitivity towards immune effectors such as NK cells, and that blockade of NKG2D leads to the reduction of tumor cell killing by NK cells (Upshaw and Leibson, 2006; Jamieson et al., 2002). Several *in vivo* studies also showed that ectopic expression of NKG2DL in tumor cells lacking these molecules leads to the rejection of these tumor cells upon grafting. As an example, Diefenbach and colleagues (2001) used the B16-BL6 melanoma cell line that is highly tumorigenic and one of the least immunogenic cell lines, and transfected them with Raet1 or H60, resulting in their efficient rejection involving NK and CD8 T cells (Diefenbach et al., 2001). In clinic, NKG2DL expression was demonstrated to have an impact on patient survival in several cancers such as ovarian cancer in which high expression of NKG2DL correlated with a significantly higher 5-year survival rate (Conejo-Garcia et

al., 2004). In human colorectal cancer too, high expression of MIC and *RAET1G/ULBP5* were shown to correlate with NK cell infiltration and longer patient survival (McGilvray et al., 2009).

5.3 Down-modulation of NKG2D in tumor immunity

Although expression of NKG2DL on cancer cells trigger the activation of immune effectors such as NK cells, it was shown that the chronic stimulation of NKG2D by exposure to membrane-bound NKG2DL or soluble NKG2DLs can downregulate NKG2D expression (Molfetta et al., 2017). The presence of NKG2DLs in serum has been correlated with a worse prognosis in some cancers, in particular with a shorter survival in melanoma and ovarian cancers (Li et al., 2009; Paschen et al., 2009). On the contrary, Von Lilienfeld-Toal and colleagues (2010) showed that in multiple myeloma there is no correlation between the increased levels of soluble NKG2DLs and reduced NKG2D function (Lilienfeld-Toal et al., 2010). One of the hypotheses that may explain the divergence of these results lies in the source of the soluble ligands. Indeed, it was shown that the ability of NKG2DL to down-modulate NKG2D is different when the soluble ligands result from proteolytic cleavage or from exosome-release. Thereby, exosome-released ligands turned out to be more potent NKG2D repressors and this could be explained by a difference of the NKG2D avidity for the two types of soluble NKG2DLs (Clayton et al., 2008). Interestingly too, Molfetta and colleagues (2014) showed that the various NKG2DLs do not have the same ability to down-regulate NKG2D function. Indeed, they found that both MICA and ULBP2 were able to down-modulate NKG2D receptor function but MICA was the most potent one in promoting NKG2D receptor down-modulation leading to the impairment of NKG2D-dependent NK cell cytotoxicity (Molfetta et al., 2014). Another hypothesis that might explain this difference lies in the different modes of membrane anchor (transmembrane and Glycosyl-Phosphatidyl-Inositol-linked) that could impact the avidity of the NKG2DL for NKG2D.

5.4 NKG2D/NKG2DL-mediated immune escape

During tumor progression, cancer cells are able to develop multiple escape mechanisms to prevent NKG2D mediated killing. One of the strategies is to down-regulate the expression of NKG2DL. Among these mechanisms one can cite the

ones that have already been discussed above such as the action of ADAM/MMP molecules and exosomes leading to the shedding of NKG2DL from the cell surface and their release as soluble form, and miRNA overexpression by cancer cells thus impairing NKG2DL expression. Cancer cells are also able to alter cell surface glycosylation leading to the inhibition of NKG2DL expression (Frazao et al., 2019; Mellergaard et al., 2014). In addition, it was shown that chromatin remodeling involving histone deacetylases can regulate the expression of NKG2DL (López-Soto et al., 2009). Other than that, NKG2DL expression is also altered by soluble factors including TGF- β and IL-10. Indeed, it was shown that regulatory immune cells and cancer cells themselves are able to secrete these cytokines leading to the inhibition of NKG2DL expression on the surface of cancer cells, thereby impairing immune effector mediated tumor cell destruction (Zafirova et al., 2011; Frazao et al., 2019). Another strategy used by cancer cells is to induce high levels of NKG2DL. As discussed above, the chronic stimulation of NKG2D by tumor cells expressing NKG2DL can lead to the down-modulation of NKG2D presumably by an unknown negative feedback mechanism. In addition, another mechanism results in the selection of NKG2D-resistant tumor cells (Zafirova et al., 2011; Frazao et al., 2019). Cancer cells expressing high levels of NKG2DL are eliminated by immune effectors resulting in the progressive emergence of NKG2D-resistant variants lacking NKG2DL expression. Altogether these multiple mechanisms show the capacity of cancer cells to adapt towards their microenvironment to evade from NKG2D-mediated immune surveillance.

5.5 NKG2D/NKG2DL as a target in cancer therapy

The impact of NKG2D/NKG2DL axis in anti-tumor immunity is now well established. Therefore, targeting this axis appeared to be a relevant and promising approach to study in cancer treatment. Understanding the mechanisms involved in this axis is crucial to develop efficient treatments since an over-expression of NKG2DL can have a Janus-faced role by promoting on one side more efficient destruction of tumor cells but triggering on the other side the emergence of NKG2D resistant tumor cells. Basically, all the mechanisms triggering the down-regulation of NKG2D/NKG2DL axis efficacy and the mechanisms involved in the immune escape explained above could

represent potential targets in therapy development. Here, I will give a non-exhaustive description of some targets.

5.5.1 Targeting the down-regulation of NKG2DL expression

A promising approach for cancer therapy might reside in the use of ADAM and MMP inhibitors leading to the blockade of ligand shedding. In this context, lomofungin (an antifungal drug) was recently found to significantly decrease ADAM17 activity in hepatocellular carcinoma cells and this blockade leads to the impairment of MICA shedding (Arai et al., 2018a). Another study showed that treatment with regorafenib (a multi-kinase inhibitor that has shown good response rates in colon and pancreatic neuroendocrine tumors) triggers the upregulation of MICA by impairing ADAM9 and ADAM10 function in hepatoma cells (Arai et al., 2018b). Another strategy is the inhibition of MICA/MICB proteolytic cleavage by using antibodies that target the protein domain of the MIC proteins involved in the cleavage. Indeed, it was shown *in vitro* in human cancer cells and *in vivo* in humanized mouse models that targeting the $\alpha 3$ domain of MICA/B using an antibody prevents proteolytic shedding leading to reduced tumor growth (de Andrade et al., 2018). It is also important to note that these strategies could be used in combination with “classical” treatment approaches such as radiotherapy or chemotherapy.

5.5.2 Targeting NKG2DL with engineered T cells

Chimeric antigen receptor (CAR) T-cell therapy consists in genetically engineered patient-derived T cells to express a synthetic receptor that binds a tumor antigen (Feins et al., 2019). This recent therapeutic strategy has already shown improved outcomes in cancer patients. In the NKG2D CAR expressing T cells, the CAR represents a fusion of the full-length NKG2D receptor, the zeta-chain of CD3 (CD3 ζ) and DAP10. These engineered T cells are thus able to recognize any NKG2DL expressed on tumor cells through the CAR receptor in a T-cell receptor independent manner thus triggering activation of these T cells resulting in the secretion of pro-inflammatory cytokines (Chang et al., 2013). It was also shown in a murine ovarian cancer model that immunotherapy with NKG2D CAR T cells leads to a long-term tumor-free survival by inducing the development of a host tumor-specific T cell

memory response (Barber et al., 2008). Thereby this strategy represents a promising immunotherapeutic strategy for cancer treatment.

5.5.3 Targeting NKG2D using bispecific proteins

Another strategy consists to use a bispecific protein targeting NKG2D receptor. In their multiple myeloma model, Pogge von Strandmann and colleagues (2006) have designed and used a bispecific ULBP2-BB4 protein (von Strandmann et al., 2006). BB4 is an antibody recognizing syndecan-1 (CD138) that is overexpressed in multiple myeloma. BB4 serves here as a tumor-antigen directed antibody that has been fused to ULBP2. Thus in this complex ULBP2 binds to the NKG2D receptor while BB4 binds to CD138. The authors showed *in vitro* and *in vivo* that this protein is able to strongly activate and enhance NK-mediated lysis of human CD138⁺ multiple myeloma cells suggesting a potential clinical use of this strategy. Another group developed a bispecific protein in which the extracellular domain of NKG2D receptor was fused to an anti-CD3 single chain variable fragment (scFv) (Zhang and Sentman, 2011). The scFv-NKG2D complex can thereby bind to NKG2D ligand-positive tumor cells and simultaneously to T cells enabling the recognition of tumor cells by T cells that become activated and trigger cytotoxicity.

5.5.4 Cross-talk between immune checkpoint therapy and NKG2D/NKG2DL activation

The presence of soluble NKG2DL in the serum of cancer patients was correlated with tumor progression and less favorable response to immunotherapy. In this context, Maccalli and colleagues (2017) measured soluble immunomodulatory factors in serum of melanoma patients undergoing anti-CTLA4 therapy with Ipilimumab, and showed that the absence of some soluble NKG2DL correlated with better response to the immunotherapy (Maccalli et al., 2017). In cancer patients, MICA was shown to be the most expressed NKG2DL that down-regulates the expression of NKG2D on the cell surface of immune cells. Also, the presence of soluble MICA in the serum of patients was correlated with clinical parameters such as worse prognosis and decreased response to immunotherapy (Sharma et al., 2017). Jinushi and colleagues (2006) showed that the blockade of CTLA-4 even induced anti-MICA antibodies in melanoma patients (Jinushi et al., 2006). These therapy-induced anti-MICA

antibodies can block the decrease of NKG2D expression and effectively opsonize cancer cells that would enhance dendritic cell mediated cross-presentation of tumor antigens (Zafirova et al., 2011; Maccalli et al., 2017). The mechanism underlying the crosstalk between immune checkpoint therapy and NKG2D/NK2DL axis is not well understood yet and needs further investigation. The challenge in this context is to find suitable models for pre-clinical investigation since for example no MIC homolog is found in mice.

All these information emphasize the close relation between the different component of the TME and their impact on tumor progression. Yet, there are still grey area remaining to be lightened and notably concerning the ECM impact on anti-tumor immunity.

Thesis Objectives

It is now well known that high TNC expression correlates with poor overall and poor metastasis-free survival in breast cancer patients (Lowy and Oskarsson, 2015; Oskarsson et al., 2011). This has been explained by the different pro-tumorigenic impacts of TNC such as promoting angiogenesis, cancer cell proliferation, migration, and invasiveness abilities (Midwood et al., 2016; Orend and Chiquet-Ehrismann, 2006). Some studies have also shown the immunomodulatory effects of TNC (Parekh et al., 2005; Jachetti et al., 2015; Deligne et al., 2020), but the underlying mechanisms are still poorly understood.

The aim of my thesis project was to study the impact of TNC on anti-tumor immunity in a breast cancer progression model. To do that, I used an orthotopic syngeneic breast cancer model established previously in my host laboratory named NT193 model. This grafting model is based on the MMTV-NeuNT mouse model, a genetic model where the oncogene Neu, the rat homologue of ErbB2, is expressed under the control of the mouse mammary tumor virus (MMTV) enhancer (Muller et al., 1988). In this model the oncogene Neu is mutated leading to its constitutive activation. These mice develop spontaneous multifocal primary breast tumors and lung metastasis. The NT193 breast cancer cell line has been established from a primary tumor of a MMTV-NeuNT mouse and upon orthotopic grafting in mice mimics the genetic model in a shorter period of time. Both models have been engineered to modulate the expression of TNC and enable us to study the roles of both stromal and host-derived TNC. These models were used to achieve the following two aims:

Aim 1: Investigate TNC effects on the immune cell infiltrate and its impact on tumor progression

Aim 2: Investigate the impact of TNC on the NKG2D/NKG2DL axis

Tenascin-C immobilizes infiltrating T lymphocytes through CXCL12 promoting breast cancer progression

Devadarssen Murdamoothoo^{1,2,3,4,†} , Zhen Sun^{1,2,3,4,5,6,†} , Alev Yilmaz^{1,2,3,4,†} , Gilles Riegel^{1,3,4} , Chérine Abou-Faycal^{1,2,3,4} , Claire Deligne⁷ , Ines Velazquez-Quesada^{1,2,3,4} , William Erne^{1,2,3,4}, Marine Nascimento^{1,3,4}, Matthias Mörgelin⁸ , Gérard Cremel^{2,3,4} , Nicodème Paul^{3,4,9} , Raphael Carapito^{3,4,9} , Romain Veber¹⁰ , Hélène Dumortier¹⁰ , Jingping Yuan¹¹, Kim S Midwood⁷ , Thomas Loustau^{1,3,4}  & Gertraud Orend^{1,2,3,4,*} 

Abstract

Immune checkpoint therapy, where CD8 tumor infiltrating T lymphocytes (TIL) are reactivated, is a promising anti-cancer treatment approach, yet with low response rates. The extracellular matrix, in particular tenascin-C, may generate barriers for TIL. To investigate this possibility, we used a MMTV-NeuNT and syngeneic mammary gland grafting model derived thereof with engineered tenascin-C levels and observed accumulation of CD8 TIL in tenascin-C-rich stroma. Inhibition studies revealed that tenascin-C induced CXCL12 through TLR4. By binding CXCL12, tenascin-C retained CD8 TIL in the stroma. Blockade of CXCR4, the receptor of CXCL12, enhanced macrophage and CD8 TIL infiltration and reduced tumor growth and subsequent metastasis. Retention of CD8 TIL by tenascin-C/CXCL12 was also observed in human breast cancer by tissue staining. Moreover, whereas high CD8 TIL numbers correlated with longer metastasis-free survival, this was not the case when also tenascin-C and CXCL12 levels were high. Altogether, these results may be useful for improving tumor immunity as diagnostic tool and to formulate a future “TIL-matrix-release-and-reactivate” strategy.

Keywords CD8 tumor infiltrating lymphocytes; CXCL12; extracellular matrix; tenascin-C; Tumor immune microenvironment

Subject Categories Cancer; Immunology

DOI 10.1525/emma.202013270 | Received 11 August 2020 | Revised 12 April 2021 | Accepted 12 April 2021 | Published online 14 May 2021
EMBO Mol Med (2021) 13: e13270

Introduction

Immune checkpoint therapy (ICT) is a promising approach to activate the body’s immune system to fight cancer. Yet, in most breast cancer patients, ICT is only efficient in up to 20% of patients (Duraiswamy *et al*, 2013). Inactive CD8 TIL can get reactivated with antibodies targeting PD1, PD-L1, or CTLA (Duraiswamy *et al*, 2013; Huang *et al*, 2017); however, CD8 TIL are often either scarce or located inside the tumor stroma not reaching the tumor cells (Joyce & Fearon, 2015). The “immune contexture” and tumor microenvironment (TME) have been identified as potential obstacle in ICT (Fridman *et al*, 2012; Zemek *et al*, 2020). In particular, the so-called “immunoscore” takes into account the exclusion of CD8 TIL from tumor cell clusters (Galon & Bruni, 2019) which are often organized as nests surrounded by stroma, that is rich in extracellular matrix (ECM) (Pickup *et al*, 2014; Spenlé *et al*, 2015). Yet, the roles of the ECM in controlling CD8 TIL infiltration are not well understood (Erdag *et al*, 2012; Galon *et al*, 2012; Joyce & Fearon, 2015).

1 The Tumor Microenvironment Laboratory, INSERM UMR_S 1109, Faculté de Médecine, Hopital Civil, Institut d’Hématologie et d’Immunologie, Strasbourg, France

2 The Microenvironmental Niche in Tumorigenesis and Targeted Therapy (MN3T), INSERM UMR_S 1109, Faculté de Médecine, Hautepierre, France

3 Université Strasbourg, Strasbourg, France

4 Fédération de Médecine Translationnelle de Strasbourg (FMTS), Strasbourg, France

5 Department of Gastrointestinal Surgery, Tongji Hospital, Tongji Medical College in Huazhong University of Science and Technology, Wuhan, China

6 Tongji Cancer Research Institute, Tongji Hospital, Tongji Medical College in Huazhong University of Science and Technology, Wuhan, China

7 Kennedy Institute of Rheumatology, University of Oxford, Oxford, UK

8 Colzyx AB, Lund, Sweden

9 GENOMAX platform, INSERM UMR_S 1109, Institut thématique interdisciplinaire (ITI) de Médecine de Précision de Strasbourg, Transplantex NG, Faculté de Médecine, Fédération Hospitalo-Universitaire OMICARE, LabEx TRANPLANTEX, Strasbourg, France

10 Institut de Biologie Moléculaire et Cellulaire, CNRS, UPR3572 Immunologie, Immunopathologie et Chimie Thérapeutique, Institut de Biologie Moléculaire et Cellulaire, Strasbourg, France

11 Department of Pathology, Renmin Hospital of Wuhan University, Wuhan, China

*Corresponding author. Tel: +33 368 85 40 11; E-mail: gertraud.orend@inserm.fr

†These authors contributed equally to this work

The ECM molecule tenascin-C (TNC) is highly expressed in the tumor stroma in regions called tumor matrix tracks (TMT), that are composed of several matrix molecules and are enriched with fibroblasts and leukocytes (Spenné *et al*, 2015; Spenné *et al*, 2020). TNC is also expressed in regions with high collagen-rich tumor-associated collagen signatures (TACS) that correlate with poor breast cancer patient survival (Tomko *et al*, 2018). TNC has many context-dependent functions (Midwood *et al*, 2016). TNC can impair adhesion, proliferation, and function of cytotoxic T lymphocytes (CTL) and can be degraded by autophagy that is defective in triple-negative breast cancer causing CTL impairment (Rüegg *et al*, 1989; Hemesath *et al*, 1994; Hauzenberger *et al*, 1999; Parekh *et al*, 2005; Huang *et al*, 2010; Li *et al*, 2020). TNC skewed macrophages toward a M2 phenotype through TLR4 promoting lung metastasis in the syngeneic NT193 breast cancer model, that has been used in the current study (Deligne *et al*, 2020). Moreover, in an oral squamous cell carcinoma model, TNC promoted an immune suppressive TME through CCR7/CCL21 (Spenné *et al*, 2020). Altogether, TNC may contribute to evasion from immune surveillance in breast cancer by regulating CTL function but how is largely unknown.

Here, by investigating two breast cancer progression models with engineered high and low TNC levels, we demonstrated that TNC contributes to the escape from anti-tumor immunity by regulating CD8 TIL. TNC impaired CD8 TIL function through induction of CXCL12. TNC bound CXCL12, thus immobilizing CD8 TIL in the matrix. Subsequently, these lymphocytes were impaired in reaching and killing the tumor cells. Upon inhibition of CXCR4, CD8 TIL were released from the TNC-rich stroma, now accessing and killing the tumor cells causing reduced tumor growth and subsequent metastasis. This mechanism may be relevant in human breast cancer where CD8 TIL accumulation in the TNC-rich stroma in context of high CXCL12 correlated with shortest survival of breast cancer patients.

Results

TNC regulates expression of immunity-associated genes in the MMTV-NeuNT model

To investigate how TNC impacts tumor growth, we used the MMTV-NeuNT (NeuNT) model on a wild-type (WT) and TNC knockout (KO) background. In this model, we have previously shown that TNC increased tumor onset and lung metastasis (Sun *et al*, 2019). We compared overall gene expression in tumors isolated from WT and TNCKO mice by an Affymetrix chip array. This analysis revealed 2,260 genes to be differently regulated between tumors of both genotypes ($P < 0.05$) (Fig 1A–C,

Appendix Table S1). Gene ontology analysis showed differential expression of several genes including 136 immune-related genes (75 downregulated (Fig 1B) and 61 upregulated (Fig 1C)) and reduced expression of type I interferon (IFN) responsive genes in WT compared to TNCKO tumors (Figs 1A and EV1A, B, Appendix Fig S1A and B, Appendix Table S1). We also noticed that more than 10 *Mhc type II* molecules and chemokines such as *Cxcl12* were higher and lower in the absence of TNC, respectively, suggesting an impact of TNC on tumor immunity (Fig 1B and C). By flow cytometry, we investigated the immune cell infiltrate and observed that $F4/80^+$ and $iNOS^+$ macrophages were more and less abundant in WT than TNCKO tumors, respectively (Fig 1D and E). Moreover, T cell subtype numbers and in particular CD8 T cells ($CD44^+$ and $PD-1^+$) were in general very low in these late-stage tumors with no difference between genotypes (Appendix Fig S1C–F). Interestingly, the CD8 T cell activation marker *Perforin* and several T cell-regulating genes were higher in TNCKO tumors, indicating that TNC impacts CTL function (Figs 1B and EV1B, Appendix Fig S1G).

TNC promotes stromal CD8 TIL enrichment and enhances survival of tumor cells in the syngeneic NT193 breast cancer grafting model

Due to poorly abundant CD8 TIL in late-stage NeuNT tumors (confirmed by immunofluorescence staining (IF), Appendix Fig S1C and S2A), we decided to use our novel syngeneic orthotopic NT193 grafting model with more numerous CD8 TIL (Deligne *et al*, 2020). In the previous study, the TNC-low condition had some residual TNC that was provided by the host. Here, we engrafted *Tnc* knockdown (shTNC) NT193 tumor cells into a TNCKO host to obtain a close to TNC-negative condition where indeed TNC is almost undetectable (Sun *et al*, 2019). For some experiments, it is relevant to use a TNCKO host to mimic the TNC-negative condition as host TNC plays a role in promoting lung metastasis by impacting tumor cell survival and plasticity in the blood vessel invasions (BVI), an important precursor of metastasis (Siegel *et al*, 2003; Sun *et al*, 2019). As illustrated in Fig EV1C and D, we compared tumors with high and low TNC levels. In the TNC-high condition control (shC), tumor cells were engrafted into a WT host (WT/shC). For TNC-low tumors, a WT or TNCKO host was engrafted with shTNC cells, giving rise to WT/shTNC or KO/shTNC tumors, respectively. We used different time points (4, 5, 7, and 11 weeks) and grafting methods (iv, orthotopic) as indicated and outlined in Fig EV2. We investigated gene expression in all grafted tumors by RNA-seq analysis and compared gene expression levels to that in NeuNT tumors (Fig EV1B–D). This comparison revealed clear differences between tumors and showed that in tumors with lowered TNC, gene

Figure 1. Loss of the TNC protein in NeuNT tumors impacts gene expression and the immune cell infiltrate.

A–C Display of differentially expressed genes in NeuNT tumors (WT, TNCKO) as volcano plot (A) and heatmaps (B, C) representing all (A) and immunity-associated genes to be low (B) or high (C) in WT tumors. $N = 3$ tumors per genotype. (A) \log_2 fold change (x-axis) and the negative \log_{10} (P -Value) (y-axis) is displayed, the blue line indicating $P = 0.05$ (y-axis), points above the line, $P < 0.05$. The dashed red lines indicate the \log_2 fold change cutoff of -0.25 and 0.25 , respectively (x-axis). Green dots represent genes that display both statistical significance ($P < 0.05$) and fold changes -0.25 and 0.25 , respectively. Selected genes regulated by TNC are marked in red (type I interferon response) or pink (*Cxcl12* dot).

D, E Infiltration of $F4/80^+$ macrophages determined by flow cytometry. (WT, $N = 10$, TNCKO, $N = 7$ tumors), $*P = 0.0304$, unpaired t-test and $iNOS^+$ macrophages (WT, $N = 9$, TNCKO, $N = 7$ tumors) $*P = 0.0197$, unpaired t-test. Mean \pm SEM.

Source data are available online for this figure.

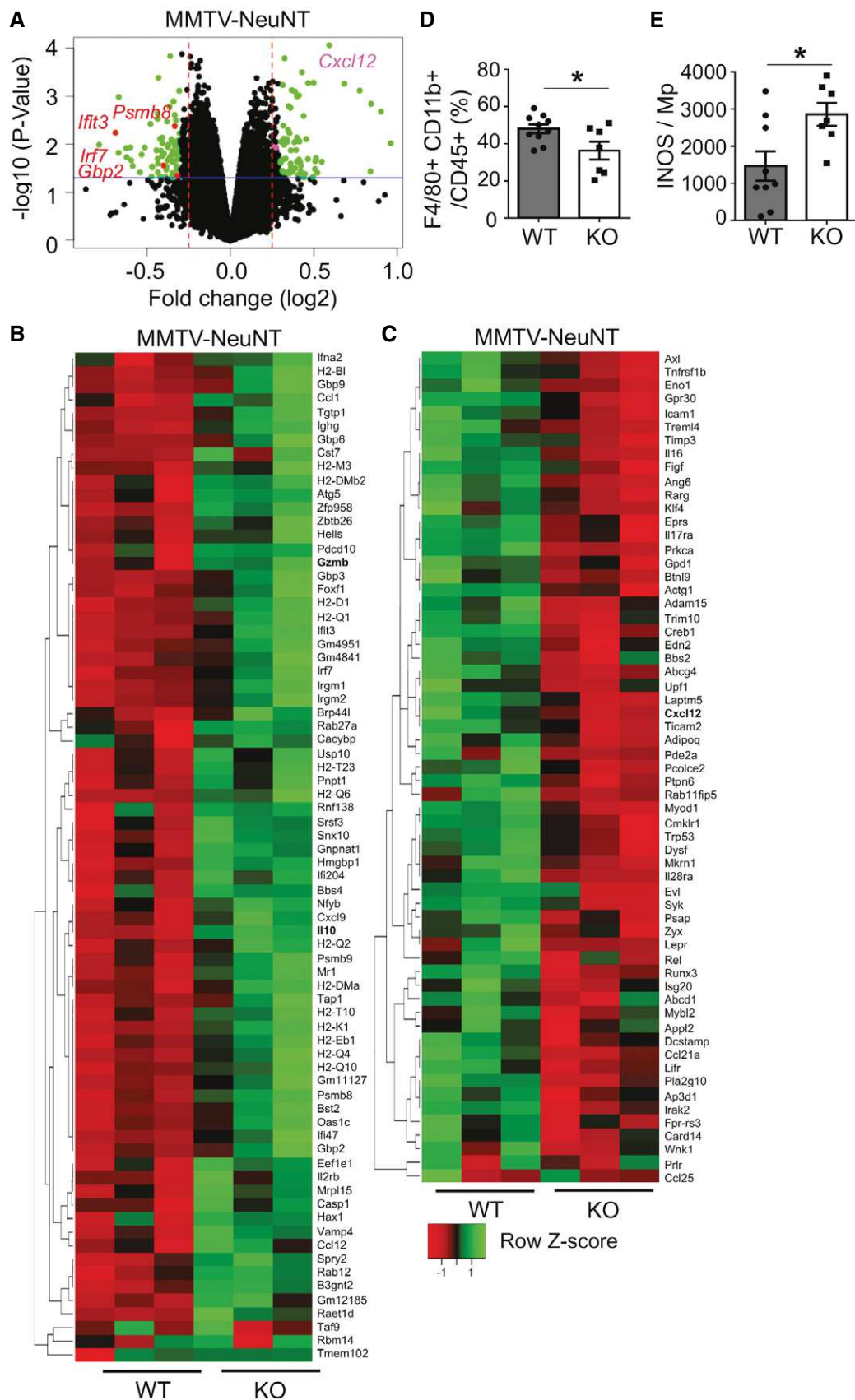


Figure 1.

expression was clearly different to tumors with abundant TNC. Moreover, similarities in gene expression were seen in the TNC-high group (NeuNT-WT, WT/shC) and TNC no/low group (NeuNT-KO, WT/shTNC, KO/shTNC), respectively (Fig EV1B and D, Appendix Table S2).

We previously noticed that macrophages were abundant in the stroma of TNC-high (WT/shC) tumors (Deligne *et al*, 2020). Now we wondered whether TNC influenced the localization of macrophages and other immune subtypes which we addressed by tissue staining in the 11-week model (Fig EV2) and observed that CD45⁺ leukocytes were present inside the stroma as well as in the tumor cell nests. As previously seen for macrophages (F4/80) (Deligne *et al*, 2020), also CD4 T cells and CD11c myeloid/dendritic cells were present inside the tumor nests and the stroma with no apparent difference between genotypes (Fig 2A). This was different for CD8 TIL. Whereas CD8 TIL were similarly abundant in TNC-high and TNC-low (KO/shTNC) tumors (Fig 2B), they resided predominantly inside the stroma of TNC-high tumors, in contrast to TNC-low (KO/shTNC) tumors where CD8 TIL more frequently invaded the tumor cell nests (Fig 2A and C). As CD8 TIL were found in the stroma, we asked what contribution tumor and stromal TNC has on this retention. Therefore, we quantified CD8 TIL in WT/shTNC tumors and compared results to KO/shTNC and WT/shC tumors which revealed a tendency of more CD8 TIL infiltration when tumor cell-derived TNC was lowered (WT/shTNC). However, tumor nest infiltration of CD8 TIL was only significantly higher in the absence of host TNC (KO/shTNC). This result clearly shows that host TNC is important in retaining CD8 TIL (Appendix Fig S2B). To address whether CD8 TIL in the tumor nests had an impact on survival, we stained for cleaved caspase 3 (Cl. casp3) and saw more apoptosis in TNC-low (KO/shTNC) than in TNC-high tumors (Fig 2D and E). Costaining for CD8 and Cl. casp3 revealed no colocalization, but vicinity, suggesting a paracrine mechanism (Fig 2F). In support, we saw higher expression of *Granzyme B* (*Gzmb*) and *Perforin* (secreted by activated CD8 TIL (Kelsel *et al*, 2002)) in TNC-low (KO/shTNC) than TNC-high tumors (Fig 2G and H). As TNC is expressed in the lungs of NT193 tumor mice (Sun *et al*, 2019), we addressed whether TNC also impacted CD8 TIL in lung metastasis by determining the abundance of CD8 TIL by tissue staining. We noticed a higher infiltration of CD8 TIL in lung metastases from WT than TNCKO mice (Fig 2I and J) correlating with higher metastasis in WT mice (Sun *et al*, 2019). Altogether, our results point at CD8 TIL localization and function to be regulated by TNC.

Tenascin-C upregulates and binds CXCL12

To gain insight into the underlying mechanism, we consulted our RNA-seq results which revealed 1,502 genes to be differently expressed, including *Cxcl12*. Here, we focused on CXCL12, a known regulator of tumor immunity (Okabe *et al*, 2005; Zhang *et al*, 2019) that was more expressed in TNC-high in comparison to TNC-low (WT/shTNC, KO/shTNC) tumors and in cultured tumor cells which we confirmed by qRT-PCR and ELISA (Figs 3A–C and EV3A and B, Appendix Table S2). Tumors derived from shC-engrafted tumor cells had the highest CXCL12 levels irrespective of the host, and shTNC-engrafted tumor cells expressed less CXCL12 altogether pointing at the tumor cells as major source of CXCL12 (Figs 3B and). We confirmed higher *Cxcl12* levels also in NeuNT-WT than TNCKO tumors (qRT-PCR) and in the supernatant (conditioned medium, CM) of shC in comparison to shTNC cells (qRT-PCR, ELISA) (Figs 3C and D, and EV3D). Next, we addressed how TNC induced *Cxcl12* by using inhibitors according to established protocols for tyrosine kinase inhibitors (sunitinib), integrin $\alpha 4\beta 1$ and $\alpha 9\beta 1$ (BOP), TGF β receptor 1 (TGF β RI, GW788388), and Toll-like receptor 4 (TLR4, Cli95) on tumor cells stimulated with TNC. In contrast to BOP, GW, and sunitinib that did not affect *Cxcl12* expression, Cli95 reduced TNC-induced *Cxcl12* demonstrating that TNC regulates CXCL12 expression through the known TNC receptor TLR4 like other molecules (Fig 3E; Midwood *et al*, 2009; Spenlé *et al*, 2020).

Next, we used tissue staining to assess the relative distribution of CXCL12 within the tumor. We noticed higher CXCL12 expression in the tumor nests than in the stroma as also documented in human tumors (Toullec *et al*, 2010; Lefort *et al*, 2017). In contrast, TNC was highly expressed in the stroma but not in the tumor nest which we confirmed by using 3 different antibodies (Appendix Fig S2B and C). We cannot explain how CXCL12 expression is regulated in the tumor nests. TNC may play a role by inducing CXCL12 in the stroma to either bind to TNC and/or diffuse into the tissue. CXCL12 gradients in tumors have been described but how they are established is not well understood (Spinosa *et al*, 2017).

TNC interacts with many molecules (De Laporte *et al*, 2013; Midwood *et al*, 2016; Spenlé *et al*, 2020). Therefore, we asked whether TNC potentially binds CXCL12. Indeed, by surface plasmon resonance measurement, CXCL12 was found to bind TNC in a range of 790 nM (35-fold lower than binding to CXCR4; Richter *et al*, 2014; Fig 3F). Moreover, by negative staining electron microscopy, we confirmed CXCL12 binding to TNC. CXCL12 labeled with colloidal gold particles bound to TNC predominantly inside the

Figure 2. Impact of TNC on CD8 TIL in the syngeneic NT193 breast cancer model.

- A Representative staining images ($N = 5$) of tissue from TNC-high (WT/shC) and TNC-low (KO/shTNC) tumors ($N = 5$ per condition) with the indicated antibodies. Arrows point at the respective immune subtype. Scale bar, 50 μ m.
- B, C Quantification of CD8 TIL upon tissue staining as total number per field (B) and in the stroma or tumor cell nest (C), expressed as relative ratio, *** $P = 0.0002$, Fisher's exact test and in TNC-high ($N = 5$) and TNC-low tumors ($N = 5$). 3 sections per tumor and 8 random fields per section. Mean \pm SEM.
- D, E Apoptosis measurement upon tumor staining for cl. casp3 (D) and signal quantification per field (E) in TNC-high and TNC-low tumors ($N = 7$ per condition), 2 sections per tumor, 5 random fields. *** $P = 0.0006$, Mann-Whitney test, mean \pm SEM. Scale bar, 50 μ m.
- F Representative staining images ($N = 5$ tumors, 3 sections per tumor) for the indicated molecules. Scale bar, 50 μ m. Arrows point at CD8 TIL.
- G, H *Gzmb* and *Perforin* expression as determined by qRT-PCR. $N = 6$ tumors per condition. ** $P = 0.0022$ for both graphs, Mann-Whitney test. Mean \pm SEM.
- I, J Detection (I) and quantification (J) of CD8 TIL in lung metastasis of NeuNT-WT and TNCKO mice ($N = 3$ mice, $n = 7$ and 12 lung metastases, respectively). Scale bar, 100 μ m. ** $P = 0.0097$, Mann-Whitney test. Mean \pm SEM.

Source data are available online for this figure.

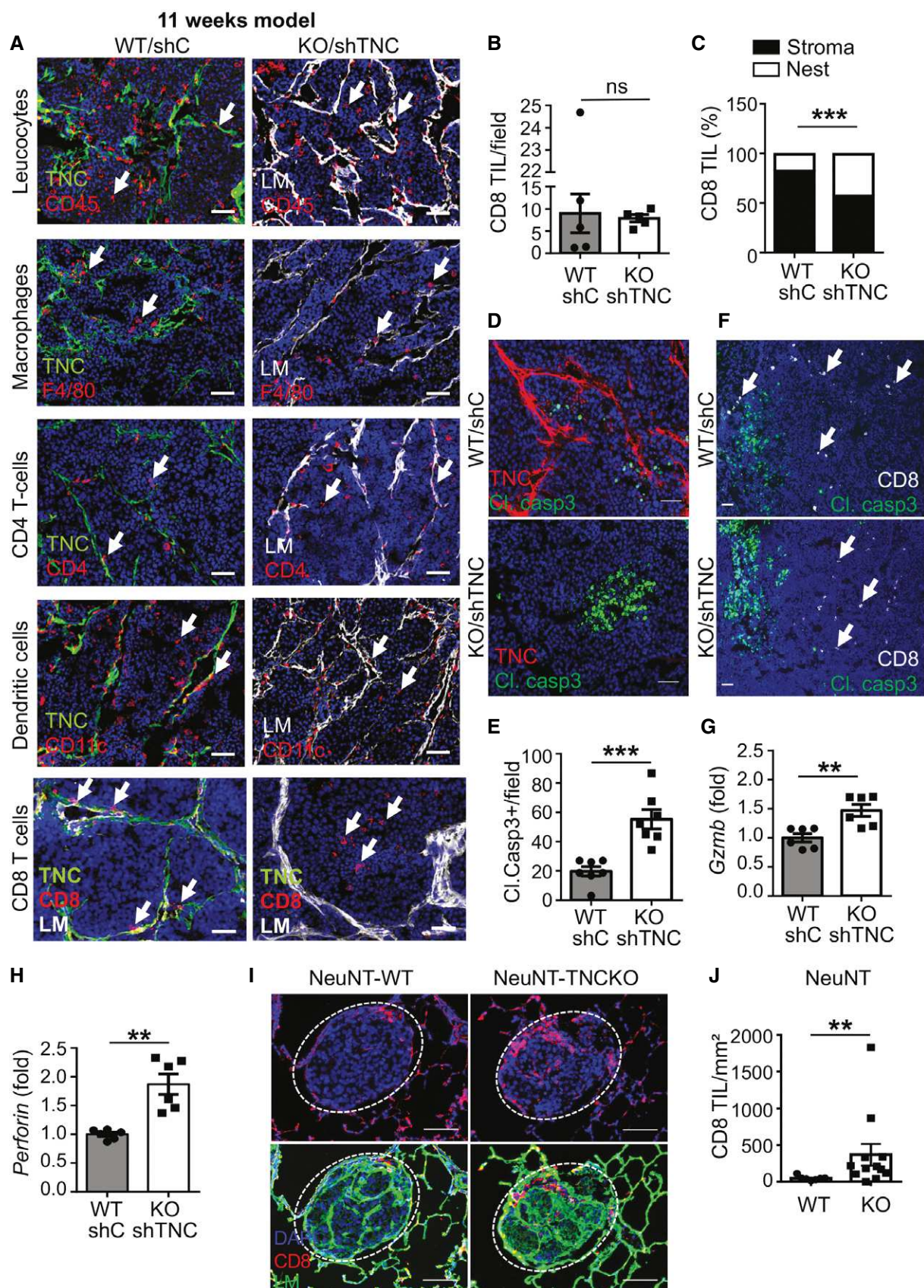


Figure 2.

fibronectin type III (FNIII) domains, including the 5th FNIII repeat that was previously shown to bind several other molecules (De Laporte *et al*, 2013; Spenlé *et al*, 2020). Additional but much lower binding was also seen in the EGFL repeats and the fibrinogen like globe (FBG) whereas control gold particles (not chemokine

coupled), or EGF- or BSA-coupled gold particles (Spenlé *et al*, 2020), did not bind TNC (Figs 3G and H, and EV3E). Moreover, binding of CXCL12-coupled beads to TNC was competed with free CXCL12 and with increasing concentrations of heparin implying interactions via charged moieties (Fig EV3F and G).

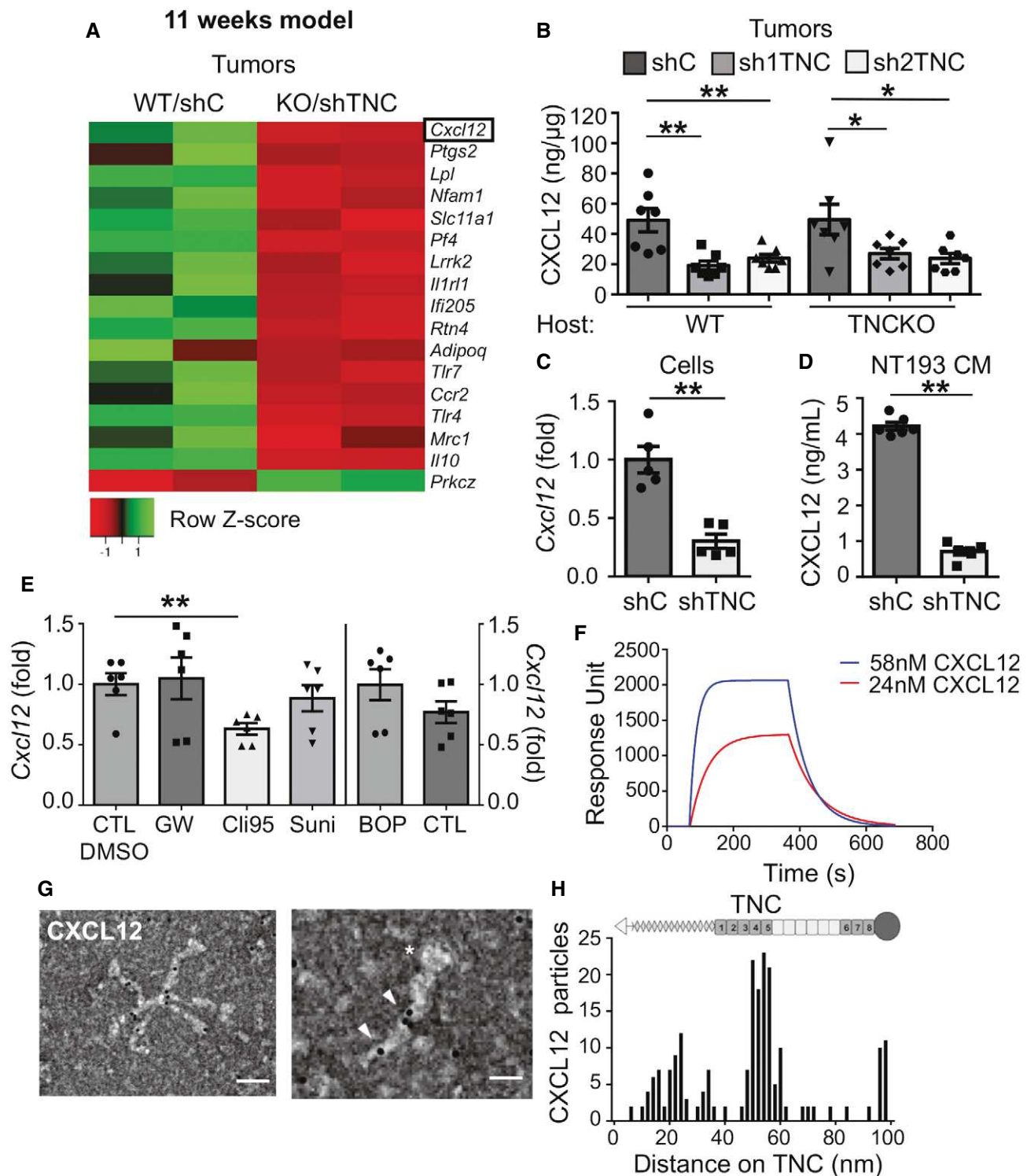


Figure 3.

Figure 3. CXCL12 expression and binding to TNC.

A Heatmap representation of the most 17 deregulated Panther identified immune-related genes in TNC-high (WT/shC) and TNC-low (KO/shTNC) tumors ($N = 2$ tumors each).

B CXCL12 protein levels in NT193 tumors (ELISA). $N = 7$ tumors per group, $**P = 0.0035$ (WT host, shC versus sh1TNC), $**P = 0.0070$ (WT host, shC versus sh2TNC), $*P = 0.0379$ (TNCKO host, shC versus sh1TNC), $*P = 0.0262$ (TNCKO host, shC versus sh2TNC), Mann-Whitney test. Mean \pm SEM.

C *Cxcl12* levels in cultured tumor cells (qRT-PCR). $N = 5$ independent experiments, $**P = 0.0079$, Mann-Whitney test. Mean \pm SEM.

D CXCL12 protein levels (ELISA) in conditioned medium (CM) from cultured tumor cells, $N = 6$ independent experiments, $**P = 0.0022$, Mann-Whitney test. Mean \pm SEM.

E Analysis of *Cxcl12* (qRT-PCR) in tumor cells upon pretreatment with the indicated inhibitors for 45 min (GW, BOP, DMSO, and PBS as control, respectively) or 60 min (Sunitinib) and 6 h (Cil95) (6 h DMSO as control) before incubation with TNC for 24 h. $N = 6$ independent experiments, $**P = 0.0022$, Mann-Whitney test. Mean \pm SEM.

F–H CXCL12 binding to TNC as determined by SPR measurement (F) and negative EM imaging (G), followed by quantification (H). (G) scale bars, 100 nm (left), 50 nm (right), the arrowheads point at gold labeled CXCL12 and the asterisk points at the fibrinogen globe of the murine TNC monomer. (H) Representation of TNC monomer, oligomerization domain (triangle) to form hexamers as seen in (G), FNIII repeats (gray boxes, constant domains, white boxes, alternative domains), fibrinogen like domain (circle). Representative result (3 independent experiments).

Source data are available online for this figure.

CXCL12 immobilizes CD8 T leukocytes in a CXCR4-dependent manner

We investigated whether TNC influenced expression of the CXCL12 receptors CXCR4 and/or CXCR7 (Bleul *et al.*, 1996; Balabanian *et al.*, 2005) and observed that *Cxcr4* levels were higher in TNC-low (WT/shTNC, KO/shTNC) tumors and in cultured tumor cells upon TNC knockdown, revealing an opposite regulation than *Cxcl12* by TNC (Appendix Fig S3A). No difference in *Cxcr7* mRNA levels was seen in cultured tumor cells in dependence of TNC (Appendix Fig S3B).

To address whether CXCL12 regulates CD8 T cell function, we compared transwell migration (attraction or retention) of CD8 T cells toward defined substrata, collagen I (COL), fibronectin (FN), or TNC together with CXCL12 and CXCL10 or CCL21, respectively, as previously described (Fig 4A, Spenlé *et al.*, 2020). CXCL12 attracted more CD8 T cells than CXCL10 or CCL21. In contrast to FN or COL, CD8 T cell attraction by CXCL12 was surprisingly largely reduced by TNC (Fig 4B). However, we found more CD8 T cells to be immobilized on TNC than on the other substrata, with a more potent effect of CXCL12 than CXCL10 or CCL21 (Fig 4C). As TNC binds CXCL12, potentially generating an adhesive substratum, we washed the coating after incubation with CXCL12 and observed that TNC plus CXCL12 indeed retained CD8 T cells whereas the other substrata did not. This effect was CXCR4 dependent as AMD3100 (AMD), a CXCR4 inhibitor, blocked CXCL12- but not CXCL10-dependent CD8 T cell retention (Fig 4D and E).

To address whether CXCL12 is the major chemoattractant by which TNC immobilizes CD8 T cells, we used conditioned medium (CM) from cultured tumor cells in the migration and retention assay, respectively. In contrast to CM from shTNC cells (low CXCL12) that was poorly cell attracting, CM from shC cells (high CXCL12) strongly attracted CD8 T cells toward the FN and COL but less to the TNC coating (Fig 4F). As for CXCL12, also with the CM from shC cells more CD8 T cells adhered on TNC than on the other substrata which were not seen with CM from shTNC cells (Fig 4G, Appendix Fig S3C and D). Finally, the TNC retention effect of the CM was abolished with AMD, supporting a role of CXCR4 signaling in CD8 T cell attraction and retention by the secretome from the tumor cells (Fig 4F and G, Appendix Fig S3C and D).

To rule out other potential effects of AMD on CD8 T cells, we investigated CD8 T cell survival, proliferation, and function upon activation by an anti-CD3 antibody and inhibition of CXCR4. In contrast to *Bax* and *Bcl-w* that were unchanged (determined by qRT-PCR), expression of apoptosis inhibitory *Bcl-2* was increased by anti-CD3, yet not affected by AMD (Appendix Fig S3E–G). With an MTS assay, proliferation was found to be increased with anti-CD3, which was not changed by AMD (Appendix Fig S3H). Moreover, upon incubation with the anti-CD3 antibody, CD8 T cells upregulated expression of *Ifng*, *Perforin*, and *Gzmb* which again was not altered by AMD (Appendix Fig S3I–K).

Finally, by higher resolution tissue staining of TNC-high tumors, we noticed a punctate CXCL12 signal in the stroma, importantly colocalizing with TNC and CD8 TIL, altogether suggesting that the described chemoretention by TNC/CXCL12 might be relevant for tethering CD8 TIL in the tumor stroma (Appendix Fig S3L).

Inhibition of CXCR4 restores CD8 TIL tumor nest infiltration triggering tumor cell death

We investigated by flow cytometry whether TNC influenced CD8 TIL function *in vivo* through CXCL12, by blocking CXCR4 with AMD (for 2 weeks) in tumor-bearing mice in the 4-week model (Figs EV2 and EV4A–H). We observed a tendency toward more CD8 TIL in TNC-high tumors upon AMD treatment ($P = 0.07$). This was different to TNC-low (WT/shTNC) tumors with no change in CD8 TIL levels (Fig EV4A). Whereas a tendency toward more CD4 and B cells and less macrophages, DC, NK cells, and neutrophils was seen in the TNC-high tumors upon CXCR4 inhibition, respectively, there was clearly no difference in TNC-low tumors suggesting that CXCR4 inhibition may have an impact on the immune cell infiltrate in the presence but not in the absence of TNC (Fig EV4A–G).

We considered that in the 4-week model, the full effect of AMD may not have developed yet; therefore, we used other AMD treatment protocols (Azab *et al.*, 2009; Domanska *et al.*, 2012; Fig EV2). In the 7-week model, we observed a reduced tumor weight in AMD-treated mice, indicating that inhibition of CXCR4 reduced tumor growth (Fig 5A). In accordance, we observed more apoptosis (quantification of the cl. casp3 staining signal) in the tumors upon CXCR4 inhibition (Fig 5B and C). Next, we addressed CD8 TIL tumor

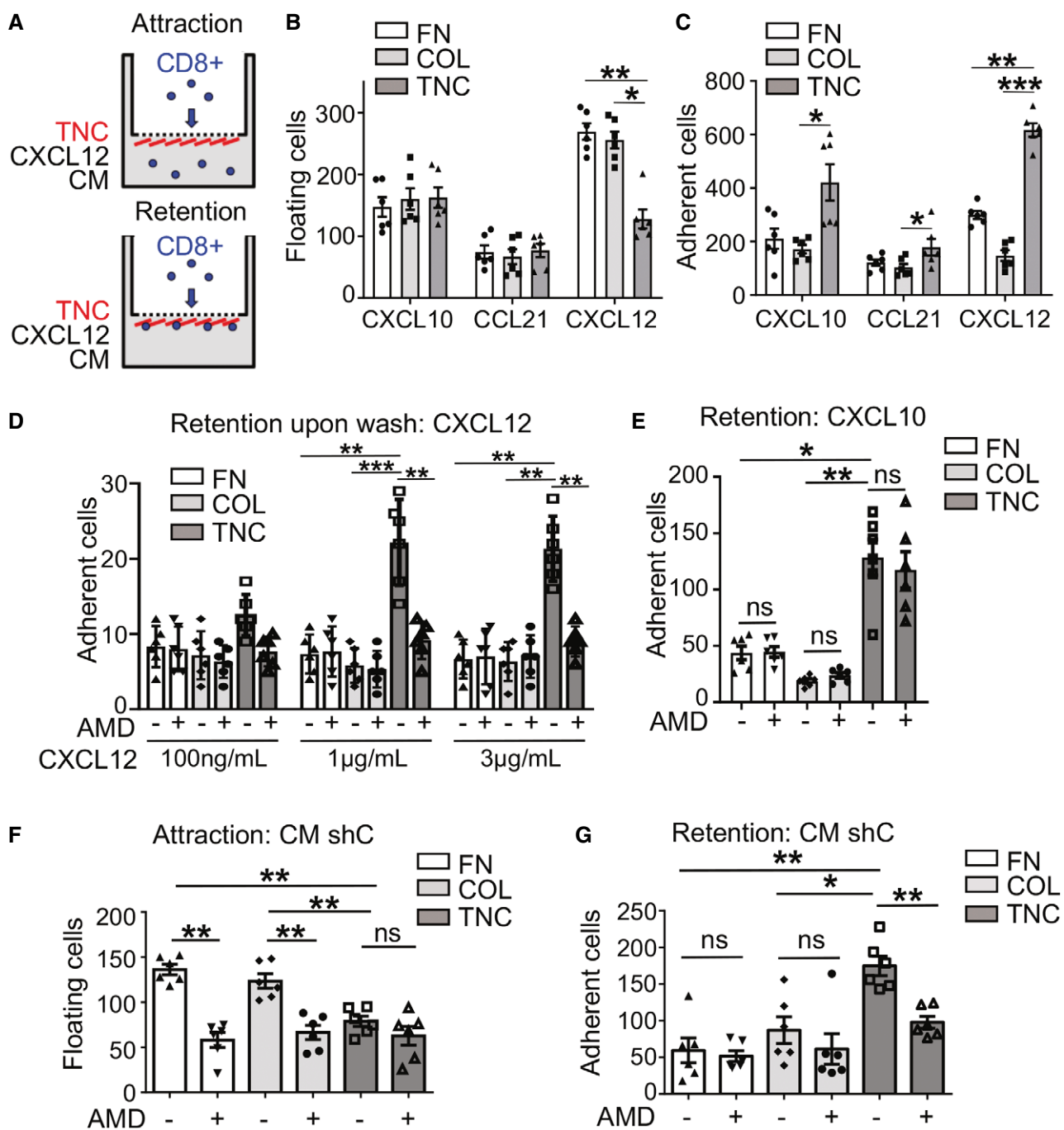


Figure 4. Chemoattraction of CD8 T leukocytes by TNC and CXCL12.

A Boyden chamber experiment to measure attraction and retention of CD8 T cells toward factors in the lower chamber. Cells in the lower chamber were measured by flow cytometry (attraction) or on the matrix coatings (retention) by counting Dapi-stained nuclei 5 h after plating.

B–G Attraction (B, F) and retention (C, D, E, G) were determined toward coatings with collagen I (COL), fibronectin (FN), or TNC in the presence of CXCL10, CCL21, CXCL12 (B, C), CXCL10 (E), or CM from shC cells (CM:shC) and upon AMD3100 (AMD, 5 µg/ml) (D–G). (D) CXCL12 (indicated concentrations) was added overnight at 4°C during the coating followed by washing (2 times with PBS) and plating CD8 T cells for 5 h before fixation and counting Dapi-stained nuclei. Three independent experiments in duplicates, Mann–Whitney test, ns > 0.05; *P < 0.05; **P < 0.01; ***P < 0.005. Mean ± SEM.

Source data are available online for this figure.

infiltration by tissue staining and observed more CD8 TIL in AMD-treated tumors (Fig 5D and E) that likely were active as *Gzmb* and *IFN γ* levels were higher upon CXCR4 inhibition (Figs 5F and EV4H).

To rule out other factors, by qRT–PCR, we determined *Cxcl12*, *Cxcr4*, and *Cxcr7* expression and did not see differences between PBS- and AMD-treated groups (Fig EV4I–K).

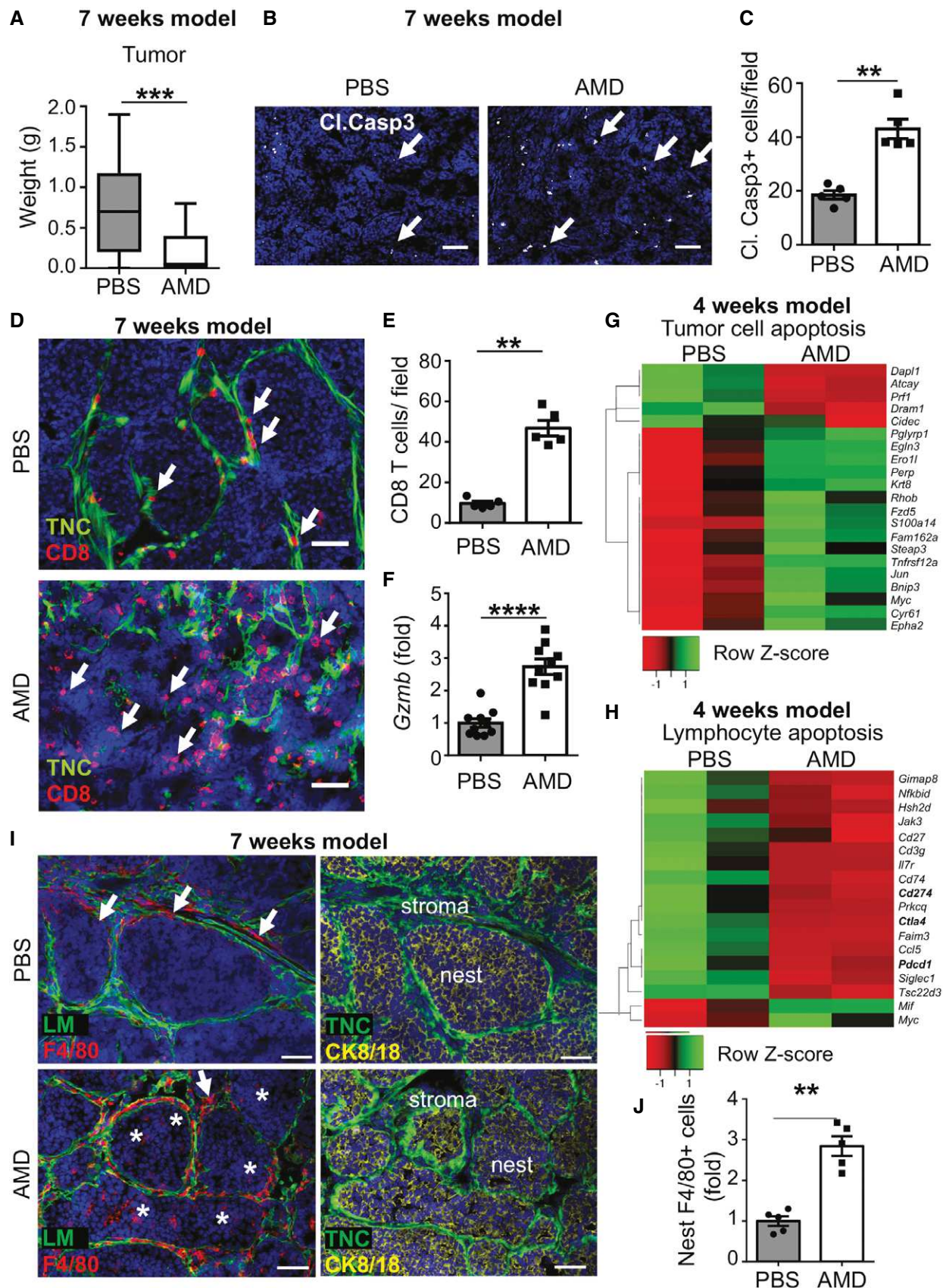


Figure 5.

Figure 5. Inhibition of CXCR4 induces infiltration of CD8 leukocytes and macrophages and reduces tumor cell death and tumor growth (7-week model).

A Growth of TNC-high (WT/shC) tumors upon cell engraftment and 5 weeks AMD treatment. $N = 20$ tumors per condition, $***P = 0.0007$, unpaired *t*-test. The central band represents the median, the ends of the box the first and the third quartiles, and the whiskers reach from each quartile to the minimum or maximum.

B, C Imaging and signal quantification upon staining for cl. casp3 and DAPI in PBS- and AMD-treated tumors, $N = 5$ tumors per condition, 2 sections per tumor, 5 random fields, $**P = 0.0079$, Mann–Whitney test. Mean \pm SEM. Scale bar, 50 μ m, arrows point at cl. Casp3.

D, E CD8 TIL abundance and localization in PBS- and AMD-treated tumors, arrow points at CD8 TIL, scale bar, 50 μ m (D). (E) Quantification of CD8 T cells per randomly chosen fields. $N = 5$ tumors per condition, 2 sections per tumor, 5 random fields, $**P = 0.0079$, Mann–Whitney test. Mean \pm SEM.

F *Gzmb* levels in PBS- and AMD-treated tumors. $N = 10$ tumors, $****P < 0.0001$, unpaired *t*-test. Mean \pm SEM.

G, H Heatmap of tumor cell apoptosis-associated (G) and lymphocyte apoptosis-associated (H) genes differentially expressed in PBS- and AMD-treated TNC-high (WT/shC) tumors, $N = 2$.

I, J Abundance and quantification of F4/80 $^{+}$ macrophages in PBS- and AMD-treated tumors, (I) staining for the indicated molecules, (arrow, macrophages in the stroma; asterisk, macrophages in the tumor nest), (J) quantification of F4/80 $^{+}$ cells inside the tumor nest. $N = 5$ tumors per condition, 2 sections per tumor, 5 random fields, $**P = 0.0079$, Mann–Whitney test. Mean \pm SEM. Scale bar, 50 μ m.

Source data are available online for this figure.

To gain more insight into the underlying mechanisms, we compared gene expression in PBS with AMD-treated conditions (TNC-high) in the 4-week model, by RNA-seq analysis, and noticed profound differences between the groups. 1,287 genes were deregulated with 269 up- and 1,018 downregulated upon CXCR4 inhibition (Appendix Table S3). The large majority of genes in a signature associated with tumor cell apoptosis were upregulated upon AMD treatment (Fig 5G). In contrast, signatures associated with angiogenesis, lymphocyte apoptosis, immune suppression, and IL10 production and response were downregulated upon CXCR4 inhibition in comparison to the PBS control (Figs 5H and EV5A–E). Also, CD8 T cell inhibitory *Pdcd-1*, *Cd274*, and *Ctla4* were reduced upon AMD treatment (Figs 5H and EV5D). As TNC impacted expression of *Cd274*, we investigated gene expression with inhibitors as described (Fig 3E) and found that *Cd274* was reduced in the tumor cells with the TLR4 inhibitor Cli95 yet not with the other inhibitors (Fig EV5F). Moreover, upon CXCR4 inhibition, several genes regulating lymphocyte differentiation, T cell activation, and IFN γ production were deregulated mimicking gene expression of tumors with low TNC (WT/shTNC) (1,753 deregulated genes, 470 up- and 1,283 downregulated), altogether suggesting that immunity is largely regulated by CXCR4 signaling in these tumors in a TNC-dependent manner (Fig EV5D and E, Appendix Table S4).

As we had previously seen that TNC promoted an M2 macrophage phenotype (Deligne *et al*, 2020), we wondered whether CXCR4 inhibition potentially impacted macrophages. By staining of TNC-high tumor tissue from the 7-week model for F4/80, we observed more activated macrophages upon AMD treatment compared to PBS. More importantly, largely present in control tumors, macrophages were even more abundant upon CXCR4 inhibition, now clearly infiltrating the tumor nests (Figs 5I and J, and EV5G). By tissue staining for CD206, we confirmed M2 macrophage infiltration of TNC-high tumors (Deligne *et al*, 2020) which we noticed to be abolished with AMD as no M2 macrophages were detectable anymore (Fig EV5H).

Thus, we conclude that TNC plays an important role in regulating macrophages and CD8 TIL through CXCL12/CXCR4 signaling thereby impairing tumor cell killing and promoting tumor growth.

Impact of CXCR4 inhibition on lung metastasis

As CXCR4 signaling is known to promote cell migration and metastasis (Chatterjee *et al*, 2014), we investigated whether CXCR4 inhibition by AMD had an effect on lung metastasis in the spontaneous NeuNT and grafting NT193 models, respectively, as detailed in Fig 6A, D, and H. Due to variable latency and multi-focal tumor

Figure 6. Impact of CXCR4 inhibition on lung metastasis.

A Schematic depiction of the AMD treatment protocol before sacrifice and analysis of the lungs. Intraperitoneal (ip) injection of 5 mg/kg/day AMD into NeuNT mice (daily for 2 weeks, week 27–29).

B IF tissue staining identifying blood vessel invasions (BVI), surrounded by an EC monolayer (arrow) and expanded EC (asterisk), scale bar, 50 μ m.

C Quantification of BVI with normal (EC monolayer) and aberrant (expanded EC) phenotype expressed as ratio. $N = 5$ mice (PBS), $n = 3$ sections, $n = 15$ BVI, $n = 7$ PM (parenchymal metastasis); $N = 5$ mice (AMD), $n = 3$ sections, $n = 12$ BVI, $n = 2$ PM, $****P < 0.0001$, Fisher's exact test.

D Schematic depiction of the AMD treatment protocol before sacrifice and analysis of the lungs. Tail vein (iv) tumor cell-engrafted mice (WT/shC, WT/shTNC) were ip injected (daily for one week, week 4–5) with AMD 7.5 mg/kg/day. Metastasis assessment in the 5 weeks iv orthotopic grafting model (D–G).

E Ratio of mice with and without lung metastasis determined by H&E tissue staining. $N = 8$ mice (shC, PBS), $N = 7$ mice (shC, AMD), $N = 7$ mice (shTNC, PBS), $N = 7$ mice (shTNC, AMD). $P < 0.0001$, chi-square test. Fisher's exact test was used to compare the conditions pairwise $*P < 0.05$, $**P < 0.001$, $P = 0.0109$ (shC/PBS versus shTNC/PBS), $P = 0.0001$ (shC/AMD versus shTNC/AMD).

F, G Ratio of BVI and PM in lungs from shC-engrafted (F) and shTNC-engrafted (G) mice. $N = 8$ mice (shC, PBS), $n = 4$ BVI, $n = 13$ PM; $N = 7$ mice (shC, AMD), $n = 15$ BVI, $n = 21$ PM; $N = 7$ mice (shTNC, PBS), $n = 8$ BVI, $n = 9$ PM; $N = 7$ mice (shTNC, AMD). $N = 5$ BVI, $n = 1$ PM, $***P < 0.001$, $****P < 0.0001$. $P = 0.0009$ (shC/PBS versus shC/AMD) and $P = 0.0001$ (shTNC/PBS versus shTNC/AMD), Fisher's exact test.

H Schematic depiction of the AMD treatment protocol before sacrifice and analysis of the lungs. Mice with mammary gland (MG)-engrafted tumor cells (WT/shC) were daily injected peritumorally (pt) for 5 weeks with 5 mg/kg/day (week 2–7). Metastasis assessment in the 7 weeks orthotopic grafting model (H–L).

I–L qRT–PCR assessment of *Neu* (I), *Cd8a* (J), *Ifn γ* (K), and *Gzmb* (L) by qRT–PCR. PBS-treated ($N = 16$) and AMD-treated ($N = 19$) mice, $*P = 0.0364$, Mann–Whitney test (I), $**P = 0.0086$ unpaired *t*-test (J), $**P = 0.0055$, unpaired *t*-test (K), $***P = 0.0003$ unpaired *t*-test (L), respectively. The central band represents the median, the ends of the box the first and the third quartiles, and the whiskers reach from each quartile to the minimum or maximum.

Source data are available online for this figure.

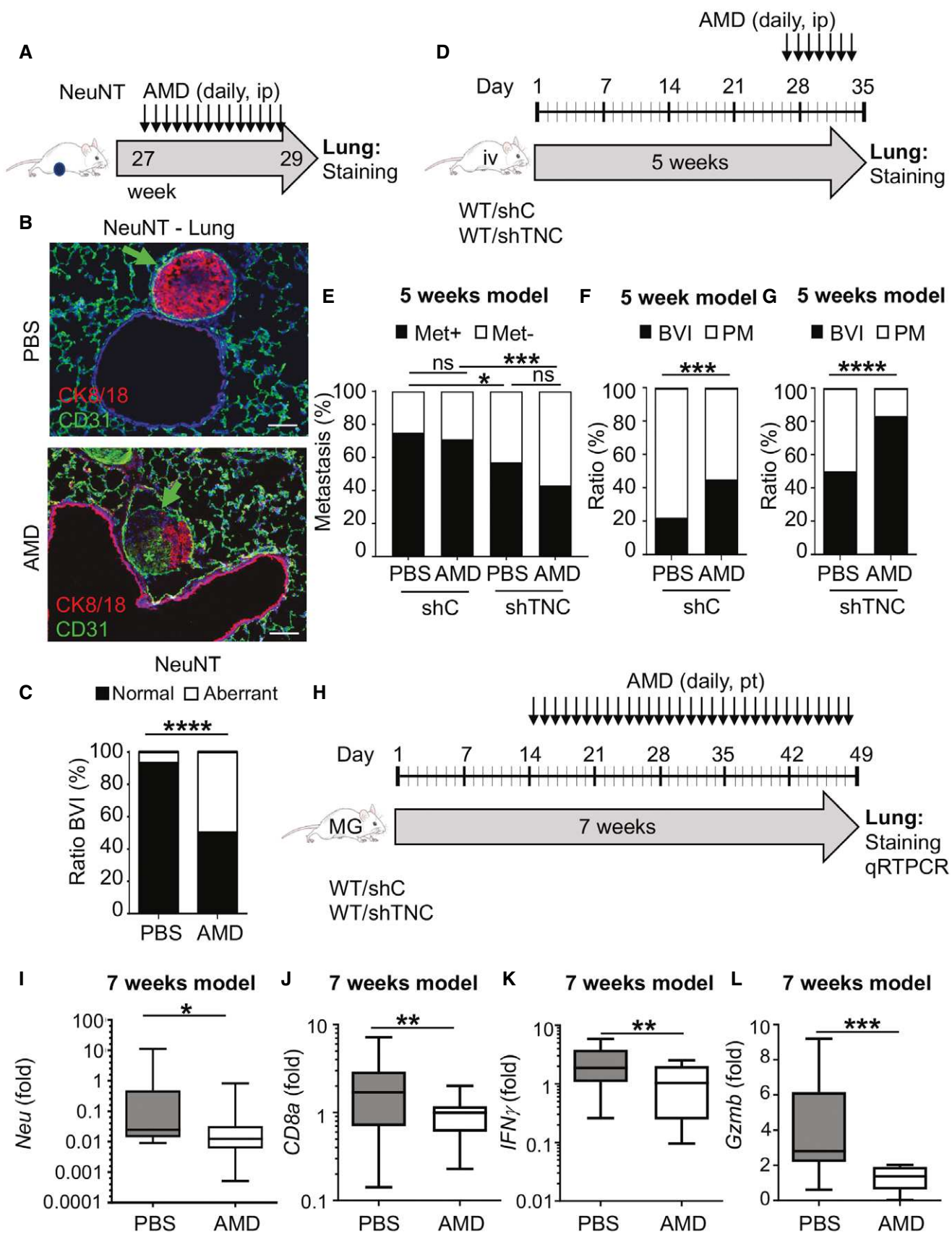


Figure 6.

onset, the NeuNT model is poorly suitable for general metastasis assessment. However, upon AMD treatment, we noticed differences in the phenotype of blood vessel invasions (BVI), important precursors of parenchymal metastasis in this model (Fig 6B; Siegel *et al*, 2003; Sun *et al*, 2019). Whereas tumor cells were surrounded by an endothelial cell (EC) monolayer in BVI of PBS-treated mice (like in untreated mice; Sun *et al*, 2019), we noticed a prominent EC expansion in the BVI of AMD-treated mice which may impact progression into parenchymal metastasis (Fig 6B and C, Appendix Fig S4A and B; Sun *et al*, 2019).

To address a potential role of CXCR4 signaling on homing and tumor outgrowth in the NT193 model, we engrafted shC or shTNC cells via tail vein (iv) injection into a WT host followed by a daily AMD treatment for one week as previously described (Yang *et al*, 2019) (5-week model, Fig 6D). By a stereological approach, we assessed lung metastasis (Saupe *et al*, 2013) and observed that the majority of shC-engrafted mice got metastases, however with no impact of AMD. In contrast, engrafted shTNC cells caused less metastases which again was not affected by AMD, supporting a potential role of TNC in tumor cell homing to the lung as previously described for another model (Fig 6E; Oskarsson *et al*, 2011). We further found that the number and size of metastases was not different in the TNC-high condition (Appendix Fig S4C and D). Moreover, we noticed prominent round structures with flat nuclei at the rim (representing EC), reminiscent of blood vessel invasions (BVI) in the lungs of iv tumor cell-engrafted mice (similar to the orthotopic grafting condition (Sun *et al*, 2019)) (Appendix Fig S4E). Upon CXCR4 inhibition, BVI were more abundant in TNC-high conditions in expense of parenchymal metastasis (PM) (in comparison to PBS controls) (Fig 6F). The PM/BVI ratio was even further reduced upon AMD treatment in the TNC-low (WT/shTNC) condition suggesting a stronger effect of CXCR4 inhibition in the absence of TNC (Fig 6G). These results show that CXCR4 inhibition impacts BVI potentially delaying parenchymal metastasis.

Next, we used the 7-week model where mice with shC orthotopically engrafted tumor cells were treated with AMD for 5 weeks according to established protocols (Azab *et al*, 2009, Domanska *et al*, 2012; Fig 6H). We had observed a clear effect of AMD on tumor growth inhibition that may have an effect on lung metastasis; therefore, we examined the abundance of tumor cells in the lungs. As we could not detect tumor cells by tissue staining at this early time point, we used qRT-PCR for *Neu* which revealed expression in PBS controls that was lower upon CXCR4 inhibition, indicative of less tumor cells in the lung (Fig 6I). We considered that tumor cells invading the lung may elicit an immune response as seen (Fig 2I);

therefore, we used qRT-PCR to determine expression of *Cd8*, *Ifn γ* , and *Gzmb* that was indeed seen in PBS conditions, however with lower levels upon CXCR4 inhibition potentially reflecting less tumor cells in the lungs (Fig 6J-L).

Altogether, these results suggest that reduced metastasis is likely due to a major impact of CXCR4 inhibition on tumor growth.

Combined abundance of CD8 TIL and high TNC and CXCL12 expression correlate with worsened breast cancer patient survival

To address whether the results from the murine tumor models are relevant in human breast cancer, we stained a human breast cancer tissue microarray (Chen *et al*, 2010, 2011) for TNC and CD8. We used a limited dilution approach for TNC that allowed to discriminate between tumors expressing high (TNC $^+$) and low TNC (TNC $^-$) levels, respectively (Fig 7A, Appendix Fig S5A and B). TNC $^-$ and TNC $^+$ groups almost equally distributed between breast cancer subtypes except for Her2 $^+$ breast cancer specimens where the TNC $^+$ phenotype was more prominent (41%) than the TNC $^-$ phenotype (29%) (Table 1). Moreover, CD8 TIL were more abundant in TNC $^-$ tumors which was pronounced in basal-like cases (Fig 7B, Appendix Fig S5C). A closer investigation of CD8 TIL distribution showed that in both tumors (TNC $^-$ and TNC $^+$) CD8 TIL were more abundant in the stroma than in the nests, which applied to all three (Her2 $^+$, basal, and luminal) subtypes (Appendix Fig S5D-G, Table 2). However, the ratio of nest-to-stroma CD8 TIL was lower in TNC $^+$ than in TNC $^-$ tumors (Fig 7C). Also in TNC $^+$ tumors, nest infiltration of CD8 TIL was lower than in TNC $^-$ tumors supporting that TNC may play a role in retaining CD8 TIL in the stroma (Appendix Fig S5H and I).

Next, we asked whether TNC expression and CD8 TIL abundance potentially had an impact on patient survival. By Kaplan-Meier analysis of the TMA cohort, we first observed that high TNC levels (above the median) correlated with shorter metastasis-free survival (MFS) as previously seen in other patient cohorts (Fig 7D; Minn *et al*, 2005; Oskarsson *et al*, 2011). Importantly, higher CD8 TIL levels were seen in patients with longer MFS (Fig 7E). However, the survival benefit of high CD8 TIL seemed to be abolished when TNC levels were also high (Fig 7F). In CD8 $^-$ tumors, TNC levels did not correlate with survival (Appendix Fig S5J). High or low abundance of CD8 TIL in the tumor nest also showed no difference in MFS (Appendix Fig S5K). In contrast, stromal CD8 TIL abundance and TNC levels, CD8 $^+$ /TNC $^-$, correlated with longest MFS whereas CD8 $^+$ /TNC $^+$ and CD8 $^-$ conditions correlated with shorter MFS (Fig 7G, Appendix Fig S5J and K).

Figure 7. TNC expression, abundance, and localization of CD8 TIL in breast tumors and survival of human breast cancer patients.

A-C Adjacent human breast cancer tissue microarray (TMA) sections were stained with the indicated antibodies, scale bar, 50 μ m, arrows point at CD8 TIL (A), and CD8 TIL were counted per field (B), or in the stroma and nest, respectively (C), $N = 103$ TNC $^+$ tumors, $N = 116$ TNC $^-$ tumors. (B) ** $P = 0.0055$, Fisher's exact test. The central band represents the median, the ends of the box the first and the third quartiles, and the whiskers reach from each quartile to the minimum or maximum. (C) ** $P = 0.0055$, Mann-Whitney test.

D-G Kaplan-Meier analysis to address correlation of TNC expression (D), total numbers of CD8 TIL (E), combined high (above median) CD8 TIL and high or low (above/below median) TNC (F) and stromal CD8 cells (G) with metastasis-free survival (MFS) of breast cancer patients. Stromal CD8 $^-$ or CD8 $^+$ is defined as below or above median stromal CD8 TIL per area. Log-rank test.

H, I Correlation of TNC and CD8 α levels with overall survival (OS) using survival analysis on breast cancer patient cohort GSE 19783-GPL6580. Hazard ratio (HR) and p values are indicated in Appendix Fig S5N. Log-rank test.

Source data are available online for this figure.

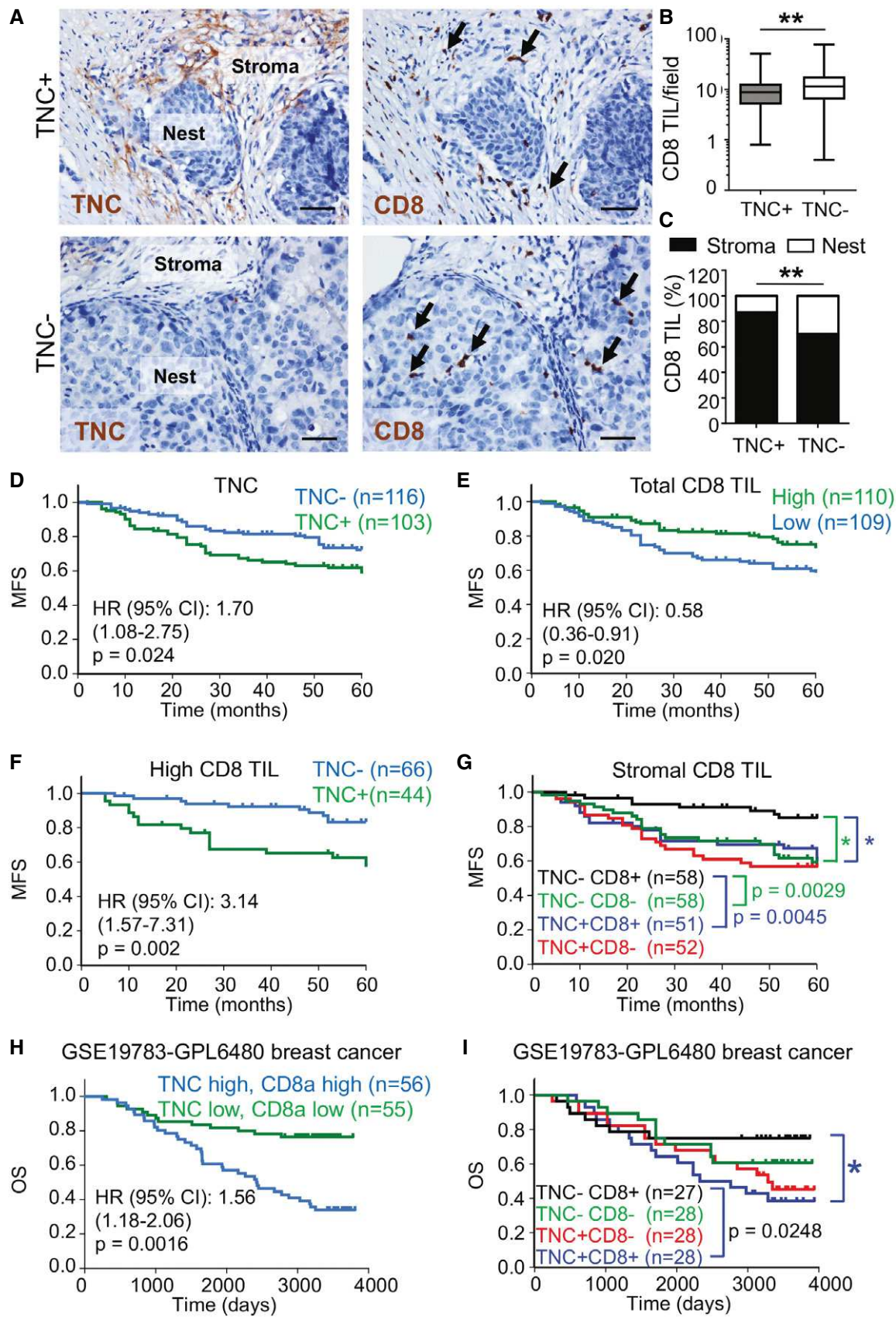


Figure 7.

Table 1. Comparison of TNC expression with clinicopathological characteristics in breast cancer patients.

Parameter	TNC ⁻ patients (n = 116) (%)	TNC ⁺ patients (n = 103) (%)	P value
MFS (months), mean (95% CI)	51.5 (48.5–54.5)	45.1 (41.0–49.1)	0.024*
Age (year), median (range)	47 (31–75)	48 (29–76)	
< 50	56 (60.2)	80 (63.5)	0.570
≥ 50	37 (39.8)	46 (36.5)	
Molecular type: n (%)			
Luminal	55 (47.4)	40 (38.8)	0.202
Her-2 ⁺	34 (29.3)	42 (40.8)	
Basal-like	27 (23.3)	21 (20.4)	
TNM stage: n (%)			
TNM 1	7 (6.1)	5 (4.9)	0.738
TNM 2	76 (65.5)	64 (62.1)	
TNM 3	33 (28.4)	34 (33.0)	
Histological grade: n (%)			
Well-differentiated	16 (13.8)	18 (17.5)	0.571
Moderately differentiated	71 (61.2)	56 (54.4)	
Poorly/undifferentiated	29 (25.0)	29 (28.2)	
Pathological type: n (%)			
Invasive ductal cancer	78 (67.2)	83 (80.6)	0.052
Invasive lobular cancer	16 (13.8)	7 (6.8)	
Mixture	16 (13.8)	4 (3.9)	
Others	6 (5.2)	9 (8.8)	
Neoadjuvant chemotherapy: n (%)			
Yes	68 (58.6)	54 (52.4)	0.357
No	48 (41.4)	49 (47.6)	

Comparisons of variables in the TMA cohort (Chen *et al*, 2010, 2011) were performed by using the chi-square test.

*MFS (metastasis-free survival) was analyzed by log-rank test.

In the well-studied breast cancer patient cohort GSE 19783-GPL6580 representing all subtypes (Enerly *et al*, 2011), high TNC levels (above the median) and combined high TNC and high CD8

Table 2. Comparison of TNC expression with CD8 and CXCL12 expression in breast cancer patients.

Parameter	TNC ⁻ patients (n = 116) (%)	TNC ⁺ patients (n = 103) (%)	P value
CD8 ⁺ Leukocytes: n (%)			
< 9.4	50 (43.1)	59 (57.3)	0.036
≥ 9.4	66 (56.9)	44 (42.7)	
Nest CD8 ⁺ Leukocytes: n (%)			
< 1.7	36 (31.0)	74 (71.8)	< 0.001
≥ 1.7	80 (69.0)	29 (28.2)	
Stromal CD8 ⁺ Leukocytes: n (%)			
< 7.6	58 (50.0)	52 (50.5)	0.943
≥ 7.6	58 (50.0)	51 (49.5)	
CXCL12: n (%)			
Low	63 (54.3)	46 (44.7)	0.154
High	53 (45.7)	57 (55.3)	

Numbers of CD8 T leukocytes and expression of CXCL12 in the TMA cohort (Chen *et al*, 2010, 2011) was determined on two separate sections per tumor using the median value. Comparison of variables by using the chi-square test.

TIL correlated with shorter overall survival (Fig 7H and I, Appendix Fig S5L). Moreover, a combined high expression of TNC together with either high CD8 α (HR 1.56) or CD8 β (HR 1.57), GZMB (HR 1.52), IFN γ (HR 1.76), and Perforin (HR 1.75), respectively, correlated with a shorter overall survival and stronger power than TNC alone (HR 1.37) suggesting that stromal CD8 TIL tethering by TNC may be more important than CD8 TIL activation which does not seem to be linked to TNC (Appendix Fig S5N–U).

Next we stained the breast cancer TMA for CXCL12 and observed similar staining patterns as reported (Toullec *et al*, 2010; Lefort *et al*, 2017). We discriminated 4 staining intensities with no or low CXCL12 and high CXCL12 in tumor nests only, or combined high expression in tumor nest and stroma (Fig 8A). As in the grafting model, CXCL12 showed a punctate expression in the stroma (Fig 8A). As previously done, we combined intensity and abundance of CXCL12 expression in the so-called Hscore (Lefort *et al*, 2017) that we then used to assess whether CXCL12 expression is correlated with TNC levels. Indeed, TNC⁺ tumors had a higher CXCL12 Hscore than TNC⁻ tumors (Fig 8B). The CXCL12 Hscore was similar in the different tumor subtypes (Appendix Fig S6A, Table 2). More detailed analysis revealed that the CXCL12 Hscore was higher when TNC and CD8 TIL were abundant (Fig 8C).

Figure 8. CXCL12 expression in human breast cancer and patient survival.

A Representative IHC images of CXCL12 intensity and staining pattern in the TMA. N = 219 tumors. Upper panel, scale bar, 400 μ m; lower panel, scale bar, 100 μ m. Arrows point at punctate staining in the stroma.

B, C Histological score of CXCL12 staining in TNC⁺ and TNC⁻ tumors in combination with CD8⁺ (above median) and CD8⁻ (below the median). *P = 0.0206, **P = 0.0040, unpaired t-test. The central band represents the median, the ends of the box the first and the third quartiles, and the whiskers reach from each quartile to the minimum or maximum.

D Kaplan–Meier survival analysis of breast cancer patients upon stratification into tumors with a CXCL12 Hscore below or above the median, P = 0.002. Mann–Whitney test.

E Survival analysis of breast cancer patients in the GSE 19783-GPL6580 cohort upon stratification into tumors with high or low expression of TNC and CXCL12. Log-rank test. HR and P values are indicated, see also Appendix Fig S6B.

Source data are available online for this figure.

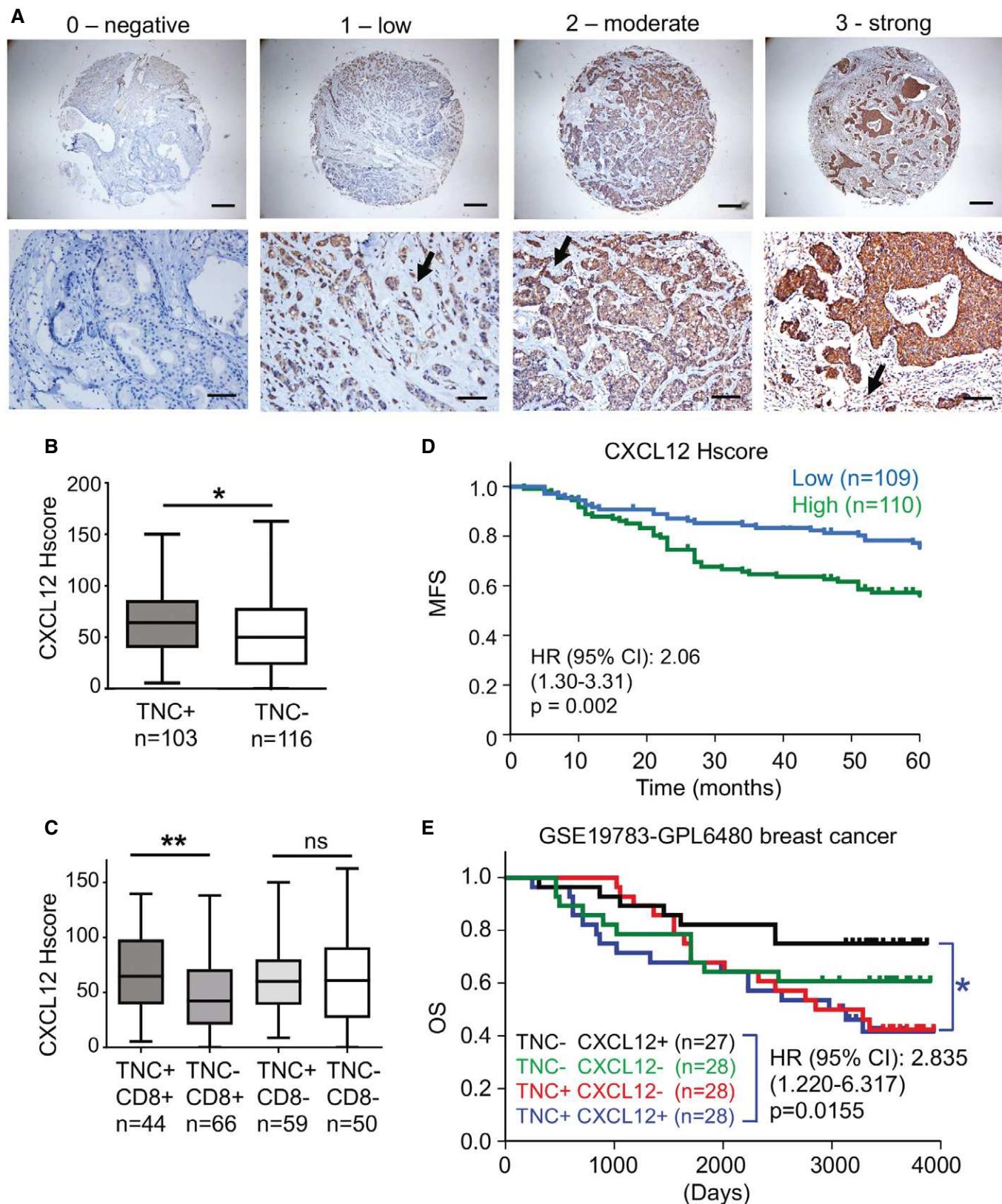


Figure 8.

Moreover, high TNC correlated with shorter overall survival when CXCL12 levels were high or the CXCL12 Hscore was above the median, whereas the TNC level was not prognostic in patients with tumors that had CXCL12 levels below the median (Fig 8D and E, Appendix Fig S6B).

Altogether, our results suggest that TNC regulates macrophages and CD8 TIL involving their positioning inside the stroma. By upregulating CXCL12 through TLR4 and binding to CXCL12, we showed that TNC generates stromal niches that attract and immobilize CD8 TIL. Subsequently, CD8 TIL may be impaired in reaching and killing the tumor cells, contributing to the well-known immune exclusion phenotype (Fig 9, Galon & Bruni, 2019). Here we showed that high CD8 TIL in the TNC stroma and combined high TNC and CXCL12 expression are parameters that define the immune exclusion phenotype which correlates with shorter survival of breast cancer patients

that could have therapeutic value as seen in the preclinical models upon CXCR4 inhibition (Fig 9).

Discussion

Tumors are complex ecosystems where the matrix is an instrumental component not only providing architectural but also signaling cues to cells (Lu *et al*, 2012; Pickup *et al*, 2014). In particular, the matrix molecule TNC that is highly abundant in (breast) cancers plays an instructive role in many steps during cancer progression including regulation of tumor immunity (Jachetti *et al*, 2015; Midwood *et al*, 2016; Deligne *et al*, 2020; Spenlé *et al*, 2020).

We revealed a novel mechanism of CD8 T cell impairment by TNC, retaining CD8 TIL inside the tumor stroma. We showed that

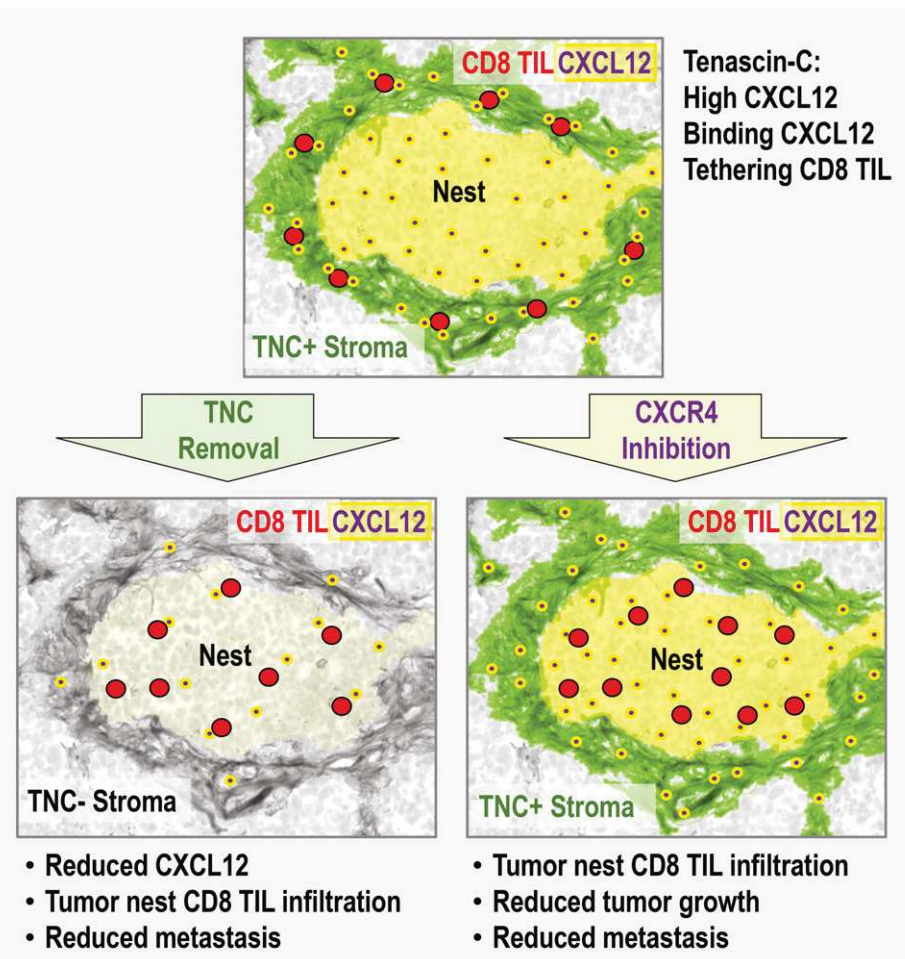


Figure 9. “TIL-matrix-release-and-reactivate” strategy through targeting TNC and CXCR4.

TNC contributes to an immune suppressive TME in breast cancer by retaining CD8 TIL in the stroma. TNC induces CXCL12 in a TLR4-dependent manner. The TNC protein binds CXCL12 generating a substratum that tethers CD8 TIL in the stroma thus preventing infiltration of CD8 TIL into the tumor nests and subsequent tumor cell killing. This mechanism could be relevant in human breast cancer as patients with tumors of high TNC expression show high CD8 TIL in the (TNC-rich) stroma which correlates with shorter MFS. (Lower left) Upon removal of TNC anti-tumor immunity is activated and characterized by lower CXCL12 expression, higher CD8 TIL nest infiltration, and a reduced metastasis rate as previously shown (Sun *et al*, 2019). In human breast cancer, low TNC and high CD8 TIL correlate with longest MFS. (Lower right) TNC impacts CD8 TIL through CXCL12/CXCR4. Inhibition of CXCR4 led to increased CD8 TIL infiltration, higher tumor cell apoptosis, and reduced tumor growth and subsequent lung metastasis. Also macrophages, loosing their M2 phenotype, infiltrate the tumor nests more numerous contributing to the observed activated CD8 TIL phenotype (e.g., less PD-L1, CTLA4). Targeting TNC and CXCL12 could direct a novel “TIL-matrix-release-and-reactivate” strategy to improve ICT in breast cancer.

TNC regulates CXCL12 expression through TLR4. We further showed that as in the murine model also in human breast cancer CXCL12 is predominantly expressed by the tumor cells. However, CXCL12 was also but less expressed by stromal cells presumably fibroblasts as seen in a murine pancreatic cancer model (Feig *et al*, 2013). Most importantly, we described that CXCL12 binds to TNC and turns the TNC matrix normally poorly adhesive for T cells (Hauzenberger *et al*, 1999; Huang *et al*, 2001), into a substratum that retains CD8 TIL in the TNC-rich stroma. This mechanism seems to be relevant in human breast cancer as high TNC and high stromal CD8 TIL correlate with shorter MFS. High CXCL12 levels, potentially acting as protective shield toward CD8 TIL (by an unknown mechanism) (Vianello *et al*, 2006; Guyon, 2014), may even further potentiate CD8 TIL exclusion from the tumor nest. We have shown that inhibition of CXCR4 releases the matrix-retained, now active CD8 TIL (as *Ifny* and *Gzmb* expression was elevated) to infiltrate the tumor tissue thus increasing tumor cell death and reducing tumor growth and subsequently metastasis. This mechanism could be clinically relevant as combined high TNC and high CXCL12 correlated with shortest MFS.

CXCR4 signaling is active in many cell types (Döring *et al*, 2014); thus, it is possible that CXCR4 inhibition also affects, for example, other immune subtypes or the vasculature. In support by RNA-seq analysis, we observed a reduced angiogenesis-associated gene signature and an aberrant EC phenotype in BVI upon AMD treatment. CXCR4 inhibition also increased the number and infiltration of activated macrophages whereas tumor-promoting M2 macrophages disappeared. Moreover, CXCR4 inhibition reduced expression of immune suppressive IL10-production/IL-10 response-associated genes and CD8 T cell inhibitory CTLA4, PD-L1, and PD1, altogether presumably boosting CD8 TIL. However, our results propose that tumor cell-directed cytotoxicity may only be accomplished upon release of the CD8 TIL from the matrix where TNC binding CXCL12 could be crucial and exploitable for therapy. It is conceivable that targeting matrix potentiates ICT. This is supported by published work showing that blocking the TLR4/TNC interaction increased the anti-PD-L1 effects on metastasis inhibition (Deligne *et al*, 2020) and that combined treatment of anti-PD-L1 with AMD increased TIL infiltration reducing tumor growth in a pancreatic tumor model (Feig *et al*, 2013).

Previously, the so-called immunoscore, reflecting the abundance of CTL and memory T cells in the tumor cell nest or in the stroma, was identified as a better predictive tool for survival of colorectal carcinoma patients than the TNM classification (Galon *et al*, 2006; Galon *et al*, 2012). No information about a potential link to TNC or any other matrix was provided. It was also not known whether the immunoscore would also be a predictive tool in breast cancer. Here, we have shown that CD8 TIL immune exclusion in TNC-rich stroma correlates with worsened prognosis and identified novel parameters for stratification of breast cancer patients, irrespective of subtype, likely to benefit from ICT. Our results predict that patients with tumors of high levels of CD8 TIL, TNC, and CXCL12 (detectable at mRNA and protein tissue level), correlating with short MFS, may benefit from ICT in combination with CXCR4 inhibition.

Indeed, clinical trials targeting CXCR4 in cancer patients with different drugs alone or in combination with ICT are ongoing (NCT02104427, NCT01359657). A combination of the CXCR4 antagonist X4P-001 in combination with Pembrolizumab reactivating CD8

TIL (Emancipator, 2020) demonstrated a clinical response in patients with advanced melanoma (phase 1b trial, NCT02823405). Interestingly, the improved response was associated with an increased CD8 TIL density in the tumor center.

Altogether, our results propose that releasing CD8 TIL from the tumor matrix may be an important factor to empower ICT, where targeting matrix-regulated CXCR4 signaling is worth to be further explored. RNA gene expression results from our novel immune competent breast cancer model provides several molecular indicators such as TNC and CXCL12 to direct a future combined “TIL-matrix-release-and-reactivate” strategy for improving ICT in breast cancer.

Material and Methods

The experiments conformed to the principles set out in the WMA Declaration of Helsinki and the Department of Health and Human Services Belmont Report. More detailed information can be found in the Appendix Supplementary Information section.

Immunohistochemical analysis of human breast tumors

Paraffin-embedded tissue microarrays (TMA with 219 specimens with invasive breast cancer, Hubei Cancer Hospital, China, Chen *et al*, 2010; Chen *et al*, 2011) were used for hematoxylin/eosin (H&E) and antibody staining for TNC (Abcam, ab2074, 1/500), CXCL12 (Abcam, ab9797, 1/200) and CD8 (DAKO, C8/144B) (Tables 1 and 2). Informed consent was obtained from each patient and the study was approved by the hospital’s Ethics Committee. Slides were independently investigated blinded by two investigators. Duplicates were counted and the average signal count per slide was used for statistical analysis. The expression of TNC was scored according to the staining intensity and the proportion of positive stromal cells in the whole slide per tissue sample (Yang *et al*, 2017). CXCL12 expression is expressed as histological score (Hscore) (Lefort *et al*, 2017). CD8-stained cells were counted in five representative pictures (20 fields) according to placement in tumor nest or stroma. Numbers were determined as high or low using the median value as cutoff.

Patient survival analysis

The survival data for GSE19783-GPL6480 (Enerly *et al*, 2011) were obtained from and analyzed by a web application (<http://genomics.jefferson.edu/proggene/index.php>) as described elsewhere (Goswami & Nakshatri, 2013). Hazard ratio above or below 1 within a confidence interval of 95% (HR, 95% CI), and *P* values were determined using the log-rank test.

Experimental mice and study design

MMTV-NeuNT female mice in FVB/NCrl (WT or TNCKO background; more than 10 backcrosses into FVB (Sun *et al*, 2019)) were bred in parallel from heterozygous parents. Mice were housed and used according to the guidelines of INSERM and the ethical committee of Alsace, France (CREMEAS), and agreement number D 67-482-033 at the animal facilities of INSERM U682 and U1109 under pathogen-free conditions in cages providing disposable homes and

nesting paper, together with food and water at discretion. Before begin of the experiment, female mice (8–10 weeks of age) were acclimatized in the procedure room for at least two weeks and were daily checked for good health and welfare throughout the whole experiment (including posture and activity). Experimental groups consisted of at least 5 mice per time point and per genotype. Cages with experimental mice were placed in random order, which was then used throughout the experiment. Upon sedation with 4% isoflurane (Isoflurin® 1,000 mg/g, Axience), female WT or TNCKO FVB mice were grafted with 1×10^7 NT193 cells (shC, *Tnc* knock-down (sh1TNC, sh2TNC; Sun *et al*, 2019) in the surgically opened left fourth mammary gland that was surgically closed afterward. For most experiments, sh2TNC cells were used and defined as “shTNC” if not further specified. Tumor growth was assessed by measuring the tumor size, and tumor volume was determined using the following calculation $V = (\text{width})^2 \times \text{length}/2$. Tumor-bearing mice (or mice with iv engrafted tumor cells) were daily treated with AMD3100 (Sigma, A5602) at 5 mg/kg or PBS as control by peritumoral (pt) injection (4- and 7-week model), intraperitoneal injection (ip) (NeuNT model), or at 7.5 mg/kg ip injection (5-week model). Mice were euthanized by cervical dislocation. Tumors and lungs were processed for freezing in liquid nitrogen (protein and mRNA analysis), or embedding in OCT (Sakura Finetek) or paraffin (Leica, 39601006) for immunostaining. The experimental setup is explained in the text and in Figs 6 and EV1, and EV2.

Flow cytometry

Tumor tissue was digested in RPMI medium, 5% fetal bovine serum, penicillin (10,000 U/ml), streptomycin (10 mg/ml), Liberase TM (500 μ g/ml), and DNase (Thermo Fischer Scientific, 18047019, 100 μ g/ml). Cells were separated through a 70- μ m cell strainer (BD Falcon, 352350) and counted. Flow cytometry with the indicated antibodies (Appendix Table S5) was performed with a LSR Fortessa machine (BD Biosciences) or a Beckman Coulter Gallios flow cytometer. FlowJo was used for the data analysis.

Immunofluorescence (IF) and H&E staining

OCT-embedded tissue sections were incubated with a blocking solution before incubation with the indicated primary antibody, washed, incubated with the secondary antibodies (Appendix Table S6), and DAPI (Sigma, catalog number D9542) followed by embedding with FluorSave™ Reagent (Calbiochem, 345789). Images were analyzed with a Zeiss Axio Imager Z2 microscope with constant acquisition setting (microscope, magnification, light intensity, exposure time) and quantified by the ImageJ (National Institutes of Health) software using a constant threshold.

Real-time quantitative-PCR analysis

Total RNA was extracted from frozen tumors, lungs, and cultured cells with TRIzol (Invitrogen, 12044977). cDNAs (synthesized using random primers and Moloney murine leukemia virus reverse transcriptase (MultiScribe, Applied Biosystems, 10117254)) were used for qRT-PCR in an Mx3005P Real-Time PCR System (Thermo Fisher Scientific) with Sybr Green Master mix (Thermo Fisher Scientific, 4344463) or Fast Taqman mix (Thermo Fisher Scientific, 4444557).

Expression of mouse *Gapdh* mRNA (Life Technology, 433764T) was used as endogenous control in the comparative cycle threshold method ($2^{-\Delta\Delta C_t}$) with the listed primers (Appendix Table S7).

Cell culture

NT193 tumor cells (Sun *et al*, 2019) were cultured in DMEM-glucose (Dutscher) complemented with 10% of fetal bovine serum (FBS, Dutscher). Silencing of TNC was done by short hairpin (sh)-mediated gene expression knock down and was confirmed by qRT-PCR and Western blot (Sun *et al*, 2019). Tumor cells were pretreated with inhibitors for TGF β RI (GW788388, 10 μ M, 45 min, Selleckchem, S2750), TLR4 (Cli95, 1 μ g/ml, 6 h, InvivoGen, tlr1-cl95), receptor tyrosine kinases (SU6668, 30 μ M, 60 min, Tocris bioscience, 3335), and α 4 β 1/ α 9 β 1 (BOP, 1 μ M, 45 min, Tocris bioscience, 6047) according to the manufacturer’s instructions and as published (Sun *et al*, 2019; Deligne *et al*, 2020; Spenlé *et al*, 2020). Inhibitor-treated tumor cells were then incubated with TNC (10 μ g/ml) (Huang *et al*, 2001) for 24 h before RNA extraction. Purification of recombinant his-tagged human TNC was done as described (Huang *et al*, 2001). The absence of endotoxins was determined with the PyroGene Recombinant Factor C Endpoint Fluorescent Assay (Lonza 50-658 U) according to the manufacturer’s instruction.

CD8 T leukocyte isolation and attraction and retention assay

CD8 T leukocytes were sorted by using the murine CD8a $^+$ T Cell Isolation Kit (Miltenyi Biotec, 130-104-075) from spleens of FVB mice as described (Deligne *et al*, 2020). The lower surface of polycarbonate membrane transwells (Costar, 5 μ m-pore size, 3421) was coated with matrix molecules, washed with PBS, and blocked with 1% BSA overnight at 4°C. The lower chambers of the transwells were filled with TexMACS medium (Miltenyi Biotec, 130-097-196) containing CXCL12 (1 μ g/ml, R&D Systems, 460-SD-050) or conditioned medium (CM) from shC or shTNC cells. AMD3100 (Sigma, A5602) at 5 μ g/ml was added to the CD8 T cells for 1 h at 37°C before seeding cells in the upper chamber for 5 h at 37°C followed by collection of the medium in the lower chamber for cell counting by flow cytometry (Appendix Table S5). Cells on the surface of the lower side of the insert were fixed with 4% PFA (Santa Cruz, sc-281692), stained with DAPI and imaged. Pictures were analyzed with the ImageJ software.

Surface plasmon resonance (SPR) analysis

In SPR binding experiments (Biacore 2000 instrument (Biacore Inc.)), recombinant human TNC was immobilized (Spenlé *et al*, 2020). CXCL12 (R&D Systems, 460-SD-050) (from 0.6×10^{-7} M to 6×10^{-7} M) was added to the chip at pH 7.4 (10 mM HEPES, 150 mM sodium chloride, 0.005% (v/v) surfactant P20), at a flow rate of 10 μ L/min. A steady-state condition was used to determine the affinity of CXCL12 for TNC. The dissociation constant (Kd) was determined using the 1:1 Langmuir association model.

Negative staining, transmission electron microscopy, and CXCL12 binding assay

The interaction of murine TNC (Spenlé *et al*, 2020) with CXCL12 (R&D Systems, 460-SD-050) was visualized by negative staining and

The paper explained

Problem

Immune checkpoint therapy (ICT), where CD8 tumor infiltrating T lymphocytes (TIL) get reactivated, is a promising anti-cancer treatment approach, yet with low response rates in breast cancer. Immune exclusion by the matrix, in particular by the highly abundant matrix molecule tenascin-C, forming spatial niches separating tumor cell nests, may generate barriers for TIL.

Results

We combine evidence from clinical material and experimental models to reveal that through induction (involving TLR4) and binding of CXCL12, tenascin-C impairs macrophages and CD8 TIL. We report that a tenascin-C/CXCL12 substratum retains CD8 TIL in the matrix impairing tumor cell killing. This molecular axis is important as inhibition of CXCR4 (CXCL12 receptor) restores anti-tumor immunity by activating and releasing CD8 TIL from the matrix, promoting CD8 TIL tumor infiltration and tumor cell apoptosis, and causing reduced tumor growth and subsequent lung metastasis. Notably, in human breast cancer patients, we document an immune exclusion phenotype correlating with shorter survival characterized by CD8 TIL retention in tenascin-C-rich stroma, together with high CXCL12.

Impact

This study provides novel insight into how matrix retains CD8 TIL contributing to the immune exclusion phenotype, information that could be exploited to formulate a novel "TIL-matrix-release-and-reactivate" strategy. Moreover, our results provide rationale for targeting matrix plus CXCR4 for improving ICT in particular in tumors with high tenascin-C, high CXCL12, and high CD8 TIL as this combination correlates with short breast cancer patient survival.

transmission electron microscopy as described (Bober *et al.*, 2010; Spenlé *et al.*, 2020). For inhibition experiments, TNC samples were pre-incubated with the indicated concentrations of heparin dp10 (AMS Biotechnology, AMS.HO10). Specimens were examined in a Philips/FEI CM 100 TWIN transmission electron microscope operated at 60 kV accelerating voltage. Images were recorded with a side-mounted Olympus Veleta camera and the ITEM acquisitions software. Binding of CXCL12 to TNC was determined by counting the number of colloidal gold particles along the length of the TNC monomer. Numbers of molecules from 500 randomly picked distinct TNC molecules were determined. Competition was done with increasing concentration of CXCL12 in TBS (50 mM Tris, 150 mM NaCl, pH 7.9).

Gene expression analysis

The sequencing library was prepared from mRNA derived from tumors, shC, and shTNC cells, respectively, with the Ion Total RNA-Seq Kit v2 (Thermo Fisher Scientific, 4475936). Sequencing was performed on an Ion Proton sequencer with the Ion PI™ Hi-Q™ Sequencing 200 Kit (Thermo Fisher Scientific A26433). The transcriptome data were processed by the RNASeqAnalysis plugin from the Torrent Suite Software 5.06 (Thermo Fisher Scientific). RNA from MMTV-NeuNT-WT and TNCKO mammary tumors were used for the Affymetrix Microarray experiments, performed at the IGBMC Sequencing Core Facility (Illkirch, France).

Statistical analysis

Gaussian distribution was tested by the D'Agostino-Pearson normality test. When data followed a Gaussian distribution, statistical differences were analyzed by unpaired *t*-test (with Welch's correction in case of unequal variance) or ANOVA one-way with Tukey post-test. Otherwise, the Mann-Whitney test or a non-parametric ANOVA followed by Dunn's post-test were used to verify significance of the observed differences. All statistical analyses were performed using the GraphPad Prism software. All results were compared to the respective control by the indicated statistical test, and only $P < 0.05$ are mentioned in the figure legends. Mean \pm SEM. $P < 0.05$ were considered as statistically significant, $*P < 0.05$; $**P < 0.01$; $***P < 0.001$.

Data availability

Microarray data generated for this study have been submitted to ArrayExpress under the accession numbers <https://www.ebi.ac.uk/arrayexpress/experiments/E-MTAB-10149> and <https://www.ebi.ac.uk/arrayexpress/experiments/E-MTAB-10135>.

Expanded View for this article is available online.

Acknowledgments

We acknowledge personnel from INSERM U682 and U1109, M. van der Heyden, O. Lefebvre, F. Steinbach, A. Klein, C. Arnold, T. Hussenet, A. Mariotte, A. De Cauwer, and staff of the BioEM lab (Biozentrum, University of Basel) in particular C. Tiberi, C. Alampi, and M. Chami and staff of the Core Facility for Integrated Microscopy (CFIM), Panum Institute, University of Copenhagen in particular K. Qvortrup (FCIM) for technical support, the staff of the animal facilities, and the staff of the Genomax facility (INSERM U1109). We like to thank Nathalie Salome for critically reading the manuscript and assistance with editing. Funding was provided by Worldwide Cancer Research WCR/AICR grant 14-1070 (GO, KM), Ligue Régionale contre le Cancer CCIR-Est (GO), Ligue contre le Cancer AAP2017.LNCC (GO), EUCOR seed money-2020 (GO), INSERM (GO), University Strasbourg (GO), Institut National contre le Cancer (INCa) TENPLAMET (GO), INCa TENMAX (GO), ANR (AngioFib) (GO), the European regional development fund INTERREG V program (project PERSONALIS; RC), a MSDAvenir grant (Autogen project; RC), National Natural Science Foundation of China (Grant No. 81802655) to SZ and through personnel fellowships, Versus Arthritis Senior fellowship (20003) to KM, the Fondation ARC (DM), Chinese Scholarship Council CSC (ZS), Conacyt Mexico (IVQ), and French ministry fellowship grants (AY, WE).

Author contributions

DM, ZS, KM, TL, and GO conceptualized the study. DM, ZS, AY, GR, CAF, CD, IVQ, WE, MN, MM, GC, NP, RV, JY, and TL performed experiments, analyzed, and interpreted the data. RC and HD supervised the RNA profiling and flow cytometry experiments. Experiments were performed as follows: SRP by GC, negative EM imaging by MM, RNA-seq analysis by NP, IVQ, TL, and RC, human tissue microarray staining and patient survival analysis by ZS and JY, analysis and treatment of mice with AMD by DM, AY, GR, CAF, flow cytometry by DM, CD, RV, staining by DM, ZS, WE, AY, MN, CAF, preparation of human TNC by DM, WE, AY, CAF, TL, cell culture experiments by DM, AY, TL. DM, TL, GO wrote the manuscript, DM, ZS, AY, CAF, KM edited the manuscript. GO supervised the study. All authors read and discussed the manuscript.

Conflict of interest

The authors declare that they have no conflict of interest.

References

Azab AK, Runnels JM, Pitsillides C, Moreau AS, Azab F, Leleu X, Jia X, Wright R, Ospina B, Carlson AL et al (2009) CXCR4 inhibitor AMD3100 disrupts the interaction of multiple myeloma cells with the bone marrow microenvironment and enhances their sensitivity to therapy. *Blood* 113: 4341–4351

Balabanian K, Lagane B, Infantino S, Chow KYC, Harriague J, Moepps B, Arenzana-Seisdedos F, Thelen M, Bachelerie F (2005) The chemokine SDF-1/CXCL12 binds to and signals through the orphan receptor RDC1 in T lymphocytes. *J Biol Chem* 280: 35760–35766

Bleul CC, Fuhlbrigge RC, Casasnovas JM, Aiuti A, Springer TA (1996) A highly efficacious lymphocyte chemoattractant, stromal cell-derived factor 1 (SDF-1). *J Exp Med* 184: 1101–1109

Bober M, Enochsson C, Collin M, Mörgelin M (2010) Collagen VI is a subepithelial adhesive target for human respiratory tract pathogens. *J Innate Immun* 2: 160–166

Chatterjee S, Azad BB, Nimmagadda S (2014) The intricate role of CXCR4 in cancer. *Adv Cancer Res* 124: 31–82

Chen C, Sun S-R, Gong Y-P, Qi C-B, Peng C-W, Yang X-Q, Liu S-P, Peng J, Zhu S, Hu M-B et al (2011) Quantum dots-based molecular classification of breast cancer by quantitative spectroanalysis of hormone receptors and HER2. *Biomaterials* 32: 7592–7599

Chen C, Xia H-S, Gong Y-P, Peng J, Peng C-W, Hu M-B, Zhu X-B, Pang D-W, Sun S-R, Li Y (2010) The quantitative detection of total HER2 load by quantum dots and the identification of a new subtype of breast cancer with different 5-year prognosis. *Biomaterials* 31: 8818–8825

De Laporte L, Rice JJ, Tortelli F, Hubbell JA (2013) Tenascin C promiscuously binds growth factors via its fifth fibronectin type III-like domain. *PLoS One* 8: e62076

Deligne C, Murdamoothoo D, Gammage AN, Gschwandtner M, Erne W, Loustau T, Marzeda AM, Carapito R, Paul N, Velazquez-Quesada I et al (2020) Matrix-Targeting Immunotherapy Controls Tumor Growth and Spread by Switching Macrophage Phenotype. *Cancer Immunol Res* 8: 368–382

Domanska UM, Timmer-Bosscha H, Nagengast WB, Oude Munnink TH, Kruizinga RC, Ananias HJK, Kliphuis NM, Huls G, De Vries EGE, de Jong IJ et al (2012) CXCR4 inhibition with AMD3100 sensitizes prostate cancer to docetaxel chemotherapy. *Neoplasia* 14: 709–718

Döring Y, Pawig L, Weber C, Noels H (2014) The CXCL12/CXCR4 chemokine ligand/receptor axis in cardiovascular disease. *Front Physiol* 5: 212

Duraiswamy J, Kaluza KM, Freeman GJ, Coukos G (2013) Dual blockade of PD-1 and CTLA-4 combined with tumor vaccine effectively restores T-cell rejection function in tumors. *Cancer Res* 73: 3591–3603

Emancipator K (2020) Keytruda and PD-L1: a Real-World Example of Co-development of a Drug with a Predictive Biomarker. *AAPS J* 23: 5

Enerly E, Steinfeld I, Kleivi K, Leivonen S-K, Aure MR, Russnes HG, Rønneberg JA, Johnsen H, Navon R, Rødland E et al (2011) miRNA-mRNA integrated analysis reveals roles for miRNAs in primary breast tumors. *PLoS One* 6: e16915

Erdag G, Schaefer JT, Smolkin ME, Deacon DH, Shea SM, Dengel LT, Patterson JW, Slingluff CL (2012) Immunotype and immunohistologic characteristics of tumor-infiltrating immune cells are associated with clinical outcome in metastatic melanoma. *Cancer Res* 72: 1070–1080

Feig C, Jones JO, Kraman M, Wells R, Deonarine A, Chan DS, Connell CM, Roberts EW, Zhao Q, Caballero OL et al (2013) Targeting CXCL12 from FAP-expressing carcinoma-associated fibroblasts synergizes with anti-PD-L1 immunotherapy in pancreatic cancer. *Proc Natl Acad Sci USA* 110: 20212–20217

Fridman WH, Pagès F, Sautès-Fridman C, Galon J (2012) The immune contexture in human tumours: impact on clinical outcome. *Nat Rev Cancer* 12: 298–306

Galon J, Bruni D (2019) Approaches to treat immune hot, altered and cold tumours with combination immunotherapies. *Nat Rev Drug Discovery* 18: 197–218

Galon J, Costes A, Sanchez-Cabo F, Kirilovsky A, Mlecnik B, Lagorce-Pagès C, Tosolini M, Camus M, Berger A, Wind P et al (2006) Type, density, and location of immune cells within human colorectal tumors predict clinical outcome. *Science* 313: 1960–1964

Galon J, Pagès F, Marincola FM, Angell HK, Thurin M, Lugli A, Zlobec I, Berger A, Bifulco C, Botti G et al (2012) Cancer classification using the Immunoscore: a worldwide task force. *J Transl Med* 10: 205

Goswami CP, Nakshatri H (2013) PROgene: gene expression based survival analysis web application for multiple cancer. *J Clin Bioinforma* 22: 3–22

Guyon A (2014) CXCL12 chemokine and its receptors as major players in the interactions between immune and nervous systems. *Front Cell Neurosci* 8: 65

Hauzenberger D, Olivier P, Gundersen D, Rüegg C (1999) Tenascin-C inhibits beta1 integrin-dependent T lymphocyte adhesion to fibronectin through the binding of its fnIII 1–5 repeats to fibronectin. *Eur J Immunol* 29: 1435–1447

Hemesath TJ, Marton LS, Stefansson K (1994) Inhibition of T cell activation by the extracellular matrix protein tenascin. *J Immunol* 152: 5199–5207

Huang AC, Postow MA, Orlowski RJ, Mick R, Bengsch B, Manne S, Xu W, Harmon S, Giles JR, Wenz B et al (2017) T-cell invigoration to tumour burden ratio associated with anti-PD-1 response. *Nature* 545: 60–65

Huang J-Y, Cheng Y-J, Lin Y-P, Lin H-C, Su C-C, Juliano R, Yang B-C (2010) Extracellular matrix of glioblastoma inhibits polarization and transmigration of T cells: the role of tenascin-C in immune suppression. *J Immunol* 185: 1450–1459

Huang W, Chiquet-Ehrismann R, Moyano JV, Garcia-Pardo A, Orend G (2001) Interference of tenascin-C with syndecan-4 binding to fibronectin blocks cell adhesion and stimulates tumor cell proliferation. *Cancer Res* 61: 8586–8594

Jachetti E, Caputo S, Mazzoleni S, Brambillasca CS, Parigi SM, Grioni M, Piras IS, Restuccia U, Calcinotto A, Freschi M et al (2015) Tenascin-C protects cancer stem-like cells from immune surveillance by arresting T-cell activation. *Cancer Res* 75: 2095–2108

Joyce JA, Fearon DT (2015) T cell exclusion, immune privilege, and the tumor microenvironment. *Science* 348: 74–80

Kelso A, Costelloe EO, Johnson BJ, Groves P, Buttigieg K, Fitzpatrick DR (2002) The genes for perforin, granzymes A-C and IFN-γ are differentially expressed in single CD8⁺ T cells during primary activation. *International Immunology* 14: 605–613

Lefort S, Thuleau A, Kieffer Y, Sirven P, Bieche I, Marangoni E, Vincent-Salomon A, Mechta-Grigoriou F (2017) CXCR4 inhibitors could benefit to HER2 but not to triple-negative breast cancer patients. *Oncogene* 36: 1211–1222

Li Z-L, Zhang H-L, Huang Y, Huang J-H, Sun P, Zhou N-N, Chen Y-H, Mai J, Wang Y, Yu Y et al (2020) Autophagy deficiency promotes triple-negative breast cancer resistance to T cell-mediated cytotoxicity by blocking tenascin-C degradation. *Nat Commun* 11: 3806

Lu P, Weaver VM, Werb Z (2012) The extracellular matrix: A dynamic niche in cancer progression. *J Cell Biol* 196: 395–406

Midwood KS, Chiquet M, Tucker RP, Orend G (2016) Tenascin-C at a glance. *J Cell Sci* 129: 4321–4327

Midwood K, Sacre S, Piccinini AM, Inglis J, Trebaul A, Chan E, Drexler S, Sofat N, Kashiwagi M, Orend G et al (2009) Tenascin-C is an endogenous activator of Toll-like receptor 4 that is essential for maintaining inflammation in arthritic joint disease. *Nat Med* 15: 774–780

Minn AJ, Kang Y, Serafina I, Gupta GP, Giri DD, Doubrovin M, Ponomarev V, Gerald WL, Blasberg R, Massagué J (2005) Distinct organ-specific metastatic potential of individual breast cancer cells and primary tumors. *J Clin Invest* 115: 44–55

Okabe S, Fukuda S, Kim Y-J, Niki M, Pelus LM, Ohyashiki K, Pandolfi PP, Broxmeyer HE (2005) Stromal cell-derived factor-1alpha/CXCL12-induced chemotaxis of T cells involves activation of the RasGAP-associated docking protein p62Dok-1. *Blood* 105: 474–480

Oskarsson T, Acharya S, Zhang XH-F, Vanharanta S, Tavazoie SF, Morris PG, Downey RJ, Manova-Todorova K, Brogi E, Massagué J (2011) Breast cancer cells produce tenascin C as a metastatic niche component to colonize the lungs. *Nat Med* 17: 867–874

Parekh K, Ramachandran S, Cooper J, Bigner D, Patterson A, Mohanakumar T (2005) Tenascin-C, over expressed in lung cancer down regulates effector functions of tumor infiltrating lymphocytes. *Lung Cancer* 47: 17–29

Pickup MW, Mouw JK, Weaver VM (2014) The extracellular matrix modulates the hallmarks of cancer. *EMBO Rep* 15: 1243–1253

Richter R, Jochheim-Richter A, Ciuculescu F, Kollar K, Seifried E, Forssmann U, Verzijl D, Smit MJ, Blanchet X, von Hundelshausen P et al (2014) Identification and characterization of circulating variants of CXCL12 from human plasma: effects on chemotaxis and mobilization of hematopoietic stem and progenitor cells. *Stem Cells Dev* 23: 1959–1974

Ruegg CR, Chiquet-Ehrismann R, Alkan SS (1989) Tenascin, an extracellular matrix protein, exerts immunomodulatory activities. *Proc Natl Acad Sci* 86: 7437–7441

Saupe F, Schwenzer A, Jia Y, Gasser I, Spenlé C, Langlois B, Kammerer M, Lefebvre O, Hlushchuk R, Rupp T et al (2013) Tenascin-C downregulates wnt inhibitor dickkopf-1, promoting tumorigenesis in a neuroendocrine tumor model. *Cell Rep* 5: 482–492

Siegel PM, Shu W, Cardiff RD, Muller WJ, Massagué J (2003) Transforming growth factor beta signaling impairs Neu-induced mammary tumorigenesis while promoting pulmonary metastasis. *Proc Natl Acad Sci USA* 100: 8430–8435

Spenlé C, Gasser I, Saupe F, Janssen K-P, Arnold C, Klein A, van der Heyden M, Mutterer J, Neuville-Méchine A, Chenard M-P et al (2015) Spatial organization of the tenascin-C microenvironment in experimental and human cancer. *Cell Adh Migr* 9: 4–13

Spenlé C, Loustau T, Murdamoothoo D, Erne W, Beghelli-de la Forest D, Divonne S, Veber R, Petti L, Bourdely P, Mörgelin M, Brauchle E-M et al (2020) Tenascin-C orchestrates an immune-suppressive tumor microenvironment in oral squamous cell carcinoma. *Cancer Immunol Res* 8: 1122–1138.

Spinosa PC, Lucker KE, Luker GD, Linderman JJ (2017) The CXCL12/CXCR7 signaling axis, isoforms, circadian rhythms, and tumor cellular composition dictate gradients in tissue. *PLoS One* 12: e0187357

Sun Z, Velázquez-Quesada I, Murdamoothoo D, Ahowesso C, Yilmaz A, Spenlé C, Averous G, Erne W, Oberndorfer F, Oswald A et al (2019) Tenascin-C increases lung metastasis by impacting blood vessel invasions. *Matrix Biol* 83: 26–47

Tomko LA, Hill RC, Barrett A, Szulczewski JM, Conklin MW, Eliceiri KW, Keely PJ, Hansen KC, Ponik SM (2018) Targeted matrisome analysis identifies thrombospondin-2 and tenascin-C in aligned collagen stroma from invasive breast carcinoma. *Sci Rep* 8: 12941

Toullé A, Gerald D, Despouy G, Bourachot B, Cardon M, Lefort S, Richardson M, Rigaill G, Parrini M-C, Lucchesi C et al (2010) Oxidative stress promotes myofibroblast differentiation and tumour spreading. *EMBO Mol Med* 2: 211–230

Vianello F, Papeta N, Chen T, Kraft P, White N, Hart WK, Kircher MF, Swart E, Rhee S, Palù G et al (2006) Murine B16 melanomas expressing high levels of the chemokine stromal-derived factor-1/CXCL12 induce tumor-specific T cell chemorepulsion and escape from immune control. *J Immunol* 176: 2902–2914

Yang F, Takagaki Y, Yoshitomi Y, Ikeda T, Li J, Kitada M, Kumagai A, Kawakita E, Shi S, Kanasaki K et al (2019) Inhibition of dipeptidyl peptidase-4 accelerates epithelial-mesenchymal transition and breast cancer metastasis via the CXCL12/CXCR4/mTOR axis. *Cancer Res* 79: 735–746

Yang Z, Ni W, Cui C, Fang L, Xuan Y (2017) Tenascin C is a prognostic determinant and potential cancer-associated fibroblasts marker for breast ductal carcinoma. *Exp Mol Pathol* 102: 262–267

Zemek RM, Chin WL, Nowak AK, Millward MJ, Lake RA, Lesterhuis WJ (2020) Sensitizing the tumor microenvironment to immune checkpoint therapy. *Front Immunol* 11: 223

Zhang B, Wu C, Zhang Z, Yan K, Li C, Li Y, Li L (2019) CXCL12 is associated with FoxP3⁺ tumor-infiltrating lymphocytes and affects the survival of patients with oral squamous cell carcinoma. *Oncol Lett* 18: 1099–1106



License: This is an open access article under the terms of the Creative Commons Attribution License, which permits use, distribution and reproduction in any medium, provided the original work is properly cited.

Expanded View Figures

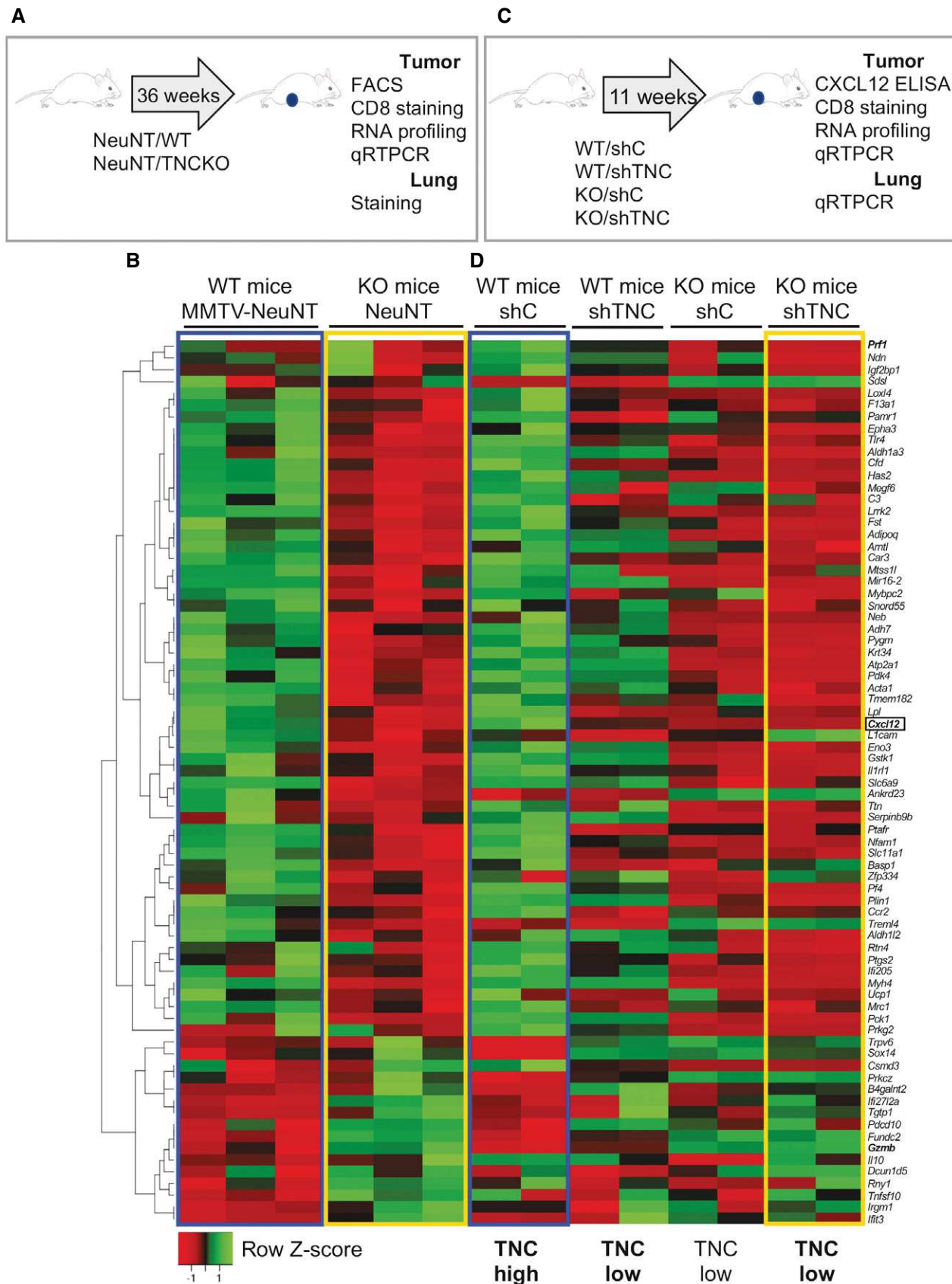


Figure EV1.

Expanded View Figures

Figure EV1. Loss of the TNC protein in both cancer and stromal cells impacts tumor gene expression.

A Schematic depiction of the experimental setup in NeuNT mice with a WT or TNCKO background.

B Juxtaposed heatmaps representing RNA chip analysis data of MMTV-NeuNT tumors (WT, TNCKO; $N = 3$).

C Schematic depiction of the experimental setup in the NT193 grafting model followed by analysis of the tumor and the lungs as indicated. In the grafting experiments, four conditions were used where shC or shTNC tumor cells (sh1, sh2) were engrafted into the mammary gland of a WT or TNCKO (KO) host giving rise to TNC-high (WT/shC) and TNC-low tumors (WT/shTNC, KO/shC, KO/shTNC).

D Juxtaposed heatmaps representing the RNA sequencing results from NT193 tumors (WT and TNCKO mice injected with shC or shTNC cells; $N = 2$). Conditions further used in the study are shown in bold as TNC high and TNC low, respectively. Note, juxtaposition shows similarities in the pattern of gene expression between TNC-high (MMTV-NeuNT/WT, WT/shC) tumors (blue squares) (B) and TNC-low (MMTV-NeuNT/KO, WT/shTNC, KO/shTNC) tumors (yellow squares) (D).

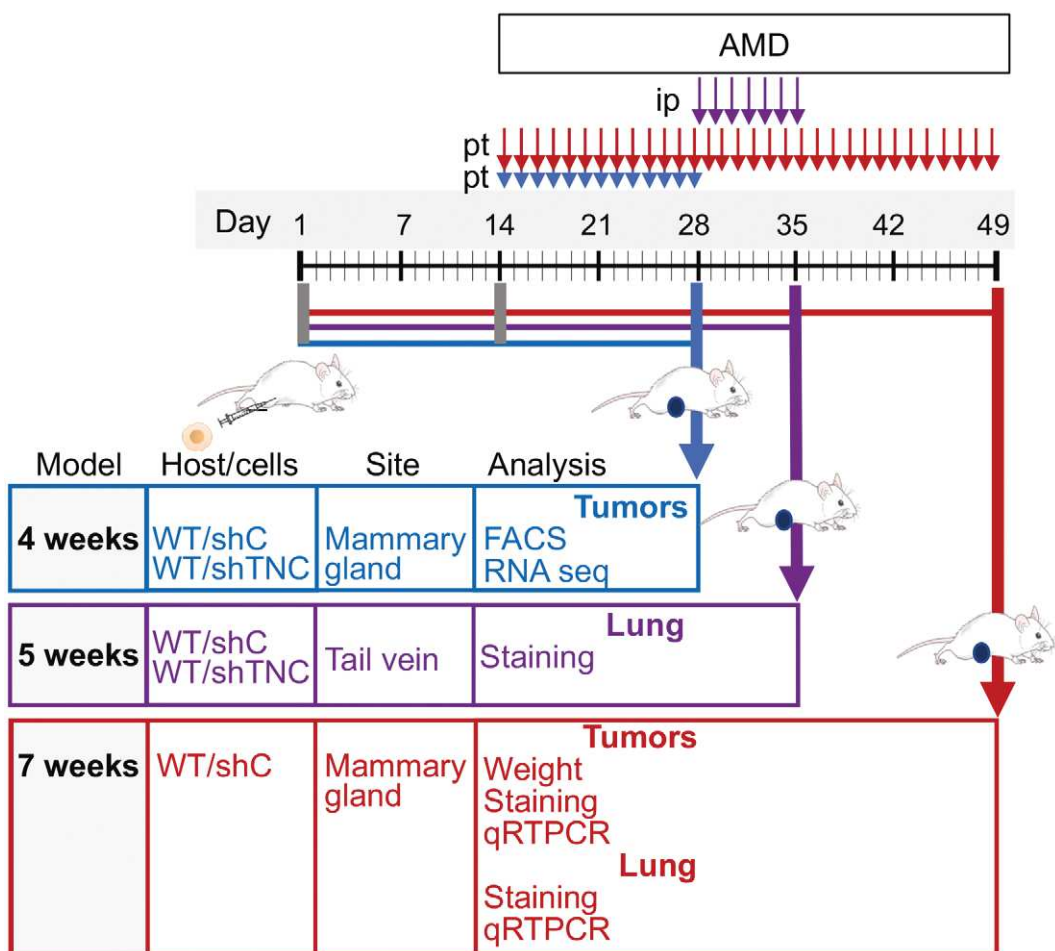


Figure EV2. Experimental setup of the CXCR4 inhibition experiments in the NT193 grafting model.

Experimental setup for the 4, 5, and 7 weeks protocols. 4-week model: WT mice were engrafted with shC or shTNC tumor cells in the mammary gland followed by AMD treatment (5 mg/kg/day, peritumoral (pt)) for 2 weeks (week 2–4) before sacrifice and investigation of the primary tumor by flow cytometry and RNA-seq (WT/shC and WT/shTNC). 5-week model: WT mice were iv engrafted with shC or shTNC tumor cells for 4 weeks followed by AMD treatment (7.5 mg/kg/day, ip) for 1 week (week 5) before sacrifice and analysis of the lungs by tissue staining. 7-week model: WT mice were engrafted with shC tumor cells into the mammary gland followed by AMD treatment (5 mg/kg/day, pt) for 5 weeks (week 2–7) before sacrifice and investigation of the tumor (weight, tissue staining, qRT-PCR) and the lungs (tissue staining, qRT-PCR).

Figure EV3. CXCL12 expression and binding to TNC.

- A, B RNA-seq gene expression results represented as heatmap for the fifty most deregulated genes in TNC-high (WT/shC) and TNC-low (KO/shTNC) tumors ($N = 2$ tumors per condition), 11-week model (A) and in shC and shTNC cells ($N = 2$) (B).
- C CXCL12 mRNA levels in NT193 tumors, 11-week model ($N = 7$ tumors for WT/shC, WT/sh1TNC, TNCKO/sh1TNC, and TNCKO/sh2TNC conditions, $N = 8$ tumors for WT/sh2TNC and TNCKO/shC conditions), $*P = 0.0205$, Mann–Whitney test. Mean \pm SEM.
- D CXCL12 mRNA levels in MMTV-NeuNT/WT compared to TNCKO tumors as determined by qRT-PCR ($N = 13$ and 6 tumors, respectively), $*P = 0.0123$, Mann–Whitney test. Mean \pm SEM.
- E–G Negative EM analysis of binding of unlabeled beads to TNC (E) and upon binding of CXCL12-adsorbed gold beads upon incubation with unlabeled CXCL12 (F) and heparin (G) at the indicated molar ratios to TNC. Asterisk points at fibrinogen globe. Scale bars, 100 nm (top), 50 nm (bottom), (E). Representation of TNC monomer, oligomerization domain (triangle) to form hexamers as seen in (E) FNIII repeats (gray boxes, constant domains, white boxes, alternative domains), fibrinogen like domain (circle). Representative result (3 independent experiments, $n = 500$ TNC molecules each). Mean \pm SEM.

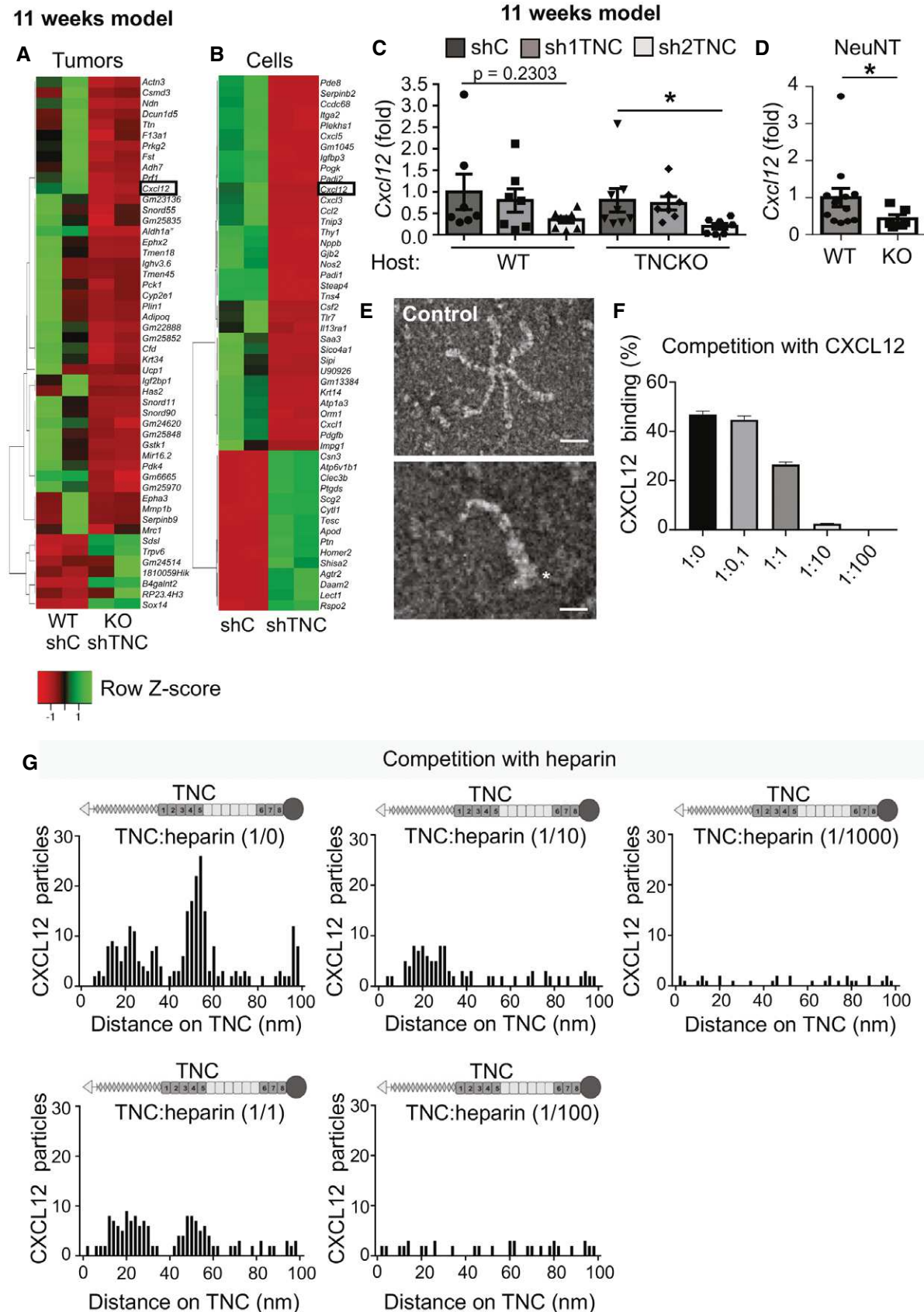


Figure EV3.

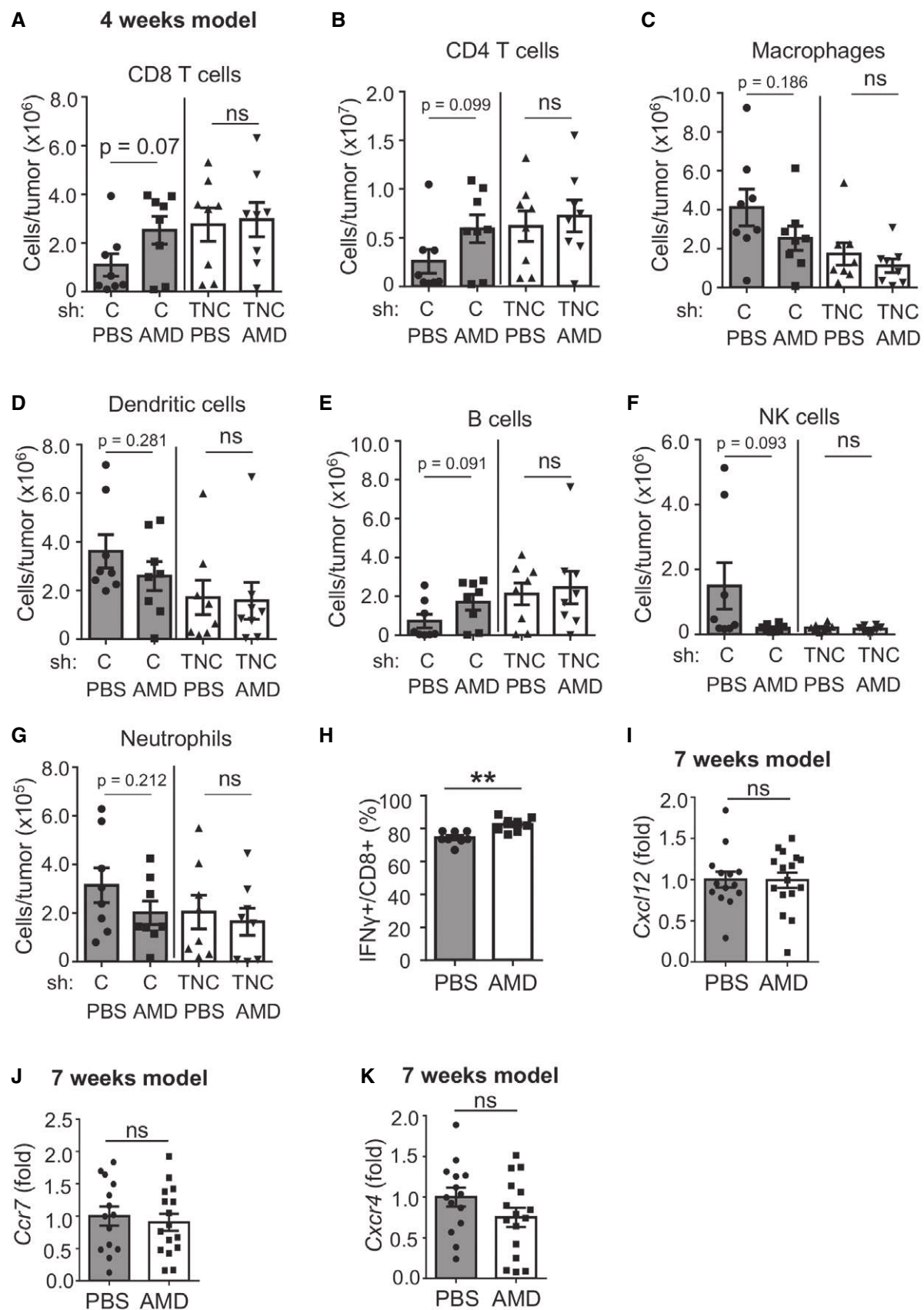


Figure EV4.

Figure EV4. Impact of CXCR4 on the tumor immune cell infiltrate and gene expression in the tumors.

A–G 4-week model. Abundance of the indicated immune cell subtypes per tumor as determined by flow cytometry. $N = 8$ tumors per condition. ns: $P > 0.05$, Mann–Whitney test. Mean \pm SEM.

H 4-week model. IFN γ expression in MACS isolated CD8 T leukocytes as determined by flow cytometry. $N = 8$ tumors per group, ** $P = 0.0015$, unpaired t -test. Mean \pm SEM.

I–K 7-week model. Expression of the indicated molecules in tumors as determined by qRT–PCR. $N = 14$ (PBS), $N = 16$ (AMD) tumors. ns: $P > 0.05$, unpaired t -test. Mean \pm SEM.

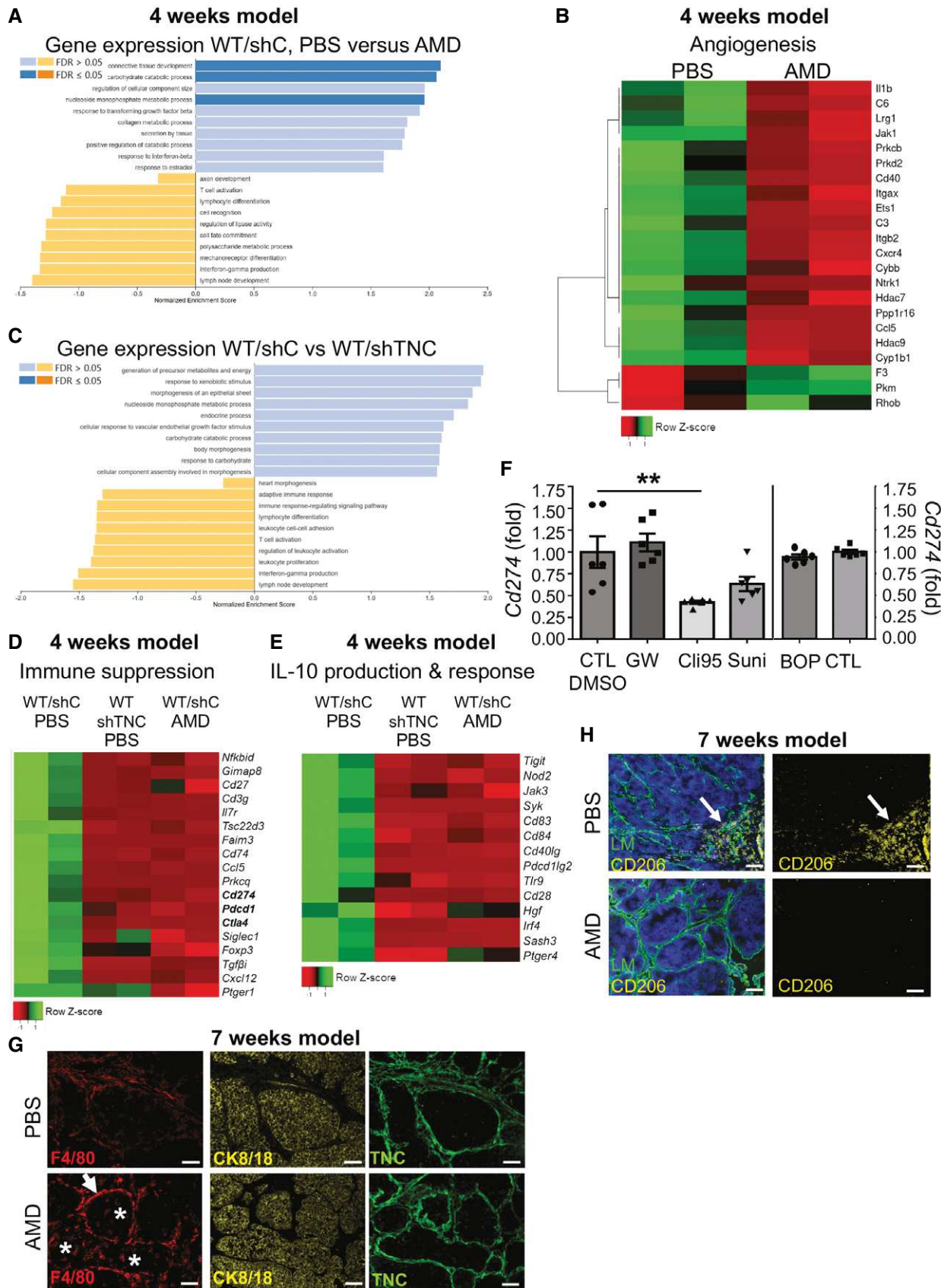


Figure EV5.

Figure EV5. Impact of CXCR4 on gene expression and abundance of macrophages.

A–E 4-week model. Gene set enrichment analysis of differentially expressed genes in TNC-high (WT/shC) tumors treated with PBS or AMD (A, B, D, E) and in WT/shC and WT/shTNC tumors treated with PBS (C, D, E). (A, C) False discovery rate (FDR) > 0.05 and ≤ 0.05 . $N = 2$ tumors per group. RNA-seq gene expression results represented as heatmap for genes that belong to the angiogenesis pathways ($P = 2.31 \times 10^{-9}$) (B), immune suppression ($P = 7.87 \times 10^{-7}$) (D), IL-10 production and response signaling ($P = 8.12 \times 10^{-8}$) (E) according to the Panther software and Geneontology functional database.

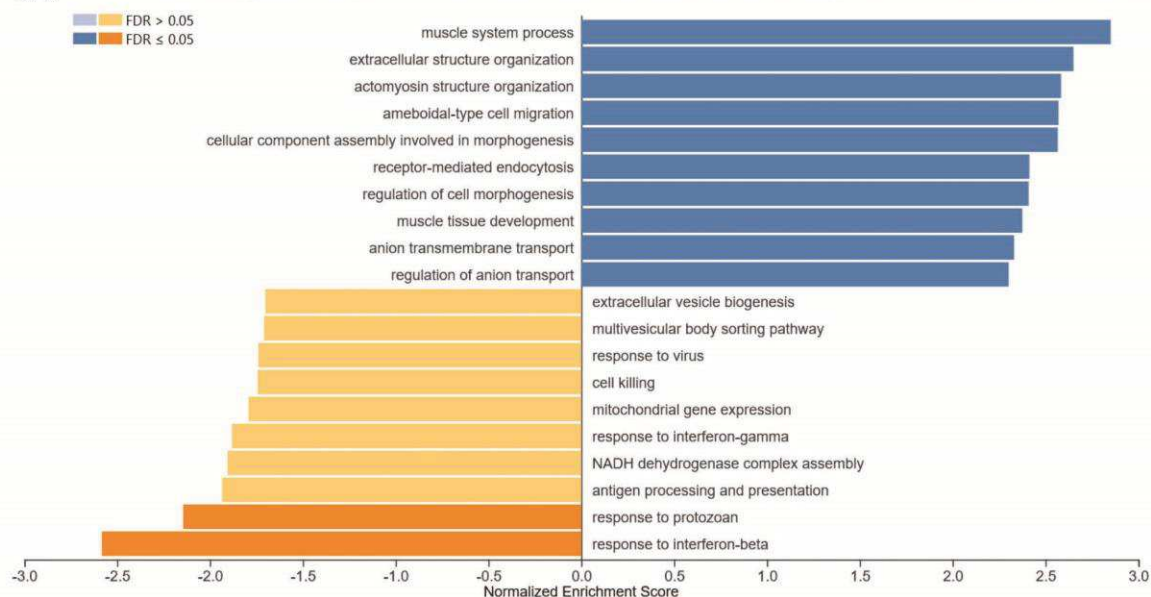
F Analysis of *Cd274* levels by qRT-PCR in shC tumor cells upon treatment with the indicated inhibitors, $N = 6$ independent experiments, ** $P = 0.0022$, Mann-Whitney test. Mean \pm SEM.

G, H 7-week model. Staining of tumor tissue (WT/shC) for the indicated molecules. Scale bar, 50 μ m. $N = 5$ tumors, $n = 2$ slides per condition. Arrows point at F4/80 $^{+}$ (G) and CD206 $^{+}$ cells (H). Asterisks point at the F4/80 $^{+}$ cells localized in the tumor cell nest (G).

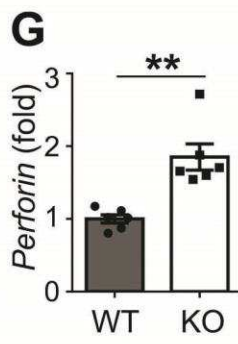
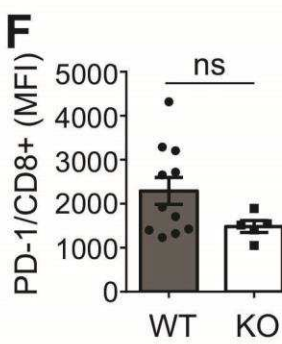
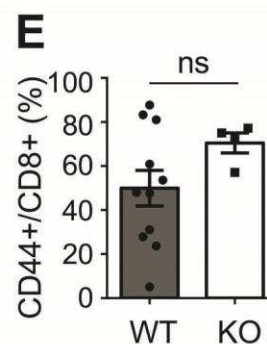
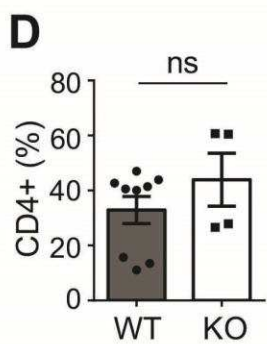
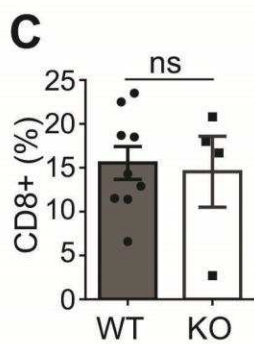
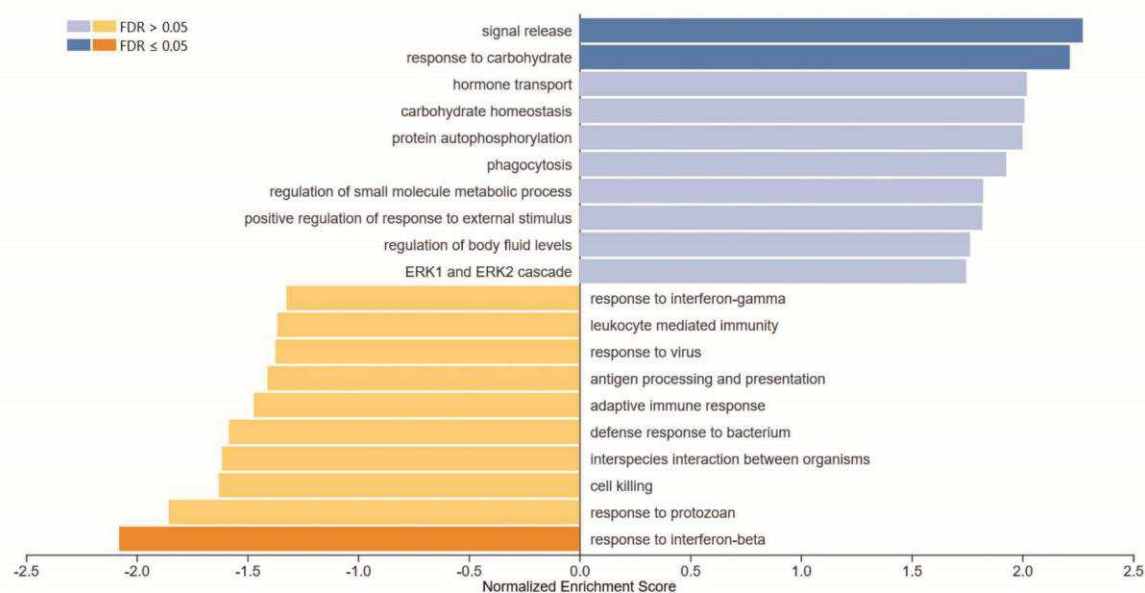
Appendix Figures S1-6

Appendix Fig. S1

A Global gene expression in MMTV-NeuNT WT compared to TNCKO tumors



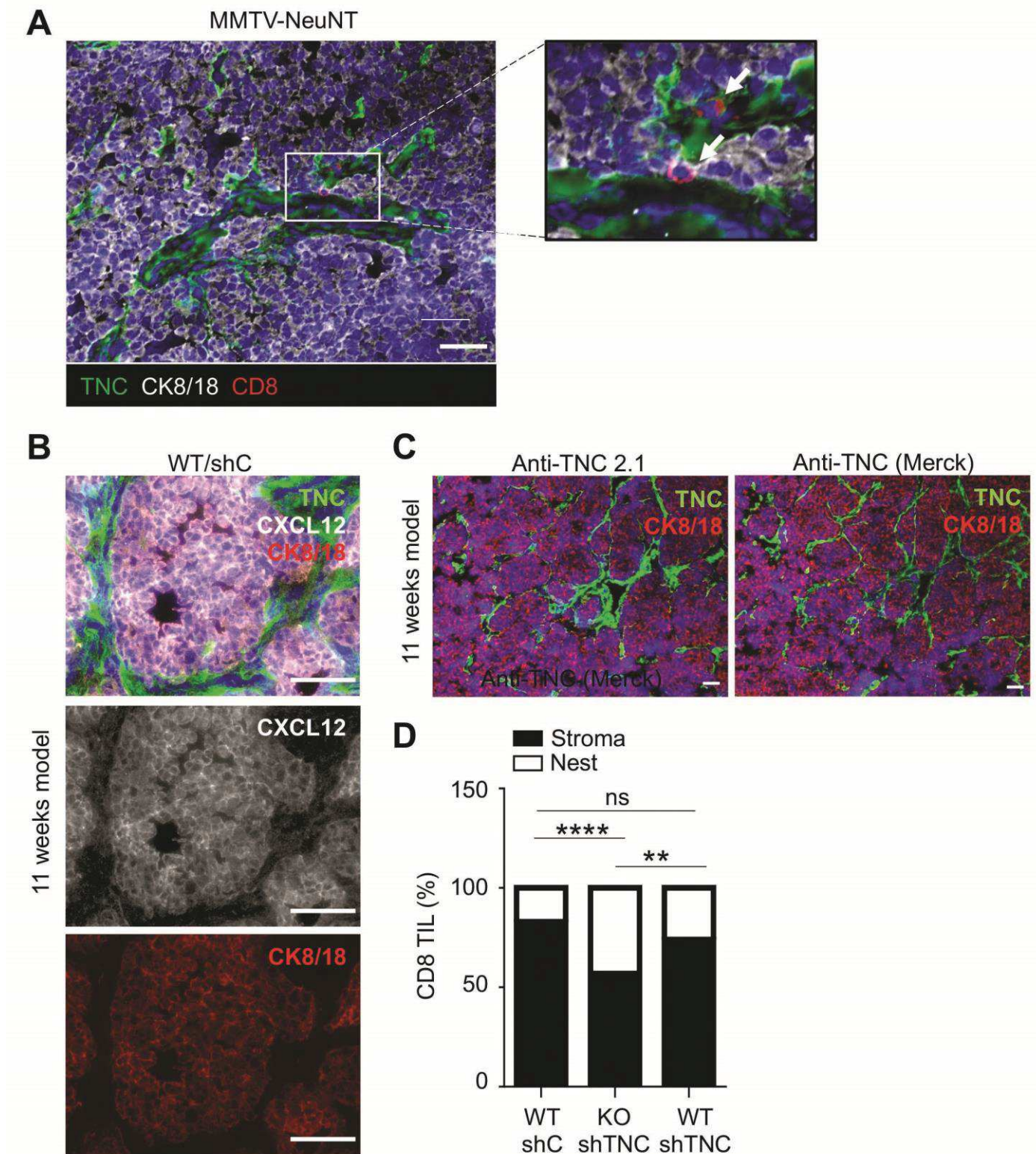
B Immunity related gene expression in MMTV-NeuNT WT compared to TNCKO tumors



Appendix Fig. S1 Gene ontology representation and immune cell infiltrate in MMTV-NeuNT tumors

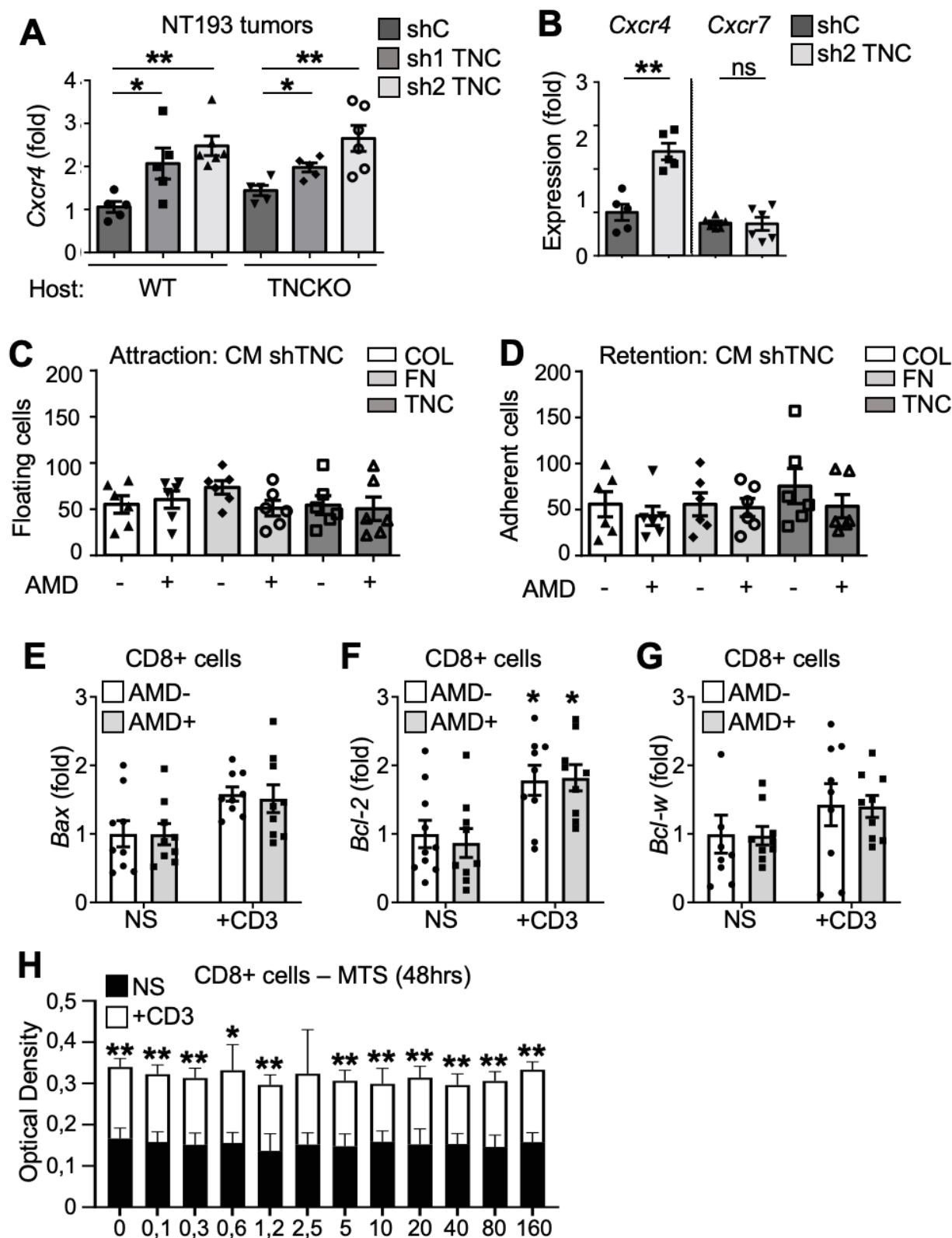
(A) Gene set enrichment analysis (GSEA) of the 2260 differentially expressed genes in MMTV-NeuNT tumors from TNC WT vs. KO mice. Up-regulated pathways are those enriched in the over-represented gene sets (Geneontology database) and are represented on the right. Down-regulated pathways are those enriched in the negatively regulated gene sets and represented on the left. The analysis showed that in the TNC WT tumors muscle extracellular and actomyosin structure organization were upregulated, while genes involved in interferon responses were down-regulated. False discovery rate (FDR) $> 0,05$ and $\leq 0,05$. **(B)** Gene set enrichment analysis of differentially expressed immune-related genes in MMTV-NeuNT WT versus TNCKO tumors. False discovery rate (FDR) $> 0,05$ and $\leq 0,05$. **(C - F)** Tumor infiltrating immune cells determined by flow cytometry for the indicated markers expressed as % of T cells. N = 9 WT, N = 4 TNCKO **(C, D)** and % of CD8 T cells, N = 11 WT, N = 4, **(E, F)**. $p > 0,05$, Mann-Whitney test **(C - F)**. **(G)** Differential expression of *Perforin* as determined by qRT-PCR. N = 6 WT, N = 6 TNCKO, $p = 0,0011$, unpaired t-test.

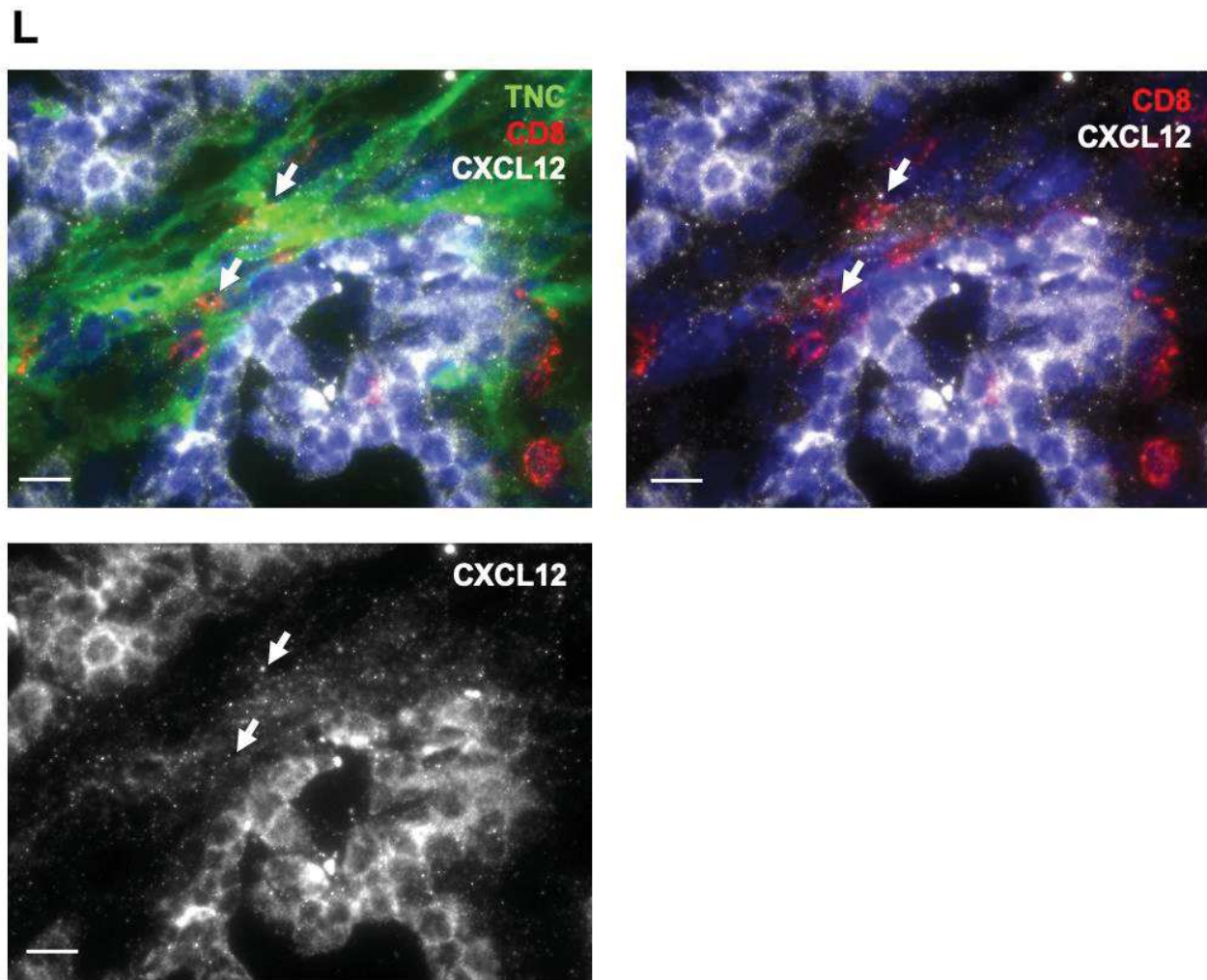
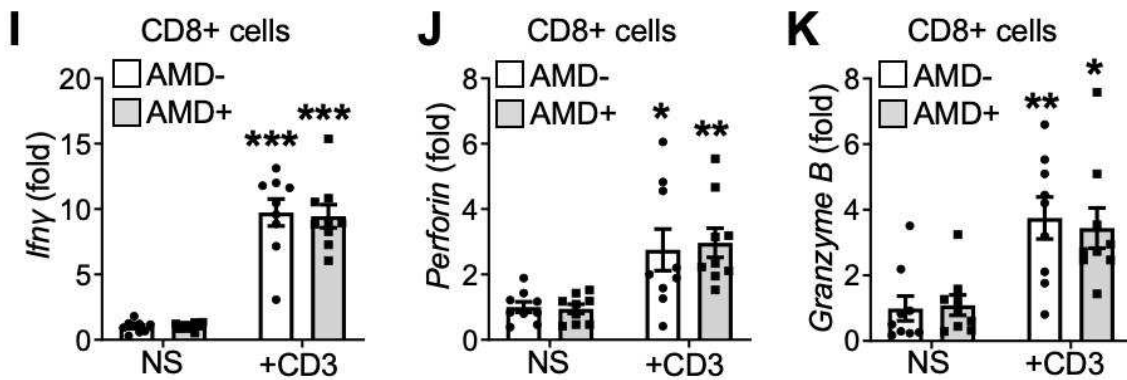
Appendix Fig. S2



Appendix Fig. S2 Expression of TNC and localisation of CD8 TIL in NeuNT and NT193 tumors (A)
 Tissue staining of a NeuNT tumor for the indicated molecules, revealing very low abundance of CD8 TIL. Scale bar, x μ m. **(B, C)** Staining of a TNC high (WT/shC) tumor for TNC with the rat monoclonal MTn12 **(B)** and rabbit polyclonal TNC2.1 and Merck antibodies **(C)** revealing expression of the TNC protein in the stroma but not in the tumor cell nests (CK8/18).

Appendix Fig. S3



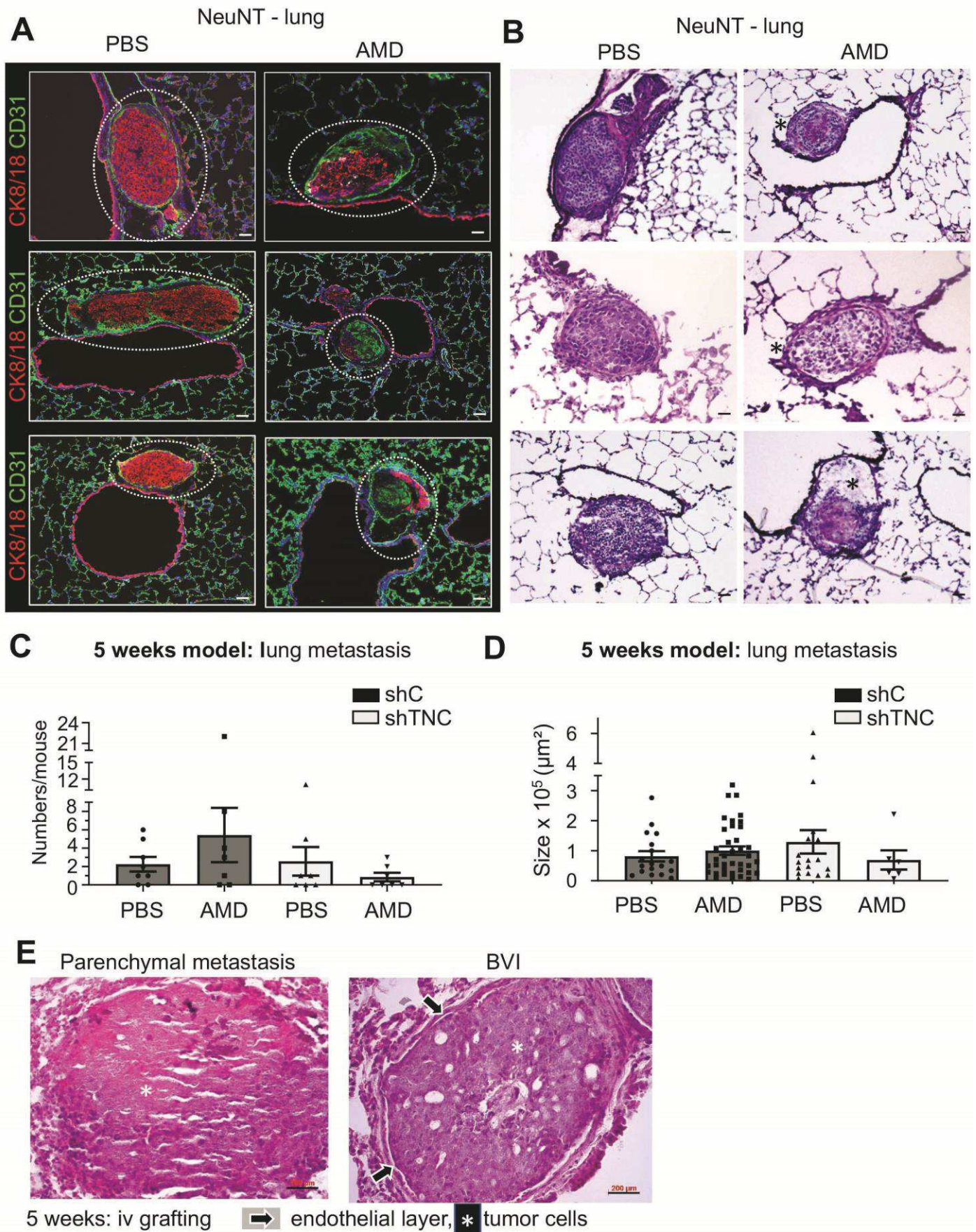


Appendix Figure S3 CXCL12 receptor expression and CD8 T leukocyte migration and function upon CXCR4 inhibition

(A, B) mRNA levels of CXCR4 and CXCR7 **(B)** in NT193 tumors **(A)** and cultured NT193 cells **(B)**. **(A)** N = at least 5 tumors per group, ** p = 0.0043 (WT host, shC versus sh2TNC), * p = 0.0159 (WT host, shC versus sh1TNC), ** p = 0.0087 (TNCKO host, shC versus sh2TNC), * p = 0.0159 (TNCKO host, shC versus sh1TNC), Mann-Whitney test. **(B)** N = at least 5 tumors per group, ** p = 0.0079 **(C)** Migration and **(D)** retention of CD8 T leukocytes with CM from shTNC cells upon coating of the lower insert surface with the indicated matrix molecules. Cells were quantified upon addition of AMD3100 (AMD), 1 hour pretreatment (5 µg/ml AMD) for 5 hours, **(C)** N = 6 per group, t-test, ns > 0.05. **(D)** N = 6 per group, Mann-Whitney test, ns

> 0.05. **(E – G, I - K)** Gene expression (qRTCP) of *Bax* (**E**), *Bcl-2* (**F**), *Bcl-w* (**G**), *Ifny* (**I**), *Perforin* (**J**), *Granzyme B* (**K**) in CD8 T cells treated *in vitro* with a CD3 mouse antibody (1 μ g/mL; +CD3) or not (Non-stimulated; NS) for 24 hours and incubation for 45 min with AMD (5 μ g/mL; AMD+) or not (AMD-). N = 9 (3 independent experiments in triplicate). Values are normalized to *Gapdh* and are expressed as relative ratio to control CD8 T cells (NS, AMD-). Mean \pm SEM, Two way-AVOVA and Tukey's post-test. * relative to NS condition (* p < 0,05; **p < 0.01; ***p < 0.005). **(H)** MTS cell proliferation of CD8 T cells after CD3+ stimulation or not and 48 hours of incubation with the indicated AMD concentrations (μ g/mL, n = 2 experiments, n = 8 replicates). Two way-AVOVA and Tukey's post-test, mean \pm SEM, * relative to corresponding NS condition (* p < 0,05; **p < 0.01). **(L)** Representative staining image (N = 5 tumors) of a TNC+ tumor for the indicated molecules. Scale bars, 50 μ m. Note punctate CXCL12 expression in the tumor cells and at lower level in the stroma colocalizing with CD8 and TNC (arrows).

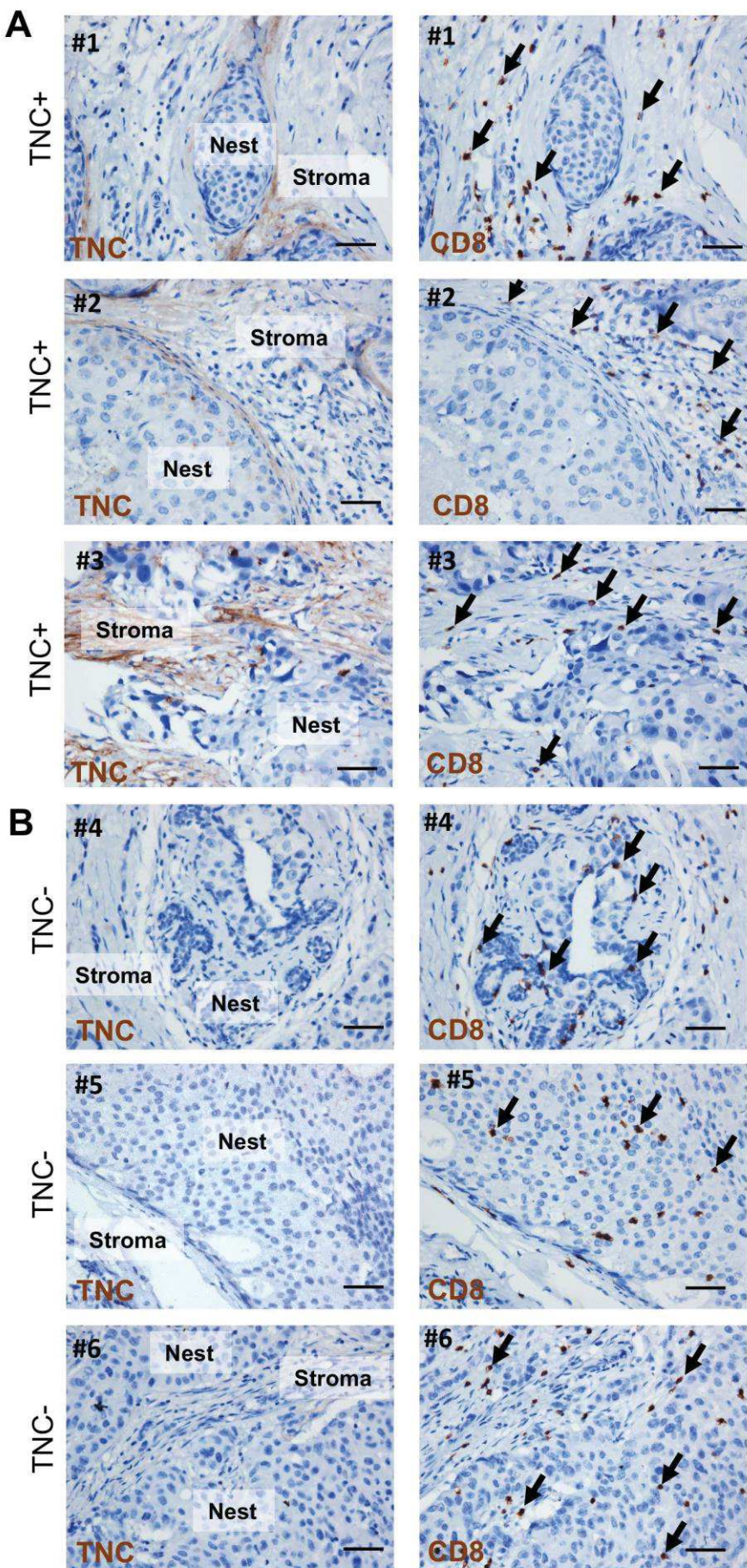
Appendix Fig. S4

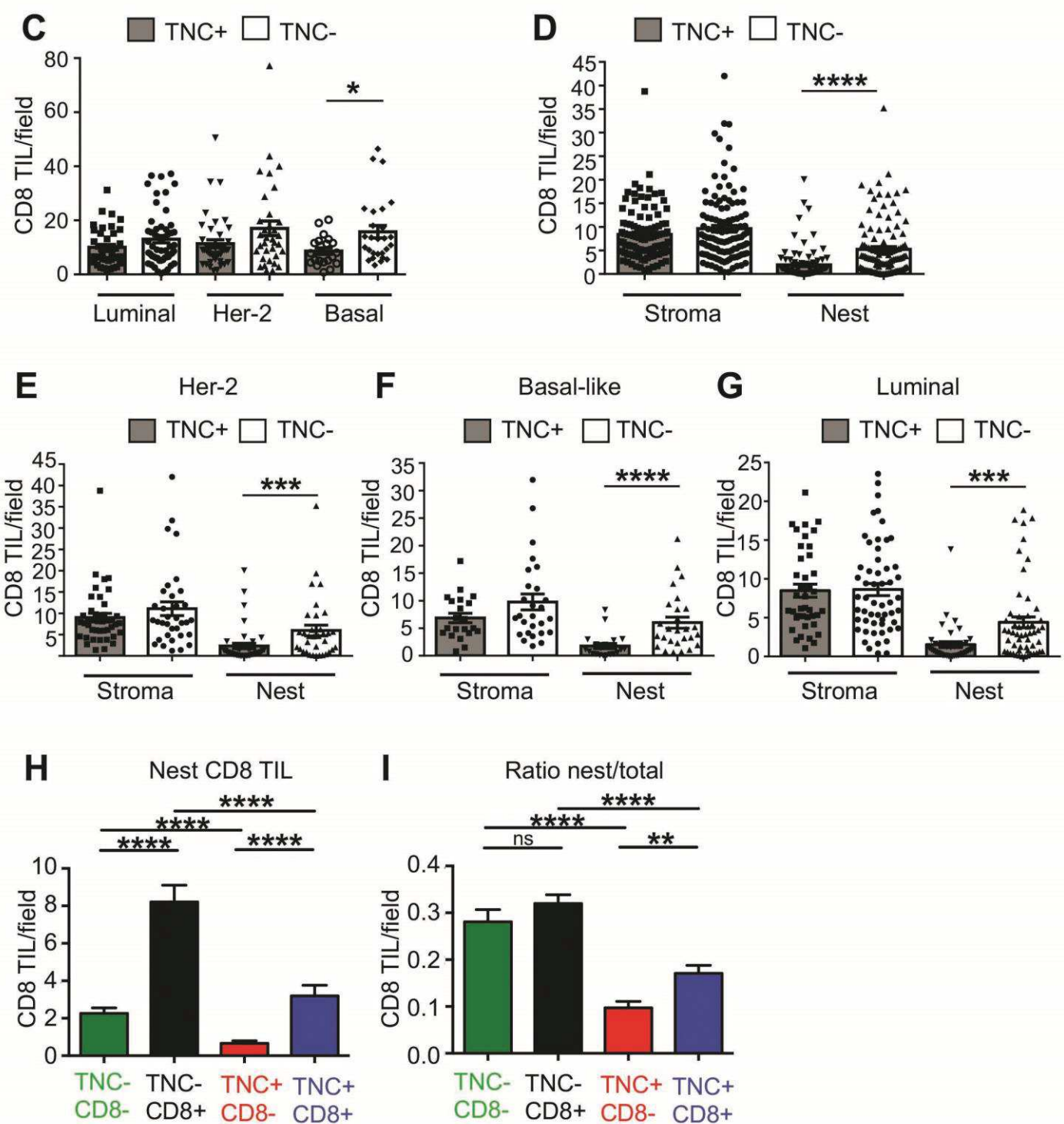


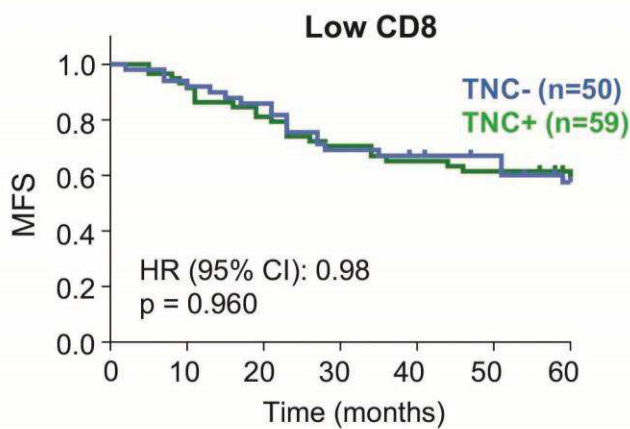
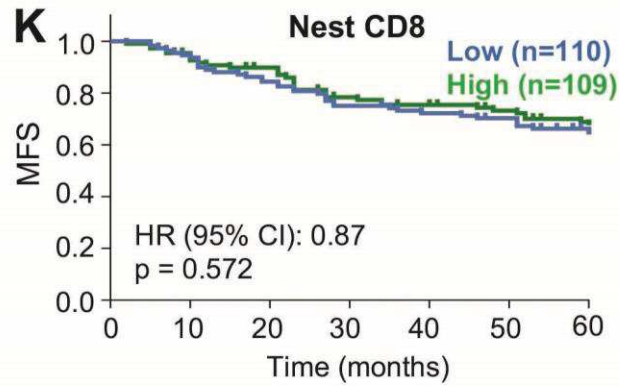
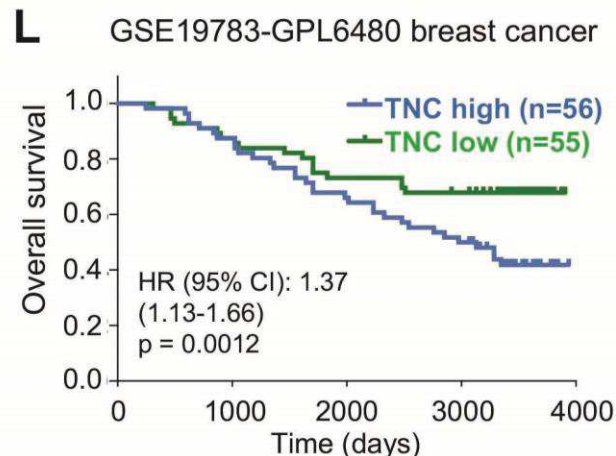
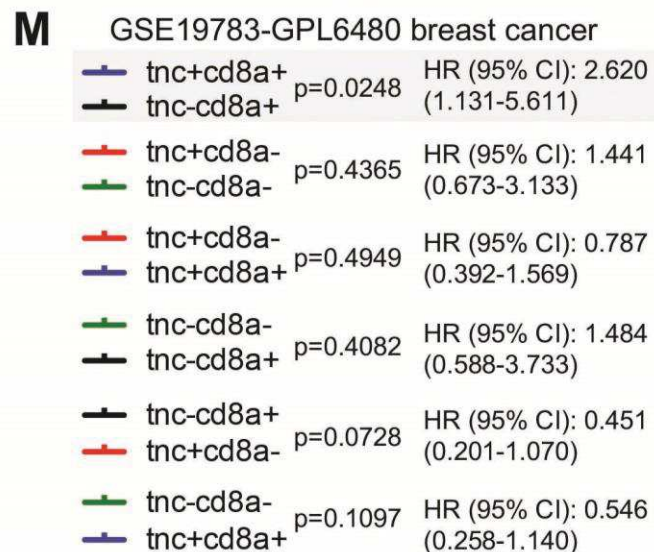
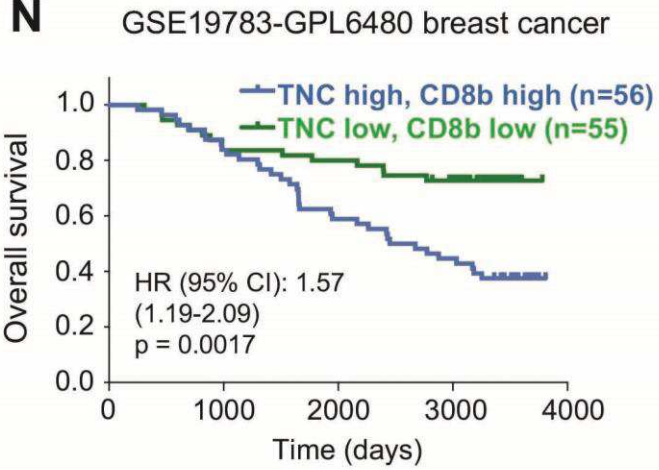
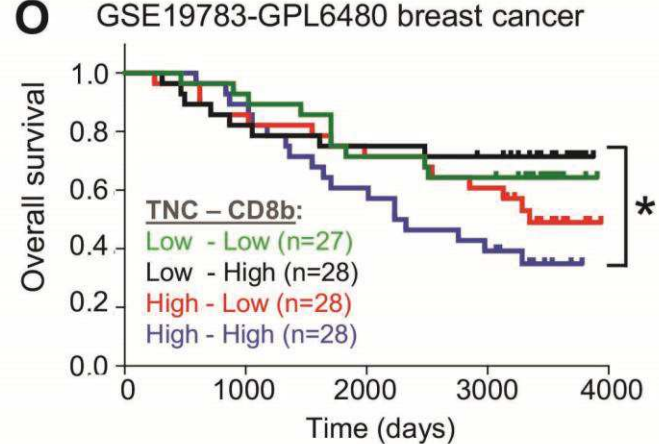
Appendix Figure S4 Impact of CXCR4 inhibition on BVI in NeuNT mice

Metastasis assessment in lungs from NeuNT mice by IF (**A**) and H&E staining (**B**). BVI are encircled with a broken white line. Representative images of N = 5 mice, PBS and N = 5 mice, AMD, scale bar, 50 μ m. (**C-E**) 5 weeks model. Number (**C**) and size (**D**) of lung metastases upon iv grafting of shC or shTNC cells followed by stereological analysis by H&E staining. N = 8 mice (shC, PBS), N = 7 mice (shC, AMD), N = 7 mice (shTNC, PBS), N = 7 mice (shTNC, AMD). No statistical difference was observed by Kruskal Wallis statistical test, p > 0.05. (**E**) Representative image of parenchymal metastasis and BVI. Scale bar, 200 μ m.

Appendix Fig. S5

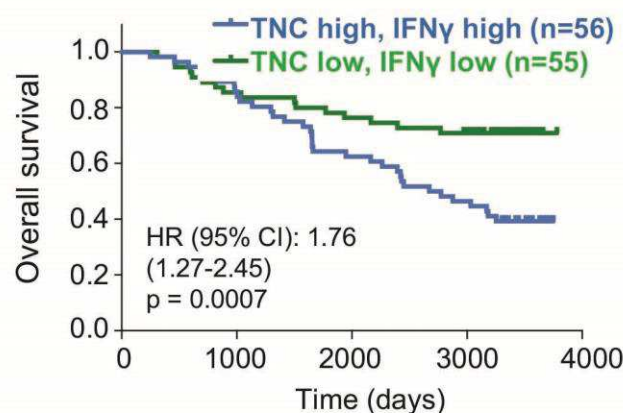




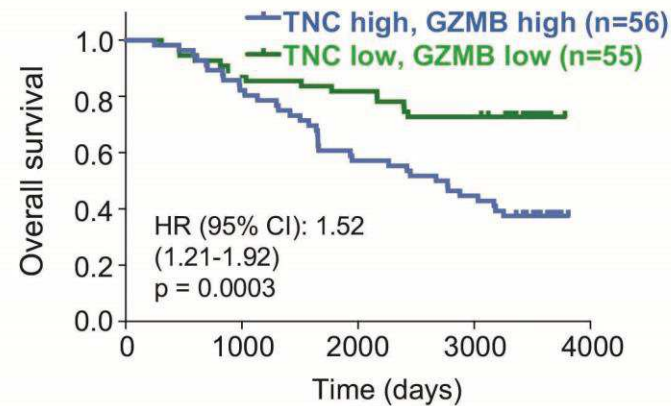
J**K****L****M****N****O**

tnc+cd8b+	p=0.0244	HR (95% CI): 2.501 (1.129-5.265)
tnc-cd8b+		
tnc+cd8b-	p=0.3520	HR (95% CI): 1.462 (0.659-3.267)
tnc-cd8b-		
tnc+cd8b-	p=0.2256	HR (95% CI): 0.654 (0.323-1.299)
tnc+cd8b+		
tnc-cd8b-	p=0.7339	HR (95% CI): 1.173 (0.466-2.962)
tnc-cd8b+		
tnc-cd8b+	p=0.1887	HR (95% CI): 0.564 (0.247-1.314)
tnc-cd8b-		
tnc-cd8b-	p=0.0382	HR (95% CI): 0.454 (0.215-0.951)
tnc+cd8b+		

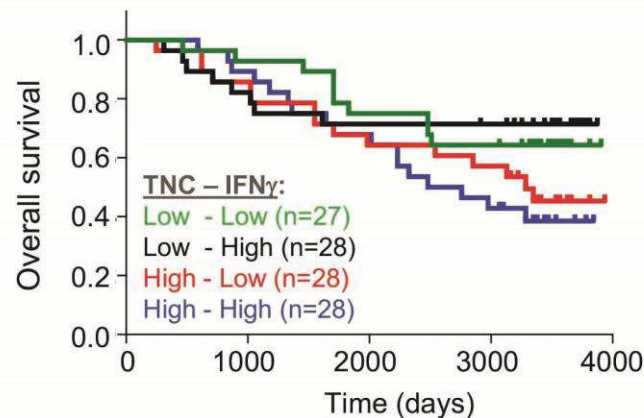
P GSE19783-GPL6480 breast cancer



R GSE19783-GPL6480 breast

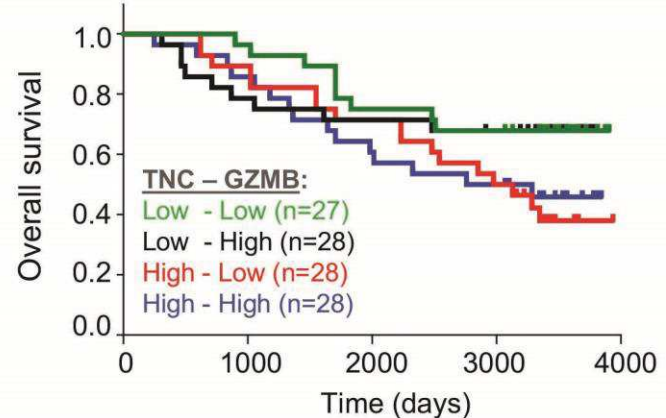


Q GSE19783-GPL6480 breast cancer

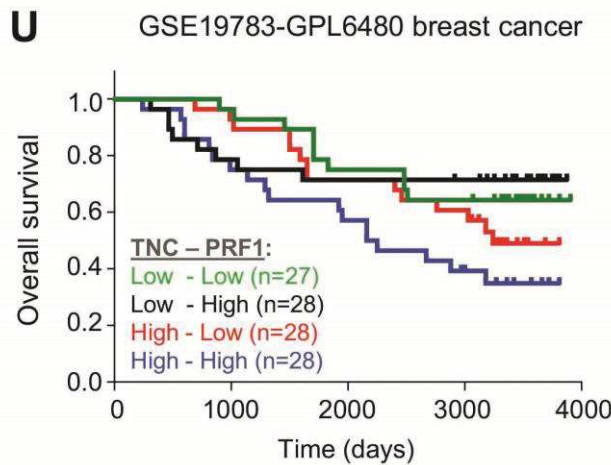
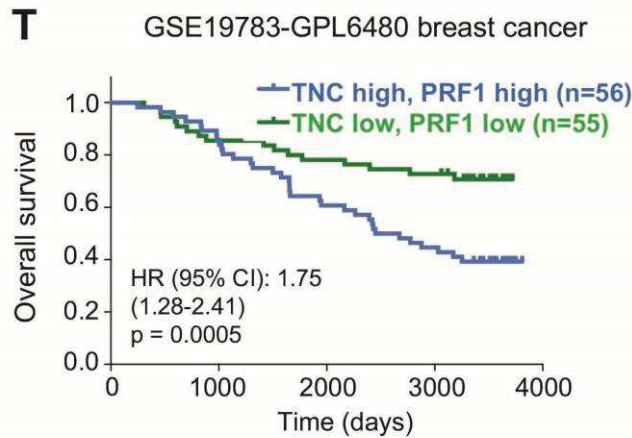


TNC+IFNG+	p=0.0595	HR (95% CI): 2.187
TNC-IFNG+		(0.975-4.678)
TNC+IFNG-	p=0.1982	HR (95% CI): 1.673
TNC-IFNG-		(0.767-3.690)
TNC+IFNG-	p=0.6038	HR (95% CI): 0.833
TNC+IFNG+		(0.416-1.662)
TNC-IFNG-	p=0.8074	HR (95% CI): 1.122
TNC-IFNG+		(0.445-2.833)
TNC-IFNG+	p=0.1239	HR (95% CI): 0.518
TNC+IFNG-		(0.231-1.187)
TNC-IFNG-	p=0.0654	HR (95% CI): 0.491
TNC+IFNG+		(0.228-1.038)

S GSE19783-GPL6480 breast cancer



TNC+GZMB+	p=0.2028	HR (95% CI): 1.697
TNC-GZMB+		(0.757-3.753)
TNC+GZMB-	p=0.0489	HR (95% CI): 2.185
TNC-GZMB-		(1.014-4.736)
TNC+GZMB-	p=0.8682	HR (95% CI): 0.943
TNC+GZMB+		(0.471-1.886)
TNC-GZMB-	p=0.7713	HR (95% CI): 0.873
TNC-GZMB+		(0.345-2.198)
TNC-GZMB+	p=0.1102	HR (95% CI): 0.526
TNC+GZMB-		(0.247-1.147)
TNC-GZMB-	p=0.0849	HR (95% CI): 0.493
TNC+GZMB+		(0.220-1.097)

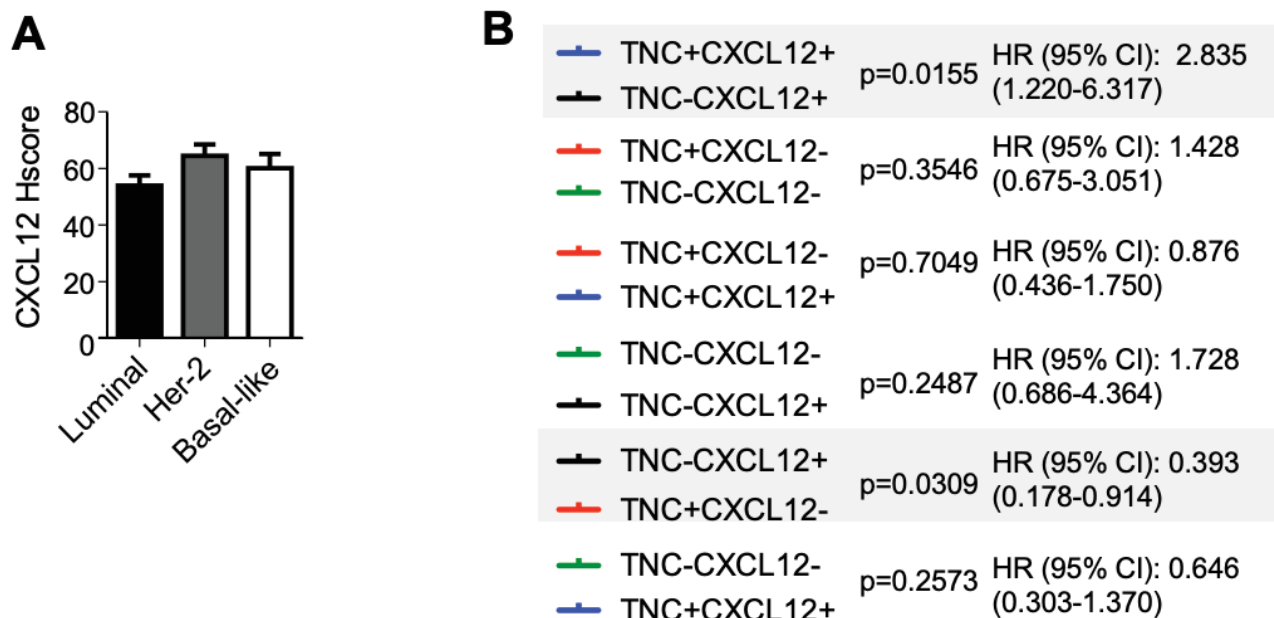


TNC+PRF1+	p=0.0248	HR (95% CI): 2.495
TNC-PRF1+		(1.125-5.246)
TNC+PRF1-	p=0.2886	HR (95% CI): 1.543
TNC-PRF1-		(0.695-3.448)
TNC+PRF1-	p=0.1485	HR (95% CI): 0.603
TNC+PRF1+		(0.296-1.197)
TNC-PRF1-	p=0.8436	HR (95% CI): 0.911
TNC-PRF1+		(0.361-2.298)
TNC-PRF1+	p=0.2388	HR (95% CI): 0.598
TNC+PRF1-		(0.262-1.392)
TNC-PRF1-	p=0.0239	HR (95% CI): 0.424
TNC+PRF1+		(0.199-0.886)

Appendix Figure S5 Correlation of TNC expression and CD8 TIL abundance with breast cancer patient survival

(A, B) Representative adjacent sections of human breast cancer tissue (TMA, N = 219) stained with antibodies specific for TNC or CD8. Scale bar = 50 μ m. **(C - G)** Determination of CD8 TIL in TNC+ and TNC- tumors of the different molecular subtypes. **(C)** Total and **(D - I)** nest or stromal numbers of CD8 TIL. Nest CD8- or CD8+ or stromal CD8- or CD8+ is defined as below/above median of nest or stromal CD8 TIL per area. **(C)** * p = 0.0161 **(D)** **** p < 0.0001 **(E)** *** p = 0.0007 **(F)** **** p < 0.0001 **(G)** *** p = 0.0003, **(H, I)** **** p < 0.0001, ** p < 0.01, Mann-Whitney test. **(J - U)** Survival analysis for the indicated molecules in patient cohort of the TMA **(J, K)** and cohort GSE19783 **(L - U)**. Values are shown above or below the median, HR and p values are indicated for the different comparisons. Log-rank test.

Appendix Fig. S6



Appendix Figure S6 Correlation of TNC and CXCL12 expression with breast cancer patient survival

(A) Histological score of CXCL12 staining in different molecular subtypes of breast cancer patients, TMA cohort, one way Anova. $p > 0.05$. **(B)** HR and p values are indicated for the different comparisons of TNC and CXCL12 expression with survival used in **Fig. 8E**. Log-rank test.

II. Unpublished results: TNC impacts tumor onset and NKG2DL expression in the NT193 model

1.1 Introduction

Tumors are complex ecosystems where the malignant cells interact with the surrounding environment and form altogether the tumor microenvironment (TME). In addition to tumor cells, TME comprises stromal cells including immune cells and cancer-associated fibroblasts, soluble factors and the extracellular matrix (ECM). More than providing only a physical scaffold, the ECM plays an active role in cancer progression by modulating the behavior of TME components (Yue, 2015). The ECM molecule tenascin-C (TNC) that is mostly absent from normal tissues, is highly expressed in tumor tissue and this high expression has been associated with poor overall and metastasis-free survival in breast cancer patients (Lowy and Oskarsson, 2015; Oskarsson et al., 2011). This correlation can be explained by the multiple effects of TNC described to promote cancer progression. TNC was reported to promote tumor-associated angiogenesis and to enhance cancer cell aggressiveness by increasing their proliferation, survival and invasion (Saupe et al., 2013; Orend and Chiquet-Ehrismann, 2006). TNC has also an impact on immune responses in cancers. In lung and prostate cancer models, TNC was reported to inhibit the activation and proliferation of T lymphocytes and the production of cytokines (Parekh et al., 2005; Jachetti et al., 2015). In breast cancer models TNC can impair the infiltration of monocytes and macrophages (Talts et al., 1999) and can favor macrophages to switch towards a M2 phenotype (Deligne et al., 2020). Our recent study in a cancer progression model demonstrated that TNC impairs the infiltration of CD8 T lymphocytes by sequestering them into the tumor matrix tracks through CXCL12/CXCR4 signaling (Murdamoothoo et al., 2021). However, the plethora of immunomodulatory functions of TNC are context-dependent and in some cases such as in chronic inflammation (Midwood et al., 2009) and more recently also in an oral squamous cell carcinoma (OSCC) model (Spenlé et al., 2020) and in our NT193 model (Deligne et al., 2020), TNC was reported to upregulate molecules involved in triggering anti-tumor immunity. Anti-tumor responses are notably mediated by

receptors expressed on immune effector cells that can detect molecules expressed by cancer cells. This detection triggers the activation of immune effector cells leading to the elimination of tumor cells. The Natural Killer Group 2 member D (NKG2D)/NKG2D ligand (NKG2DL) axis is a major regulator of immune responsiveness and several studies reported its importance in anti-tumor immunity (Diefenbach et al., 2001; Duan et al., 2019). Given that TNC is an important regulator of anti-tumor immunity and that we found by RNA seq analysis several NKG2DL to be expressed on cultured NT193 cells and in NT193 tumors in a TNC dependent manner, we considered the possibility that TNC may also have an impact on the NKG2D/NKG2DL axis.

Here we asked the following questions:

- 1.- Does TNC impact NKG2DL expression in the grafted NT193 tumor cells?
- 2.- Do NKG2DL expression levels impact NT193 tumor engraftment and metastasis?
- 3.- Does the immune cell repertoire impact tumor cell engraftment, growth and metastasis, in dependence of TNC?

1.2 Results

TNC expression impacts tumor growth in the NT193 model

As TNC can exist in many proteoforms with so far poorly understood functions we wanted to know whether host and tumor cell derived TNC had a specific impact on tumorigenesis and metastasis in the NT193 grafting model. By using a host lacking the TNC protein (TNCKO) and NT193 cells with repressed TNC expression (shRNA mediated) we previously showed that host TNC promotes lung metastasis by impacting the formation of blood vessel invasions (BVI) that represent a precursor of parenchymal metastasis (Sun et al., 2019 (see Appendix I)). We also noticed different growth properties of the engrafted tumor cells in a wildtype (WT) and TNCKO host. By grafting NT193 cells engineered to repress TNC (shTNC) or control NT193 cells (shC) into the mammary gland of either a WT or TNCKO host we noticed that all engrafted tumor cells induced tumors in a TNCKO host (**Fig. 1A-C**). However, whereas growth of shC cell derived and shTNC cell derived tumors was undistinguishable in a TNCKO host, shC tumor cells were rejected after 28 days in 50% of WT mice (**Fig. 1B**). The other 50% of WT mice got tumors undergoing a partial rejection (leading to reduced tumor volume) starting at 3 weeks post engraftment followed by tumor regrowth at 5 weeks reaching a comparable volume as all other tumors at the end of the experiment at 11 weeks (**Fig. 1 C**). Notably, no difference in the lung surface covered by tumor cells has been seen despite some significant differences in the BVI (Sun et al., 2019 (see Appendix I)). Altogether, these results suggest a role of TNC in tumor cell engraftment and that a combined expression of host- and tumor cell-derived TNC triggered tumor cell rejection which interestingly occurred with a 3 weeks delay only in a WT but not a TNCKO host.

NT193 model is a mixture of tumor cells with epithelial and mesenchymal properties impacting tumorigenesis

We hypothesized that tumor cell rejection may be impacted by the epithelial (E) and mesenchymal (M) properties of the cultured NT193 cells as these cells form clusters of E cells surrounded by M cells in cell culture (**Fig. 2 A**). To address a potential role of cell phenotype on tumorigenesis we first isolated NT193 cells with an E and M phenotype by differential trypsinization and confirmed their particular molecular E and M phenotype by RNA sequencing, immunofluorescence (IF), and western blot (WB)

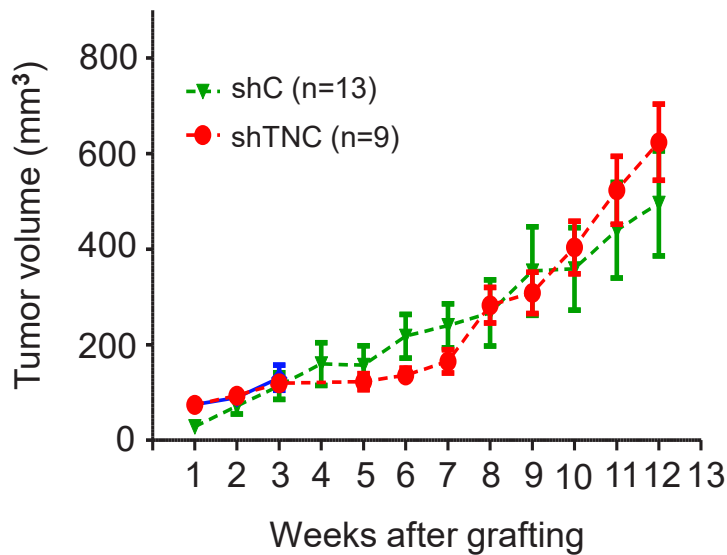
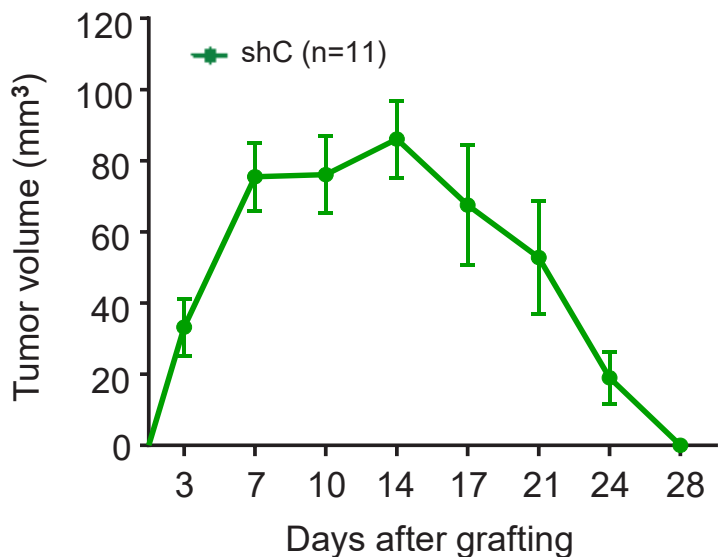
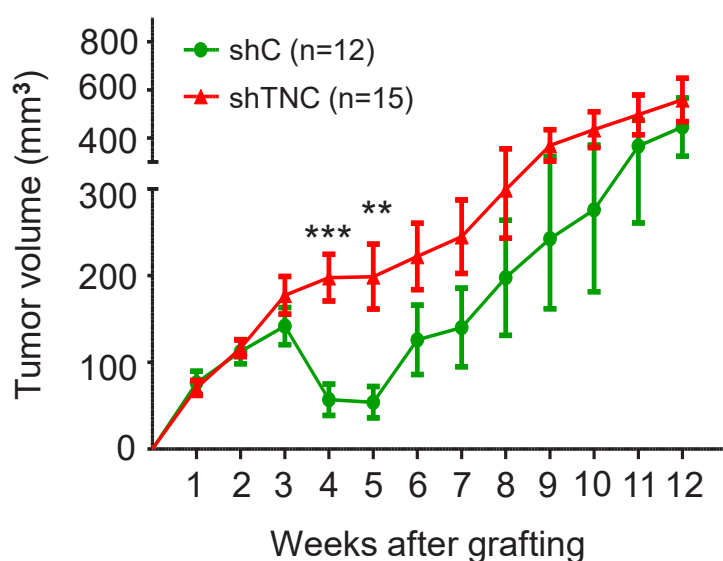
A**TNCKO host****B****WT host****C****WT host**

Figure 1: Combined expression of host- and tumor cell-derived TNC triggers partial tumor cell rejection. (A-C) Growth curves of NT193 (1×10^7) shC and shTNC cell derived tumors upon engraftment into a syngeneic FVB TNCKO (A) and FVB WT host (B,C), respectively. Multiple t-test, mean \pm SEM, ** $p < 0,01$, *** $p < 0,001$.

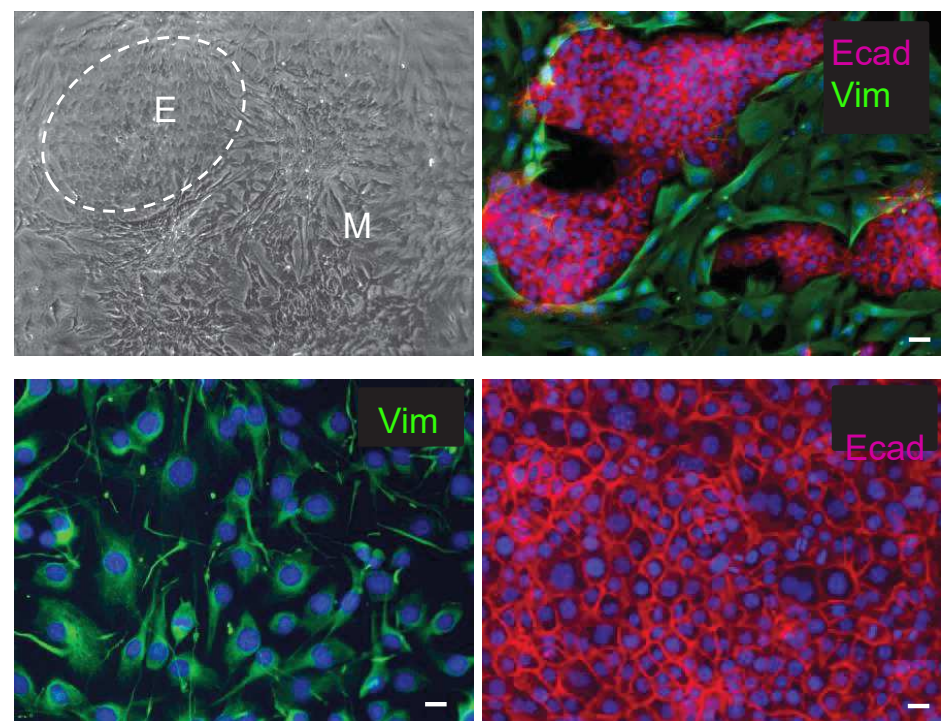
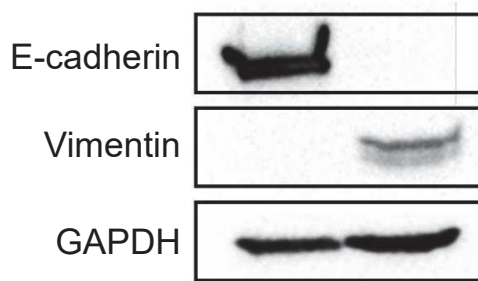
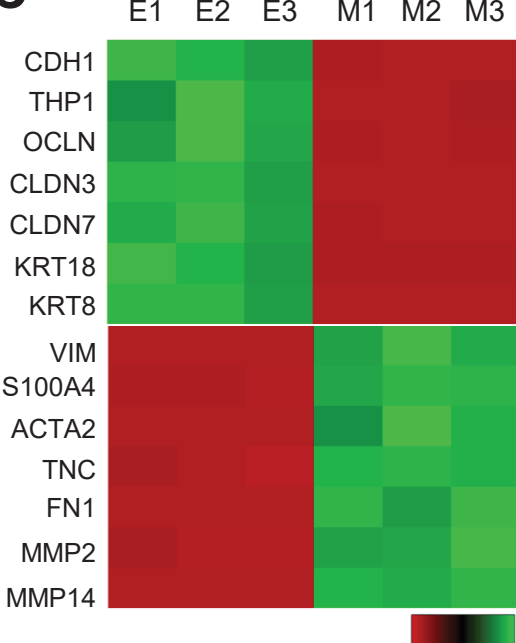
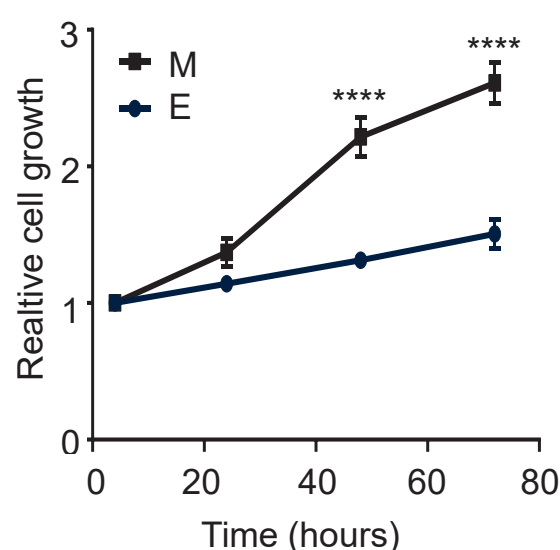
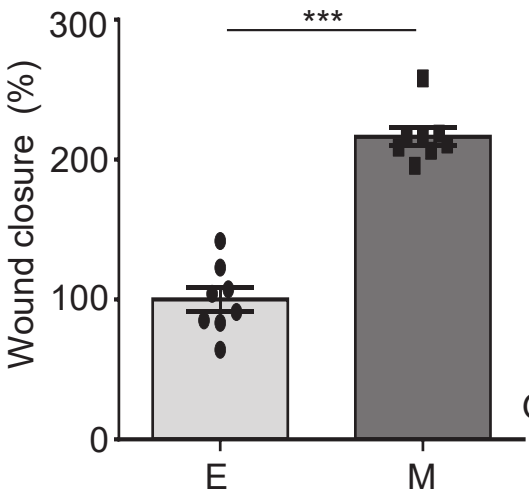
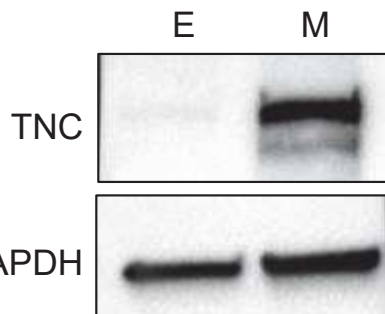
A**B****C****D****E****F**

Fig.2 Characterization of NT193E and NT193M cell lines. (A,B) Expression of epithelial and mesenchymal markers (phenotype, E-cadherin (Ecad) and vimentin (Vim), respectively) in E and M cells (A) upon phase contrast and immunofluorescence imaging, representative images ($N = 5$), scale bar 20 μ m, (B) and by immunoblotting ($N = 3$ experiments). (C) Expression of genes related to epithelial and mesenchymal properties in E and M cells determined by RNA seq analysis. $N = 3$ different passages. Limma moderated t-test, $p < 0,05$. red = low, green = high expression according to the provided scale (Row Z-Score). (D) Comparison of E and M cell proliferation, $N = 3$ experiments in triplicates. Multiple t-test, mean \pm SEM, $****p < 0,0001$. (E) Wound closure of E and M cells, $N = 4$ experiments in duplicates. Mann-Whitney test, mean \pm SEM, $***p < 0,001$. (F) Representative ($N = 3$ experiments) immunoblot for TNC in E and M cells.

(**Fig. 2 A-C**). RNA sequencing showed the presence of 12220 genes differentially expressed between E and M cells. By using panther gene ontology program we found that these genes are notably associated with cancer cell stemness, epithelial-to-mesenchymal transition, drug resistance and negative regulation of immune system processes (**Fig. S1**). Moreover, the RNAseq data indicate that the oncogene ErbB2 is found highly expressed in E cells compared to M cells. In addition, by performing functional assays we observed that M cells have a higher ability to proliferate and migrate compared to E cells (**Fig. 2D,E**). Also, high expression of TNC was found in M cells whereas no TNC expression was detectable in E cells (**Fig. 2F**). Altogether, these results show that E and M cells forming the NT193 model display distinct properties suggesting a different behavior *in vivo*.

M cells grafted in the mammary gland do not induce primary tumor development in the first 6 weeks post engraftment but disseminate to the lungs

In order to test whether E and M cells have a different behavior *in vivo* we grafted these cells in the mammary gland of FVB mice and observed that 100% of mice grafted with E cells developed primary tumors whereas no host engrafted with M cells got tumors 6 weeks post engraftment (**Fig. 3A**). To investigate the *in vivo* fate of these cells we analyzed the mammary gland of the mice by hematoxylin and eosin staining and IF, and observed that half of the grafted mice display a cancer cell cluster in the mammary gland tissue even though no palpable primary tumors developed suggesting that at least some M cells survived (**Fig. 3B**). Moreover, by analyzing the expression of the oncogene *Neu* (rat homologue of ErbB2) in the lungs of all mice by real time quantitative PCR (RTqPCR) we found a higher expression of this marker in the mice engrafted with M than with E cells, suggesting that some M cells escaped from immune surveillance and disseminated to the lungs (**Fig. 3C**).

M cells express NKG2DL and TNC triggers NKG2DL expression

In vitro, the proliferation ability of M cells was higher than E cells thus one would expect M cells to grow faster *in vivo* upon engraftment in comparison to E cells. However, this seems not to be the case as M cells did not form tumors. We used the RNA sequencing data to find gene expression differences between M and E cells that could explain why M cells do not give rise to palpable tumors *in vivo* during the 6 weeks' time frame of the experiment. We observed that M cells highly express the

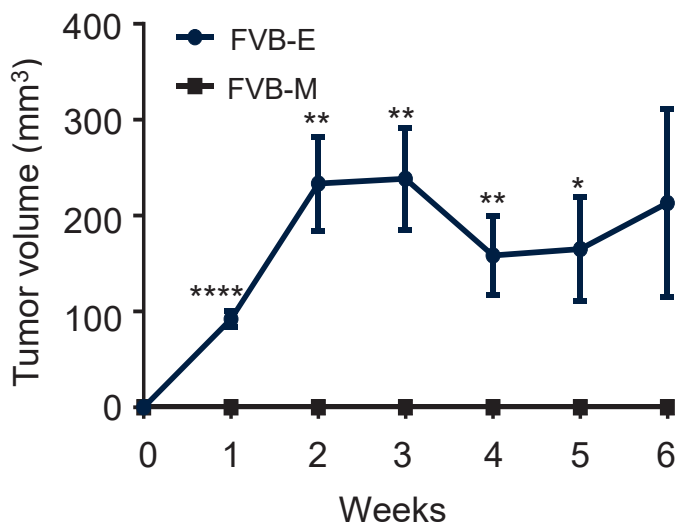
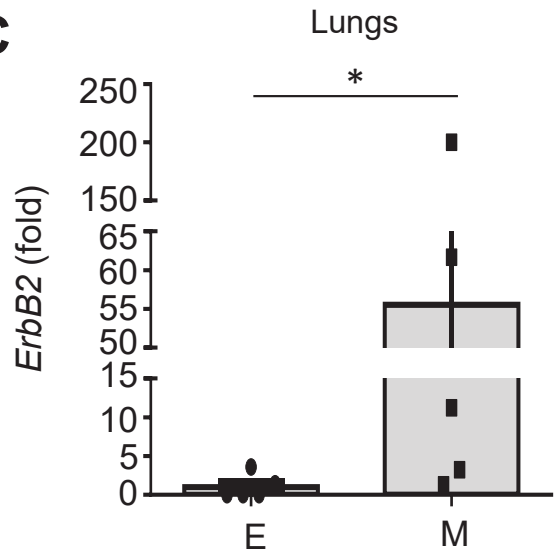
A**C****B**

Fig.3 Tumor growth and metastasis of orthotopically engrafted NT193 E and M cells. (A) Growth of E (5×10^6) and M (5×10^6) cell derived tumors upon engraftment into the mammary gland (MG) of a FVB host. N = 5 mice/group. Multiple t-test, \pm SEM, *p < 0,05, **p < 0,01, ****p < 0,0001. **(B)** Representative images of control (healthy) MG (N = 5) and MG from M cell engraftment (6 weeks) by H&E and immunofluorescent imaging for ErbB2 (far right). Note that tumor cells are found as clusters in half of the M cell-engrafted mice. N = 5 mice/group, scale bar, 50 μm . **(C)** Expression of ErbB2 in lungs of mice engrafted with E or M cells, respectively as determined by RTqPCR, N = 5 mice/group, Mann-Whitney test mean \pm SEM, *p < 0,05.

NKG2DL *H60b/c* and *Raet1d/e* but not *Mult1* (**Fig. 4A**). This was the opposite for E cells that expressed *Mult1* but not *H60* nor *Raet1*. We confirmed these results for H60 and Raet1 at protein level by WB (**Fig. 4B**).

Next, we determined whether TNC has an impact on NKG2DL expression and observed by RTqPCR and WB that the expression of *H60b*, *Raet1* and *Mult1* are significantly reduced in shTNC compared to shC cells suggesting that TNC may upregulate NKG2DL expression (**Fig. 4C-G**). This possibility was confirmed for H60 and Raet1 upon addition of soluble TNC to the shTNC cells (**Fig. 4H,I**). As no *Mult1* antibody was available that would recognize *Mult1* by western blot we could not determine *Mult1* protein expression levels.

Knockdown of TNC in M cells promotes tumor cell engraftment and tumor growth

As NKG2DL expression is known to enable cancer cell recognition by immune effector cells expressing NKG2D (NK and other cells) (Nausch and Cerwenka, 2008), and since we showed that TNC increases NKG2DL expression, we hypothesized that TNC may cause M cell recognition by NKG2D expressing immune cells through induction of H60 and/or Raet1 *in vivo* leading thereby to tumor cell elimination blocking tumor growth. First, we asked the question whether M cells with lowered TNC level (MshTNC) induce tumors. Our hypothesis was indeed confirmed as we observed that 50% of mice grafted with MshTNC cells developed a primary tumor already after 10 days and almost all mice (90%) showed tumors 20 days post engraftment (**Fig. 5 A,C**). After this initial phase, we observed a similar rejection pattern as observed after grafting of NT193 pool shC cells. Indeed, around 50% of MshTNC tumors that developed within 20 days post engraftment regressed progressively starting from day 35 and were totally rejected after 50 days post grafting (**Fig. 5 A-C**). At the latest time point of 90 days only 50 % of mice grafted with MshTNC cells had still a tumor (**Fig. 5C**). Nevertheless, those tumors that did not get rejected continued to grow (**Fig. 5A**) suggesting two groups of tumors, one that gets rejected and another that evades rejection. What is also intriguing is at first a rapid tumor induction that is followed by a prominent rejection starting after an extended period of time of some 20-30 days (**Fig. 5 A-C**). This observation suggests that the immune system may need time to get elicited and then acts on some but not

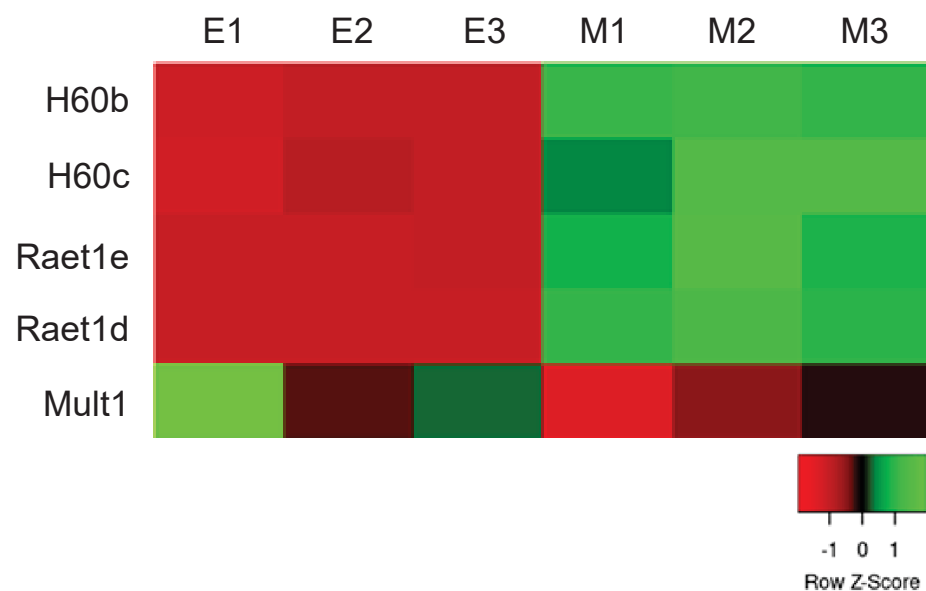
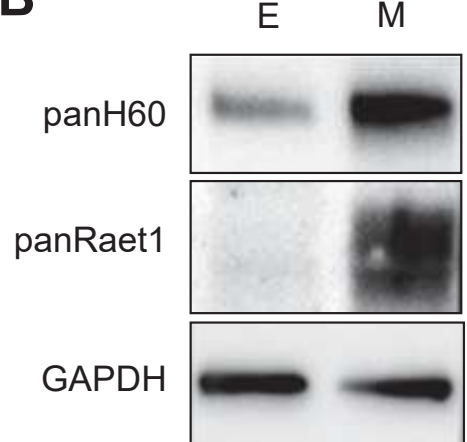
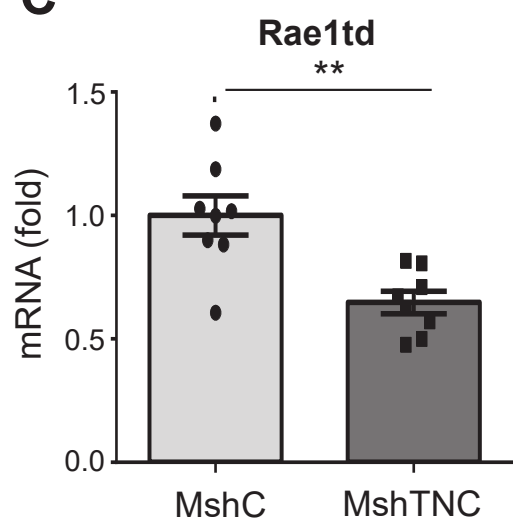
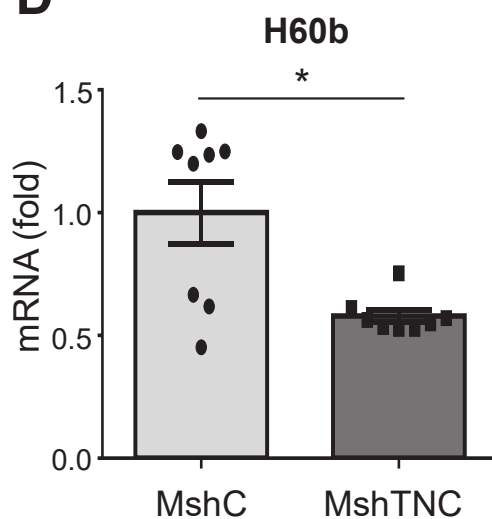
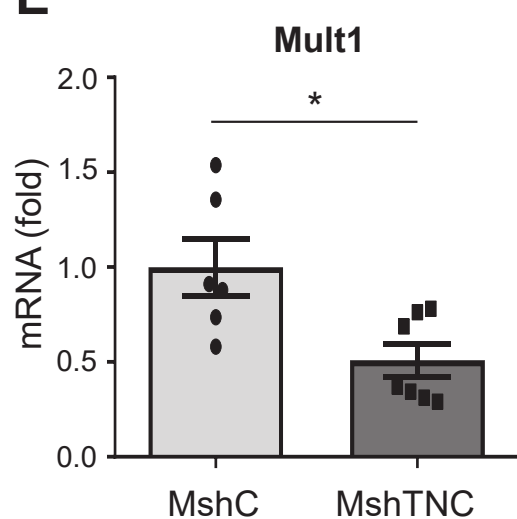
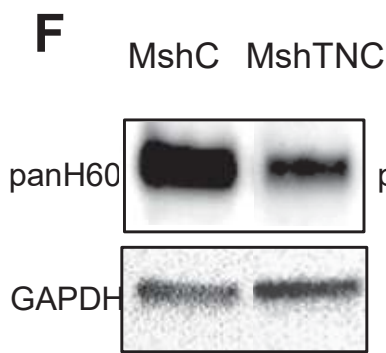
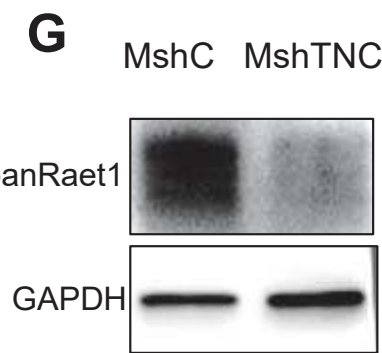
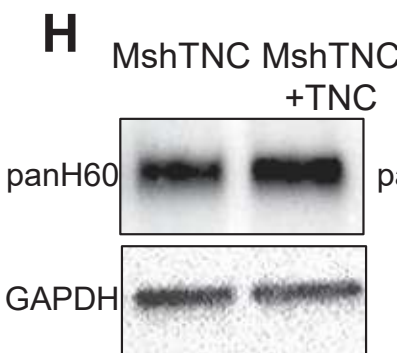
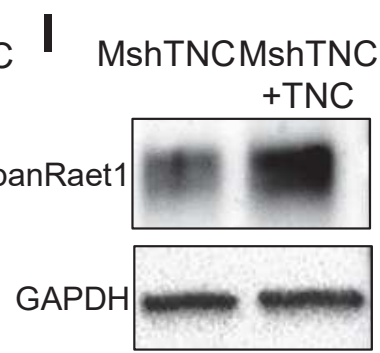
A**B****C****D****E****F****G****H****I**

Fig.4 Expression of NKG2DL in M cells in dependence of TNC. (A, B) NKG2DL expression determined (A) by RNAseq analysis (red = low, green = high expression) (N = 3 different cell passages) (B) and by immunoblotting in E and M cells (N = 2 experiments). (C-G) Expression of Raet1, H60 and Mult1 in MshC and MshTNC cells as determined by RTqPCR, N = 8 experiments, Unpaired t-test, mean \pm SEM, **p < 0,01 (C,E) and by immunoblotting (F, G). (H-I) Expression of H60 (H) and Raet1 (I) as determined by immunoblotting upon addition of soluble TNC (10 μ g/ml for 24 hours) to the cells (N = 2 experiments).

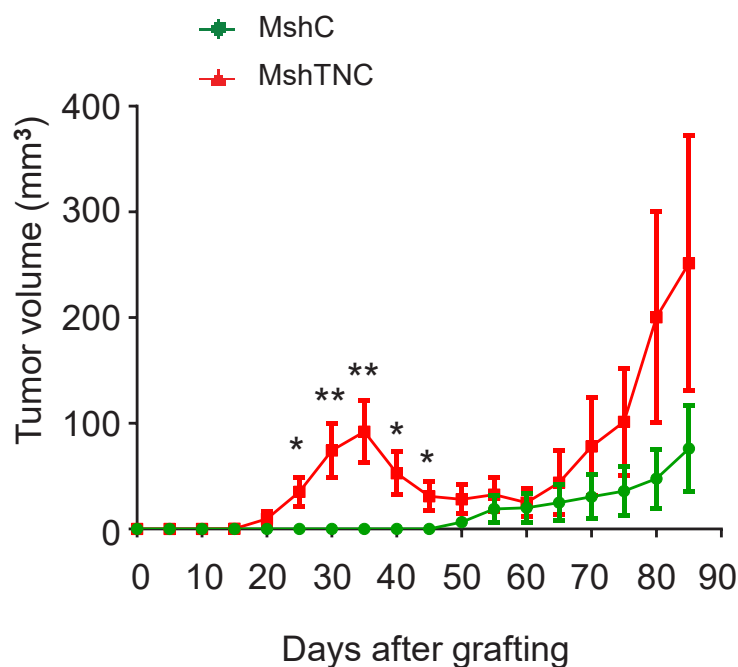
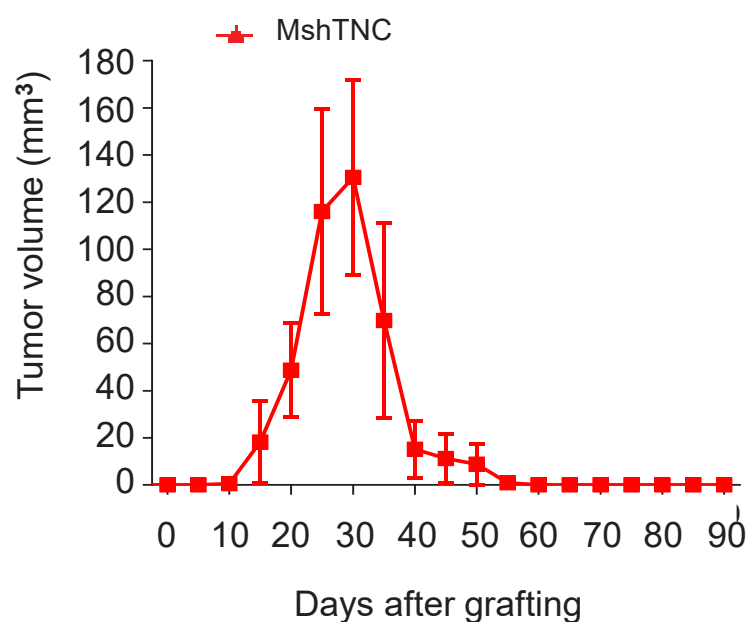
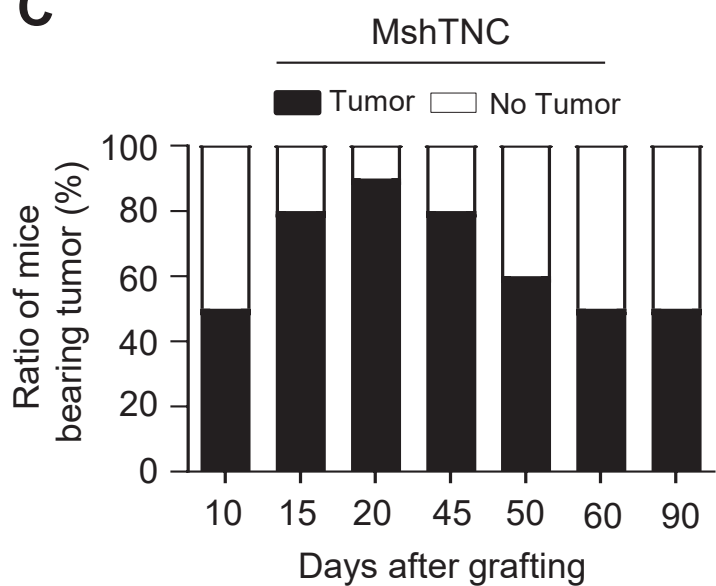
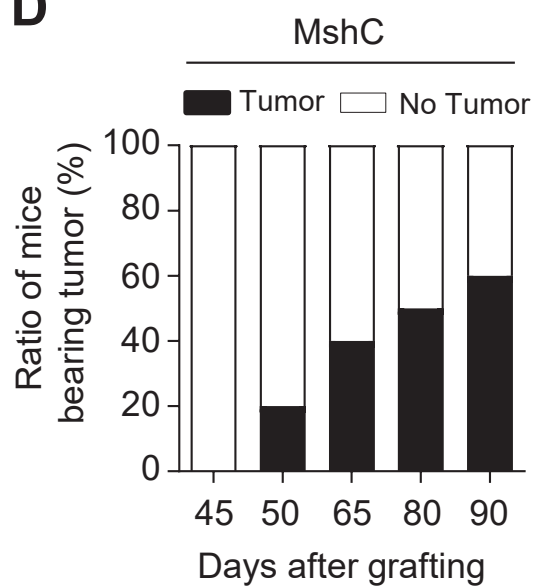
A**B****C****D**

Fig.5: Growth of engrafted MshC and MshTNC cells in the MG of a syngeneic host. (A,B) Growth of MshC (5×10^6) and MshTNC (5×10^6) cell-derived tumors upon engraftment into the MG of a FVB host. N = 10 mice/group, Multiple t-test, * $p < 0,05$, ** $p < 0,01$. (C,D) Ratio of mice bearing tumor over time after engraftment of the corresponding cancer cells.

all tumor cells which is associated with expression of TNC by the tumor cells. Unlike the rapid tumor onset in mice engrafted with MshTNC cell, none of the mice grafted with MshC cells developed tumor until day 50 post grafting (**Fig. 5 A,D**). Interestingly, later mice grafted with MshC developed progressively primary tumors starting after day 50, with tumor onset in 20% of mice at day 50, and tumors in 50% of mice after day 90 post grafting (**Fig. 5 A,D**). These results suggest a role of TNC in M tumor cell engraftment, growth and rejection. As the host is also expressing TNC and impacts anti-tumor immunity it will be important to determine whether in the absence of host TNC MshTNC cells still get rejected or now fully establish a tumor immediately upon grafting (indicating that host TNC is important for educating the immune system)

Crossregulation of NKG2DL expression

We wanted to know whether expression of NKG2DL in M cells represents an important obstacle for M cells to give rise to primary tumor. To test this hypothesis, we engineered M cells to downregulate either *H60* (shH60) or *Raet1* (shRaet1) with the aim to test their tumorigenic potential *in vivo* later. Upon selection of engineered cells we first confirmed a reduced expression of *H60* in Msh60 and *Raet1* in MshRaet1 cells by RTqPCR and WB (**Fig. 6A-D**). Interestingly, we observed *in vitro* a cross regulation among the NKG2DL family members which was unknown so far. In particular, *Raet1* expression was not only reduced by the KD of *Raet1* but was also reduced by the KD of *H60* and to a lesser extent it was also the case for *H60* that was reduced upon KD of *Raet1* (**Fig. 6E, F**). Moreover, we observed by RTqPCR that the KD of either *Raet1* or *H60* led to an increased *Mult1* expression suggesting a potential compensatory mechanism enforcing expression of at least one NKG2DL molecule (**Fig. 6G,H**). Due to the lack of a functional antibody specific for *Mult1* it was not feasible to assess *Mult1* protein levels upon *Raet1* and *H60* knockdown, respectively.

Simultaneous KD of the three NKG2DL families leads to decreased TNC expression but does not induce tumors

In order to avoid any potential *in vivo* compensatory mechanisms amongst NKG2DL members, we established a triple shNKG2DL M cell line (3-shNKG2DL) and a corresponding control cell line (3-shC). First we confirmed downregulation of the three NKG2DL family members by RTqPCR and WB (**Fig. 7 A-E**). The KD at mRNA

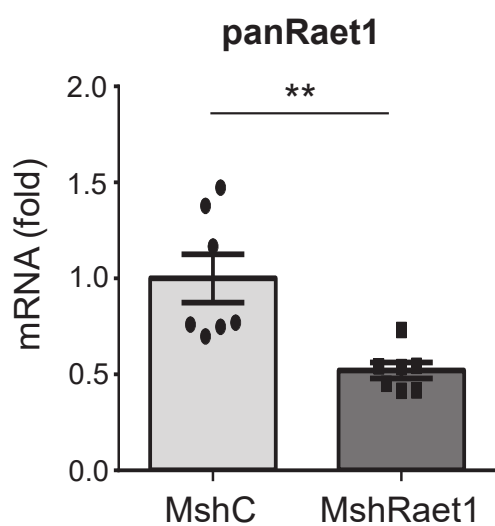
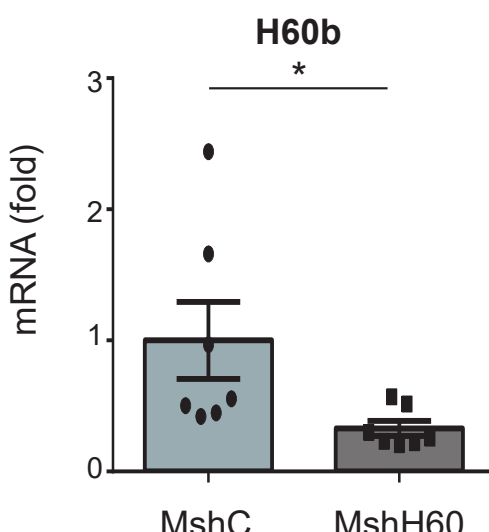
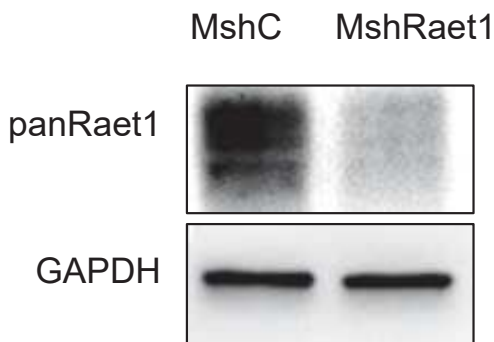
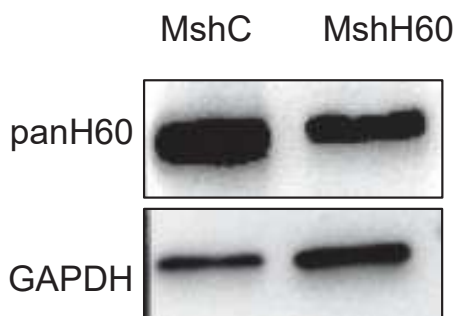
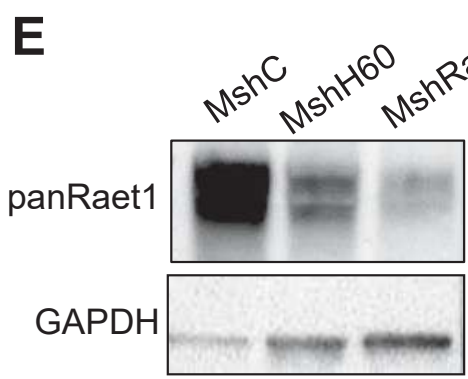
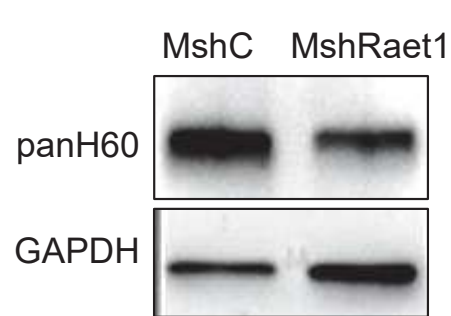
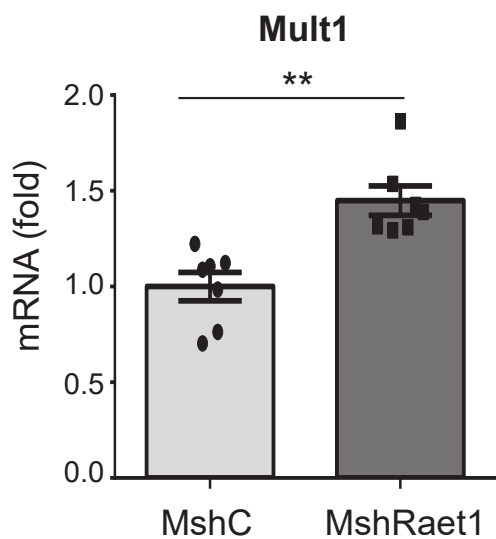
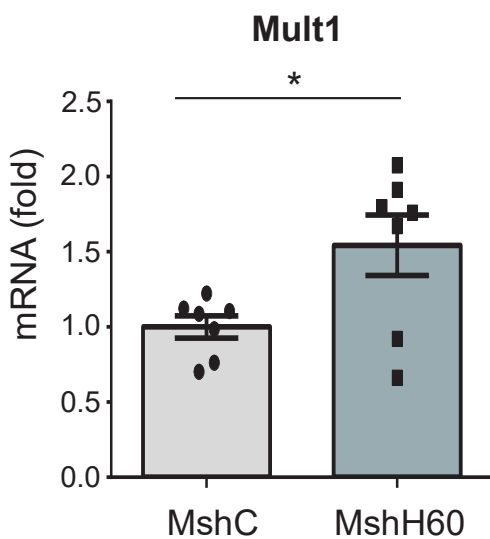
A**B****C****D****E****F****G****H**

Fig.6. Mult1 expression in NT193 M cells upon knockdown of H60 or Raet1, respectively.
(A-D) Expression of Raet1 (A,C), H60 (B,D) and Mult1 (G, H) as determined by RTqPCR, N = 7 experiments, Mann-Whitney test, mean \pm SEM, **p < 0,01 (A, B) Unpaired t-test, mean \pm SEM, *p<0,05, **p<0,01 (G, H) and immunoblotting (C - F), N = 2 experiments.

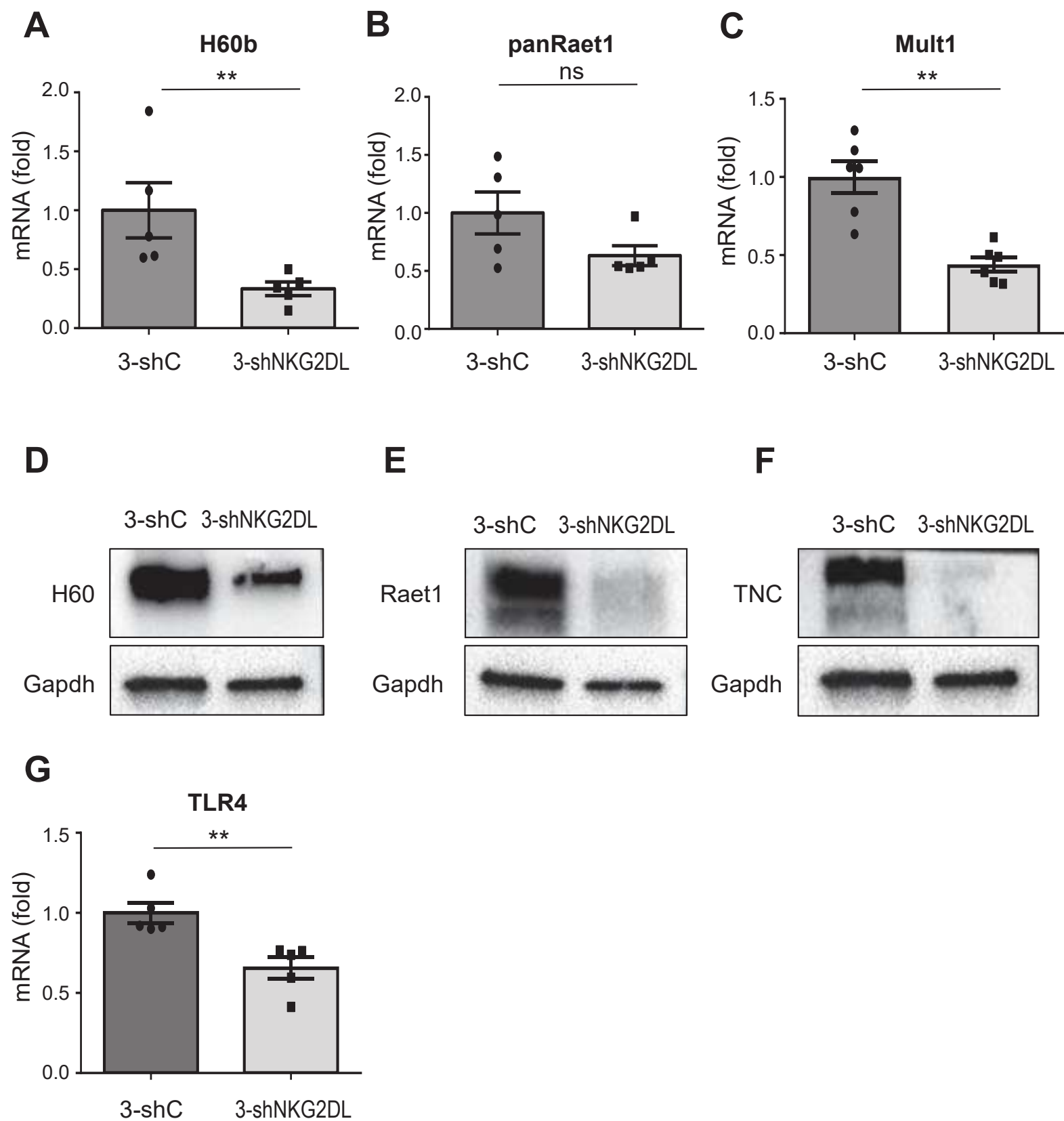


Fig.7. Impact of triple NKG2DL knockdown in M cells on NKG2DL and TNC expression.

(A-E) Expression of H60 (**A,D**), Raet1 (**B,E**) and Mult1 (**C**) as determined by RTqPCR, N = 5 experiments, Mann-Whitney test, mean \pm SEM, **p < 0,01 (**A-C**) and by immunoblotting, N = 2 experiments (**D,E**) in NT193 M cells with triple knockdown for all NKG2DL (3-shNKG2DL) or 3 control shRNA (3-shC). **(F)** Expression of TNC in 3-shNKG2DL and 3-shC cells. N = 2 experiments. **(G)** Expression of TLR4 in 3-shNKG2DL and 3-shC cells as determined by RTqPCR, N= 5 experiments, Mann-Whitney test, mean \pm SEM, **p < 0,01.

level was at least 50% for each molecule and even more pronounced at protein level for H60 and Raet1 (**Fig. 7A-E**). Again, it was not feasible to check *Mult1* protein levels. As we knew that TNC plays an important role in tumor cell engraftment, we wondered whether the triple NKG2DL KD had an impact on TNC expression which we investigated by western blot. Surprisingly, we observed a reduced expression of TNC in 3-shNKG2DL in comparison to 3-shC cells (**Fig. 7F**). As TLR4 is an important receptor for TNC and triggers signaling promoting immunity (Midwood et al., 2009b) we also investigated TLR4 expression by RTqPCR and again observed *Tlr4* reduction in the 3-shNKG2DL cells (**Fig. 7G**). Whether also TLR4 protein levels are reduced has to be determined in the future. Altogether these results revealed interdependence between the expression of H60, Raet1 and *Mult1* that has to be investigated in more detail in the future. We also discovered a crosstalk of NKG2DL and TNC and *Tlr4* expression. As M cells with reduced TNC expression (shTNC) induced tumors more robustly and faster than shC cells it is possible that reduced TNC levels may impact engraftment and growth of 3-shNKG2DL cells *in vivo*.

Now that we had generated M cells with a triple KD of the NKG2DL and saw downregulation of H60, Raet1 and *Mult1* we tested our hypothesis that NKG2DL expression on M cells caused their rejection *in vivo*. For that we engrafted the 3-shNKG2DL M cells into the mammary gland of FVB mice. However, until 90 days after engraftment none of the mice developed tumors. Either more time is needed for tumors to form, or expression of any of the NKG2DL is too high *in vivo* to prevent a NKG2D expressing immune cell response. Therefore, more work is needed to address NKG2DL and TNC levels in the mammary gland tissue. It is possible that the engrafted cells persisted in the mammary gland as observed for the shC M cells. If this is the case, it will be interesting to see whether immune cells and in particular those expressing NKG2D have infiltrated the tissue. As we already observed that M cells induced lung metastasis it is also possible that the KD of the NKG2DL impacted lung metastasis formation by the M cells.

Impact of host immune cell repertoire on tumor cell engraftment

So far we have investigated how expression of TNC or NKG2DL by the tumor cells impacts their engraftment, survival and lung metastatic potential. Now we asked whether the absence of important immune cell subtypes such as T, B and NK cells

impacted tumor cell engraftment, growth and metastasis. First we engrafted the same number of E and M cells (5×10^6) in the mammary gland of an immune competent FVB host or into immune compromised CB17 Scid mice (lacking for effective T and B cells) or Scid Beige mice (lacking for effective T, B and NK cells). We noticed that whereas E cells formed tumors in all mice (5/5) the M cells did not (**Fig. 8A**). We observed that the growth of E cell derived tumors was faster in immune deficient mice, indicating that E cell tumor growth is controlled by NK, B and T cells (**Fig. 8A**). When we performed this experiment we did not know that with prolonged tumor latency (over 50 days) some M cells start to generate tumors. Nevertheless, this experiment clearly showed that despite the absence of important immune subtypes M cells did not form tumors immediately until engraftment for 42 days.

Next we investigated whether the engrafted M cells potentially persisted in the mammary gland, and indeed by tissue staining for ErbB2 we found cell clusters in 60% (3/5) of FVB, Scid Beige and CB17 Scid mice (**Fig. 8B**). We then asked whether some tumor cells may have got an epithelial phenotype which we addressed by staining for CK8/18. Indeed, in all 3 hosts, some tumor cells expressed CK8/18 with no obvious differences (**Fig. 8B**). Moreover, staining for TNC revealed different expression patterns. Whereas in a Scid Beige or CB17 Scid Beige host TNC formed tracks like fibers this was not seen in the FVB host (**Fig. 8B**).

Next we asked whether the host specific immune cell repertoire had an impact on lung metastasis. It is well known that even without an apparent primary tumor metastasis can occur (Klein 2009). NT193 cells metastasize to the lung (Sun et al., 2019 (see Appendix I)), therefore we looked whether we can detect disseminated tumor cells in the lung by RTqPCR for *ErbB2* the oncogene that is ectopically expressed by the NT193 cells. Indeed, we could detect *ErbB2*+ E and M tumor cells in the lungs of FVB mice (**Fig. 3C**). This result indicates that M cells have homed to the lung despite the absence of a primary tumor. Interestingly, the *ErbB2* levels were several folds higher in the lungs of M-cell than in E-cell engrafted mice. Moreover, we observed a higher *ErbB2* expression in lungs of E-cell engrafted immunocompromised hosts than in FVB host with similar levels in Scid Beige and CB17 Scid lungs (**Fig. 8C**). This result indicates that the absence of T and B cells promotes lung metastasis in this model, but that an additional compromise in NK cell

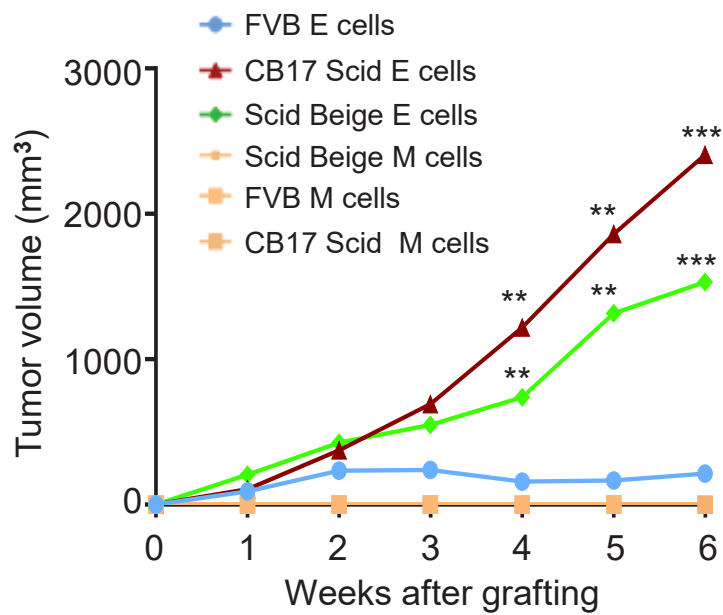
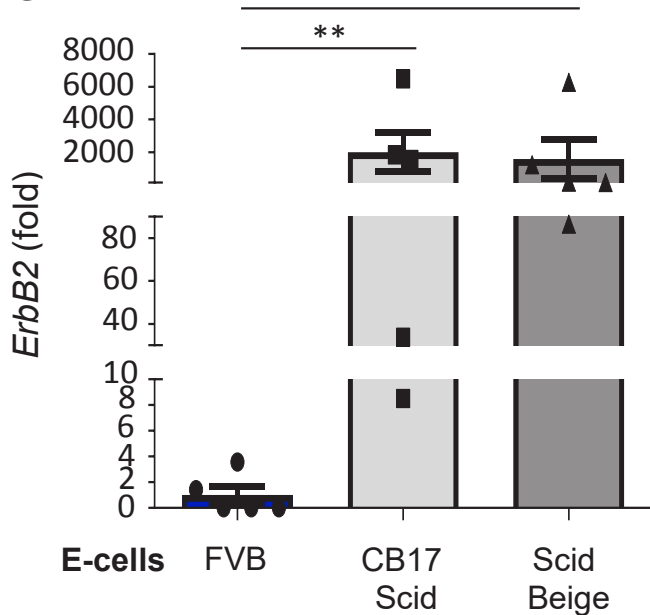
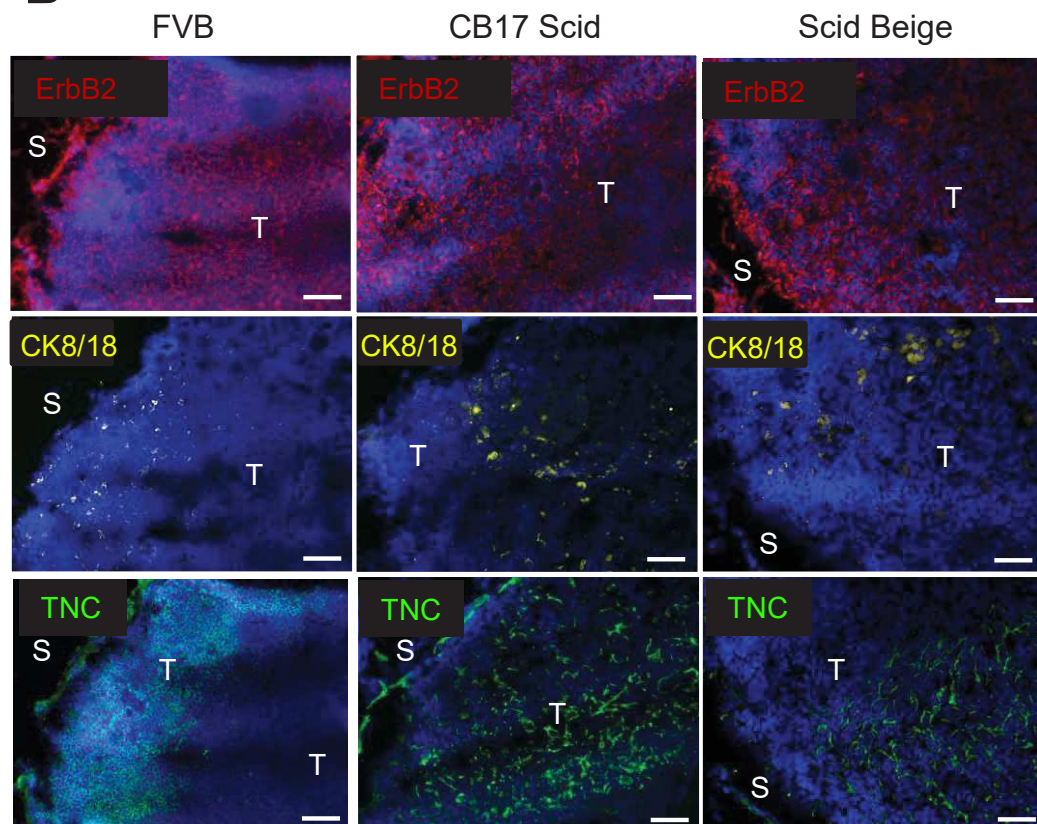
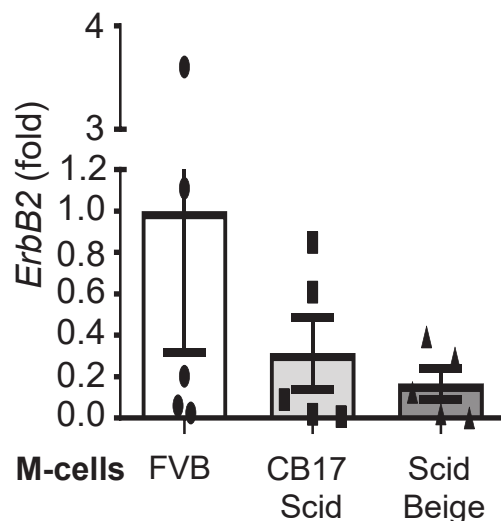
A**C****B****D**

Fig.8. Impact of host immune cell repertoire on tumor cell engraftment. (A) Growth of E and M (5×10^6) cell derived tumors upon engraftment into the mammary gland of a FVB, CB17 Scid and Scid Beige host. Multiple t-test, \pm SEM, **p < 0,01, ***p < 0,001. (B) Representative images (N=4) of mammary gland tissue immunofluorescence staining for the indicated markers. N= 3 mice/group, S: Stroma, T: Tumor, scale bar 50 μ m. (C,D) Expression of ErbB2 in lungs of mice engrafted with E (C) and M (D) cells as determined by RTqPCR, N = 5 mice/group, Mann-Whitney test mean \pm SEM, **p < 0,01.

function does not further promote lung metastasis. Interestingly, there was a tendency towards more *ErbB2*⁺ M cells in a FVB host than in the two immune compromised hosts (**Fig. 8D**). More experiments are necessary to evaluate this result.

Altogether, these results suggest that the immune system recognizes E and M cells differently and that a pronounced rejection effect on a mixture of E and M cells (pool NT193) is seen after a 3 weeks latency period. TNC plays a role in tumor cell rejection where a combined expression of TNC by the host and tumor cells drives total or partial rejection. Whereas E cell engraftment gives rise to primary tumor quickly (2 weeks post engraftment), M cell engraftment is largely delayed. This is overcome when M cells express little TNC (shTNC). Nevertheless, despite the failure to induce a primary tumor, M cells persisted in the mammary gland and homed to the lung. Future studies have to determine whether M cells have a defect in proliferation and/or apoptosis. Moreover, whether M cells form full blown metastasis has also to be addressed in the future. Another interesting question is how E cells evade immune surveillance and induce tumors that appear not to be rejected. Here the differential expression of the NKG2DL could be important.

1.3 Material and methods

Mice model and animal experiments

All mice were housed and handled according to the guidelines of INSERM and the ethical committee of Alsace, France (CREMEAS) (Directive 2010/63/EU on the protection of animals used for scientific purposes).

TNC +/- mice in the 129/Sv genetic background provided by Reinhard Fässler (Talts et al. 1999) were crossed 10 consecutively times with FVB/NCrl mice (Charles River) to homogenize the background before crossing TNC+/- males with TNC+/- females to obtain TNC +/+ (WT) and TNC -/- (KO) littermates. Female immune deficient mice (Scid Beige and CB17 Scid) were purchased from Charles River. All female mice were used at 2-3 months of age. For the orthotopic syngeneic model, 5×10^6 of the indicated cells were diluted in 50 μ l of phosphate buffer saline (PBS) solution and injected orthotopically into the left fourth mammary glands of the indicated mice. Tumor size was measured every 4 to 6 days with a caliper, and tumor volume was calculated using the formula $V = (a^2 \times b)/2$, where b is the longest axis and a is the perpendicular axis to b. Mice were euthanized at the indicated time points and breast tumors, lungs and mammary gland tissue were removed for analysis. Tissues were frozen in liquid nitrogen for RTqPCR or embedded in OCT for Hematoxylin-Eosin and IF stainings.

Hematoxylin-Eosin staining (HE)

OCT-embedded tissue was cut in 7 mm thick sections, dewaxed and rehydrated with 100% toluene with 2 washes of 15 min, and then incubated in 100% -70% alcohol solutions for 10min each before staining with hematoxylin for 5 min and washing with tap water. Sections were then processed with differentiation solution (1% HCl in absolute ethanol) for few seconds and washed under tap water for 10 min. Then the sections were incubated with eosin for 10 seconds, washed and dehydrated by rapid bath in 70% - 100% alcohol solutions before a final wash in toluene for 15 min. Slides were finally mounted in Eukitt solution (Sigma).

Cell lines, transduction, and culture

NT193 cell line has been previously established in the laboratory from a primary MMTV-NeuNT breast tumor (Arpel et al. 2014). NT193 cells were cultured in Dulbecco's modified Eagle's medium (DMEM) containing 4.5 g/L glucose supplemented with 10% of inactivated fetal bovine serum (FBS), penicillin (10 000 U/ml), streptomycin (10 mg/ml) and Gentamicin (40 µg/ml).

Silencing of TNC in the NT193 cells was done previously in the laboratory by short hairpin (sh) RNA mediated gene expression knock down (KD). Transduction with a lentivirus expressing a shRNA vector specific for TNC was used and a lentivirus encoding a non-targeting shRNA vector was used as a control (shC: SHC202V, Sigma) (Sun et al., 2019 (see Appendix I)). Transduced cells (shC and shTNC) were selected with the classical medium described above supplemented with puromycin (1 µg/ml). NT193 E and NT193 M cell lines were generated from NT193 shC and shTNC by applying differential trypsinizations during 5 passages and were cultured in the classical medium described above described above supplemented with puromycin (1 µg/ml). shH60 M cell line was generated from M cell line using a lentivirus with shRNA against *H60* and was cultured with the classical medium described above supplemented with puromycin (1 µg/ml). shRae1 M cell line was generated from M cell line using a lentivirus with shRNA against *Rae1* and was cultured with the classical medium described above supplemented with puromycin (1 µg/ml). Triple shNKG2DL M cell line was generated from M cell line using the same sequences than for shH60 and shRae1 in addition to lentivirus with shRNA against *Mult1*. Three lentivirus encoding non-targeting shRNA were used as control (shC1, shC2, shC3). Transduced cells were cultured with the classical medium described above supplemented with puromycin (1 µg/ml), hygromycin (100 µg/ml) and blasticidin (1 µg/ml). All oligonucleotide sequences used for gene expression KD are listed in **Table 1**. All cell lines were maintained at 37°C in a humidified atmosphere of 5% CO₂ and the selection pressure was maintained in all *in vitro* experiments.

Cell expansion measurement

E and M cells were seeded into 96-well plates (1000 cells/well) and cultured in normal medium at 37°C in a humidified atmosphere of 5% CO₂. Cell growth was

assessed by using the CellTiter 96® Aqueous Non-Radioactive Cell Proliferation Assay (Promega G5421) according to the manufacturer's instructions. Briefly, cells were incubated with the CellTiter 96® for 2 hours at 37°C and cell expansion was measured after 4,24, 48 and 72 hours. The optical density (OD:490) was measured with a Varioskan LUX Multimode Microplate Reader (ThermoFisher).

Wound healing assay

E and M cells were grown to confluence in 24-well plates in normal medium before starving in medium containing no FBS during 6 hours. Confluent cell monolayers were then treated with mitomycin C at 2 µg/ml for 2 hours to inhibit cell proliferation before application of a scratch wound with a pipet tip. Cell debris was removed by washing with PBS before incubating cells in serum free medium. Pictures of each wound were acquired directly after the scratch and after 16 hours of incubation at 37°C in a humidified atmosphere of 5% CO₂. The relative wound closure was calculated by measuring the surface of the cell-free area at the time of injury and at the end point of the experiment.

Real Time quantitative PCR (RT-qPCR)

Total RNA was extracted from frozen tissues and cultured cells using TriReagent (Life Technologies) according to the manufacturer's instructions. RNA concentration and purity was determined with a NanoDrop 2000 (ThermoFisher). RNA was then treated with DNase I (Roche). After inactivation of DNase I RNA was reverse transcribed (MultiScribe reverse transcriptase, Applied Biosystems) and qPCR was done on cDNA (diluted 1:5 in water) with a QuantStudio™ 5 Real-Time PCR System (Applied Biosystems) using Taqman™ Fast Advanced Master Mix (Applied Biosystems). Expression of mouse *GAPDH* mRNA was used as housekeeping gene in the comparative cycle threshold method (2-ddCt). Primers used for qPCR are listed in the **Table 2**.

Gene expression analysis by RNA-sequencing

Total RNA was prepared as described for RT-qPCR. RNA integrity was determined with the Agilent Bioanalyzer 2100 (Pico Kit, Agilent Technologies). Sequencing library was prepared with the Ion Total RNA-sep kit v2 (ThermoFisher) according to the

manufacturer's protocol. Libraries were loaded at a concentration of 20 pM on an Ion PI™ Chip Kit v3 (ThermoFisher) using the Ion Chef Instrument (ThermoFisher). Sequencing was performed on an Ion Proton sequencer with the Ion PI™ Hi-Q™ Sequencing 200 Kit (ThermoFisher). The transcriptomic data were processed using the RNASeqAnalysis plugin from the Torrent Suite Software 5.06 and the reads were mapped using STAR and Bowtie2 (Dobin et al., 2013, Langmead and Salzberg 2012). The total mapped reads were finally available in Binary Alignment Map (BAM) format for raw read count extraction. Read counts were found with the HTseq-count tool of the Python package HTSeq (Anders et al., 2015). Differential analyses were performed using the DESEQ2 package of the Bioconductor framework (Love et al., 2014). Up-regulated and down-regulated genes were selected based on the adjusted p-value (<0.10) and the heatmapping was done using online heatmapper.

Western blotting (WB)

Cell lysates were prepared using Radioimmunoprecipitation (RIPA) lysis buffer (50mM Tris-HCl pH8, 150mM NaCl, 1% NP-40, sodium deoxycholate, 0.1% SDS) supplemented with protease and phosphatase inhibitor (Pierce EDTA-Free mini tablets, ThermoFisher). Protein concentration was determined with a Bradford Assay (BioRad). After addition of Laemmli buffer (Biorad) containing 10% of β mercaptoethanol (Merck), 20-40 μ g of proteins were loaded into precasted 4-20% gradient gels (BioRad) and separated by SDS-PAGE. Separated proteins were transferred on nitrocellulose membranes (Biorad) using TransBlot Turbo™ Transfer System (Biorad). The membrane was incubated in blocking solution (5% non-fat milk diluted in 0.1% PBS-Tween20) during 1 hour at room temperature and incubated with the primary (overnight at 4°C) and the corresponding secondary antibodies (1 hour at room temperature) in 1.5% blocking solution. Protein bands were detected in a ChemiDoc™ Imager (BioRad) using the Amersham ECL Western Blotting detection reagent (GE Healthcare) or SuperSignal™ West Femto Maximum Sensitivity Substrate (ThermoFisher). Antibodies are listed in the **Table 3**.

Tissue Immunofluorescence staining (IF)

OCT-embedded tissue was cut in 7 mm thick sections and incubated for 1 hour at room temperature with a blocking solution (5% normal goat serum (NGS) in PBS)

before overnight incubation with the indicated primary antibodies at 4°C. Slides were washed and incubated with the corresponding secondary antibody for 1 hour at room temperature and then washed before incubation with DAPI (Sigma) for 10 min at room temperature. After washes the slides were mounted with Fluoromount-G™ (ThermoFisher). Images were acquired with a Zeiss Axio Imager Z2 microscope. Antibodies are listed in **Table 3**.

Cells Immunofluorescence staining (IF)

Cells were cultured in Nunc™ Lab-Tek™ II Chamber Slides™ (ThermoFisher) and were then fixed with 4% paraformaldehyde (PFA, Santa Cruz) in PBS for 10 min before permeabilization with 0.25% Triton (Euromedex) in PBS for 15 min. Then cells were washed and blocked with NGS for 30 min before incubation with primary antibody for 1 hour at room temperature. After washing cells were incubated with the corresponding secondary antibodies for 45 min, then washed, incubated with DAPI for 10 min and washed again. Slides were mounted with Fluoromount-G™ (ThermoFisher). Images were acquired with a Zeiss Axio Imager Z2 microscope. Antibodies are listed in **Table 3**.

Statistical analysis

Statistical analysis and graphical representations of data were done using GraphPad Prism software (version 6). Gaussian distribution was tested by using the Agostino-Pearson normality test. The data following a normal distribution were analyzed by using an unpaired t-test. The data not following a Gaussian distribution were analyzed by Mann Whitney test. Cell and tumor growth were analyzed using Multiple t-test, RNAseq data were analyzed using a Limma moderated t-test. Data representative of at least 3 individual experiments, expressed as the mean \pm SEM. p-values smaller than 0.05 were considered as significant (*, p<0.05, **, p<0.01, ***, p<0.001, ****p<0.0001).

1.4 Tables

Table 1: Oligonucleotide sequences used for cell transduction

Target Gene	Oligonucleotide sequence
TNC	5'-CCGGGCATCAACACAAACCAGTCTAACTCGAGTTAGACTGGTT GTGTTGATGCTTTTG-3'
H60	5'-CCGGGATGAACAGCATAGCATCTACCTCGAGGTAGATGCTAT GCTGTTCATCTTTTG-3'
Raet1	5'-CCGGCCAGTATCACCCAGCTTACATCTCGAGATGTAAGCTGG GTGATACTGGTTTTG-3'
Mult1	5'-CCGGAGCTGACTGCCAGTAACAAGGCTCGAGCCTTGTACTG GCAGTCAGCTTTTG-3'
shC1	5'-CCGGCAACAAGATGAAGAGCACCAACTCGAGTTGGTGTCTT CATCTTGTGTTTTG-3'
shC2	5'-CCGGGCGCGATAGCGCTAATAATTCTCGAGAAATTATTAGC GCTATCGCGCTTTTG-3'
shC3	5'-CCGGTCCTAAGGTTAAGTCGCCCTCCTCGAGGAGGGCGACT TAACCTTAGGATTTTG-3'

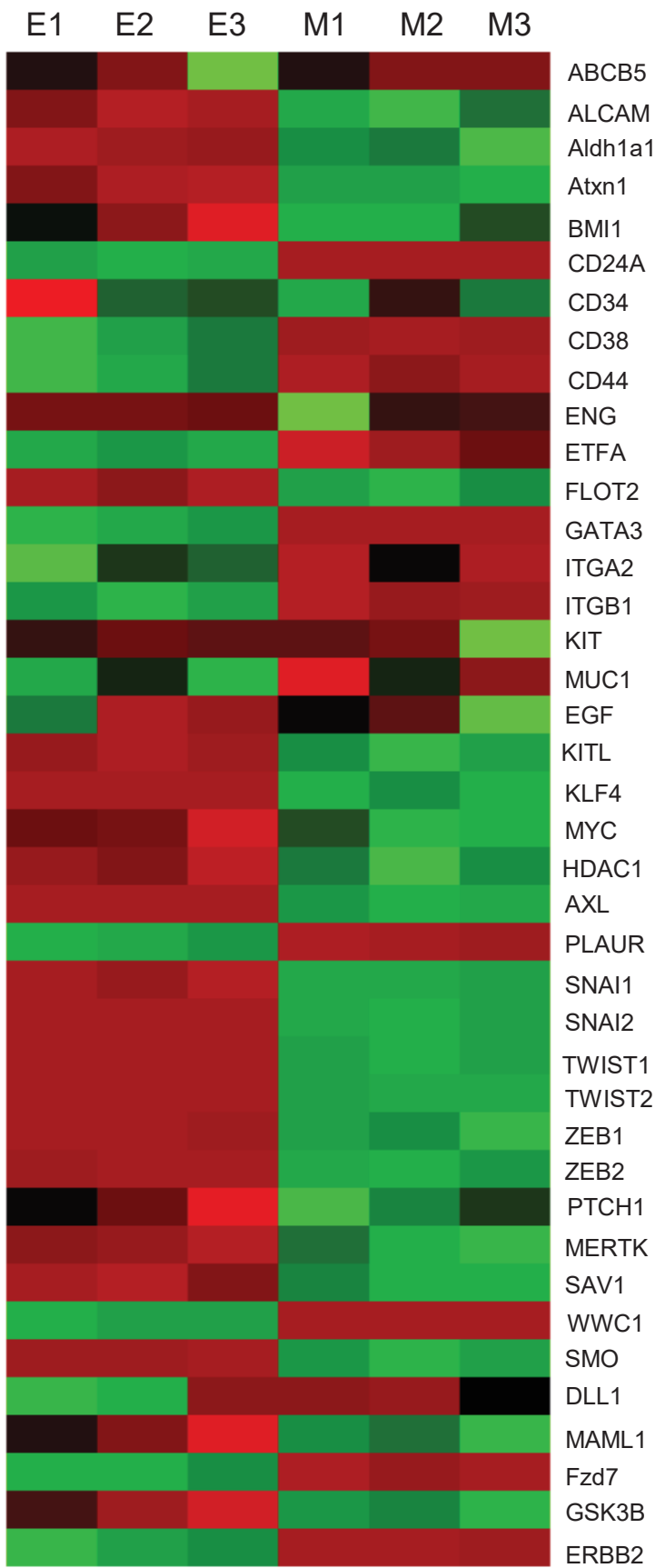
Table 2: Primers used for qPCR

Target Gene	Primer references
ErbB2	Taqman probe: Rn00566561_m1, ThermoFisher
Raet1d	Taqman probe: Mm02394669_sH, ThermoFisher
panRae1	Taqman probe: Mm04206137_gH, ThermoFisher
H60b	Taqman probe: Mm04243254_m1, ThermoFisher
Mult1	Taqman probe: Mm01180648_m1, ThermoFisher
GAPDH	Taqman probe: 4352661, Applied Biosystem

Table 3: Antibodies used for IF and WB

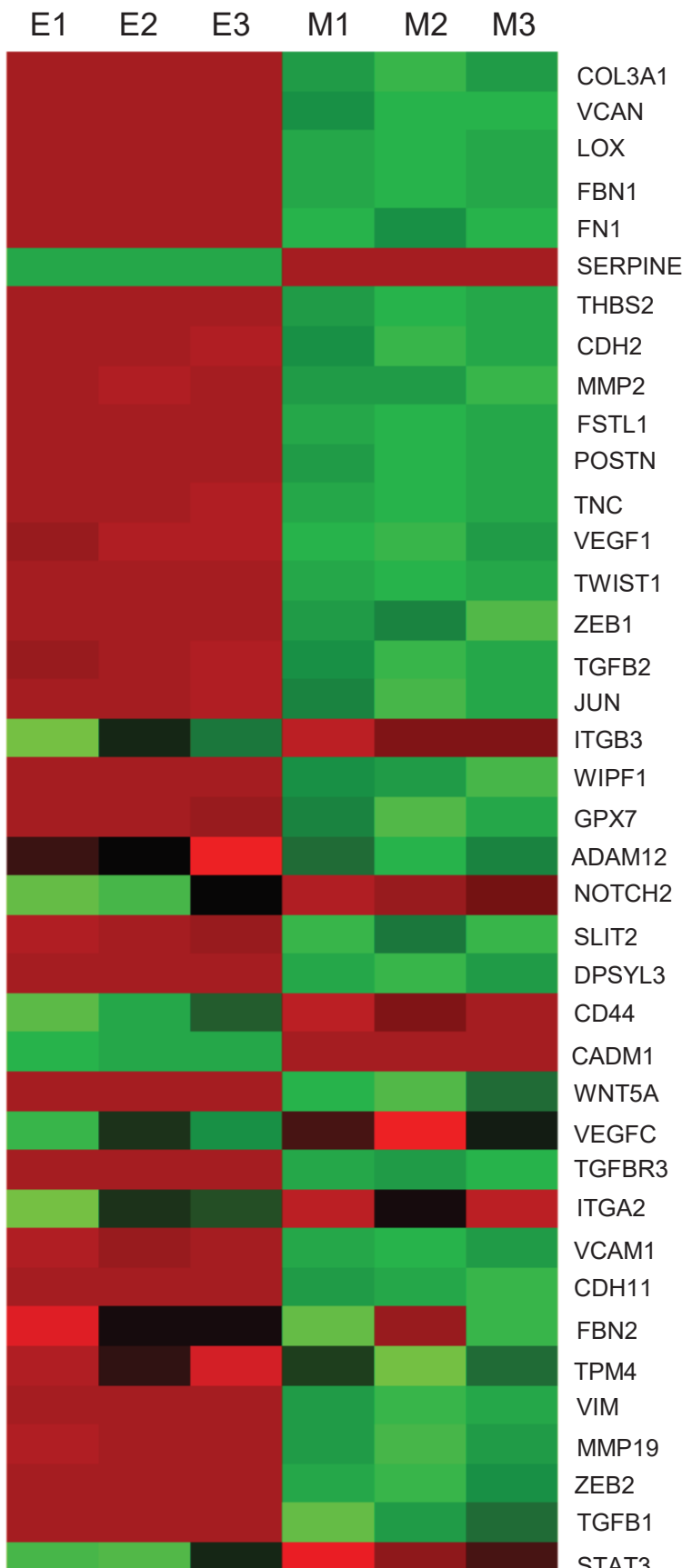
Target	Antibody type/Application	References
GAPDH	Primary / WB	Cell Signaling 2118S
Vimentin	Primary / WB, IF	Cell Signaling 5741S
E-cadherin	Primary / WB, IF	ThermoFisher 13-1900
TNC	Primary / WB	G.OREND laboratory
ErbB2	Primary / IF	Cell Signaling 2242L
panH60	Primary / WB	RD system AF1155
panRaet1	Primary / WB	RD system AF1136
Mult1	Primary / WB	RD system MAB2588
Anti-Goat	Secondary / WB	Santa Cruz sc-2354
Anti-rabbit	Secondary / WB	Cell Signaling 7074S
Anti-rat	Secondary / WB	Cell Signaling 7077S
Anti-rabbit	Secondary / IF	Jackson Lab 111-165-003
Anti-rat	Secondary / IF	Jackson Lab A11006

A Cancer stemness-related genes



Row Z-Score

B EMT-related genes



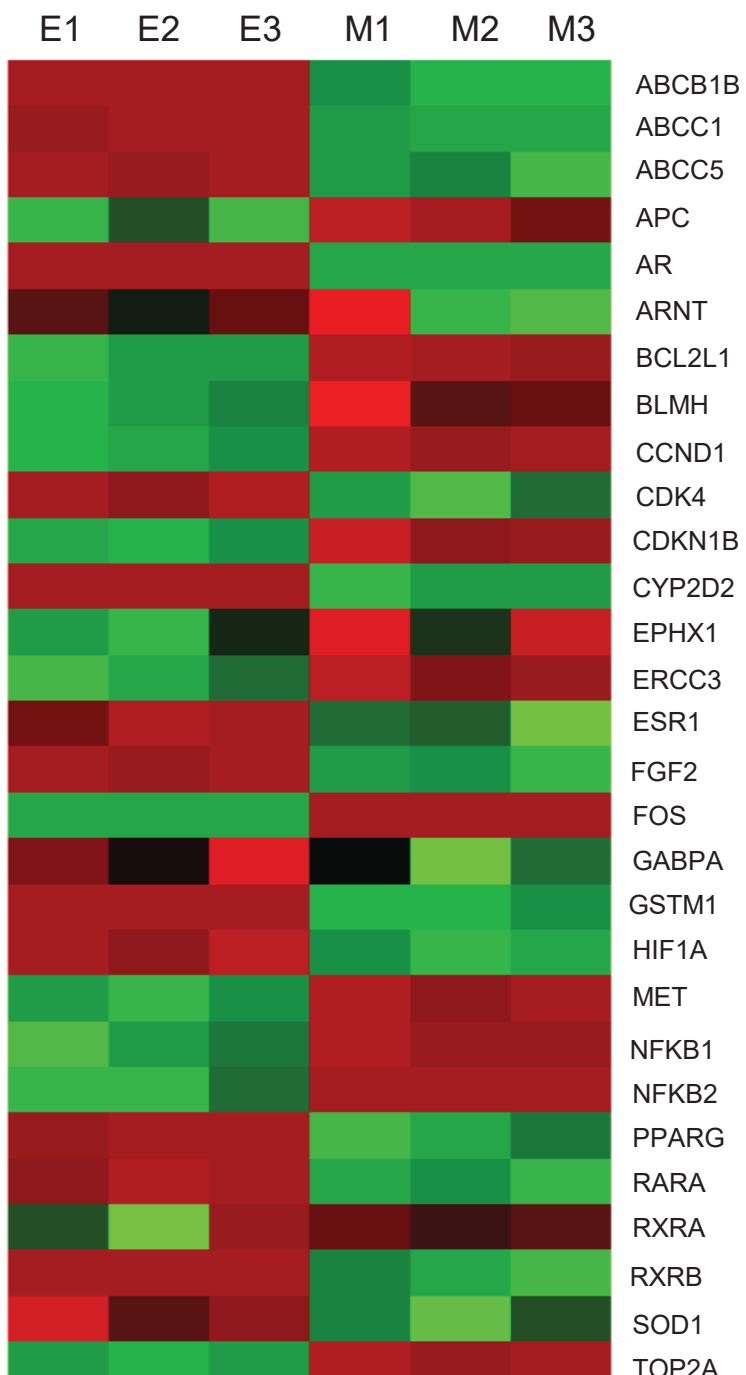
Row Z-Score

Fig. S1: Gene expression in NT193 E and NT193 M cells as determined by RNA seq analysis

(A-D) Panther guided sorting into genes related to cancer cell stemness **(A)**, epithelial-to-mesenchymal transition **(B)**, drug resistance **(C)** and to negative regulation of immune system processes **(D)**. N = 3 different cell passages, Limma moderated t-test, $p < 0.05$.

C

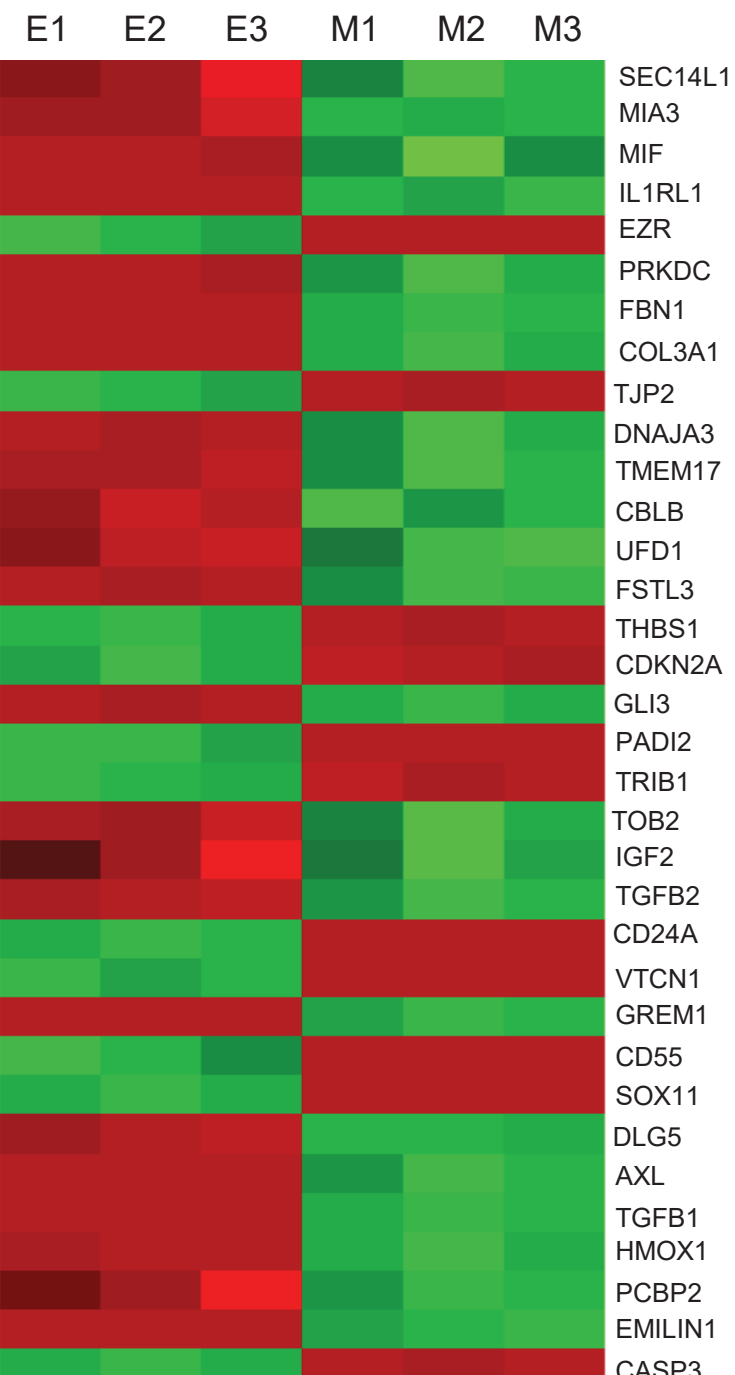
Drug resistance-related genes



Row Z-Score

D

Genes related to negative regulation of immune system process



Row Z-Score

DISCUSSION AND PERSPECTIVES

Nowadays, it is well accepted that cancer progression is not only dependent on tumor cells but also on all the other components of the TME with a particular ECM that actively shapes tumor progression through interactions with its embedded cells. Indeed, these interactions mediated by receptors trigger signaling that modulates tumor cell proliferation, survival and invasion, but also angiogenesis, metastasis and anti-tumor immunity (Lu et al., 2012; Pickup et al., 2014). TNC, an ECM molecule whose expression in adult tissues is largely restricted to a few areas, is found to be highly expressed *de novo* in pathological conditions such as chronic inflammation and cancers (Midwood and Orend, 2009). In many cancers such as breast and colorectal cancers, high expression of TNC is associated with poor metastasis-free and poor overall patient survival (Lowy and Oskarsson, 2015; Oskarsson et al., 2011). Many papers have shown the plethora functions of TNC in promoting tumor progression by impacting angiogenesis and tumor cell aggressiveness but only few have described its impact on anti-tumor immunity (Deligne et al., 2020; Parekh et al., 2005; Jachetti et al., 2015). So far, TNC has been described to affect CD8 T cell functions in a prostate cancer model, and to corrupt anti-tumor immunity by orchestrating a lymphoid immune suppressive TME in a head and neck tumor model (Jachetti et al., 2025; Spenlé et al., 2020).

Our laboratory has developed a novel orthotopic, syngeneic and immunocompetent cancer progression model based on our NT193 breast cancer cell line derived from a MMTV-NeuNT primary tumor (Muller et al., 1988). Engineering of TNC levels in both NT193 cells and in the host enabled us to investigate the impact of both host- and tumor cell-derived TNC on cancer progression and lung metastasis development (Sun et al., 2019 (see Appendix I)). Also, using the same model, TNC was shown to promote a M2 macrophage phenotype promoting tumor growth and metastatic spread (Deligne et al., 2020).

During my thesis, I worked mainly on two projects using the MMTV-NeuNT and the NT193 models for investigating TNC impact on anti-tumor immunity. On one side, we demonstrated that TNC impacts anti-tumor immunity by immobilizing CD8 T

lymphocytes within the matrix tracks impairing thereby their immune effector functions. We identified the CXCL12/CXCR4 signaling axis as being a major underlying mechanism through which TNC triggers CD8 T lymphocyte sequestration. On the other side, our yet unpublished results show that high TNC expression in mesenchymal tumor cells leads to their *in vivo* rejection in an early phase post grafting. Moreover, we showed that TNC upregulates the expression of NKG2DL which could be one of the TNC-triggered downstream mechanisms potentially impacting tumor cell rejection, dormancy and reawakening.

I. Tenascin-C immobilizes infiltrating T lymphocytes through CXCL12 promoting breast cancer progression

1. Experimental models used in the study

The genetic model used in the study is the well described MMTV-NeuNT breast cancer model that is widely used in the breast cancer research field (Muller et al., 1988). In this model, the transgenic mice carry an activated form of the rat homologue of HER2 (ErbB2) oncogene (neu) that is especially expressed in the mammary epithelium under the control of the MMTV promoter. This leads to the spontaneous development of multifocal mammary tumors in all female mice at a median age of 5-10 months with frequent potential to develop lung metastasis (around 30%) (Taneja et al., 2009). This genetic model appears to be highly relevant as HER2 has been reported to be overexpressed in 20-30% of human breast cancers, and the model mimics progression of HER2+ human breast cancer (Taneja et al., 2009). Also, the long kinetic for tumor onset and metastasis development may allow the establishment of a TME mimicking the TME observed in human breast cancer. However, despite its relevance, the long kinetics and the multifocal tumor origin create some heterogeneity that often compromises the use of this model in particular for drug targeting.

The NT193 model is a novel orthotopic grafting model in an immune competent host (syngeneic) that was established in our laboratory from a primary tumor of a MMTV-NeuNT mouse. The NT193 cell line derived thereof is grafted in the surgically opened mammary fat pad of a syngeneic FVB/NCrI host. 50% of the grafted mice develop a

mammary gland tumor starting from 2 weeks post grafting and lung metastasis after 11-14 weeks post grafting. The histological comparison between tumors from the genetic model and the grafting model revealed no obvious differences concerning tissue architecture and expression of ErbB2 and other markers (PR+, ER+), and their extensive characterization showed a similar tumor matrix organization as matrix tracks in both models. These observations brought us to consider the NT193 model as a good surrogate for the genetic model allowing us to decrease our *in vivo* experimentation duration. Not to forget an ethical consideration namely a shorter time of mice in the experiment. In cell culture, the NT193 cell line is a mixture of both epithelial and mesenchymal cells but interestingly the grafting of this mixture of cells gives rise to tumors expressing only epithelial markers. The NT193 model is also a good surrogate model for cancer progression as in this model so called blood vessel invasions (BVI) representing a step towards parenchymal metastasis are formed in a TNC-regulated manner (Sun et al., 2019 (see Appendix I)). We described the cellular and molecular composition of BVI in the NT193 (and NeuNT model) and found that they share similarities with BVI in the aforementioned human cancers. We had identified TNC, TGF β signaling, platelets and endothelial cells as important targets to prevent extravasation of cancer cells from the BVI into the lung parenchyma (Sun et al., 2019 (see Appendix I)).

2. TNC impacts immune-related gene expression in the MMTV-NeuNT model

TNC has been reported to promote tumor growth in many cancer types and notably in breast cancer (Oskarsson et al., 2011) but until recently TNC impact on anti-tumor immunity remained poorly examined. Yet understanding tumor immunity and the crosstalk between the ECM and immune cells appears to be crucial for improving anti-cancer therapies and bears the potential to increase the low response rate to immunotherapy observed in cancer patients (Sharma et al., 2017). By using the MMTV-NeuNT breast cancer model on WT and TNCKO background, our previous study has shown that TNC increases tumor onset and lung metastasis (Sun et al., 2019 (see Appendix I)). Here, we used the same model and the non-biased investigation of overall gene expression in tumors from WT and TNCKO mice that showed more than 2 000 genes to be differentially expressed between the two

groups, among which many genes related to immunity including the expression of T cell-regulation-associated genes that were higher in tumors from TNCKO mice. Moreover, even if the abundance of most of the immune cell types was not different between WT and TNCKO groups, we observed a lower expression of CD8 T cell activation marker *Perforin* in tumors from WT mice. These results are in concordance with studies on other models having shown that TNC can impact T cells. For instance, Jachetti and colleagues (2015) showed that TNC inhibits T-cell receptor-dependent T-cell activation and cytokine production in a prostate cancer model by inhibiting the actin-based cytoskeleton reorganization required for T cell activation through the interaction with $\alpha 5\beta 1$ integrin found on T cell surface (Jachetti et al., 2015). Altogether these data show that TNC has an impact on tumor immunity and notably on CD8 T cells. The end stage of the MMTV-NeuNT is not suited model to investigate an impact on CD8 T cells as these cells were rare, presumably because the immune exhausted state has been reached. Thus, CD8 T cell abundance should be investigated in this model at an earlier time point. Although rare, no difference was seen in CD8 T cell abundance between the two genotypes of tumors, likely due to the multifocal nature of tumorigenesis that precludes investigation of immune editing along tumor growth and progression.

3. The NT193 model is a relevant model to investigate TNC impact on tumor immunity

TNC has been reported to be expressed by tumor and stromal cells in the TME and TNC from both sources has an impact on clinical prognosis of breast cancer patients with a worsened overall survival in patients displaying combined high TNC expression in the cancer and stromal cells (Ishihara et al., 1995). However, the lack of suitable immunocompetent *in vivo* models with a long kinetic that is necessary to establish a proper tumor relevant ECM precluded for investigating the impact of ECM on tumor immunity in breast cancer so far. Here, we decided to use our immunocompetent NT193 grafting model that has previously been used to study the distinct roles of host- and tumor cell-derived TNC on several pro-tumorigenic events such as breast cancer lung metastasis development and the establishment of an immune suppressive TME. This was accomplished by grafting shC or shTNC cells in a WT or TNCKO host, respectively (Sun et al., 2019 (see Appendix I)). Also, more

numerous infiltrating CD8 T cells were found in the grafting model compared to the MMTV-NeuNT model, which allows investigating the impact of TNC on CD8 T cells.

Recently, TNC has been described in several cancer types such as in human and murine insulinoma and colorectal cancers, to be organized in tumor matrix tracks (TMT) together with other ECM molecules such as collagen IV, fibronectin and laminins (Spenlé et al., 2015). These TMT have been found to be enriched in stromal cells including endothelial cells, fibroblasts and immune cells and several data suggested that these TMT provide a hospitable microenvironment for the stromal cells that may generate an immune tolerogenic TME (Spenlé et al., 2015). Organization of TNC and other ECM into TMT has not only been seen in the NeuNT and NT193 models but also in other cancer types such as in glioblastoma and in head and neck squamous cell carcinoma models (Rupp et al, 2016; Sun et al., 2019; Spenlé et al., 2020).

4. TNC impacts infiltrating CD8 T cell localization

By using the NT193 model, Deligne and colleagues (2020) showed that more M2-like macrophages are present in the stroma of tumors with high TNC expression (WT/shC) (Deligne et al., 2020). Here we were wondering whether TNC has an impact on the spatial distribution of the immune infiltrate and observed that unlike the other immune cells, the spatial distribution of CD8 T cells is different within the tumors expressing high and low TNC, respectively. In particular, we found that CD8 T cells are preferentially enriched in TMT (highly expressing TNC) rather than in the tumor cell nests. This observation further correlated with decreased mRNA levels of granzyme B and perforin and a reduced number of apoptotic cells in TNC-high compared to TNC-low tumors, suggesting that TNC may retain CD8 T cells in the stroma thus impairing their cytotoxic functions.

As previously discussed in the introduction of this manuscript (see part 4.4) the immune contexture characterized by the type, density and location of immune cells within the tumor site, has been reported to be crucial for predicting cancer patient survival but also the response to immunotherapy (Fridman et al., 2012). In this context, high infiltration of CD8 T cells was reported in many cancers including breast cancer, for being associated with good clinical outcome and better response to

immunotherapy (Galon and Bruni, 2019). Moreover, the so called “immunoscore” based on the quantification of CD8 T cells at the invasive margin and at the core of the tumor enabled to classify tumors in three distinct phenotypes: the immune-inflamed phenotype with high cytotoxic T cell infiltration in the tumor, the immune-excluded phenotype with CD8 T cells only present at the invasive margins and the immune-deserted phenotype largely lacking CD8 T cells, both in the core and the tumor margins (Galon and Bruni, 2019). Retention of CD8 T cells by the stroma and in particular TNC was not only seen in the NT193 model but also in human breast cancer irrespective of the subtype and represents a novel mechanism of escape from tumor immune surveillance. The principle of immune cell retention in the stroma by TNC may apply to other immune subtypes as recently seen in a carcinogen-induced OSCC model and human OSCC tissue where TNC immobilized CD11c+ myeloid/dendritic cells in the stroma (Spenlé et al., 2020).

5. CD8 T sequestration by TNC is mediated through CXCL12

Our RNA-seq data obtained on WT/shC and TNCKO/shTNC tumors showed that more than 1 000 genes are differently expressed between the two conditions, including the chemokine CXCL12 that was upregulated in tumors with high TNC. CXCL12 is a highly interesting candidate molecule since several studies showed its multiple functions promoting cancer progression and also regulating immunity. For instance, CXCL12 and its receptor CXCR4 that is highly expressed on cancer cells have been reported to promote angiogenesis and tumor cell survival and proliferation through signaling such as PI3K, Akt and Wnt (Burger and Kipps, 2006; Shi et al., 2020). Moreover, the CXCL12/CXCR4 axis was described in many studies for regulating metastasis in breast cancer. The first evidence was provided by the study of Müller and his colleagues (2001) showing that in response to CXCL12, CXCR4-mediated signaling triggers chemotactic and invasive responses leading to the homing of breast cancer cells in the lungs (Müller et al., 2001). Analogous findings were observed in several cancer types such as glioblastoma and hepatocellular carcinoma where the CXCL12/CXCR4 axis was shown to stimulate cancer cell invasion this time by promoting EMT (Shi et al., 2020). In addition, the CXCL12/CXCR4 signaling was also reported to regulate T cell migration. While low concentrations of CXCL12 act as a chemoattractant for T cells, high concentrations

can repel and reverse T cell infiltration *in vivo* however how this is accomplished is unknown (Poznansky et al., 2000).

As CXCL12 was upregulated in TNC-high tumors we hypothesized that TNC-mediated CD8 T cell immobilization in the TMT may involve CXCL12/CXCR4 signaling and found that our results supported this hypothesis. We showed that TNC binds CXCL12 and upregulates CXCL12 in both the genetic and grafting model and that the major source of CXCL12 is the tumor cells despite its presence also in the stroma at a weaker level presumably expressed by fibroblasts as seen in another study (Feig et al., 2013). These results suggest that on one side the high CXCL12 concentration within the tumor nest might create a CD8 T cell repelling environment holding them away from the tumor nest. On the other side through binding to TNC, CXCL12 can immobilize CD8 T cells in the stroma, again keeping CD8 T cells away from the tumor cell nest. Moreover, by investigating how TNC triggers CXCL12 expression using inhibitors for distinct signaling pathways, we found that TNC induced CXCL12 through TLR4. TLR4 is a receptor responsible for pattern recognition in innate immunity that has been widely shown as being overexpressed on tumor cells and in the TME in many cancer types such as breast cancer, and has been associated with cancer progression (Oblak and Jerala., 2011). Moreover, TLR4 is a known interactor of TNC, capable not only of inducing but also of being induced by TNC (Midwood et al., 2009). Our result is strengthened by other studies showing that the LPS, a major TLR4 ligand, is able to induce CXCL12 expression for instance in monocytes and macrophages (Lu et al., 2017). Also, TLR4 was reported to induce CXCL12 production in a neurodegenerative disease (Li et al., 2019).

6. CXCL12-mediated CD⁺ T immobilization requires CXCR4

After having demonstrated by functional assays that TNC ability to immobilize CD8 T cells is enhanced by CXCL12, we showed that this effect is CXCR4 dependent as its chemical inhibition by AMD3100 blocks CXCL12-mediated CD8 T cell retention *in vitro* and restores infiltration of CD8 T cells in the tumor nest *in vivo*. Indeed, in the 7-weeks *in vivo* model we showed that inhibition of CXCR4 by AMD3100 increases CD8 T cell infiltration into the tumor nest correlating with higher tumor cell apoptosis, reduced tumor weight and reduced subsequent metastasis.

7. Combined high expression of TNC and CXCL12 as predictive marker of immune checkpoint inhibitor treatment efficacy

Our results showed that CXCR4 signaling is crucial for tumor progression as it impacts anti-tumor immunity by distinct mechanisms. One of the highly interesting results is the downregulation of genes involved in the impairment of CD8 T cell activity among which *Cd274* in AMD-treated conditions. *Cd274*, also commonly referred to as PDL1, is an immune checkpoint protein expressed on cancer cells that binds to PD-1 expressed on T cells triggering inhibition of T cell proliferation leading to tumor immune suppression (Han et al., 2020). PDL1 has been reported in many cancers such as breast cancer as playing a crucial role in cancer immune escape and tumor progression. Immune checkpoint inhibitors used in immunotherapy are able to block checkpoint proteins from binding with their partner proteins, preventing the switch off signal emitted by this interaction. Thereby, T cells can proliferate and remain operational for killing cancer cells. However, even if the T cells are activated they cannot fulfill their immune effector functions as they are excluded from the tumor nest (Galon and Bruni, 2019).

In our study we found that PLD1 (CD274) is upregulated in WT/shC tumors and that CXCR4 inhibition decreases *CD274* expression. It is thereby possible that a combined high expression of TNC together with CXCL12 may render tumors poorly responsive to immune checkpoint therapies.

We investigated the relevance of our results obtained in the murine tumor models by analyzing human breast cancer tissue microarray cohort (over 200 samples) for TNC and CD8 expression and observed more CD8 T cells infiltrating the tumor nest in tumors expressing low TNC suggesting that also in human breast cancer TNC may play a role in retaining CD8 T cells in the stroma. Moreover by Kaplan-Meier analysis of the two distinct breast cancer patient cohorts we found that despite higher CD8 T cell infiltration correlating with better overall patient survival, this survival benefit is counteracted by TNC. In addition our murine tumor models showed also as being relevant for CXCL12 expression pattern observed in human breast cancer. Indeed, we observed the presence of CXCL12 mainly in the tumor nest but also within the stroma at a lower level. By investigating CXCL12 expression on the previous breast cancer microarray cohort we showed a higher CXCL12 expression in tumors with

high TNC expression and the highest CXCL12 expression was observed in conditions with combined high TNC and CD8. Moreover, Kaplan-Meier analysis showed that the overall survival is worst in patients with combined high TNC and CXCL12.

Altogether these results found on human tumors corroborate the relevance of our murine tumor model and show the complex interaction of TNC, CXCL12 and CD8 T cells in promoting tumor immune suppression.

Our data also suggest that combined high TNC and CXCL12 expression in breast cancer patients could be used to predict the response efficacy to immune checkpoint therapies.

In the last years several papers have shown that combining CXCR4 inhibition and blockade of PD-1/PDL-1 pathway potentiates anti-tumor treatment. In a highly interesting work, Feig and colleagues (2013) showed in a pancreatic ductal adenocarcinoma model that inhibition of CXCR4 by AMD3100 induced T cell accumulation in the tumor nest and synergized with PDL-1 blockade to diminish cancer cells (Feig et al., 2013). In more recent years analogous results were observed in several other cancer types such as in colorectal and melanoma cancers (Zboralski et al., 2017; D'Alterio et al., 2019). Thus, it could be relevant to test this combined treatment in our *in vivo* models to address whether the inhibition of TNC-mediated CD8 T cell retention through CXCR4 cooperates with PD-1/PDL-1 blockade. Also, our data suggest that targeting TNC before applying combined CXCR4 and PDL-1 blockade may enhance CTL release and functions.

II. TNC impacts tumor onset and NKG2DL expression in the NT193 grafting model

1. The origin of TNC has an impact on tumor growth

In our previous study using the NT193 model where TNC levels were engineered in the grafted tumor cells and in the host, we showed that stromal and tumor cell-derived TNC have distinct functions in tumor progression (Sun et al., 2019 (see Appendix I)). Indeed, our results demonstrate that host-derived TNC promotes breast cancer lung metastasis by increasing blood vessel invasions (BVI). Here, using the same model we observed that tumor cell and host-derived TNC have also distinct effects on primary tumor growth. Indeed, we observed tumor rejection on half of the mice in condition where both host and tumor cells express TNC and a transient tumor regression in the other half, which is not observed when TNC is expressed by either only tumor cells or only host. TNC has previously been shown to serve as a DAMP molecule in a non-tumor context, triggering chronic inflammation through TLR4 and integrin $\alpha 9\beta 1$ (Midwood et al., 2009). It might be thereby possible that this is also the case in our model and that the immune system recognizes TNC-mediated danger signals enabling the establishment of an immune response in an early phase after engraftment. Moreover, other data from our laboratory (Deligne et al., 2020; Spenlé et al., 2020) suggest that tumor cell-derived TNC induces genes related to antigen presentation in the host that could be involved in the rejection/transient regression of the primary tumor. Also, comparison of TNCKO/shC and WT/shC tumors showed that these genes are more expressed in shC tumors from WT than from TNCKO host, which might explain why the rejection/regression is observed when TNC is expressed in both host and tumor cells. Furthermore, in the study of Deligne and colleagues (2020) that used also NT193 cells, no rejection of NT193 cells was observed when the cells were injected through the nipple, and not grafted in the mammary gland after a surgical wounding (Deligne et al., 2020). This difference suggests that the surgical wounding might trigger immune cell priming enabling them to face tumor cells leading to tumor rejection/regression in an early phase.

2. Characterization of NT193E and NT193M cell lines shows different features suggesting distinct tumorigenic properties

The NT193 cell line is composed of epithelial (E) and mesenchymal (M) cells. For understanding the *in vivo* behavior we established an E and M cell line from the NT193 pool of cells. Then we performed different analysis such as IF and WB for assessing their expression of typical E and M markers and functional assays in terms of cell growth and migration. It turned out that M cells have a higher ability to proliferate and to migrate compared to E cells. Interestingly, we showed that while TNC expression is almost absent in E cells it is highly expressed by M cells. Moreover, analysis of RNA-seq performed on these two cell lines showed an upregulation of genes associated with epithelial-to-mesenchymal transition (EMT) in M cells. EMT is a process playing a key role in embryonic development, in fibrosis and also in diseases such as cancer (Thiery et al., 2009). In that latter case, this process was shown to promote tumor invasion and metastatic spread enabling cells to acquire enhanced migratory and invasive properties (Bonnomet et al., 2012). It has also been demonstrated that EMT confers properties related to cancer stemness, drug resistance and immune evasion (Polyak and Weinberg, 2009). Our RNA-seq data are in agreement with this information. Indeed, we observed an upregulation in most of the genes related to cancer stemness and to negative regulation of immunity in M cells compared to E cells. Knowing that M cells have a high ability to proliferate and migrate, and that they display a strong expression of TNC and EMT-related genes reported for being associated with migratory and invasive properties, we could hypothesize that M cells might have a higher tumorigenic capacity *in vivo* than E cells.

3. *In vivo* behavior of E and M cells

E and M cells were grafted separately in the mammary gland of FVB mice and contrary to our previous hypothesis none of the mice grafted with M cells developed a primary tumor within the first 6 weeks post grafting whereas 100% of mice that were engrafted with E cells generated a primary tumor. Moreover, after E cell engraftment we observed a transient stop of exponentially tumor growth that may resemble the transient regression observed after shC NT193 pool cell engraftment in a WT host,

however interestingly the regression was less drastic for the E cells. These observations suggest that the presence of M cells in the NT193 pool cells could contribute to the rejection/transient regression. By investigating the *in vivo* fate of M cells we found that half of the mammary glands grafted with M cells display the presence of tumor cells as clusters. More extensive experiments are needed to characterize these tumor cell clusters and investigate why they are present in only half of the mice. Indeed, it would be relevant to know whether this cluster is composed of M cells or whether the grafted M cells have undergone a mesenchymal-to-epithelial transition (MET). If M cells need to undergo MET to establish a primary tumor this could be one of the explanation to the non-systematic tumor development. Indeed, not all tumor cells have sufficient plasticity to re-epithelialize and microenvironmental factors might also contribute to MET, leading to heterogeneity within mice. Another interesting perspective would be to characterize the immune cell infiltrate within the grafting site. This would enable to assess whether the immune system is involved in this phenomenon. Besides immune infiltrate, investigating proliferative markers such as ki-67 and apoptotic ones such as cleaved-caspase 3 would enable to understand whether primary tumor does not develop due to a lack of proliferative cancer cells or an excess of dying cancer cells. One of the hypotheses would be that we are in presence of what is called “the equilibrium state” of the cancer immunoediting concept where the adaptive immunity and cancer cells coexist and immune responses are able to restrain but not to fully eradicate tumor cells. The equilibrium state was reported to generate a dormant phase in cancer during which a tumor does not develop but the selection pressure on cancer cells leads to the emergence of cancer cells carrying mutations providing them increased resistance to immune attacks (Teng et al., 2008). Thereby, it would be also relevant to investigate whether these tumors express genes related to dormancy.

In addition to the mammary gland analysis we started to study the lungs of mice grafted with either E or M cells and found a higher expression of ErbB2 in mice grafted with M than with E cells. This result suggests that even if no primary tumor developed within the first 6 weeks some M cells disseminated to the lungs. Several papers have reported that cancer cells need to lose polarity and cell-cell adhesions to initiate tumor dissemination and these changes occur in cells undergoing EMT (Wodarz and Nähke, 2007). We could thus hypothesis that M cells have a greater

ability to invade and disseminate toward the lung. Staining of lung tissues would enable to investigate M cell location and whether M cells give rise to blood vessel invasions as we observed in our published paper for NT193 pool cells (Sun et al., 2019 (see Appendix I)). Moreover, investigating immune infiltrate within E and M lung tissues would be highly relevant for comparing tolerogenic properties of both cells.

4. NKG2DL expression in M cells and its link with TNC

By analyzing RNA-seq data we observed that M cells overexpress the NKG2DL *H60* and *Raet1* but not *Mult1* compared to E cells. Moreover, our results show that TNC upregulates NKG2DL expression. This result is highly interesting as it is the first time that a matrix molecule, namely TNC is shown to regulate NKG2DL expression. Knowing that M cells highly express TNC that upregulates NKG2DL, and that NKG2DL expression in cancer cells has been reported by many studies as being involved in cancer progression (Raulet, 2003; Jamieson et al. 2002), we hypothesized that TNC triggers NKG2DL in M cells leading to their *in vivo* recognition and destruction by the immune system explaining their rejection. Yet how TNC triggers NKG2DL expression remains unknown and additional experiments are needed to answer this question.

5. Janus-faced impact of TNC in tumor development

Based on this assumption we hypothesized that grafting of M cells engineered to express low TNC levels may induce tumors. This time, we grafted either MshC or MshTNC cells in 10 mice and stopped the experiment 13 weeks post grafting. This experiment gave us several highly interesting results. First, we observed that 90% of mice grafted with MshTNC cells developed primary tumor starting from 2 weeks post grafting. This result supports our hypothesis that TNC has an impact on the rejection of M cells at an early phase post engraftment. Interestingly we observed over time a rejection of some established primary tumors starting from 7 weeks post grafting. At the end of the experiment only 50% of mice grafted with MshTNC cells had still tumors, which seem to converge with what was observed after NT193 pool cell grafting but after a longer time frame. Concerning grafted MshC cells we observed that no tumor occurred until week 7 post grafting. Then progressively 60% of mice

developed a primary tumor over the last 6 weeks of the experiment. This is highly intriguing as the time frame before rejection of MshTNC primary tumor corresponds to the same time frame before MshC cells give rise to a primary tumor. We could hypothesize that there is a shift of TNC function at this stage. Several hypotheses can be ventured and have to be addressed by further analysis:

It is possible that first TNC acts as DAMP and triggers an immune response leading to an equilibrium state between immune and cancer cells, and then promotes the aggressiveness of cancer cells that have accumulated mutations under the selection pressure, rendering them immune resistant.

Another hypothesis that would converge with our previous hypothesis involving NKG2DL is that first TNC induces the expression of NKG2DL enabling NKG2D expressing immune cells, notably NK cells, to recognize and kill cancer cells leading to an equilibrium state. Then occurs the shift of TNC function where a potential cleavage of the NKG2DL may induce shedding from the cancer cell surface thus leading to cancer cell immune escape.

6. Downregulation of NKG2DL expression in M cells

In order to investigate the second part of our hypothesis postulating that the expression of NKG2DL in M cells is an important impediment for tumor growth we established single KD for *Raet1* and *H60*. It turned out that downregulation of either *Raet1* or *H60* leads to the upregulation, at least at mRNA level, of *Mult1* that was not expressed in M cells according to our RNA-seq data. How this compensatory mechanism occurs remains yet unknown and needs further investigation. As E cells express *Mult1* without getting rejected, it is possible that *Mult1* has other functions than playing a role in NKG2D mediated cell killing. It also remains to be determined how the KD of one family member affects the expression levels of another family member. So far nothing is known.

To avoid any potential compensation amongst NKG2DL family members we established a novel M cell line by knocking down simultaneously the three NKG2DL family members by shRNA technology. Surprisingly, it turned out that the downregulation of the 3 NKG2DL leads to the downregulation of TNC and *Tlr4* expression. TLR4 signaling was reported by few studies as being involved in the expression of NKG2DL in different myeloid cells such as macrophages and DCs but

so far such a regulation was not known for tumor cells which should be addressed in more detail in the future (Stojanovic et al., 2018; Eissmann et al., 2010). Knowing that TNC activates TLR4 inducing inflammatory cytokines, it is possible that TNC-mediated NKG2DL induction involves TLR4 signaling. . It is intriguing to note that TNC and NKG2DL expression seem to counter regulate each other which suggests that TNC may be an important regulator of NKG2D/NKG2DL axis. In this context it is interesting to note that TNC and adaptive immunity appear to have evolved at the same time and one could question whether the same tool kit used in innate immunity such as TLR4 also finds application e.g. by TNC in regulating immunity (Orend and Tucker, 2021).

We then hypothesized that grafting of this newly established M cells expressing low NKG2DL may give rise to a primary tumor. However, so far *in vivo* we did not observe any tumor formation 13 weeks after engraftment. An important caveat is that the reduction in NKG2DL expression may not be sufficient to abolish NK cell function. For that we need to determine expression of all NKG2DL molecules *in vivo*. First, we have to see whether the engrafted tumor cells persisted in the mammary gland. If cells remain in the mammary gland this could represent a state of dormancy. It would be important to determine if cells are proliferating or silent and if they proliferate whether apoptosis would keep the cells in check. One has to look for markers that are associated with dormancy such as high nuclear p27^{KIP1} levels that would block CDK2/4 and G1 cell cycle progression and were associated with dormancy (Sharma and Pledger). It is possible that NKG2DL expression promotes cell survival and/or cancer stemness, thus by FACS it should be determined how abundant are the M tumor cells having CD44⁺/CD24⁻ properties. Moreover, the CXCL12/CXCR4 signaling was shown to regulate dormancy, thus expression of CXCL12 and CXCR4 upon triple knockdown of the NKG2DL has to be determined. In case M cells are present in the mammary gland we can investigate NKG2DL expression by RTqPCR and mass spectrometry analysis of the proteome. In case the knockdown was not sufficient *in vivo* a full KO can be achieved by the CRISPR/cas9 technology.

Engraftment of MshTNC cells gave rise to a tumor starting 10 days after engraftment. A reduced TNC expression in 3-shNKG2DL cells that was observed in the cultured cells may also promote tumor induction, however this is not the case until 13 weeks

of engraftment. Therefore, the TNC expression levels should be determined in the mammary gland and/or tumors. It is possible that either the TNC levels are not reduced *in vivo* in the 3-shNKG2DL engrafted cells and/or that there is a residual expression of TNC with different qualities due to different proteoforms which should be addressed by a proteomics analysis. It is also possible that the knockdown of the NKG2DL had an impact on other genes that potentially behave as tumor antigens and/or deregulate immune surveillance. Therefore, a proteomics analysis is needed to solve these possibilities.

It is also possible that NKG2DL expression is not the major obstacle impairing tumor onset. The analysis of the immune infiltrate within tumors and the mammary gland with no tumors but tumor cell clusters may give us some clues to guide our future investigations. As NK cells were recently found to mediate breast cancer cell dormancy in the liver (Correia et al., 2021), it will be interesting to determine whether NK cells are more abundant in the mammary gland with “dormant” tumor cell clusters than in M and E cell tumors. CD206⁺ M2 macrophages have been associated with dormancy and M1 macrophages with tumor growth, so determining the macrophage subtypes present within tumors would also be relevant. Also the role of the endothelin (ET)/ET receptor signaling axis should be investigated in more detail as activation of the endothelin receptor type A (ETA) results in activation of anti-apoptotic Bcl-xL molecule and tumor cell survival, whereas the activation of ETB induces tumor cell apoptosis (Nelson et al., 2005). Here, it could be relevant as TNC was shown to induce the ETA in cultured glioblastoma cells which may promote survival (Lange et al., 2007). Thus, it has to be determined whether ETA levels potentially are higher in M than E cells and higher in MshC than MshTNC cells, respectively. Interestingly, in the T89G glioblastoma cells the ETA signaling caused cell rounding which may impact YAP/TAZ signaling. This could have far reaching consequences as previously shown in KRIB osteosarcoma cells where integrin $\alpha 9\beta 1$ mediated cell rounding by TNC inhibited YAP and caused repression of TNC and other genes promoting their amoeboid migration, invasion and metastasis *in vivo* (Sun et al., 2018). However, it was not investigated whether this signaling has an impact on dormancy. Thus one has to determine whether M cells and in particular upon KD of NKG2DL express different levels of ETA and/or ETB. Moreover, several studies reported the involvement of CD8 T cells and IFNy in inducing and maintaining tumor cell

dormancy (Aqbi et al., 2019; Kmiecik et al., 2013). In mouse mammary tumor cells the expression levels of IFN- γ R α was shown to determine whether IFN- γ eliminates tumor cells or establishes tumor cell dormancy. Indeed, while CD8 T cell eliminate tumor cells expressing high levels of IFN- γ R α , tumor cells expressing low IFN- γ R α levels do not die and remain dormant and quiescent in the presence of IFN- γ producing CD8 T cells (Aqbi et al., 2019). Moreover, the activation of the IFN- γ /STAT1 pathway results in the establishment of tumor cell dormancy in melanoma. Thus, analyzing this signaling pathway and the IFN- γ R α expression level in our tissue could be relevant.

Summary

Altogether, this study provided evidence for a complex role of TNC in immune surveillance determining breast tumor growth and lung metastasis. We have shown that:

- 1.- TNC is an important regulator of tumor immunity employing CXCL12/CXCR4 signaling to retain CD8 T cells in the stroma thus blocking their function, corrupting anti-tumor immunity and promoting lung metastasis (Murdamoothoo et al., 2021).
- 2.- TNC plays a role in immune editing with different roles in the early and late phase, respectively. In the early phase TNC promotes tumor cell rejection, in the late phase TNC generates a CD8 T cell retaining stroma, thus blocking tumor cell rejection.
- 3.- The cellular source of TNC matters and regulates tumor growth and rejection, respectively. TNC (expressed by the host) promotes tumor cell rejection presumably through induction of an antigen presenting and processing signature (Deligne et al., 2020, Spenle et al., 2020). TNC expressed by the tumor cells is also relevant in activating immune surveillance (by an unknown mechanism) since only combined expression of TNC by the host and the tumor cells leads to tumor rejection.
- 4.- The plastic phenotype of the NT193 cells is important in triggering tumor cell rejection and dormancy. In particular M cells are prone to rejection and dormancy. As NK cells can regulate tumor dormancy (Correia et al., 2021) and we have seen that TNC regulates NKG2DL expression in M cells, TNC may regulate tumor dormancy through NKG2D activation in NK cells. Our tumorigenesis experiments with 3-shNKG2DL M cells that is in progress may provide further information.
- 5.- As TNC regulates CXCL12/CXCR4 signaling (Murdamoothoo et al., 2021) that was shown to be important in inhibiting NK cell functions in dormancy (Correia et al., 2021) TNC induction and binding of CXCL12 may play a role in the decision whether tumor cells remain dormant or expand.

References

Al-thoubaity, F.K., 2020. Molecular classification of breast cancer: A retrospective cohort study. *Annals of Medicine and Surgery* 49, 44–48.

Anders, S., Pyl, P.T., Huber, W., 2015. HTSeq--a Python framework to work with high-throughput sequencing data. *Bioinformatics* 31, 166–169.

Arai, J., Goto, K., Stephanou, A., Tanoue, Y., Ito, S., Muroyama, R., Matsubara, Y., Nakagawa, R., Morimoto, S., Kaise, Y., Lim, L.A., Yoshida, H., Kato, N., 2018a. Predominance of regorafenib over sorafenib: Restoration of membrane-bound MICA in hepatocellular carcinoma cells: Superiority of regorafenib to sorafenib. *Journal of Gastroenterology and Hepatology* 33, 1075–1081.

Arai, J., Goto, K., Tanoue, Y., Ito, S., Muroyama, R., Matsubara, Y., Nakagawa, R., Kaise, Y., Lim, L.A., Yoshida, H., Kato, N., 2018b. Enzymatic inhibition of MICA sheddase ADAM17 by lomofungin in hepatocellular carcinoma cells. *Int J Cancer* 143, 2575–2583.

Arpel, A., Sawma, P., Spenlé, C., Fritz, J., Meyer, L., Garnier, N., Velázquez-Quesada, I., Hussenet, T., Aci-Sèche, S., Baumlin, N., Genest, M., Brasse, D., Hubert, P., Crémel, G., Orend, G., Laquerrière, P., Bagnard, D., 2014. Transmembrane Domain Targeting Peptide Antagonizing ErbB2/Neu Inhibits Breast Tumor Growth and Metastasis. *Cell Reports* 8, 1714–1721.

Ascierto, M., Idowu, M.O., Zhao, Y., Khalak, H., Payne, K.K., Wang, X.-Y., Dumur, C.I., Bedognetti, D., Tomei, S., Ascierto, P.A., Shanker, A., Bear, H.D., Wang, E., Marincola, F.M., De Maria, A., Manjili, M.H., 2013. Molecular signatures mostly associated with NK cells are predictive of relapse free survival in breast cancer patients. *J Transl Med* 11, 145.

Aqbi, H.F., Wallaca, M., Sappal, S., Payne, K.K., Manjili, M.H., 2019. IFN- γ orchestrates tumor elimination, tumor dormancy, tumor escape and progression. *J Leukoc Biol* 6, 1219–1223.

Bae, Y.K., Kim, A., Kim, M.K., Choi, J.E., Kang, S.H., Lee, S.J., 2013. Fibronectin expression in carcinoma cells correlates with tumor aggressiveness and poor clinical outcome in patients with invasive breast cancer. *Human Pathology* 44, 2028–2037.

Bailey, S.R., Nelson, M.H., Himes, R.A., Li, Z., Mehrotra, S., Paulos, C.M., 2014. Th17 Cells in Cancer: The Ultimate Identity Crisis. *Front. Immunol.* 5:276.

Balkwill, F.R., Capasso, M., Hagemann, T., 2012. The tumor microenvironment at a glance. *Journal of Cell Science* 125, 5591–5596.

Barber, A., Zhang, T., Sentman, C.L., 2008. Immunotherapy with Chimeric NKG2D Receptors Leads to Long-Term Tumor-Free Survival and Development of Host Antitumor Immunity in Murine Ovarian Cancer. *J Immunol* 180, 72–78.

Bates, G.J., Fox, S.B., Han, C., Leek, R.D., Garcia, J.F., Harris, A.L., Banham, A.H., 2006. Quantification of Regulatory T Cells Enables the Identification of High-Risk Breast Cancer Patients and Those at Risk of Late Relapse. *JCO* 24, 5373–5380.

Bedel, R., Thiery-Vuillemin, A., Grandclement, C., Balland, J., Remy-Martin, J.-P., Kantelip, B., Pallandre, J.-R., Pivot, X., Ferrand, C., Tiberghien, P., Borg, C., 2011. Novel Role for STAT3 in Transcriptional Regulation of NK Immune Cell Targeting Receptor MICA on Cancer Cells. *Cancer Res* 71, 1615–1626.

Bejarano, L., Jordão, M.J.C., Joyce, J.A., 2021. Therapeutic Targeting of the Tumor Microenvironment. *Cancer Discov* 4, 933–959.

Birbrair, A. (Ed.), 2020. Tumor Microenvironment: Non-Hematopoietic Cells, Advances in Experimental Medicine and Biology. Springer International Publishing, Cham.

Biswas, S.K., Mantovani, A., 2010. Macrophage plasticity and interaction with lymphocyte subsets: cancer as a paradigm. *Nat Immunol* 11, 889–896.

Bonnomet, A., Syne, L., Brysse, A., Feyereisen, E., Thompson, E.W., Noël, A., Foidart, J.-M., Birembaut, P., Polette, M., Gilles, C., 2012. A dynamic *in vivo* model of epithelial-to-mesenchymal transitions in circulating tumor cells and metastases of breast cancer. *Oncogene* 31, 3741–3753.

Brassart-Pasco, S., Brézillon, S., Brassart, B., Ramont, L., Oudart, J.-B., Monboisse, J.C., 2020. Tumor Microenvironment: Extracellular Matrix Alterations Influence Tumor Progression. *Front. Oncol.* 10, 397.

Bruni, D., Angell, H.K., Galon, J., 2020. The immune contexture and Immunoscore in cancer prognosis and therapeutic efficacy. *Nat Rev Cancer* 20, 662–680.

Burger, J.A., Kipps, T.J., 2006. CXCR4: a key receptor in the crosstalk between tumor cells and their microenvironment. *Blood* 107, 1761–1767.

Burnet, F.M., 1970. The Concept of Immunological Surveillance, in: Schwartz, R.S. (Ed.), *Progress in Tumor Research*. S. Karger AG, pp. 1–27.

Burstein, H.J., Griggs, J.J., 2010. Adjuvant Hormonal Therapy for Early-Stage Breast Cancer. *Surgical Oncology Clinics of North America* 19, 639–647.

Busse, W.W., Lemanske Jr, R.F., 2001. Asthma. *The New England Journal of Medicine* 344(5):350-62.

Butti, R., Gunasekaran, V.P., Kumar, T.V.S., Banerjee, P., Kundu, G.C., 2019. Breast cancer stem cells: Biology and therapeutic implications. *The International Journal of Biochemistry & Cell Biology* 107, 38–52.

Cai, J., Du, S., Wang, H., Xin, B., Wang, J., Shen, W., Wei, W., Guo, Z., Shen, X., 2017. Tenascin-C induces migration and invasion through JNK/c-Jun signalling in pancreatic cancer. *Oncotarget* 8, 74406–74422.

Carapito, R., Bahram, S., 2015. Genetics, genomics, and evolutionary biology of NKG2D ligands. *Immunol Rev* 267, 88–116.

Chand-Fouché, M.-E., Lam Cham Kee, D., Gautier, M., Hannoun-Levi, J.-M., 2016. Technique d'irradiation partielle du sein : radiothérapie externe et curiethérapie. *Cancer/Radiothérapie* 20, 587–594.

Chang, Y.-H., Connolly, J., Shimasaki, N., Mimura, K., Kono, K., Campana, D., 2013. A Chimeric Receptor with NKG2D Specificity Enhances Natural Killer Cell Activation and Killing of Tumor Cells. *Cancer Res* 73, 1777–1786.

Chen, D.S., Mellman, I., 2013. Oncology Meets Immunology: The Cancer-Immunity Cycle. *Immunity* 39, 1–10.

Chiquet-Ehrismann, R., Chiquet, M., 2003. Tenascins: regulation and putative functions during pathological stress: Tenascins in pathological stress. *J. Pathol.* 200, 488–499.

Chiquet-Ehrismann, R., Orend, G., Chiquet, M., Tucker, R.P., Midwood, K.S., 2014. Tenascins in stem cell niches. *Matrix Biology* 37, 112–123.

Chiquet-Ehrismann, R., Tucker, R.P., 2011. Tenascins and the Importance of Adhesion Modulation. *Cold Spring Harbor Perspectives in Biology* 3, a004960–a004960.

Chu, D.T., Phuong, T.N.T., Tien, N.L.B., Tran, D.K., Nguyen, T.T., Thanh, V.V., Quang, T.L., Minh, L.B., Pham, V.H., Ngoc, V.T.N., Kushekhar, K., Chu-Dinh, T., 2019. The Effects of Adipocytes on the Regulation of Breast Cancer in the Tumor Microenvironment: An Update. *Cells* 8, 857.

Clayton, A., Mitchell, J.P., Court, J., Linnane, S., Mason, M.D., Tabi, Z., 2008. Human Tumor-Derived Exosomes Down-Modulate NKG2D Expression. *J Immunol* 180, 7249–7258.

Cohen, I.J., Blasberg, R., 2017. Impact of the Tumor Microenvironment on Tumor-Infiltrating Lymphocytes: Focus on Breast Cancer. *Breast Cancer: Basic and Clinical Research* 11, 117822341773156.

Condeelis, J., Pollard, J.W., 2006. Macrophages: Obligate Partners for Tumor Cell Migration, Invasion, and Metastasis. *Cell* 124, 263–266.

Conejo-Garcia, J.R., Benencia, F., Courreges, M.C., Gimotty, P.A., Khang, E., Buckanovich, R.J., Frauwirth, K.A., Zhang, L., Katsaros, D., Thompson, C.B., Levine, B., Coukos, G., 2004. Ovarian Carcinoma Expresses the NKG2D Ligand Letal and Promotes the Survival and Expansion of CD28 – Antitumor T Cells. *Cancer Res* 64, 2175–2182.

Correia, A.L., Guimaraes, J.C., Auf der Maur, P., De Silva, D., Trefny, M.P., Okamoto, R., Bruno, S., Schmidt, A., Mertz, K., Volkmann, K., Terracciano, L., Zippelius, A., Vetter, M., Kurzeder, C., Weber, W.P., Bentires-Alj, M., 2021. Hepatic stellate cells suppress NK cell-sustained breast cancer dormancy. *Nature* 7864, 566–571.

Cserni, G., Chmielik, E., Cserni, B., Tot, T., 2018. The new TNM-based staging of breast cancer. *Virchows Arch* 472, 697–703.

Curiel, T.J., Coukos, G., Zou, L., Alvarez, X., Cheng, P., Mottram, P., Evdemon-Hogan, M., Conejo-Garcia, J.R., Zhang, L., Burow, M., Zhu, Y., Wei, S., Kryczek, I., Daniel, B., Gordon, A., Myers, L., Lackner, A., Disis, M.L., Knutson, K.L., Chen, L., Zou, W., 2004. Specific recruitment of regulatory T cells in ovarian carcinoma fosters immune privilege and predicts reduced survival. *Nat Med* 10, 942–949.

D'Alterio, C., Buoncervello, M., Ieranò, C., Napolitano, M., Portella, L., Rea, G., Barbieri, A., Luciano, A., Scognamiglio, G., Tatangelo, F., Anniciello, A.M., Monaco, M., Cavalcanti, E., Maiolino, P., Romagnoli, G., Arra, C., Botti, G., Gabriele, L., Scala, S., 2019. Targeting CXCR4 potentiates anti-PD-1 efficacy modifying the tumor microenvironment and inhibiting neoplastic PD-1. *J Exp Clin Cancer Res* 38, 432.

Dangaj, D., Bruand, M., Grimm, A.J., Ronet, C., Barras, D., Duttagupta, P.A., Lanitis, E., Duraiswamy, J., Tanyi, J.L., Benencia, F., Conejo-Garcia, J., Ramay, H.R., Montone, K.T., Powell, D.J., Gimotty, P.A., Facciabene, A., Jackson, D.G., Weber, J.S., Rodig, S.J., Hodi, S.F., Kandalaft, L.E., Irving, M., Zhang, L., Foukas, P., Rusakiewicz, S., Delorenzi, M., Coukos, G., 2019. Cooperation between Constitutive and Inducible Chemokines Enables T Cell Engraftment and Immune Attack in Solid Tumors. *Cancer Cell* 35, 885-900.e10.

Darvin, P., Toor, S.M., Sasidharan Nair, V., Elkord, E., 2018. Immune checkpoint inhibitors: recent progress and potential biomarkers. *Exp Mol Med* 50, 1–11.

Dejana, E., 2010. The Role of Wnt Signaling in Physiological and Pathological Angiogenesis. *Circ Res* 107, 943–952.

Deligne, C., Murdamoothoo, D., Gammage, A.N., Gschwandtner, M., Erne, W., Loustau, T., Marzeda, A.M., Carapito, R., Paul, N., Velazquez-Quesada, I., Mazzier, I., Sun, Z., Orend, G., Midwood, K.S., 2020. Matrix-Targeting Immunotherapy Controls Tumor Growth and Spread by Switching Macrophage Phenotype. *Cancer Immunol Res* 8, 368–382.

Deryugina, E.I., Bourdon, M.A., 1996. Tenascin mediates human glioma cell migration and modulates cell migration on fibronectin. *J Cell Sci*, 643-52.

Diefenbach, A., Hsia, J.K., Hsiung, M.-Y.B., Raulet, D.H., 2003. A novel ligand for the NKG2D receptor activates NK cells and macrophages and induces tumor immunity. *Eur. J. Immunol.* 33, 381–391.

Diefenbach, A., Jamieson, A.M., Liu, S.D., Shastri, N., Raulet, D.H., 2000. Ligands for the murine NKG2D receptor: expression by tumor cells and activation of NK cells and macrophages. *Nat Immunol* 1, 119–126.

Diefenbach, A., Jensen, E.R., Jamieson, A.M., Raulet, D.H., 2001. Rae1 and H60 ligands of the NKG2D receptor stimulate tumour immunity. *Nature* 413, 165–171.

Dobin, A., Davis, C.A., Schlesinger, F., Drenkow, J., Zaleski, C., Jha, S., Batut, P., Chaisson, M., Gingeras, T.R., 2013. STAR: ultrafast universal RNA-seq aligner. *Bioinformatics* 29, 15–21.

Drăgănescu, M., Carmocan, C., 2017. Hormone Therapy in Breast Cancer. *chr* 112, 413-417.

Duan, S., Guo, W., Xu, Z., He, Y., Liang, C., Mo, Y., Wang, Y., Xiong, F., Guo, C., Li, Y., Li, X., Li, G., Zeng, Z., Xiong, W., Wang, F., 2019. Natural killer group 2D receptor and its ligands in cancer immune escape. *Mol Cancer* 18, 29.

Dunn, G.P., Bruce, A.T., Ikeda, H., Old, L.J., Schreiber, R.D., 2002. Cancer immunoediting: from immunosurveillance to tumor escape. *Nat Immunol* 3, 991–998.

Dunn, G.P., Old, L.J., Schreiber, R.D., 2004a. The Three Es of Cancer Immunoediting. *Annu. Rev. Immunol.* 22, 329–360.

Dunn, G.P., Old, L.J., Schreiber, R.D., 2004b. The Immunobiology of Cancer Immunosurveillance and Immunoediting. *Immunity* 21, 137–148.

Eagle, R.A., Trowsdale, J., 2007. Promiscuity and the single receptor: NKG2D. *Nat Rev Immunol* 7, 737–744.

Eissmann, P., Evans, J.H., Mehrabi, M., Rose, E.L., Nedvetzki, S., Davis, D.M., 2010. Multiple Mechanisms Downstream of TLR-4 Stimulation Allow Expression of NKG2D Ligands To Facilitate Macrophage/NK Cell Crosstalk. *J.I.* 184, 6901–6909.

Ehrlich, P. 1909. Über den jetzigen Stand der Chemotherapie. *Berichte der deutschen chemischen Gesellschaft* 42, 17–47.

Farc, O., Cristea, V., 2020. An overview of the tumor microenvironment, from cells to complex networks (Review). *Exp Ther Med* 21, 96.

Feig, C., Jones, J.O., Kraman, M., Wells, R.J.B., Deonarine, A., Chan, D.S., Connell, C.M., Roberts, E.W., Zhao, Q., Caballero, O.L., Teichmann, S.A., Janowitz, T., Jodrell, D.I., Tuveson, D.A., Fearon, D.T., 2013. Targeting CXCL12 from FAP-expressing carcinoma-associated fibroblasts synergizes with anti-PD-L1 immunotherapy in pancreatic cancer. *Proceedings of the National Academy of Sciences* 110, 20212–20217.

Feins, S., Kong, W., Williams, E.F., Milone, M.C., Fraietta, J.A., 2019. An introduction to chimeric antigen receptor (CAR) T-cell immunotherapy for human cancer. *Am J Hematol* 94, S3–S9.

Ferlay, J., Ervik, M., Lam, F., Colombet, M., Mery, L., Piñeros, M., Znaor, A., Soerjomataram, I., Bray, F., 2020. Global Cancer Observatory: Cancer Today. Lyon, France: International Agency for Research on Cancer. Available from: <https://gco.iarc.fr/today>

Fernández-Messina, L., Reyburn, H.T., Valés-Gómez, M., 2016. A short half-life of ULBP1 at the cell surface due to internalization and proteosomal degradation. *Immunol Cell Biol* 5, 479–85.

Ferrari de Andrade, L., Tay, R.E., Pan, D., Luoma, A.M., Ito, Y., Badrinath, S., Tsoucas, D., Franz, B., May, K.F., Harvey, C.J., Kobold, S., Pyrdol, J.W., Yoon, C., Yuan, G.-C., Hodi, F.S., Dranoff, G., Wucherpfennig, K.W., 2018. Antibody-mediated inhibition of MICA and MICB shedding promotes NK cell–driven tumor immunity. *Science* 359, 1537–1542.

Fisher, B., Anderson, S., Bryant, J., Margolese, R.G., Deutsch, M., Fisher, E.R., Jeong, J.-H., Wolmark, N., 2002. Twenty-Year Follow-up of a Randomized Trial Comparing Total Mastectomy, Lumpectomy, and Lumpectomy plus Irradiation for the Treatment of Invasive Breast Cancer. *N Engl J Med* 347, 1233–1241.

Forsberg, E., Hirsch, E., Frohlich, L., Meyer, M., Ekblom, P., Aszodi, A., Werner, S., Fassler, R., 1996. Skin wounds and severed nerves heal normally in mice lacking tenascin-C. *Proceedings of the National Academy of Sciences* 93, 6594–6599.

Fragomeni, S.M., Sciallis, A., Jeruss, J.S., 2018. Molecular Subtypes and Local-Regional Control of Breast Cancer. *Surgical Oncology Clinics of North America* 27, 95–120.

Frantz, C., Stewart, K.M., Weaver, V.M., 2010. The extracellular matrix at a glance. *Journal of Cell Science* 123, 4195–4200.

Frazao, A., Rethacker, L., Messaoudene, M., Avril, M.-F., Toubert, A., Dulphy, N., Caignard, A., 2019. NKG2D/NKG2-Ligand Pathway Offers New Opportunities in Cancer Treatment. *Front. Immunol.* 10, 661.

Fridman, W.H., Pagès, F., Sautès-Fridman, C., Galon, J., 2012. The immune contexture in human tumours: impact on clinical outcome. *Nat Rev Cancer* 12, 298–306.

Fu, C., Jiang, A., 2018. Dendritic Cells and CD8 T Cell Immunity in Tumor Microenvironment. *Front. Immunol.* 9, 3059.

Fuertes, M.B., Girart, M.V., Molinero, L.L., Domaica, C.I., Rossi, L.E., Barrio, M.M., Mordoh, J., Rabinovich, G.A., Zwirner, N.W., 2008. Intracellular retention of the NKG2D ligand MHC class I chain-related gene A in human melanomas confers immune privilege and prevents NK cell-mediated cytotoxicity. *J Immunol* 7, 4606-14.

Gabrilovich, D.I., Corak, J., Ciernik, I.F., Kavanaugh, D., Carbone, D.P., 1997. Decreased Antigen Presentation by Dendritic Cells in Patients with Breast Cancer 483–490.

Gabrilovich, D.I., Ostrand-Rosenberg, S., Bronte, V., 2012. Coordinated regulation of myeloid cells by tumours. *Nat Rev Immunol* 12, 253–268.

Galon, J., Bruni, D., 2019. Approaches to treat immune hot, altered and cold tumours with combination immunotherapies. *Nat Rev Drug Discov* 18, 197–218.

Garcia-Chagollan, M., Carranza-Torres, I.E., Carranza-Rosales, P., Guzmán-Delgado, N.E., Ramírez-Montoya, H., Martínez-Silva, M.G., Mariscal-Ramirez, I., Barrón-Gallardo, C.A., Pereira-Suárez, A.L., Aguilar-Lemarroy, A., Jave-Suárez, L.F., 2018. Expression of NK Cell Surface Receptors in Breast Cancer Tissue as Predictors of Resistance to Antineoplastic Treatment. *Technol Cancer Res Treat* 17, 153303381876449.

Goepel, C., Buchmann, J., Schultka, R., Koelbl, H., 2000. Tenascin—A Marker for the Malignant Potential of Preinvasive Breast Cancers. *Gynecologic Oncology* 79, 372–378.

Gonzalez, H., Hagerling, C., Werb, Z., 2018. Roles of the immune system in cancer: from tumor initiation to metastatic progression. *Genes Dev.* 32, 1267–1284.

Han, Y., Liu, D., Li, L., 2020. PD-1/PD-L1 pathway: current researches in cancer. *Am J Cancer Res* 10, 727-742.

Hanahan, D., Coussens, L.M., 2012. Accessories to the Crime: Functions of Cells Recruited to the Tumor Microenvironment. *Cancer Cell* 21, 309–322.

Hanahan, D., Weinberg, R.A., 2011. Hallmarks of Cancer: The Next Generation. *Cell* 144, 646–674.

Hancox, R.A., Allen, M.D., Holliday, D.L., Edwards, D.R., Pennington, C.J., Guttery, D.S., Shaw, J.A., Walker, R.A., Pringle, J.H., Jones, J.L., 2009. Tumour-associated tenascin-C isoforms promote breast cancer cell invasion and growth by matrix metalloproteinase-dependent and independent mechanisms. *Breast Cancer Res* 11, R24.

Hargadon, K.M., Bishop, J.D., Brandt, J.P., Hand, Z.C., Ararso, Y.T., Forrest, O.A., 2016. Melanoma-derived factors alter the maturation and activation of differentiated tissue-resident dendritic cells. *Immunol Cell Biol* 94, 24–38.

Hassan, 2010. Chemotherapy for breast cancer (Review). *Oncol Rep* 24, 1121-31.

He, Z.-Y., Wu, S.-G., Zhou, J., Li, F.-Y., Lin, Q., Lin, H.-X., Sun, J.-Y., 2015. Postmastectomy Radiotherapy Improves Disease-Free Survival of High Risk of Locoregional Recurrence Breast Cancer Patients with T1-2 and 1 to 3 Positive Nodes. *PLoS ONE* 10, e0119105.

Herold-Mende, C., Mueller, M.M., Bonsanto, M.M., Schmitt, H.P., Kunze, S., Steiner, H.-H., 2002. Clinical impact and functional aspects of tenascin-C expression during glioma progression. *Int. J. Cancer* 98, 362–369.

Hindermann, W., Berndt, A., Borsi, L., Luo, X., Hyckel, D., Katenkamp, D., Kosmehl, H., 1999. Synthesis and protein distribution of the unspliced large tenascin-C isoform in oral squamous cell carcinoma. *J. Pathol.* 189, 475-80.

Hirata, E., Arakawa, Y., Shirahata, M., Yamaguchi, M., Kishi, Y., Okada, T., Takahashi, J.A., Matsuda, M., Hashimoto, N., 2009. Endogenous tenascin-C enhances glioblastoma invasion with reactive change of surrounding brain tissue. *Cancer Science* 100, 1451–1459.

Huang, W., Chiquet-Ehrismann, R., Moyano, J.V., Garcia-Pardo, A., Orend, G., 2001. Interference of Tenascin-C with Syndecan-4 Binding to Fibronectin Blocks Cell Adhesion and Stimulates Tumor Cell Proliferation 61, 8586-94.

Hynes, R.O., Naba, A., 2012. Overview of the Matrisome--An Inventory of Extracellular Matrix Constituents and Functions. *Cold Spring Harbor Perspectives in Biology* 4, a004903–a004903.

Ilunga, K., Nishiura, R., Inada, H., El-Karef, A., Imanaka-Yoshida, K., Sakakura, T., Yoshida, T., 2004. Co-stimulation of human breast cancer cells with transforming

growth factor-b and tenascin-C enhances matrix metalloproteinase-9 expression and cancer cell invasion. *International Journal of Experimental Pathology* 85, 373-379.

Ishihara, A., Yoshida, T., Tamaki, H., Sakakura, T., 1995. Tenascin Expression in Cancer Cells and Stroma of Human Breast Cancer and Its Prognostic Significance. *Clinical Cancer Research* 1035-1041.

Jachetti, E., Caputo, S., Mazzoleni, S., Brambillasca, C.S., Parigi, S.M., Grioni, M., Piras, I.S., Restuccia, U., Calcinotto, A., Freschi, M., Bachi, A., Galli, R., Bellone, M., 2015. Tenascin-C Protects Cancer Stem-like Cells from Immune Surveillance by Arresting T-cell Activation. *Cancer Res* 75, 2095-2108.

Jamieson, A.M., Diefenbach, A., McMahon, C.W., Xiong, N., Carlyle, J.R., Raulet, D.H., 2002. The Role of the NKG2D Immunoreceptor in Immune Cell Activation and Natural Killing. *Immunity* 1, 19-29.

Jinushi, M., Hodi, F.S., Dranoff, G., 2006. Therapy-induced antibodies to MHC class I chain-related protein A antagonize immune suppression and stimulate antitumor cytotoxicity. *Proceedings of the National Academy of Sciences* 103, 9190-9195.

Joyce, J.A., Pollard, J.W., 2009. Microenvironmental regulation of metastasis. *Nat Rev Cancer* 9, 239-252.

Ju, J., Zhu, A.-J., Yuan, P., 2018. Progress in targeted therapy for breast cancer. *Chronic Diseases and Translational Medicine* 4, 164-175.

Juhász, A., Bárdos, H., Répássy, G., Ádány, R., 2000. Characteristic Distribution Patterns of Tenascin in Laryngeal and Hypopharyngeal Cancers: Characteristic Distribution Patterns of Tenascin in Laryngeal and Hypopharyngeal Cancers. *The Laryngoscope* 110, 84-92.

Kanayama, M., Kurotaki, D., Morimoto, J., Asano, T., Matsui, Y., Nakayama, Y., Saito, Y., Ito, K., Kimura, C., Iwasaki, N., Suzuki, K., Harada, T., Li, H.M., Uehara, J., Miyazaki, T., Minami, A., Kon, S., Uede, T., 2009. α 9 Integrin and Its Ligands Constitute Critical Joint Microenvironments for Development of Autoimmune Arthritis. *J Immunol* 182, 8015-8025.

Kato, N., Tanaka, J., Sugita, J., Toubai, T., Miura, Y., Ibata, M., Syono, Y., Ota, S., Kondo, T., Asaka, M., Imamura, M., 2007. Regulation of the expression of MHC class I-related chain A, B (MICA, MICB) via chromatin remodeling and its impact on the susceptibility of leukemic cells to the cytotoxicity of NKG2D-expressing cells. *Leukemia* 21, 2103-2108.

Katoh, D., Nagaharu, K., Shimojo, N., Hanamura, N., Yamashita, M., Kozuka, Y., Imanaka-Yoshida, K., Yoshida, T., 2013. Binding of α v β 1 and α v β 6 integrins to tenascin-C induces epithelial-mesenchymal transition-like change of breast cancer cells. *Oncogenesis* 2, e65-e65.

Klein C.A., 2009. Parallel progression of primary tumours and metastasis. *Nat Rev Cancer* 4, 302-12.

Kmiecik, M., Payne, K.K., Wang, X.Y., Manjili M.H., 2013. IFN- γ R α Is a Key Determinant of CD8+ T Cell-Mediated Tumor Elimination or Tumor Escape and Relapse in FVB Mouse. *Plos One* 12, e82544.

Konjević, G.M., Vuletić, A.M., Mirjačić Martinović, K.M., Larsen, A.K., Jurišić, V.B., 2019. The role of cytokines in the regulation of NK cells in the tumor environment. *Cytokine* 117, 30–40.

Kwon, H.-J., Kim, H.S., 2012. Signaling for Synergistic Activation of Natural Killer Cells. *Immune Netw* 12, 240.

Labani-Motlagh, A., Ashja-Mahdavi, M., Loskog, A., 2020. The Tumor Microenvironment: A Milieu Hindering and Obstructing Antitumor Immune Responses. *Front. Immunol.* 11, 940.

Lange, K., Kammerer, M., Hegi, M.E., Grotegut, S., Dittmann, A., Huang, W., Fluri, E., Yip, G.W., Götte, M., Ruiz, C., Orend, G., 2007. Endothelin receptor type B Counteracts Tenascin-C-induced Endothelin receptor type A-dependent Focal adhesion and Actin stress fiber disorganization. *Cancer Res* 13, 6163-73.

Langmead, B., Salzberg, S.L., 2012. Fast gapped-read alignment with Bowtie 2. *Nat Methods* 9, 357–359.

Lee, Y.T., Tan, Y.J., Oon, C.E., 2018. Molecular targeted therapy: Treating cancer with specificity. *European Journal of Pharmacology* 834, 188–196.

Li, K., Mandai, M., Hamanishi, J., Matsumura, N., Suzuki, A., Yagi, H., Yamaguchi, K., Baba, T., Fujii, S., Konishi, I., 2009. Clinical significance of the NKG2D ligands, MICa/B and ULBP2 in ovarian cancer: high expression of ULBP2 is an indicator of poor prognosis. *Cancer Immunol Immunother* 58, 641–652.

Li, Y., Niu, M., Zhao, A., Kang, W., Chen, Z., Luo, N., Zhou, L., Zhu, X., Lu, L., Liu, J., 2019. CXCL12 is involved in α -synuclein-triggered neuroinflammation of Parkinson's disease. *J Neuroinflammation* 16, 263. <https://doi.org/10.1186/s12974-019-1646-6>

López-Soto, A., Folgueras, A.R., Seto, E., Gonzalez, S., 2009. HDAC3 represses the expression of NKG2D ligands ULBPs in epithelial tumour cells: potential implications for the immunosurveillance of cancer. *Oncogene* 28, 2370–2382.

Love, M.I., Huber, W., Anders, S., 2014. Moderated estimation of fold change and dispersion for RNA-seq data with DESeq2. *Genome Biol* 15, 550.

Lowy, C.M., Oskarsson, T., 2015. Tenascin C in metastasis: A view from the invasive front. *Cell Adhesion & Migration* 9, 112–124.

Lu, P., Weaver, V.M., Werb, Z., 2012. The extracellular matrix: A dynamic niche in cancer progression. *Journal of Cell Biology* 196, 395–406.

Ma, Q., Dieterich, L.C., Ikenberg, K., Bachmann, S.B., Mangana, J., Proulx, S.T., Amann, V.C., Levesque, M.P., Dummer, R., Baluk, P., McDonald, D.M., Detmar, M., 2018. Unexpected contribution of lymphatic vessels to promotion of distant metastatic tumor spread. *Sci. Adv.* 4, eaat4758.

Ma, Y., Shurin, G.V., Peiyuan, Z., Shurin, M.R., 2013. Dendritic Cells in the Cancer Microenvironment. *J. Cancer* 4, 36–44.

Maccalli, C., Giannarelli, D., Chiarucci, C., Cutaia, O., Giacobini, G., Hendrickx, W., Amato, G., Annesi, D., Bedognetti, D., Altomonte, M., Danielli, R., Calabro, L., Di Giacomo, A.M., Marincola, F.M., Parmiani, G., Maio, M., 2017. Soluble NKG2D ligands are biomarkers associated with the clinical outcome to immune checkpoint blockade therapy of metastatic melanoma patients. *Oncolimmunology* e1323618.

Machino-Ohtsuka, T., Tajiri, K., Kimura, T., Sakai, S., Sato, A., Yoshida, T., Hiroe, M., Yasutomi, Y., Aonuma, K., Imanaka-Yoshida, K., 2014. Tenascin-C Aggravates Autoimmune Myocarditis via Dendritic Cell Activation and Th17 Cell Differentiation. *JAHAD* 3, e001052.

Mackie, E.J., Tucker, R.P., 1999. Tenascin-C knockout revisited. *J Cell Sci* 112, 3847–53.

Mantovani, A., Marchesi, F., Malesci, A., Laghi, L., Allavena, P., 2017. Tumour-associated macrophages as treatment targets in oncology. *Nat Rev Clin Oncol* 14, 399–416.

Marzeda, A.M., Midwood, K.S., 2018. Internal Affairs: Tenascin-C as a Clinically Relevant, Endogenous Driver of Innate Immunity. *J Histochem Cytochem.* 66, 289–304.

Masoud, V., Pagès, G., 2017. Targeted therapies in breast cancer: New challenges to fight against resistance. *WJCO* 8, 120.

Maughan, K.L., Lutterbie, M.A., Ham, P.S., 2010. Treatment of Breast Cancer. *Breast Cancer* 81, 8.

McGilvray, R.W., Eagle, R.A., Watson, N.F.S., Al-Attar, A., Ball, G., Jafferji, I., Trowsdale, J., Durrant, L.G., 2009. NKG2D Ligand Expression in Human Colorectal Cancer Reveals Associations with Prognosis and Evidence for Immunoediting. *Clin Cancer Res* 15, 6993–7002.

Mellergaard, M., Skovbakke, S.L., Schneider, C.L., Lauridsen, F., Andresen, L., Jensen, H., Skov, S., 2014. N-Glycosylation of Asparagine 8 Regulates Surface Expression of Major Histocompatibility Complex Class I Chain-related Protein A (MICA) Alleles Dependent on Threonine 24. *Journal of Biological Chemistry* 289, 20078–20091.

Midwood, K.S., Chiquet, M., Tucker, R.P., Orend, G., 2016. Tenascin-C at a glance. *Journal of Cell Science* jcs.190546.

Midwood, K.S., Hussenet, T., Langlois, B., Orend, G., 2011. Advances in tenascin-C biology. *Cell. Mol. Life Sci.* 68, 3175–3199.

Midwood, K.S., Orend, G., 2009a. The role of tenascin-C in tissue injury and tumorigenesis. *J. Cell Commun. Signal.* 3, 287–310.

Midwood K., Sacre S., Piccinini A.M., Inglis J., Trebaul A., Chan E., Drexler S., Sofat N., Kashiwagi M., Orend G., Brennan F., Foxwell B, 2009b. Tenascin-C is an

endogenous activator of Toll-like receptor 4 that is essential for maintaining inflammation in arthritic joint disease. *Nat Med.* 15, 774-80.

Minn, A.J., Kang, Y., Serganova, I., Gupta, G.P., Giri, D.D., Doubrovin, M., Ponomarev, V., Gerald, W.L., Blasberg, R., Massagué, J., 2005. Distinct organ-specific metastatic potential of individual breast cancer cells and primary tumors. *J. Clin. Invest.* 115, 44–55.

Molfetta, R., Quatrini, L., Capuano, C., Gasparrini, F., Zitti, B., Zingoni, A., Galandini, R., Santoni, A., Paolini, R., 2014. c-Cbl regulates MICA- but not ULBP2-induced NKG2D down-modulation in human NK cells: Molecular immunology. *Eur. J. Immunol.* 44, 2761–2770.

Molfetta, R., Quatrini, L., Santoni, A., Paolini, R., 2017. Regulation of NKG2D-Dependent NK Cell Functions: The Yin and the Yang of Receptor Endocytosis. *IJMS* 18, 1677.

Mouw, J.K., Ou, G., Weaver, V.M., 2014. Extracellular matrix assembly: a multiscale deconstruction. *Nat Rev Mol Cell Biol* 15, 771–785.

Müller, A., Homey, B., Soto, H., Ge, N., Catron, D., Buchanan, M.E., McClanahan, T., Murphy, E., Yuan, W., Wagner, S.N., Barrera, J.L., Mohar, A., Verástegui, E., Zlotnik, A., 2001. Involvement of chemokine receptors in breast cancer metastasis. *Nature* 410, 50–56.

Muller, W.J., Sinn, E., Pattengale, P.K., Wallace, R., Leder, P., 1988. Single-step induction of mammary adenocarcinoma in transgenic mice bearing the activated c-neu oncogene. *Cell* 54, 105–115.

Murdamoothoo, D., Sun, Z., Yilmaz, A., Riegel, G., Abou-Faycal, C., Deligne, C., Velazquez-Quesada, I., Erne, W., Nascimento, M., Mörgelin, M., Cremel, G., Paul, N., Carapito, R., Veber, R., Dumortier, H., Yuan, J., Midwood, K.S., Loustau, T., Orend, G., 2021. Tenascin-C immobilizes infiltrating T lymphocytes through CXCL12 promoting breast cancer progression. *EMBO Mol Med* 13, e13270.

Nabeshima, K., Inoue, T., Shimao, Y., Sameshima, T., 2002. Matrix metalloproteinases in tumor invasion: Role for cell migration. *Pathol Int* 52, 255–264.

Nakahara, H., Gabazza, E.C., Fujimoto, H., Nishii, Y., D'Alessandro-Gabazza, C.N., Bruno, N.E., Takagi, T., Hayashi, T., Maruyama, J., Maruyama, K., Imanaka-Yoshida, K., Suzuki, K., Yoshida, T., Adachi, Y., Taguchi, O., 2006a. Deficiency of tenascin C attenuates allergen-induced bronchial asthma in the mouse. *Eur. J. Immunol.* 36, 3334–3345.

Nascimento, R.G. do, Otoni, K.M., 2020. Histological and molecular classification of breast cancer: what do we know? *Mastology* 30, e20200024.

Nausch, N., Cerwenka, A., 2008. NKG2D ligands in tumor immunity. *Oncogene* 27, 5944–5958.

Nedvetzki, S., Sowinski, S., Eagle, R.A., Harris, J., Vély, F., Pende, D., Trowsdale, J., Vivier, E., Gordon, S., Davis, D.M., 2007. Reciprocal regulation of human natural

killer cells and macrophages associated with distinct immune synapses. *Blood* 109, 3776–3785.

Nelson, J.B., Udan, M.S., Guruli, G., Pflug, B.R., 2005. Endothelin-1 Inhibits Apoptosis in Prostate Cancer. *Neoplasia* 7, 631-637.

Nersesian, S., Schwartz, S.L., Grantham, S.R., MacLean, L.K., Lee, S.N., Pugh-Toole, M., Boudreau, J.E., 2021. NK cell infiltration is associated with improved overall survival in solid cancers: A systematic review and meta-analysis. *Translational Oncology* 14, 100930.

Noy, R., Pollard, J.W., 2014. Tumor-Associated Macrophages: From Mechanisms to Therapy. *Immunity* 41, 49–61.

Oblak, A., Jerala, R., 2011. Toll-Like Receptor 4 Activation in Cancer Progression and Therapy. *Clinical and Developmental Immunology* 2011, 1–12.

O'Connell, J.T., Sugimoto, H., Cooke, V.G., MacDonald, B.A., Mehta, A.I., LeBleu, V.S., Dewar, R., Rocha, R.M., Brentani, R.R., Resnick, M.B., Neilson, E.G., Zeisberg, M., Kalluri, R., 2011. VEGF-A and Tenascin-C produced by S100A4+ stromal cells are important for metastatic colonization. *Proceedings of the National Academy of Sciences* 108, 16002–16007.

Okabe, S., Fukuda, S., Kim, Y.-J., Niki, M., Pelus, L.M., Ohyashiki, K., Pandolfi, P.P., Broxmeyer, H.E., 2005. Stromal cell-derived factor-1 α /CXCL12-induced chemotaxis of T cells involves activation of the RasGAP-associated docking protein p62Dok-1. *Blood* 105, 474–480.

Ono, M., Tsuda, H., Shimizu, C., Yamamoto, S., Shibata, T., Yamamoto, H., Hirata, T., Yonemori, K., Ando, M., Tamura, K., Katsumata, N., Kinoshita, T., Takiguchi, Y., Tanzawa, H., Fujiwara, Y., 2012. Tumor-infiltrating lymphocytes are correlated with response to neoadjuvant chemotherapy in triple-negative breast cancer. *Breast Cancer Res Treat* 132, 793–805.

Orend, G., Chiquet-Ehrismann, R., 2006. Tenascin-C induced signaling in cancer. *Cancer Letters* 244, 143–163.

Orend, G., Huang, W., Olayioye, M.A., Hynes, N.E., Chiquet-Ehrismann, R., 2003. Tenascin-C blocks cell-cycle progression of anchorage-dependent fibroblasts on fibronectin through inhibition of syndecan-4. *Oncogene* 22, 3917–3926.

Orend, G., Tucker, R.P., 2021. Did Tenascin-C Co-Evolve With the General Immune System of Vertebrates? *Front Immunol* 12, 663902.

Orimo, A., Gupta, P.B., Sgroi, D.C., Arenzana-Seisdedos, F., Delaunay, T., Naeem, R., Carey, V.J., Richardson, A.L., Weinberg, R.A., 2005. Stromal Fibroblasts Present in Invasive Human Breast Carcinomas Promote Tumor Growth and Angiogenesis through Elevated SDF-1/CXCL12 Secretion. *Cell* 121, 335–348.

Oskarsson, T., Acharyya, S., Zhang, X.H.-F., Vanharanta, S., Tavazoie, S.F., Morris, P.G., Downey, R.J., Manova-Todorova, K., Brogi, E., Massagué, J., 2011. Breast

cancer cells produce tenascin C as a metastatic niche component to colonize the lungs. *Nat Med* 17, 867–874.

Parekh, K., Ramachandran, S., Cooper, J., Bigner, D., Patterson, A., Mohanakumar, T., 2005. Tenascin-C, over expressed in lung cancer down regulates effector functions of tumor infiltrating lymphocytes. *Lung Cancer* 47, 17–29.

Paron, I., Berchtold, S., Vörös, J., Shamarla, M., Erkan, M., Höfler, H., Esposito, I., 2011. Tenascin-C Enhances Pancreatic Cancer Cell Growth and Motility and Affects Cell Adhesion through Activation of the Integrin Pathway. *PLoS ONE* 6, e21684.

Partridge, A.H., Burstein, H.J., Winer, E.P., 2001. Side Effects of Chemotherapy and Combined Chemohormonal Therapy in Women With Early-Stage Breast Cancer. *JNCI Monographs* 2001, 135–142.

Paschen, A., Sucker, A., Hill, B., Moll, I., Zapatka, M., Nguyen, X.D., Sim, G.C., Gutmann, I., Hassel, J., Becker, J.C., Steinle, A., Schadendorf, D., Ugurel, S., 2009. Differential Clinical Significance of Individual NKG2D Ligands in Melanoma: Soluble ULBP2 as an Indicator of Poor Prognosis Superior to S100B. *Clin Cancer Res* 15, 5208–5215.

Pickup, M.W., Mouw, J.K., Weaver, V.M., 2014. The extracellular matrix modulates the hallmarks of cancer. *EMBO Rep* 15, 1243–1253.

Ping, Q., Yan, R., Cheng, X., Wang, W., Zhong, Y., Hou, Z., Shi, Y., Wang, C., Li, R., 2021. Cancer-associated fibroblasts: overview, progress, challenges, and directions. *Cancer Gene Ther.*

Pio, R., Ajona, D., Ortiz-Espinosa, S., Mantovani, A., Lambris, J.D., 2019. Complementing the Cancer-Immunity Cycle. *Front. Immunol.* 10, 774.

Pollard, J.W., 2004. Tumour-educated macrophages promote tumour progression and metastasis. *Nat Rev Cancer* 4, 71–78.

Polyak, K., Weinberg, R.A., 2009a. Transitions between epithelial and mesenchymal states: acquisition of malignant and stem cell traits. *Nat Rev Cancer* 9, 265–273.

Poznansky, M.C., Olszak, I.T., Foxall, R., Evans, R.H., Luster, A.D., Scadden, D.T., 2000. Active movement of T cells away from a chemokine. *Nat Med* 6, 543–548.

Prajapati, K., Perez, C., Rojas, L.B.P., Burke, B., Guevara-Patino, J.A., 2018. Functions of NKG2D in CD8+ T cells: an opportunity for immunotherapy. *Cell Mol Immunol* 15, 470–479.

Rakha, E.A., Reis-Filho, J.S., Baehner, F., Dabbs, D.J., Decker, T., Eusebi, V., Fox, S.B., Ichihara, S., Jacquemier, J., Lakhani, S.R., Palacios, J., Richardson, A.L., Schnitt, S.J., Schmitt, F.C., Tan, P.-H., Tse, G.M., Badve, S., Ellis, I.O., 2010. Breast cancer prognostic classification in the molecular era: the role of histological grade. *Breast Cancer Res* 12, 207.

Raulet, D.H., 2003. Roles of the NKG2D immunoreceptor and its ligands. *Nat Rev Immunol* 3, 781–790.

Raulet, D.H., Gasser, S., Gowen, B.G., Deng, W., Jung, H., 2013. Regulation of Ligands for the NKG2D Activating Receptor. *Annu. Rev. Immunol.* 31, 413–441.

Ringuette Goulet, C., Bernard, G., Tremblay, S., Chabaud, S., Bolduc, S., Pouliot, F., 2018. Exosomes Induce Fibroblast Differentiation into Cancer-Associated Fibroblasts through TGF β Signaling. *Mol Cancer Res* 16, 1196–1204.

Rotte, A., 2019. Combination of CTLA-4 and PD-1 blockers for treatment of cancer. *J Exp Clin Cancer Res* 38, 255.

Rupp, T., Langlois, B., Koczorowska, M.M., Radwanska, A., Sun, Z., Hussenet, T., Lefebvre, O., Murdamoothoo, D., Arnold, C., Klein, A., Biniossek, M.L., Hyenne, V., Naudin, E., Velazquez-Quesada, I., Schilling, O., Van Obberghen-Schilling, E., Orend, G., 2016. Tenascin-C Orchestrates Glioblastoma Angiogenesis by Modulation of Pro- and Anti-angiogenic Signaling. *Cell Reports* 17, 2607–2619.

Saga, Y., Yagi, T., Ikawa, Y., Sakakura, T., Aizawa, S., 1992. Mice develop normally without tenascin. *Genes & Development* 6, 1821–1831.

Sarkar, S., Nuttall, R.K., Liu, S., Edwards, D.R., Yong, V.W., 2006. Tenascin-C Stimulates Glioma Cell Invasion through Matrix Metalloproteinase-12. *Cancer Res* 66, 11771–11780.

Satthaporn, S., Robins, A., Vassanasiri, W., El-Sheemy, M., Jibril, J.A., Clark, D., Valerio, D., Eremin, O., 2004. Dendritic cells are dysfunctional in patients with operable breast cancer. *Cancer Immunology, Immunotherapy* 53, 510–518.

Saupe, F., Schwenzer, A., Jia, Y., Gasser, I., Spenlé, C., Langlois, B., Kammerer, M., Lefebvre, O., Hlushchuk, R., Rupp, T., Marko, M., van der Heyden, M., Cremel, G., Arnold, C., Klein, A., Simon-Assmann, P., Djonov, V., Neuville-Méchine, A., Esposito, I., Slotta-Huspenina, J., Janssen, K.-P., de Wever, O., Christofori, G., Hussenet, T., Orend, G., 2013. Tenascin-C Downregulates Wnt Inhibitor Dickkopf-1, Promoting Tumorigenesis in a Neuroendocrine Tumor Model. *Cell Reports* 5, 482–492.

Schreiber, R.D., Old, L.J., Smyth, M.J., 2011. Cancer immunoediting: integrating immunity's roles in cancer suppression and promotion. *Science* 331, 1565-70.

Shankaran, V., Ikeda, H., Bruce, A.T., White, J.M., Swanson, P.E., Old, L.J., Schreiber, R.D., 2001. IFNg and lymphocytes prevent primary tumour development and shape tumour immunogenicity 410, 5.

Shao, H., Kirkwood, J.M., Wells, A., 2015. Tenascin-C Signaling in melanoma. *Cell Adhesion & Migration* 9, 125–130.

Sharma, P., Allison, J.P., 2015. The future of immune checkpoint therapy. *Science* 348, 56–61.

Sharma, P., Hu-Lieskovan, S., Wargo, J.A., Ribas, A., 2017. Primary, Adaptive, and Acquired Resistance to Cancer Immunotherapy. *Cell* 168, 707–723.

Sharma, S.S., Pledger, W.J., 2016. The non-canonical functions of p27^{Kip1} in normal and tumor biology. *Cell Cycle* 9, 1189-1201.

Shi, M., He, X., Wei, W., Wang, J., Zhang, T., Shen, X., 2015. Tenascin-C induces resistance to apoptosis in pancreatic cancer cell through activation of ERK/NF- κ B pathway. *Apoptosis* 20, 843–857.

Shi, Y., Riese, D.J., Shen, J., 2020. The Role of the CXCL12/CXCR4/CXCR7 Chemokine Axis in Cancer. *Front. Pharmacol.* 11, 574667.

Soderquest, K., Walzer, T., Zafirova, B., Klavinskis, L.S., Polić, B., Vivier, E., Lord, G.M., Martín-Fontechá, A., 2011. Cutting Edge: CD8 + T Cell Priming in the Absence of NK Cells Leads to Enhanced Memory Responses. *J.I.* 186, 3304–3308.

Spenlé, C., Gasser, I., Saupe, F., Janssen, K.-P., Arnold, C., Klein, A., van der Heyden, M., Mutterer, J., Neuville-Méchine, A., Chenard, M.-P., Guenot, D., Esposito, I., Slotta-Huspenina, J., Ambartsumian, N., Simon-Assmann, P., Orend, G., 2015. Spatial organization of the tenascin-C microenvironment in experimental and human cancer. *Cell Adhesion & Migration* 9, 4–13.

Spenlé, C., Loustau, T., Murdamoothoo, D., Erne, W., Beghelli-de la Forest Divonne, S., Veber, R., Petti, L., Bourdely, P., Mörgelin, M., Brauchle, E.-M., Cremel, G., Randrianarisoa, V., Camara, A., Rekima, S., Schaub, S., Nouhen, K., Imhof, T., Hansen, U., Paul, N., Carapito, R., Pythoud, N., Hirschler, A., Carapito, C., Dumortier, H., Mueller, C.G., Koch, M., Schenke-Layland, K., Kon, S., Sudaka, A., Anjuère, F., Van Obberghen-Schilling, E., Orend, G., 2020. Tenascin-C Orchestrates an Immune-Suppressive Tumor Microenvironment in Oral Squamous Cell Carcinoma. *Cancer Immunol Res* 8, 1122–1138.

Stojanovic, A., Correia, M.P., Cerwenka, A., 2018. The NKG2D/NKG2DL Axis in the Crosstalk Between Lymphoid and Myeloid Cells in Health and Disease. *Front. Immunol.* 9, 827.

Stojanovic, A., Correia, M.P., Cerwenka, A., 2013. Shaping of NK Cell Responses by the Tumor Microenvironment. *Cancer Microenvironment* 6, 135–146.

Sun, Z., Schwenze, A., Rupp, T., Murdamoothoo, D., Vegliante, R., Lefebvre, O., Klein, A., Hussenet, T., Orend., G., 2018. Tenascin-C promotes tumor cell migration and metastasis through integrin α 9 β 1-mediated YAP inhibition. *Cancer Res* 4, 950–961.

Sun, Z., Velázquez-Quesada, I., Murdamoothoo, D., Ahowesso, C., Yilmaz, A., Spenlé, C., Averous, G., Erne, W., Oberndorfer, F., Oswald, A., Kain, R., Bourdon, C., Mangin, P., Deligne, C., Midwood, K., Abou-Faycal, C., Lefebvre, O., Klein, A., van der Heyden, M., Chenard, M.-P., Christofori, G., Mathelin, C., Loustau, T., Hussenet, T., Orend, G., 2019. Tenascin-C increases lung metastasis by impacting blood vessel invasions. *Matrix Biology* 83, 26–47.

Sung, H., Ferlay, J., Siegel, R.L., Laversanne, M., Soerjomataram, I., Jemal, A., Bray, F., 2021. Global Cancer Statistics 2020: GLOBOCAN Estimates of Incidence and Mortality Worldwide for 36 Cancers in 185 Countries. *CA Cancer J Clin* 71, 209–249.

Takahashi, Y., Sawada, G., Kurashige, J., Matsumura, T., Uchi, R., Ueo, H., Ishibashi, M., Takano, Y., Akiyoshi, S., Iwaya, T., Eguchi, H., Sudo, T., Sugimachi, K., Yamamoto, H., Doki, Y., Mori, M., Mimori, K., 2013. Tumor-derived Tenascin-C Promotes the Epithelial– Mesenchymal Transition in Colorectal Cancer Cells. *Anticancer Research* 33, 1927-34.

Takebe, N., Harris, P.J., Warren, R.Q., Ivy, S.P., 2011. Targeting cancer stem cells by inhibiting Wnt, Notch, and Hedgehog pathways. *Nat Rev Clin Oncol* 8, 97–106.

Takebe, N., Miele, L., Harris, P.J., Jeong, W., Bando, H., Kahn, M., Yang, S.X., Ivy, S.P., 2015. Targeting Notch, Hedgehog, and Wnt pathways in cancer stem cells: clinical update. *Nat Rev Clin Oncol* 12, 445–464.

Talts, J.F., 1992. Tenascin-C in tumor growth and metastasis. *J Cell Sci* 112, 1855–64.

Talts, J.F., Wirl, G., Dictor, M., Muller, W.J., Fässler, R., 1999. Tenascin-C modulates tumor stroma and monocyte/macrophage recruitment but not tumor growth or metastasis in a mouse strain with spontaneous mammary cancer. *J Cell Sci* 112, 1855-64.

Tanaka, K., Hiraiwa, N., Hashimoto, H., Yamazaki, Y., Kusakabe, M., 2004. Tenascin-C regulates angiogenesis in tumor through the regulation of vascular endothelial growth factor expression. *Int. J. Cancer* 108, 31–40.

Taneja, P., Frazier, D.P., Kendig, R.D., Maglic, D., Sugiyama, T., Kai, F., Taneja, N.K., Inoue, K., 2009. MMTV mouse models and the diagnostic values of MMTV-like sequences in human breast cancer. *Expert Review of Molecular Diagnostics* 9, 423–440.

Tavazoie, S.F., Alarcón, C., Oskarsson, T., Padua, D., Wang, Q., Bos, P.D., Gerald, W.L., Massagué, J., 2008. Endogenous human microRNAs that suppress breast cancer metastasis. *Nature* 451, 147–152.

Teng, M.W.L., Swann, J.B., Koebel, C.M., Schreiber, R.D., Smyth, M.J., 2008. Immune-mediated dormancy: an equilibrium with cancer. *Journal of Leukocyte Biology* 84, 988–993.

Theocharis, A.D., Skandalis, S.S., Gialeli, C., Karamanos, N.K., 2016. Extracellular matrix structure. *Advanced Drug Delivery Reviews* 97, 4–27.

Thiery, J.P., Acloque, H., Huang, R.Y.J., Nieto, M.A., 2009b. Epithelial-Mesenchymal Transitions in Development and Disease. *Cell* 139, 871–890.

Jahkola, T., Toivonen, T., von Smitten, K., Blomqvist, C., Virtanen, I., 1996. Expression of tenascin in invasion border of early breast cancer correlates with higher risk of distant metastasis. *Int J Cancer* 69, 445-7.

Tsang, J.Y.S., Tse, G.M., 2019. Molecular Classification of Breast Cancer. *Adv Anat Pathol* 27, 9.

Upshaw, J.L., Leibson, P.J., 2006a. NKG2D-mediated activation of cytotoxic lymphocytes: Unique signaling pathways and distinct functional outcomes. *Seminars in Immunology* 18, 167–175.

Van Obberghen-Schilling, E., Tucker, R.P., Saupe, F., Gasser, I., Cseh, B., Orend, G., 2011. Fibronectin and tenascin-C: accomplices in vascular morphogenesis during development and tumor growth. *Int J Dev Biol* 55, 511-25.

Vantourout, P., Willcox, C., Turner, A., Swanson, C.M., Haque, Y., Sobolev, O., Grigoriadis, A., Tutt, A., Hayday, A., 2014. Immunological Visibility: Posttranscriptional Regulation of Human NKG2D Ligands by the EGF Receptor Pathway. *Science Translational Medicine* 6, 231ra49-231ra49.

Viale, G., 2012. The current state of breast cancer classification. *Annals of Oncology* 23, x207–10.

Vivanco, I., Sawyers, C.L., 2002. The phosphatidylinositol 3-kinase–AKT pathway in human cancer. *Nat Rev Cancer* 2, 489-51.

Vivier, E., Tomasello, E., Baratin, M., Walzer, T., Ugolini, S., 2008. Functions of natural killer cells. *Nat Immunol* 9, 503–510.

von Lilienfeld-Toal, M., Frank, S., Leyendecker, C., Feyler, S., Jarmin, S., Morgan, R., Glasmacher, A., Märten, A., Schmidt-Wolf, I.G.H., Brossart, P., Cook, G., 2010. Reduced immune effector cell NKG2D expression and increased levels of soluble NKG2D ligands in multiple myeloma may not be causally linked. *Cancer Immunol Immunother* 59, 829–839.

von Strandmann, E.P., Hansen, H.P., Reiners, K.S., Schnell, R., Borchmann, P., Merkert, S., Simhadri, V.R., Draube, A., Reiser, M., Purr, I., Hallek, M., Engert, A., 2006. A novel bispecific protein (ULBP2-BB4) targeting the NKG2D receptor on natural killer (NK) cells and CD138 activates NK cells and has potent antitumor activity against human multiple myeloma in vitro and in vivo. *Blood* 107, 1955–1962.

Waks, A.G., Winer, E.P., 2019. Breast Cancer Treatment: A Review. *JAMA* 321, 288.

Wang, Q.-E., 2015. DNA damage responses in cancer stem cells: Implications for cancer therapeutic strategies. *WJBC* 6, 57.

Wawrzyniak, D., Grabowska, M., Głodowicz, P., Kuczyński, K., Kuczyńska, B., Fedoruk-Wyszomirska, A., Rolle, K., 2020. Down-regulation of tenascin-C inhibits breast cancer cells development by cell growth, migration, and adhesion impairment. *PLoS ONE* 15, e0237889.

Wensveen, F.M., Jelenčić, V., Polić, B., 2018. NKG2D: A Master Regulator of Immune Cell Responsiveness. *Front. Immunol.* 9, 441.

Wensveen, F.M., Lenartić, M., Jelenčić, V., Lemmermann, N.A.W., ten Brinke, A., Jonjić, S., Polić, B., 2013. NKG2D Induces Mcl-1 Expression and Mediates Survival of CD8 Memory T Cell Precursors via Phosphatidylinositol 3-Kinase. *J.I.* 191, 1307–1315.

Wodarz, A., Näthke, I., 2007. Cell polarity in development and cancer. *Nat Cell Biol* 9, 1016–1024.

Wylie, B., Macri, C., Mintern, J., Waithman, J., 2019. Dendritic Cells and Cancer: From Biology to Therapeutic Intervention. *Cancers* 11, 521.

Yang, Z., Zhang, C., Feng, Y., Qi, W., Cui, Y., Xuan, Y., 2019. Tenascin-C is involved in promotion of cancer stemness via the Akt/HIF1 α axis in esophageal squamous cell carcinoma. *Experimental and Molecular Pathology* 109, 104239.

Yang, Z., Zhang, C., Feng, Y., Quan, M., Cui, Y., Xuan, Y., 2020. Tenascin-C predicts poor outcomes for patients with colorectal cancer and drives cancer stemness via Hedgehog signaling pathway. *Cancer Cell Int* 20, 122.

Yang, Z., Zhang, C., Qi, W., Cui, C., Cui, Y., Xuan, Y., 2018. Tenascin-C as a prognostic determinant of colorectal cancer through induction of epithelial-to-mesenchymal transition and proliferation. *Experimental and Molecular Pathology* 105, 216–222.

Yersal, O., 2014. Biological subtypes of breast cancer: Prognostic and therapeutic implications. *WJCO* 5, 412.

Yoshida, T., Akatsuka, T., Imanaka-Yoshida, K., 2015. Tenascin-C and integrins in cancer. *Cell Adhesion & Migration* 9, 96–104.

Yoshida, T., Matsumoto, E., Hanamura, N., Kalembeysi, I., Katsuta, K., Ishihara, A., Sakakura, T., 1997. Co-expression of tenascin and fibronectin in epithelial and stromal cells of benign lesions and ductal carcinomas in the human breast. *J Pathol* 182, 421–8.

Yoshida, T., Yoshimura, E., Numata, H., Sakakura, Y., Sakakura, T., 1999. Involvement of tenascin-C in proliferation and migration of laryngeal carcinoma cells. *Virchows Archiv* 435, 496–500.

Yu, Lu, Yu, Liangli, Pham, Q., Wang, T.T.Y., 2018. Transcriptional and translational-uncoupling in regulation of the CXCL12 and its receptors CXCR4, 7 in THP-1 monocytes and macrophages. *Immunity, Inflammation and Disease* 6, 106–116.

Yue, B., 2014. Biology of the Extracellular Matrix: An Overview. *Journal of Glaucoma* 23, S20–S23.

Zafirova, B., Wensveen, F.M., Gulin, M., Polić, B., 2011. Regulation of immune cell function and differentiation by the NKG2D receptor. *Cell. Mol. Life Sci.* 68, 3519–3529.

Zagzag, D., Friedlander, D.R., Dosik, J., Chikramane, S., Chan, W., Greco, M.A., Allen, J.C., Dorovini-Zis, K., Grumet, M., 1996. Tenascin-C Expression by Angiogenic Vessels in Human Astrocytomas and by Human Brain Endothelial Cells in Vitro. *Cancer Research* 56, 183–189.

Zboralski, D., Hoehlig, K., Eulberg, D., Frömming, A., Vater, A., 2017. Increasing Tumor-Infiltrating T Cells through Inhibition of CXCL12 with NOX-A12 Synergizes with PD-1 Blockade. *Cancer Immunol Res* 5, 950–956.

Zhang, J., Basher, F., Wu, J.D., 2015. NKG2D Ligands in Tumor Immunity: Two Sides of a Coin. *Front. Immunol.* 6, 97.

Zhang, Q., Liu, L., Gong, C., Shi, H., Zeng, Y., Wang, X., Zhao, Y., Wei, Y., 2012. Prognostic Significance of Tumor-Associated Macrophages in Solid Tumor: A Meta-Analysis of the Literature. *PLoS ONE* 7, e50946.

Zhang, Qingping, Xu, B., Hu, F., Chen, X., Liu, X., Zhang, Qinghua, Zuo, Y., 2021. Tenascin C Promotes Glioma Cell Malignant Behavior and Inhibits Chemosensitivity to Paclitaxel via Activation of the PI3K/AKT Signaling Pathway. *J Mol Neurosci* 71, 1636–1647.

Zhang, T., Sentman, C.L., 2011. Cancer Immunotherapy Using a Bispecific NK Receptor Fusion Protein that Engages both T Cells and Tumor Cells. *Cancer Res* 71, 2066–2076.

Zhou, Z., Zhang, C., Zhang, J., Tian, Z., 2012. Macrophages Help NK Cells to Attack Tumor Cells by Stimulatory NKG2D Ligand but Protect Themselves from NK Killing by Inhibitory Ligand Qa-1. *PLoS ONE* 7, e36928.

Zingoni, A., Molfetta, R., Fionda, C., Soriani, A., Paolini, R., Cippitelli, M., Cerboni, C., Santoni, A., 2018. NKG2D and Its Ligands: “One for All, All for One.” *Front. Immunol.* 9, 476.

Appendix I



Tenascin-C increases lung metastasis by impacting blood vessel invasions



Zhen Sun^{a,b,c,d,1,2}, Inés Velázquez-Quesada^{a,b,c,d,2},
 Devadarssen Murdamoothoo^{a,b,c,d}, Constance Ahowesso^{a,b,c,d},
 Alev Yilmaz^{a,b,c,d}, Caroline Spenlé^{a,b,c,d}, Gerlinde Averous^e, William Erne^{a,b,c,d},
 Felicitas Oberndorfer^f, Andre Oszwald^f, Renate Kain^f, Catherine Bourdon^g,
 Pierre Mangin^g, Claire Deligne^h, Kim Midwood^h, Chérine Abou-Faycal^{a,b,c,d},
 Olivier Lefebvre^{a,b,c,d}, Annick Klein^{a,b,c,d}, Michael van der Heyden^{a,b,c,d},
 Marie-Pierre Chenard^e, Gerhard Christoforiⁱ, Carole Mathelin^j,
 Thomas Loustau^{a,b,c,d}, Thomas Hussenet^{a,b,c,d} and Gertraud Orend^{a,b,c,d}

a - INSERM U1109 - MN3T, The Microenvironmental Niche in Tumorigenesis and Targeted Therapy and, the Tumor Microenvironment group, France

b - Université de Strasbourg, Strasbourg, France

c - LabEx Medalis, Université de Strasbourg, France

d - Fédération de Médecine Translationnelle de Strasbourg (FMTS), Strasbourg, France

e - Department of Pathology, University Hospital Strasbourg, Strasbourg, France

f - Department of Pathology, Medical University of Vienna (MUW), Vienna, Austria

g - Etablissement Français du Sang, INSERM U949, Strasbourg, France

h - Kennedy Institute of Rheumatology, University of Oxford, Oxford, UK

i - Department Medicine, University Basel, Basel, Switzerland

j - Department of breast diseases and surgery, Strasbourg University Hospital, Strasbourg, France

Correspondence to Gertraud Orend: at: Institut d'Hématologie et d'Immunologie, Hôpital Civil, 4 rue Kirschleger, 67085 Strasbourg Cedex, France. gertraud.orend@inserm.fr

<https://doi.org/10.1016/j.matbio.2019.07.001>

Abstract

Metastasis is a major cause of death in cancer patients. The extracellular matrix molecule tenascin-C is a known promoter of metastasis, however the underlying mechanisms are not well understood. To further analyze the impact of tenascin-C on cancer progression we generated MMTV-NeuNT mice that develop spontaneous mammary tumors, on a tenascin-C knockout background. We also developed a syngeneic orthotopic model in which tumor cells derived from a MMTV-NeuNT tumor. Tumor cells were transfected with control shRNA or with shRNA to knockdown tenascin-C expression and, were grafted into the mammary gland of immune competent, wildtype or tenascin-C knockout mice. We show that stromal-derived tenascin-C increases metastasis by reducing apoptosis and inducing the cellular plasticity of cancer cells located in pulmonary blood vessels invasions (BVI), before extravasation. We characterized BVI as organized structures of tightly packed aggregates of proliferating tumor cells with epithelial characteristics, surrounded by Fsp1+ cells, internally located platelets and, a luminal monolayer of endothelial cells. We found extracellular matrix, in particular, tenascin-C, between the stromal cells and the tumor cell cluster. In mice lacking stromal-derived tenascin-C, the organization of pulmonary BVI was significantly affected, revealing novel functions of host-derived tenascin-C in supporting the integrity of the endothelial cell coat, increasing platelet abundance, tumor cell survival, epithelial plasticity, thereby promoting overall lung metastasis. Many effects of tenascin-C observed in BVI including enhancement of cellular plasticity, survival and migration, could be explained by activation of TGF- β signaling. Finally, in several human cancers, we also observed BVI to be surrounded by an endothelial monolayer and to express tenascin-C. Expression of tenascin-C is specific to BVI and is not observed in lymphatic vascular invasions frequent in breast cancer, which lack an endothelial lining. Given

that BVI have prognostic significance for many tumor types, such as shorter cancer patient survival, increased metastasis, vessel occlusion, and organ failure, our data revealing a novel mechanism by which stromal tenascin-C promotes metastasis in human cancer, may have potential for diagnosis and therapy.

© 2019 The Authors. Published by Elsevier B.V. This is an open access article under the CC BY license (<http://creativecommons.org/licenses/by/4.0/>).

Introduction

Despite earlier diagnosis and improved treatment a high number of cancer patients die due to cancer-related complications, tumor recurrence and, most frequently, metastasis [1]. To improve patient survival a better knowledge of the mechanisms of metastasis is required. During metastasis, tumor cells disseminate from the primary tumor and invade blood or lymphatic vessels where they can be found as circulating tumor cells appearing in a variety of forms as ranging from single cells or small cell clusters up to multicellular tumor cell aggregates or tumor emboli. Tumor emboli can be classified as blood vessel invasions (BVI) or lymphatic vessel invasions (LVI), all together covered by the term lympho-vascular invasions [2–4]. The presence of vascular invasions in the primary tumor and the distant organ correlates with poorer cancer patient survival, increased metastasis, vessel occlusion and organ failure [5,6]. Therefore, targeting vascular invasions may offer novel treatment opportunities. To date, very little is known about the cellular composition of vascular invasions, nor whether there are differences in BVI in comparison to LVI.

The tumor microenvironment (TME) comprises tumor and stromal cells, soluble factors and extracellular matrix (ECM) [7]. An important ECM molecule that enhances metastasis is tenascin-C (TNC) [8,9]. As reviewed [10], TNC plays multiple roles in cancer. Recently, this has been comprehensively demonstrated in the first stochastic neuroendocrine tumor (PNET) model with abundant and no TNC, where TNC was found to enhance survival, proliferation, invasion, angiogenesis and lung metastasis [11].

By using breast cancer xenograft models, TNC was identified as a gene that mediates metastasis to the lung relevant during early steps of lung metastasis colonization; however, its relevance in immune competent breast cancer models with spontaneous tumor onset has not been confirmed [8,9,12–14]. Moreover no model existed to address the relative contribution of host and tumor cell-derived TNC on breast cancer progression in an immune competent setting.

We have chosen the MMTV-NeuNT transgenic mouse model of metastatic cancer, ectopically expressing an active ErbB2 molecule from rat under control of the MMTV enhancer, that spontaneously develops primary mammary tumors and pulmonary BVI as precursors of parenchymal metastasis [15–17]. By using our novel cancer progression

models, we observed that TNC increases lung metastasis by impacting BVI at multiple levels. In patients, we observed BVI in human cancers to be similarly organized to those in the mouse models, and also express TNC. Our results may offer novel opportunities for cancer diagnosis and therapy.

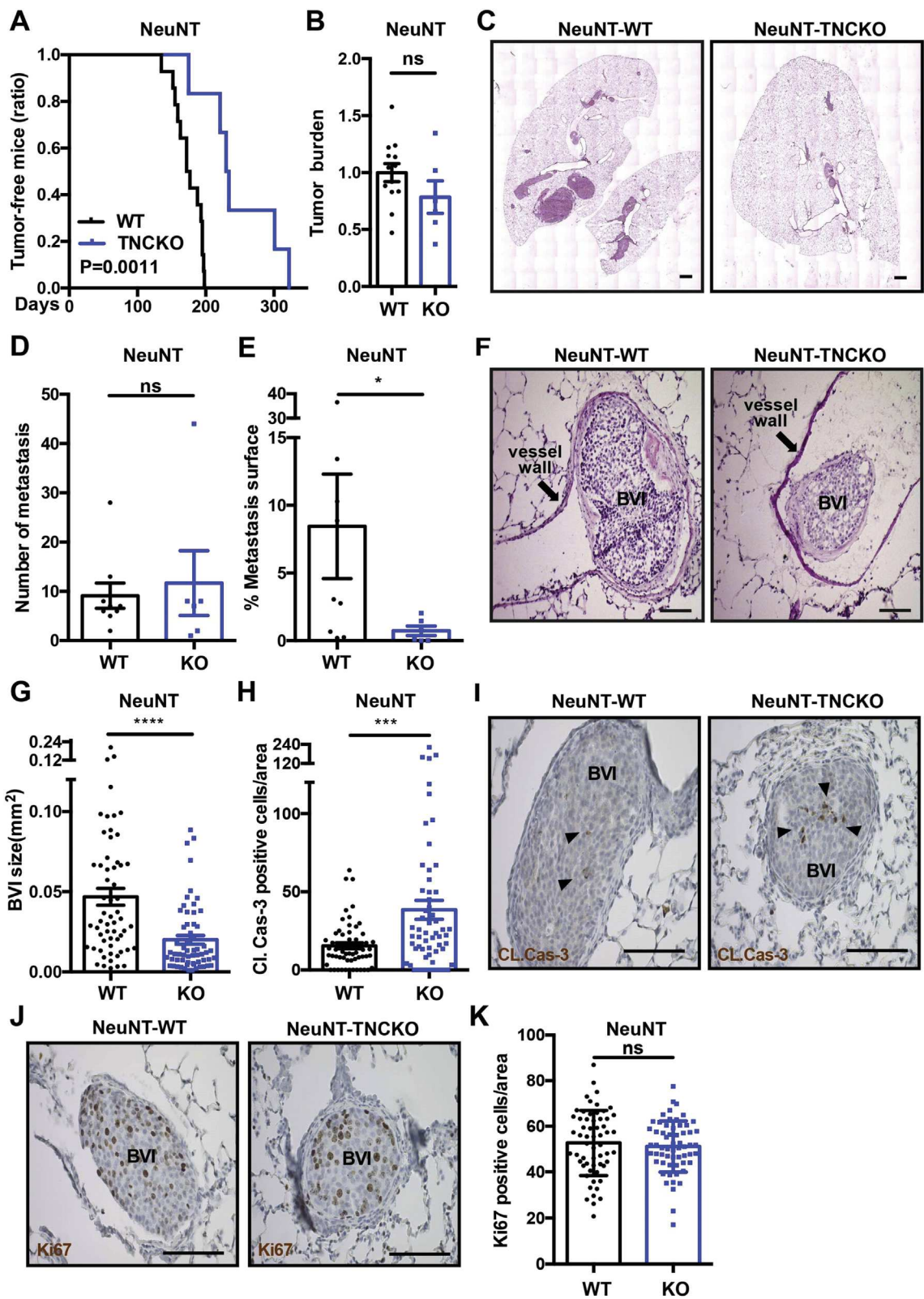
Results

Tenascin-C accelerates tumor onset

We generated compound MMTV-NeuNT tumor mice deficient in *Tnc* (NeuNT-TNCKO) and compared tumorigenesis in these mice with mice expressing normal (wildtype, WT) levels of TNC (NeuNT-WT). By immunofluorescence staining of primary tumors we found TNC expressed in tumor matrix tracks (Fig. S1A) as previously shown in other cancers [18]. No TNC protein was found in TNCKO tumors (Fig. S1A, B). We compared tumor onset and observed that tumor latency was largely delayed in NeuNT-TNCKO mice (Fig. 1A). As previously described in this model all mice developed multiple tumors [16], the number of which was not affected by TNC. Mice were sacrificed 3 months after first tumor palpation and no significant difference in tumor burden, proliferation nor apoptosis between genotypes was noted (Fig. 1B, data not shown).

Tenascin-C enhances lung metastasis

We assessed lung metastasis by a stereological analysis [19] of the left and biggest lung lobe and observed no difference in the number of metastasis between NeuNT-TNCKO and NeuNT-WT mice (Fig. 1C, D). Yet, we found a larger lung surface covered by tumor cells in NeuNT-WT compared to NeuNT-TNCKO mice (Fig. 1C, E). As pulmonary BVI have been observed in Neu models [15] and were described as precursors of lung metastasis [17], we used immunohistochemistry to assess whether BVI are also common in the NeuNT model [16]. Indeed, we observed BVI in the lungs of these mice and, also in the primary tumors which had not been documented beforehand in any MMTV-Neu model (Fig. 1C, F, Fig. S1C). Surface measurement revealed that BVI are bigger in the lungs from NeuNT-WT mice than in those from NeuNT-TNCKO mice (Fig. 1F, G). As reduced proliferation and/or



increased apoptosis could account for a difference in BVI size, we performed staining for cleaved caspase-3 (Cl. Cas-3) and Ki67, respectively. We noticed that Cl. Cas-3+ cells are less abundant in BVI from NeuNT-WT than NeuNT-TNCKO mice, indicating that TNC promotes tumor cell survival in the BVI (Fig. 1H, I). It is remarkable that some tumor cells within the BVI proliferate, yet there is no difference in the number of Ki67+ cells between tumor mice expressing or lacking TNC (Fig. 1J, K). Similar to tumor cells in the BVI, also in the parenchymal metastasis TNC did not impact cell proliferation, but enhanced tumor cell survival (Fig. S1D-G). In summary, our data indicate that in the MMTV-NeuNT model TNC promotes cancer cell survival in pulmonary BVI as well as in parenchymal metastasis which could explain the observed larger metastatic surface in lungs from WT tumor mice.

Host-derived tenascin-C promotes growth of BVI and overall metastasis

Previous reports using a xenograft model suggested that, host-derived TNC has a minor impact on lung metastasis colonization [8,9,14]. As tumor immunity largely impacts tumor growth and metastasis, which is missing in the xenograft models, we addressed how host- versus tumor cell-derived TNC impacts cancer progression in an immune competent setting. Therefore, we established a syngeneic orthotopic grafting model by using NT193 cells that we previously had established from a MMTV-NeuNT tumor [20].

We engineered NT193 cells to downregulate *Tnc* by shRNA technology. To mitigate possible off target effects we used two different shRNA sequences (sh1TNC and sh2TNC) and, grafted the tumor cells into the mammary gland of naïve WT and TNCKO FVB mice, respectively. We confirmed *Tnc* knockdown in the cultured cells by immunoblotting (Fig. S2E). Upon immunofluorescence analysis of the arising tumors in the mammary gland we noticed that TNC levels are highest in a WT host upon engraftment of shC cells (transfected with a control shRNA sequence (shC, WT/shC or TNC-high

tumors) and almost absent in KO/shTNC (or TNC-low) tumors, suggesting that the *Tnc* knockdown is stable in vivo (Fig. S2F, G). We further observed that mice with NT193 tumors develop spontaneously metastasis in the lung parenchyma as well as BVI in blood vessels of the lung. As for the MMTV-NeuNT model, with the changing levels of TNC expression we found no difference either in tumor burden (Fig. S2H) nor in lung metastasis incidence (Fig. 2A). Yet, we noticed that the lung metastasis surface is larger in TNC-high (WT/shC) than TNC-low (KO/shC) conditions. Moreover, irrespective of the cell genotype, there is a tendency towards more metastasis in WT than in TNCKO mice suggesting an involvement of host-derived TNC in promoting metastasis (Fig. 2B). Next, we determined the surface of the BVI and found that BVI derived from TNC-high (WT/shC) tumor mice are significantly bigger than from TNC-low (KO/shC) tumor mice (Fig. 2C). To address whether a difference in proliferation or survival accounts for the observed result we again stained for Ki67 and Cl. casp-3, respectively. As for the genetic MMTV-NeuNT model, in the BVI some tumor cells proliferate, yet independent of TNC (Fig. 2D, E). In contrast to proliferation, we saw that apoptosis is higher in BVI from KO tumor mice and, that in TNC-high (WT/shC) conditions apoptosis is the least (Fig. 2F, G). Altogether, these results demonstrate an important role of host-derived TNC in increasing BVI tumor cell survival and metastasis and, distinct functions of stromal and tumor cell derived TNC in metastasis.

Tenascin-C surrounds epithelial tumor cell aggregates in BVI

To understand the composition of pulmonary BVI, we analyzed tumor and lung tissue of NeuNT-WT mice. BVI were found in blood vessels of the primary tumor (Fig. S1C), and the lung, sometimes surrounded by a thick ECM layer (Fig. 3A). BVI also could completely occlude the vessel lumen and had an eventual necrotic center (Fig. 3A, S3A-C, Fig. S1C).

Fig. 1. Increased lung metastasis in the presence of TNC in MMTV-NeuNT mice **(A)** Ratio of tumor-free mice is shown for MMTV-NeuNT tumor mice with two (NeuNT-WT, $N = 13$ mice) and no (NeuNT-TNCKO, $N = 6$) TNC alleles. The absence of TNC significantly delays tumor latency (NeuNT-WT versus NeuNT-TNCKO, $p = 0.0011$; Log-rank tests). **(B)** Tumor burden of NeuNT-TNCKO tumor mice ($N = 6$) was determined and normalized to the mean tumor weight of the control group (NeuNT-WT, $N = 13$). **(C)** Representative HE images of lung metastasis from MMTV-NeuNT mice (NeuNT-WT and NeuNT-TNCKO) that had been sacrificed 3 months after tumor detection. Scale bar: 1000 μ m. **(D, E)** Number of lung metastases **(D)** and of the cumulated metastatic burden (metastatic area normalized to total lung area) **(E)** in lungs of NeuNT-WT ($N = 9$) and NeuNT-TNCKO ($N = 6$) mice. **(F, G)** HE stained lung tissue was used for BVI size determination (NeuNT-WT, $N = 6$ mice, $n = 59$ BVI; NeuNT-TNCKO, $N = 6$ mice, $n = 60$ BVI). Scale bar: 100 μ m. **(H–K)** measurement of apoptosis and proliferation by IHC analysis for cleaved caspase-3 (Cl. Cas-3) **(H, I)** and Ki67 **(J, K)** in BVI (NeuNT-WT, $N = 6$ mice, $n = 59$ BVI; NeuNT-TNCKO, $N = 6$ mice, $n = 60$ BVI). Dots represent number of apoptotic **(H)** and proliferative cells **(K)** in BVI per area (0.1 mm^2), respectively. Arrowhead denotes Cl. Cas-3 positive apoptotic cell **(I)**. Scale bar, 100 μ m. Mean \pm SEM. **(B, D, E, G, H and K)** unpaired Student t or Mann-Whitney test.

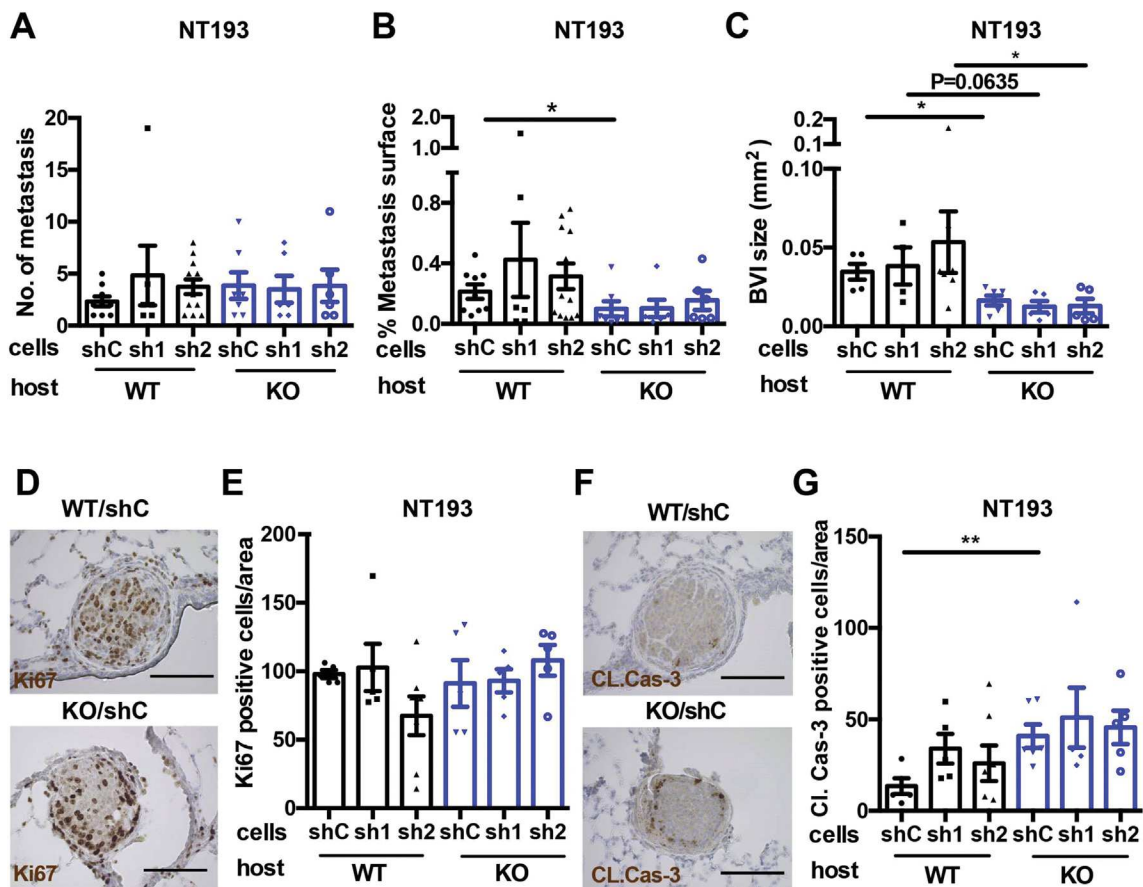


Fig. 2. Host-derived TNC promotes lung metastasis in NT193 grafted tumor mice (A-C) Quantification of the number of lung metastases (N , at least 5) (A), cumulated metastatic burden (metastatic area normalized to total lung area) (N , at least 5) (B) and size of BVI (C) in lungs of WT and TNCKO FVB hosts after engraftment of NT193 sh control (shC), sh1TNC and sh2TNC cells (WT/shC ($N = 5$ mice); WT/sh1TNC ($N = 4$ mice); WT/sh2TNC ($N = 7$ mice); KO/shC ($N = 6$ mice); KO/sh1TNC ($N = 5$ mice); KO/sh2TNC ($N = 5$ mice)). Note a bigger metastatic surface and bigger BVI in a WT host. (D-G) IHC analysis for Ki-67 (D) and cleaved caspase-3 (Cl. Cas-3) (F) in BVI of lungs from NT193 engrafted mice. Dots represent proliferative (E) and apoptotic cells in BVI (G) per 0.1 mm^2 , respectively. Note more apoptotic cells in tumors of the KO host. Scale bar, $100 \mu\text{m}$. Mean \pm SEM, unpaired Student t or Mann-Whitney test. Statistical analysis was performed between all groups. Only statistically significant ($p < 0.05$) differences are marked.

The core of the BVI is composed of cancer cells (ErbB2+) with epithelial phenotype (CK8/18+) (Fig. 3B - D). We addressed by staining whether BVI express TNC and saw indeed abundant TNC at the periphery, yet no TNC within the tumor cell cluster that homogenously expresses ErbB2 (Fig. 3B - D). We also noticed the absence of TNC when tumor cells are extravasating from the BVI into the lung parenchyma (Fig. 3B).

Since we observed that host-derived TNC promotes BVI growth we wondered which stromal cells could be a source of TNC. Considering that Fsp1+ fibroblasts/myeloid cells were described in another breast cancer model as a source of TNC (and other molecules such as VEGFA) and, have been shown to promote tumor progression [21], we evaluated their presence in BVI. Indeed, we observed Fsp1+ cells in BVI and, an overlap of the signals for Fsp1

and TNC, suggesting that Fsp1+ cells are a likely source of TNC in BVI (Fig. 3D). A similar result was obtained in the NT193 grafting model, where the Fsp1 signal also co-localized with TNC (Fig. 3E). Of note, Fsp1+ cells are also present in BVI from NeuNT mice deficient in TNC (Fig. S3E).

Together, Fsp1-expressing cells are likely candidates to express TNC in BVI of both models. This result also demonstrates a strong similarity between the genetic and grafting model.

Tenascin-C increases abundance of platelets and integrity of the surrounding endothelial monolayer of BVI

We characterized the cellular and ECM composition of pulmonary BVI of NeuNT-WT mice, by multi-channel immunofluorescence imaging of epithelial/

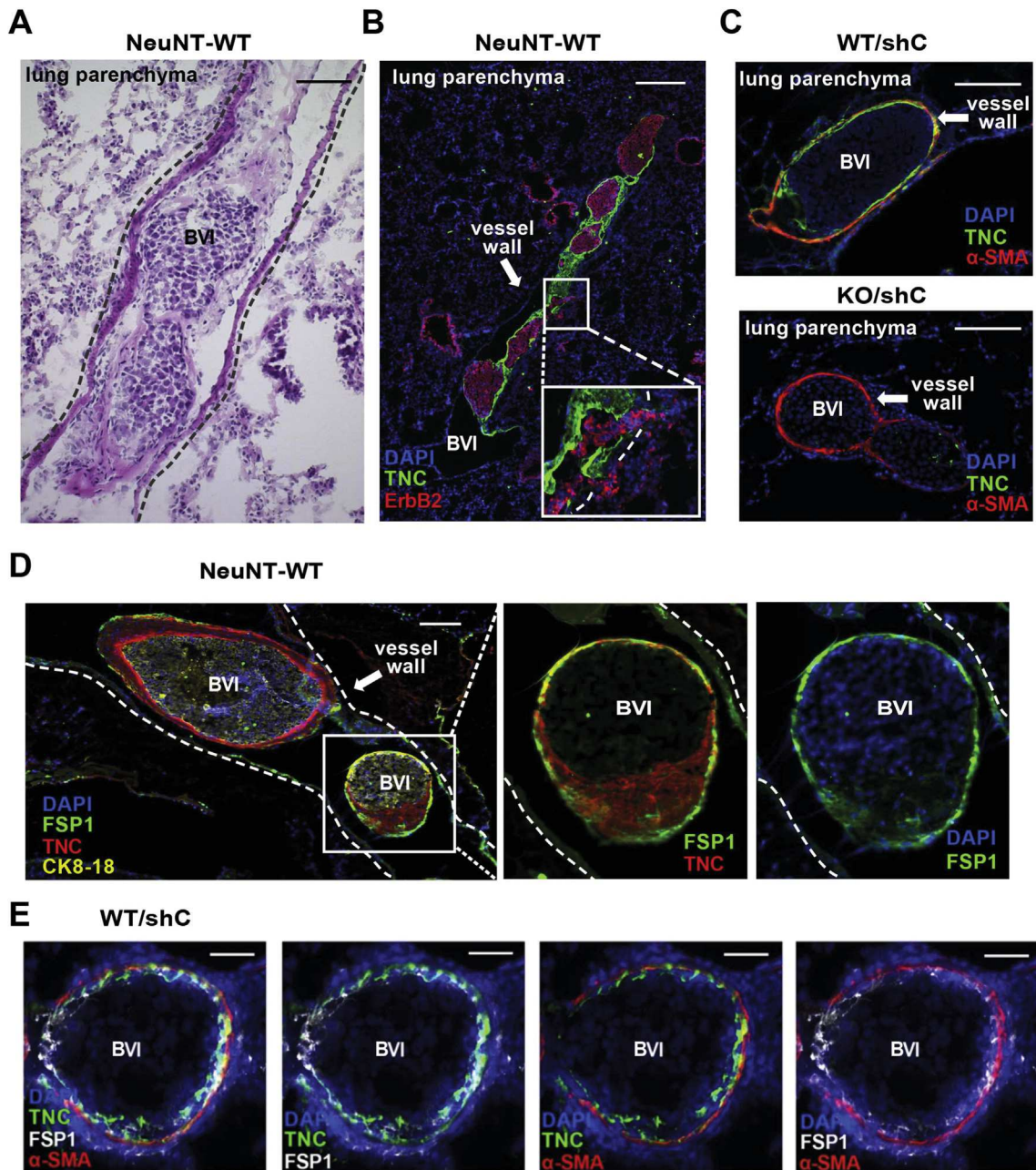
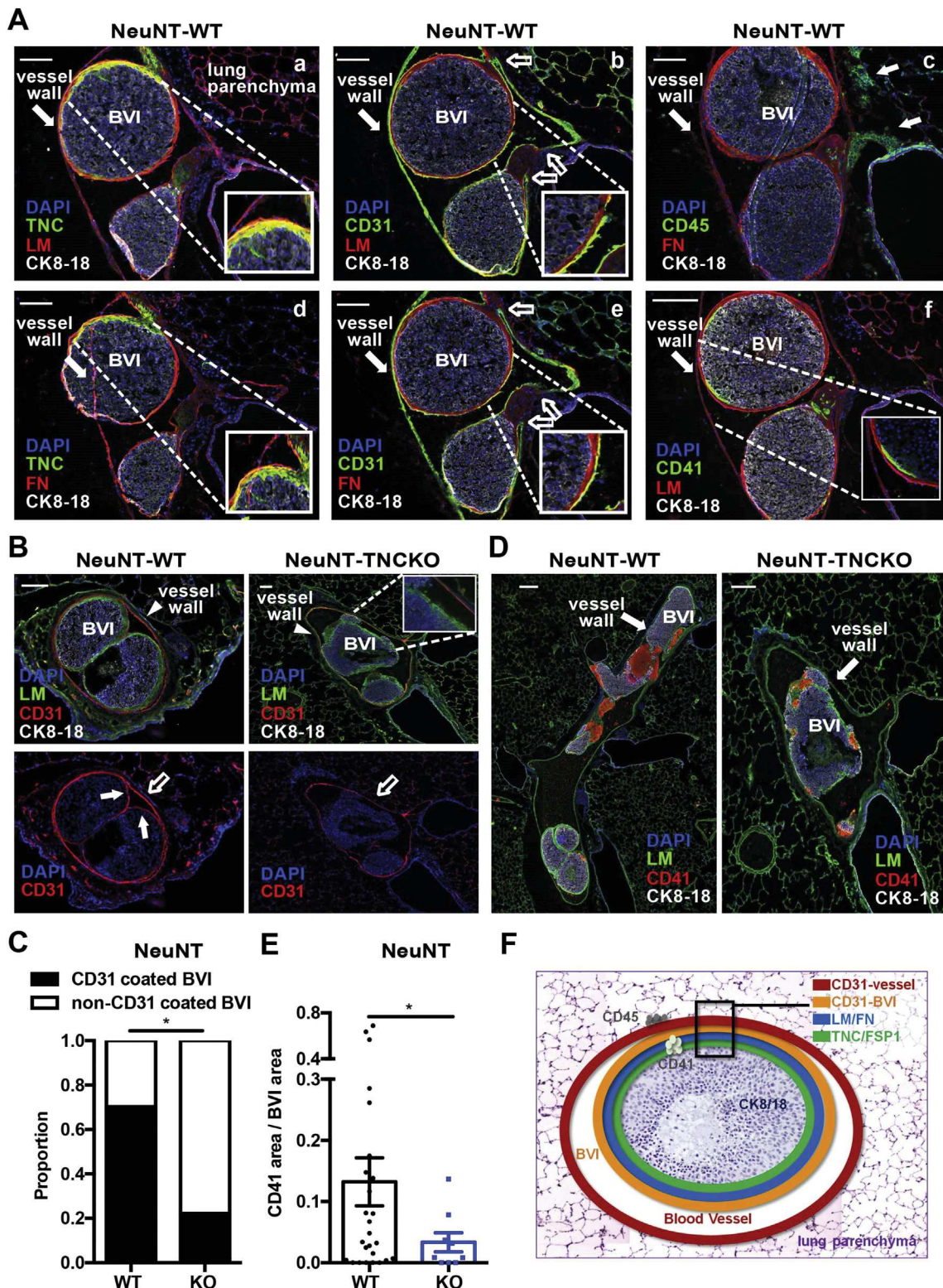


Fig. 3. TNC and Fsp1 expression in BVI **(A, B)** Representative images of BVI in NeuNT-WT lungs upon HE and IF staining for the indicated molecules. **(B)** Note that TNC (green) is expressed around tumor cells (red, ErbB2). Cell nuclei stained with DAPI. Scale bar, 100 μ m (A), 500 μ m (B). **(C)** Representative IF images for TNC (green) in BVI from WT/shC and KO/shC tumor mice. α SMA staining (red) marks the smooth muscle/pericyte layer underneath blood vessels. Note, that TNC is expressed in BVI of shC cells engrafted in a WT host, yet not in a TNCKO host indicating that TNC in BVI is of host origin. Scale bar, 100 μ m. **(D, E)** Representative IF images for Fsp1+ cells and TNC in BVI from NeuNT-WT **(D)** and WT/shC lung tissue **(E)**. Note overlap of TNC with Fsp1, yet not α SMA, suggesting Fsp1+ cells as a likely source of TNC. Scale bar: 100 μ m (D), 50 μ m (E). White square represents area of higher magnification.

tumor cells (CK8/18, ErbB2), endothelial cells (CD31), platelets (CD41, RAM1), leukocytes (CD45), fibronectin (FN) and laminin (LM) in sequential lung tissue sections. We observed that

in all BVI, cancer cells form a tightly packed tumor cell nest that is enveloped by a layer of Fsp1+ cells (Fig. 3D). Furthermore, a monolayer of endothelial cells, characterized by flat endothelial cell nuclei, is



present at the luminal side of the BVI in the genetic NeuNT-WT (Fig. 4A, S4A, B) and the syngeneic NT193 TNC-high (WT/shC) model (Fig. S4C).

Moreover, we found distinct layers of LM and FN between the endothelial layer and Fsp1+ cells. Neither FN, LM, TNC nor endothelial cells or

fibroblasts were found within the core of the tumor cell cluster (Fig. 4A). As plasticity is frequent in cancer and could give rise to cells with mixed tumor and stromal properties [22] we considered that the Fsp1+ cells may be of tumor cell origin. Yet, we did not see any signal overlap of Fsp1+ with CK8/18, nor ErbB2.

Furthermore, leukocytes (CD45+) were abundant, yet they were not associated with the BVI but were found outside the BVI at the basal side of the vessel wall facing the lung parenchyma (Fig. 4A, Fig. S4A). Most interestingly, the layered organization of BVI of the MMTV-NeuNT model is recapitulated in the NT193 grafting model. Again, BVI express a layer of TNC and display a core of proliferating cancer cells and, a layer of fibroblasts and endothelial cells that are separated by FN and LM (Fig. 3C, E, Fig. S4C).

We investigated the presence of platelets as they are frequently present in circulating tumor cell aggregates and can cause thromboembolism and vessel occlusion [23]. By staining for CD41 or RAM1 (recognizing Gp1b [24]), we found platelets located inside the BVI surrounded by the LM and endothelial layers. This observation suggests a role of platelets early in the evolution of the BVI (Fig. 4D, S4D-F). We also noticed an overlap of signals for CD41 and TNC which points at platelets as another potential source of TNC as was previously described in another model [25] (Fig. S4F).

Altogether, our detailed analysis revealed the organization of BVI as tightly packed cell clusters (positive for CK8/18 and ErbB2) where some tumor cells are proliferating. Moreover, the nest of tumor cells is enveloped by distinct layers of stromal cells. Whereas Fsp1+ cells, a likely source of TNC, are located adjacent around the tumor cell nest, a layer of endothelial cells is present at the luminal rim of the BVI. Interestingly, the endothelial cells are not in direct contact with TNC but are separated from TNC by other ECM, in particular LM and FN which is consistent with this ECM layer potentially protecting endothelial cells from TNC-induced apoptosis (Fig. 4F, [26,27]).

Since BVI are also present in lung vessels of NeuNT-TNCKO mice, we asked whether TNC had

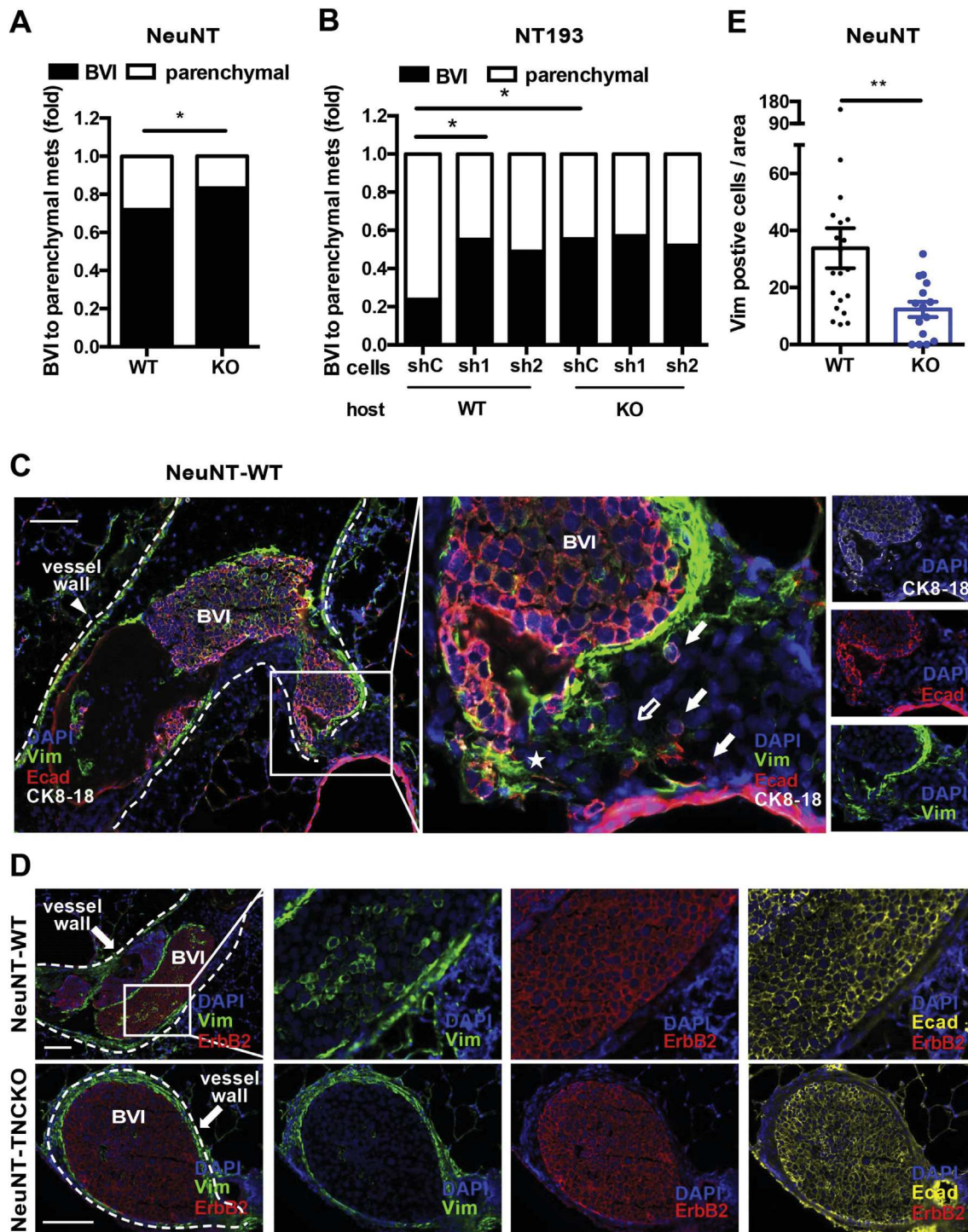
any impact on their organization. Staining for LM, FN and Fsp1 did not reveal gross differences between genotypes neither in the transgenic or syngeneic model, suggesting that TNC may not be required for BVI to form (Fig. 3C, 4B, D). Besides that, although we observed an endothelial monolayer around BVI in both genotypes (Fig. 4B, S4A - C) we noticed more BVI with an intact endothelial layer in NeuNT-WT as compared to NeuNT-TNCKO mice (Fig. 4B, C). Interestingly, we also observed an eventual cellular continuum between the endothelial layers of the BVI and the lung vessel wall (Fig. 4A). By quantification of CD41 we observed less platelets in pulmonary BVI from NeuNT-TNCKO than NeuNT-WT mice reminiscent of a role of TNC in promoting attachment of platelets, as previously described in a thrombosis model [24] (Fig. 4D-E).

Overall our data show that, whereas TNC is not required for the formation of pulmonary BVI, stromal TNC has multiple effects on the organization of BVI, promoting endothelial coat integrity, platelet recruitment and tumor cell survival.

Tenascin-C promotes extravasation of tumor cells from pulmonary BVI into the lung parenchyma

We investigated whether BVI are also precursors of parenchymal metastasis in the MMTV-NeuNT model as described in another MMTV-Neu model [17]. Indeed, we observed that the relative abundance of parenchymal metastasis increases over time on account of a reduced number of pulmonary BVI in the MMTV-NeuNT model (Fig. S5A). Notably, when we compared the ratio of BVI to parenchymal metastasis we found more parenchymal metastasis than BVI in lungs of NeuNT-WT compared to NeuNT-TNCKO mice (Fig. 5A). Similarly, in the NT193 grafting model we saw more parenchymal metastasis in TNC-high than TNC-low conditions (Fig. 5B). Interestingly, whereas at the site of extravasation TNC is absent, in the parenchymal metastasis TNC is expressed at the border and in matrix tracks (Fig. 3B, S5B-E).

Fig. 4. Cellular organization of BVI **(A)** Representative images of immunostainings for ECM molecules and cellular markers in BVI of lung tissue from NeuNT-WT **(A, B, D)** and NeuNT-TNCKO mice **(B, D)**. The empty arrows point at narrowing of endothelial layers reminiscent of fusion of the endothelial layers derived from the lung vasculature and the BVI. White squares in each panel delineate the field shown at higher magnification. In panel **A(c)** arrows point at CD45+ cells. In panel **A(d)** the vessel staining for FN on the left is an artefact due to disruption of the tissue. Scale bar, 100 μ m. **(B)** Representative images of endothelial cells. Arrows point at the endothelial monolayer of the BVI. The empty arrow points at the blood vessel wall. Scale bar, 100 μ m. **(C)** Proportion of BVI with and without a CD31 layer for each genotype (NeuNT-WT, $N = 6$ mice, $n = 27$ BVI; NeuNT-TNCKO, $N = 4$ mice, $n = 8$ BVI). Mean \pm SEM, Fisher's exact test. **(D)** Representative images of platelets (CD41+) together with LM. Scale bar, 200 μ m. **(E)** Platelet abundance (CD41+ area normalized to area of BVI), NeuNT-WT, $N = 6$ mice, $n = 26$ BVI; NeuNT-TNCKO, $N = 4$ mice, $n = 9$ BVI. Mean \pm SEM, Mann-Whitney test. **(F)** Scheme depicting the composition of BVI. Note, that cancer cells (CK8/18+) are tightly packed inside the BVI, surrounded by Fsp1+ cells, a LM/FN layer and a luminal oriented monolayer of endothelial cells (CD31+). CD45+ leukocytes are not in direct vicinity to the BVI but are present at the basal side of the vessel wall facing the parenchyma. Also, endothelial cells are not in direct contact with TNC.



Altogether, these results suggest that TNC plays a role in progression of pulmonary BVI into parenchymal metastasis. TNC also promotes outgrowth of the parenchymal metastasis by promoting survival (Fig. S1C, D), similar as seen in a xenograft tail vein injection model [9].

Tenascin-C increases cellular plasticity in pulmonary BVI and parenchymal metastasis

As pulmonary BVI can act as precursor of parenchymal metastasis, the question arises how tumor cells enter the lung parenchyma. Epithelial-to-

mesenchymal-transition (EMT) could be a possible mechanism in the MMTV-NeuNT model as was shown to occur in the MMTV-Neu model [17]. Indeed, in some sections we observed cancer cells leaving pulmonary BVI and invading the parenchymal lung tissue (Fig. 3B, 4A, 5C). We investigated the expression of the mesenchymal transition marker vimentin and the epithelial markers CK8/18 and E-cadherin, respectively, in pulmonary BVI. While all tumor cells inside the BVI express CK8/18, E-cadherin and ErbB2, some cells also co-express vimentin (Fig. 5C, E, S5F, G). By quantification we noticed more vimentin-expressing cells inside BVI from NeuNT-WT than NeuNT-TNCKO mice (Fig. 5D, E). Similarly, we also observed vimentin+ cells inside the parenchymal metastasis of NeuNT-WT tissue indicating a mixed epithelial/mesenchymal phenotype (Fig. S5C, D). Other cells at the invading front only express vimentin but not E-cadherin, nor CK8/18 or ErbB2 (Fig. 5C). A vimentin+ and Ecad+ phenotype is reminiscent of cells undergoing a partial EMT, presumably allowing cells to invade as cell cohorts as has previously reported in another model (MMTV-PyMT, [28] (Fig. 3B, 5C). In addition, a mixed tumor cell phenotype in the parenchymal tissue suggests MET that may support tumor cell outgrowth [29].

Altogether, our results suggest that TNC promotes cellular plasticity in pulmonary BVI thereby affecting tumor cell extravasation and outgrowth of parenchymal metastasis.

Tenascin-C induces EMT in cultured tumor cells, promoting cell migration and survival through TGF- β signaling

TNC has been shown to induce an EMT-like phenotype in conjunction with TGF- β in cellular models [30,31]. Therefore, we asked whether TNC induces EMT in NT193 cells. We added purified TNC to NT193 cells grown as monolayer or as spheroid cultures and indeed observed EMT as indicated by loss of E-cadherin and gain of vimentin expression as demonstrated by immunofluorescence imaging,

quantitative reverse transcription PCR (qPCR) and immunoblotting (Fig. 6A - C). Moreover, we noticed increased mRNA levels of several other EMT markers, such as *Snail*, *Slug*, *Zeb1*, *Pai-1*, *Mmp9* and *Tnc* itself upon treatment with TNC. On the contrary, mRNA levels of *E-cadherin* were found reduced (Fig. 6B).

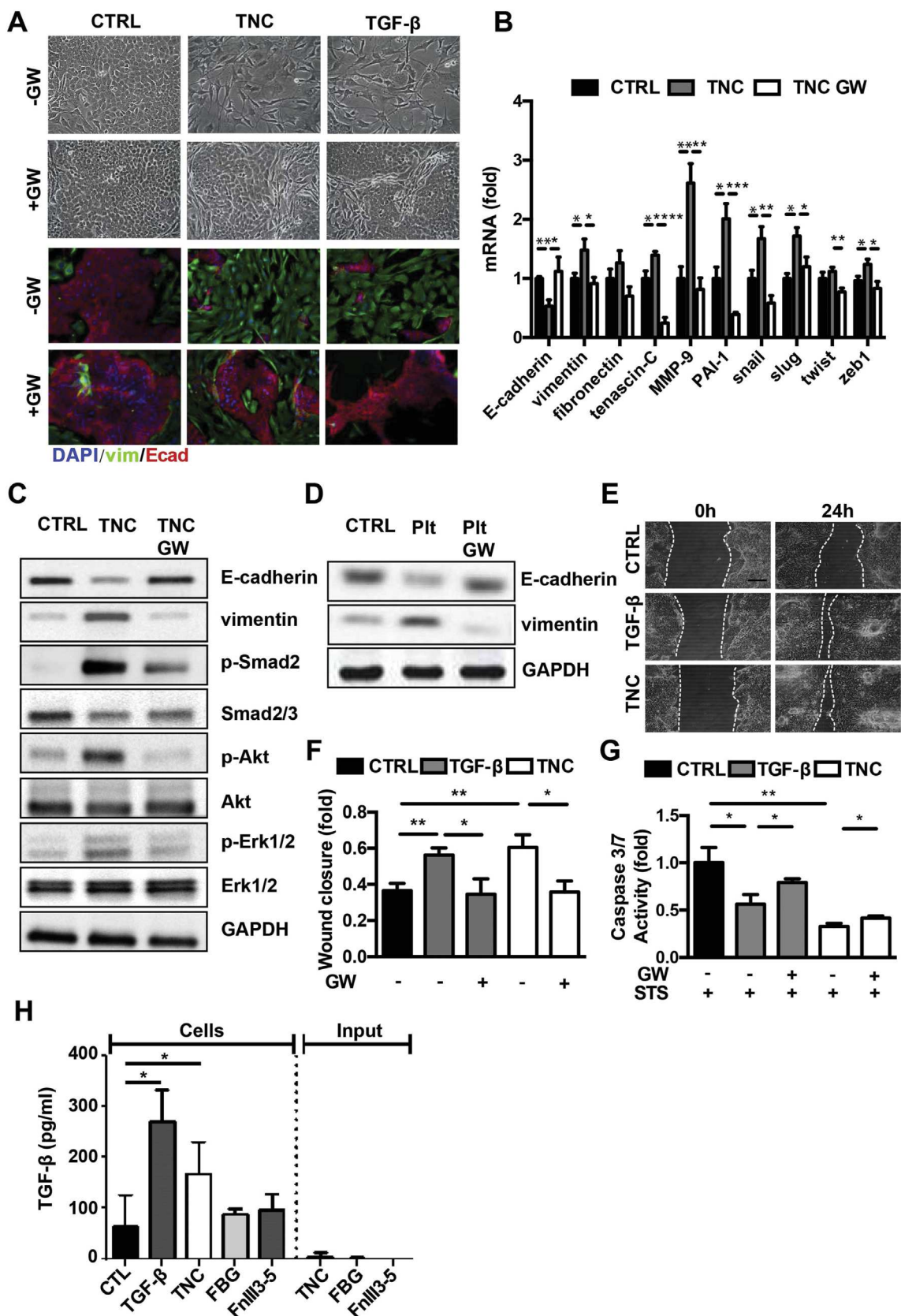
Next, we compared cell responses to TNC with that to TGF- β and, found that similar to TNC, TGF- β induces an EMT in NT193 cells as evidenced by loss of E-cadherin and gain of vimentin expression (Fig. 6A-C, Fig. S6A, B). Notably, the TGF- β signaling inhibitor GW788388 (GW) reverts the TNC-induced mesenchymal phenotype into an epithelial one, as expression of E-cadherin is increased and that of vimentin is decreased (Fig. 6A - C, Fig. S6A, B). These results demonstrate that TNC induces EMT in NT193 cells through TGF- β signaling.

We determined downstream signaling upon TNC treatment by immunoblotting and observed that in addition to phosphorylated Smad (p-Smad2) also levels of p-Akt and p-Erk1/2 increase, suggesting an induction of both canonical and non-canonical TGF- β signaling by TNC. Moreover, all three of the TNC-induced signaling pathways are TGF- β dependent as they were blocked with GW (Fig. 6C, S6B).

As we observed platelets residing inside the pulmonary BVI and platelets are known to induce an EMT [25], we considered a potential role of platelets in EMT in our models. Indeed, in cultured cells, we found that platelets induce an EMT, since E-cadherin levels are decreased and vimentin expression is increased. Similar to TNC, also the platelet-induced EMT was blocked with GW, suggesting that a platelet-induced EMT is TGF- β signaling-dependent in NT193 cells (Fig. 6D).

Next, we asked what consequences a TNC-induced TGF- β -dependent EMT has for the cells. We used a cellular wound closure assay and observed increased migration of cells upon addition of TNC, which was comparable to the treatment with TGF- β (Fig. 6E, F). Again, this effect was blocked with GW indicating that TNC-induced EMT increases NT193 cell motility through TGF- β signaling.

Fig. 5. TNC promotes extravasation and plasticity of cancer cells in BVI (A, B) Proportion of BVI to parenchymal metastasis in MMTV-NeuNT mice (A) (NeuNT-WT, $N = 6$ mice; NeuNT-TNCKO, $N = 6$ mice), $p < 0.02$, Fisher's exact test; and in NT193 grafted mice (B) (WT/shC shC, $N = 5$; WT/sh1TNC, $N = 4$; WT/sh2TNC, $N = 7$; KO/shC, $N = 6$; KO/sh1TNC, $N = 5$; KO/sh2TNC, $N = 5$. Mean \pm SEM). Chi-square test. Note, that combined TNC expression by the host and the tumor cells increases parenchymal metastasis. (C, D) Representative IF images of vimentin (green), E-cadherin (red) and CK8/18 (white) expression in BVI from NeuNT-WT mice. White squares delineate areas of higher magnification. Note, that tumor cells (CK8/18+) are invading the parenchymal lung tissue. Arrow points at single invading tumor cell with epithelial characteristics (CK8/18+ and E-cadherin+). Empty arrow points at invading vimentin+ and E-cadherin- cell. Star points at an event at the invading front. Scale bar, 100 μ m. (E) Representative IF images of cells expressing vimentin (green), ErbB2 (red) and E-cadherin (yellow) in BVI from NeuNT-WT and NeuNT-TNCKO mice. Scale bar, 100 μ m. (F) Quantification of tumor cells expressing both vimentin and ErbB2 normalized per BVI area (0.1 mm^2). MMTV-NeuNT (NeuNT-WT, $N = 6$ mice, $n = 20$ BVI; NeuNT-TNCKO, $N = 4$ mice, $n = 15$ BVI). Mean \pm SEM, Mann-Whitney test. Statistical analysis was performed between all groups. Only statistically significant ($p < 0.05$) differences are marked.



Since EMT provides tumor cells with survival resistance against toxic reagents [32], we next determined staurosporine-induced apoptosis by a caspase-3/7 activity assay and observed that pre-treatment of NT193 cells with TNC for 24 h reduces apoptosis. The TNC effect was similar to that of TGF- β and was reverted by GW, suggesting that a TNC-induced EMT protects against apoptosis where TGF- β signaling is important (Fig. 6G, Fig. S6D).

Next we investigated how TNC activates the TGF- β signaling pathway. Since TNC was shown to bind TGF- β [33], we investigated by ELISA whether our TNC preparations potentially contained TGF- β . Yet no TGF- β was found (Fig. 6H). We further determined whether cells potentially secrete more TGF- β upon treatment with TNC. Therefore, we added TNC to TNC-devoid NT193 sh2TNC cells (Fig. S2A) and, compared TGF- β secretion to cells that have been treated with TGF- β . Indeed, cells express more TGF- β upon treatment with TNC similar to levels detected in cells that were treated with TGF- β itself. This was not the case for the recombinant TNC domain molecule TNC-FGB (fibrinogen globe) and, TNC-FnIII3–5 (fibronectin type III repeat 3–5) that was described to bind TGF- β [33], despite 10-fold higher molarity than TNC (Fig. 6H).

Investigating the kinetics of canonical (Smad) and non-canonical (Akt, Erk1/2) TGF- β signaling [34], revealed rapid signaling activation by TNC which paralleled that of TGF- β itself and may contribute to enhanced survival by TNC. Phosphorylated Smad2 peaked around 2 h and was increased at 24 h comparable to the kinetics of p-Akt and p-Erk1/2. Levels of E-cadherin and vimentin started to drop and rise, respectively, upon addition of TNC similar to the treatment with TGF- β (Fig. S6E, F).

In conclusion, our results have shown that in NT193 cells TNC activates canonical and non-canonical TGF- β signaling with a similar kinetic as TGF- β itself, leading to increased abundance of TGF- β in the cell supernatant. How TNC increases TGF- β levels and induces TGF- β signaling remains

to be determined. Importantly, our study revealed an instrumental role of TNC in inducing EMT in our cellular system and, in the pulmonary BVI.

As TGF- β signaling promoted metastasis in a MMTV-Neu model [17] induction of TGF- β signaling could explain cellular plasticity and progression of BVI into parenchymal metastasis, thus elevating total metastasis burden in MMTV-NeuNT mice. A similar mechanism as recently demonstrated for fibronectin fibrils to activate TGF- β signaling should be investigated for TNC in the future [35].

Tenascin-C is expressed in BVI from human carcinomas yet not in LVI

Vascular invasions in the primary tumor comprise an important prognostic tool and can occur in blood and lymphatic vessels [36,37]. To address whether BVI and LVI of human carcinomas express TNC, we investigated tissue from several human carcinomas with and without recorded presence of vessel invasions by sequential staining for TNC, CD31, podoplanin and platelet marker CD61 (Table S1, S3, S4). We observed BVI (tumor cell clusters inside CD31+ vessels) and LVI (tumor cell clusters inside D2–40+ vessels). In particular, we saw BVI in a total of 23 tumors comprising renal cell carcinoma (RCC), hepatocellular carcinoma (HCC) and pancreatic neuroendocrine tumors (PNET) and, LVI in a total of 47 cases comprising pancreatic adenocarcinomas (PDAC (7 cases)) and mammary carcinomas (MaCa (40 cases)) (Fig. 7A-C, S7, Fig. S8, Table S1). Although we do not have evidence for a simultaneous existence of BVI and LVI in the same tumor this possibility cannot be ruled out. As in the MMTV-NeuNT model, we noted that BVI are surrounded by a luminal endothelial monolayer and a TNC layer. When BVI were bigger, TNC and endothelial cells were also detected inside the BVI (Fig. 7A, C, S7A, B and C). By contrast, LVI were neither covered by an endothelial cell layer nor did they express TNC (Fig. S8A, B, Table S1). Interestingly, tumor cell aggregates were present in

Fig. 6. In cultured NT193 cells TNC induces EMT promoting cell migration and survival **(A)** Phase contrast micrographs and IF images of E-cadherin (red) and vimentin (green) stained NT193 cells treated with TGF- β R1 inhibitor (GW788388) prior to addition of TNC and TGF- β for 24 h, respectively. Nuclei stained by DAPI. Scale bar, 20 μ m. **(B)** Relative expression (fold change) of the indicated genes in NT193 cells upon treatment with GW788388 and TNC for 24 h ($n = 5$, five independent experiments) with normalization to GAPDH. **(C)** Detection of E-cadherin, vimentin, phosphorylated pathway markers (Smad2, Akt, and Erk1/2), respectively and expression of total markers (Smad2/3, Akt, Erk1/2) by immunoblotting with GAPDH as loading control (a representative of three independent experiments is shown). **(D)** Detection of E-cadherin and vimentin expression by immunoblotting of lysates from NT193 cells upon addition of platelets for 24 h ($n = 3$, three independent experiments). **(E, F)** Wound closure of NT193 cells, $n = 14$, five independent experiments with at least two replicates. Scale bar, 20 μ m. **(G)** Assessment of staurosporine (STS) - induced apoptosis by measuring caspase-3/7 activity in NT193 cells treated as indicated, $n = 9$, three independent experiments in triplicates. **(H)** Quantification of TGF- β released by NT193 cells upon treatment with TNC, TNC-FBG and TNC-FnIII3–5 by ELISA. Note that purified TNC and recombinant TNC domain molecules are free of TGF- β . **B, F, G, H**, Mean \pm SEM, unpaired Student *t*-test. Statistical analysis was performed between all groups. Only statistically significant ($p < 0.05$) differences are marked.

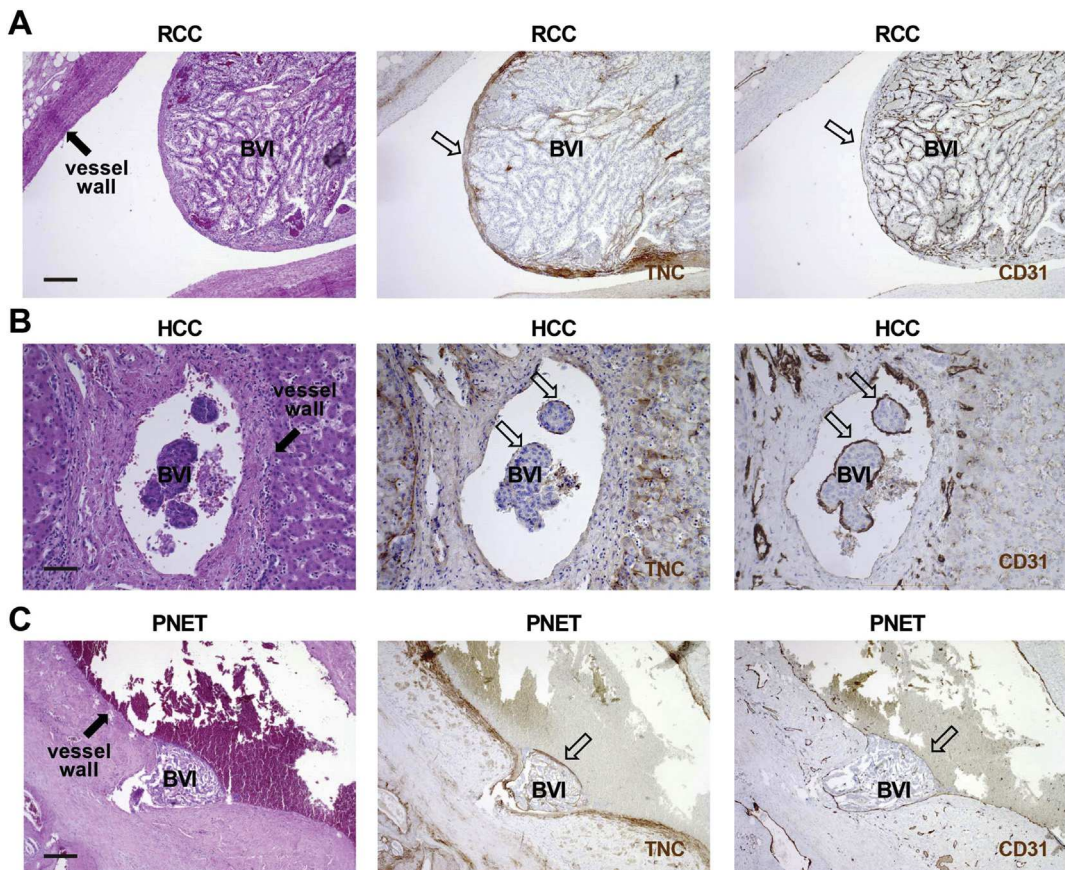


Fig. 7. BVI of human cancers are surrounded by endothelial cells and TNC. Consecutive tissue sections from human RCC, HCC and PNET were stained for H&E, CD31 and TNC. Representative images are shown. Note, that BVI are surrounded by a luminal endothelial monolayer and express TNC beneath the endothelial layer (open arrows). Note, that tumor cell clusters were found to protrude into the lumen of blood vessels (filled arrows), in particular the renal veins (RCC), the portal vein and branches of the portal vein (HCC) and the stem or branches of the superior mesenteric vein (PNET). In PNET a thrombotic reaction is observed at the luminal surface of the endothelium covering the BVI (arrow). Scale bar, 50 μ m.

lymphatic vessels (LVI) in MaCa independently of the subtype and appeared mostly as smaller floating cell clusters (Fig. S8B, Table S1). Upon an unbiased search in MaCa and the corresponding lung metastases we observed only LVI.

To our knowledge, these results demonstrate for the first time differences in cellular content and matrix composition between BVI and LVI. As in the murine metastatic models, in human cancers, BVI are enclosed by an endothelial monolayer and, express TNC.

Discussion

It is well established that the ECM plays an important role in tissue homeostasis enhancing pathologies including tumor malignancy and metastasis [7,38,39]. Moreover, the ECM molecule TNC which is abundantly expressed in cancer tissue enhances metastasis [9–11,40], yet by incompletely

understood mechanisms. To address the roles of TNC in metastasis, we have compared NeuNT (ErbB2)-driven lung metastasis in a genetic and a novel syngeneic orthotopic breast cancer model derived thereof with high TNC to that with no or low TNC, respectively. Of note ErbB2-driven models may not well recapitulate human breast cancer metastasis where LVI are frequent, but better phenocopy cancer progression of other tumors that develop BVI in blood vessels of the lung [16,17]. Our results reveal the cellular and molecular characteristics of BVI, offering future targeting opportunities. We further elucidate multiple novel functions of host-derived TNC in progression from pulmonary BVI into parenchymal metastasis that were unknown so far.

We report that pulmonary BVI are organized as clusters of proliferating epithelial tumor cells with tight junctions. Tumor cell cohesion may contribute to synoikis, a recently identified survival mechanism with relevance for targeting [2,41]. Tumor cell nests are enveloped by a luminal endothelial cell

monolayer and Fsp1+ cells, also a likely source of TNC in this model [21]. FN and LM are expressed between the two stromal cell layers (Fig. 4). Thus targeting tumor cell cohesions in BVI, endothelial cells or TNC expression itself (e.g. by Fsp1+ cells) could represent novel strategies. This could complement already identified inhibition of ErbB2 (MMTV-NeuNT) [20] and TGF- β signaling (MMTV-Neu NDL) [17] in reducing metastasis in these models.

It is interesting to note that in the MMTV-NeuNT model TNC induces a partial EMT where TGF β signaling may play a decisive role as we observed that TNC induces EMT in cultured tumor cells in a TGF β dependent manner. That only some tumor cells within the BVI as well as at the rim and site of extravasation, that are not necessarily in direct contact with TNC, have gained expression of the EMT marker vimentin, is intriguing to note and suggests a paracrine effect through which TNC impacts EMT in the BVI. In vitro, TNC-induced EMT enhances migration and survival of tumor cells which may also apply in the BVI. As TGF β signaling plays a role in promoting cancer stemness properties and survival in another model [42], future research has to clarify whether TNC also impacts cancer stemness through TGF β signaling in this model.

Due to lack of appropriate models, until now it was difficult to assign the cellular source of TNC with a function. Grafting human tumor cells with engineered TNC levels in the tail vein of immune compromised mice previously showed that tumor cell-derived TNC is relevant in early stages of lung colonization [9] but how host TNC affects spontaneous metastasis in immune competent conditions was unknown. Now, by using our novel orthotopic immune competent transplantation model with engineered TNC levels and spontaneous metastasis and, kinetics that generate a relevant TME, we showed for the first time that host-derived TNC plays a crucial role in metastasis, before tumor cell breaching. This could be relevant for future targeting as it may not suffice to kill tumor cells, but also to target stromal cells expressing TNC.

Several concepts for the formation of BVI and their endothelialization exist, as e.g. transdifferentiation of tumor cells into endothelial cells [36], budding of tumor cells from the primary tumor [43], recruitment of bone marrow-derived endothelial progenitor cells (EPC) [44] and, endothelialization [3], where endothelial cells and TNC are active participants. In a model proposed by Sugino et al., (2002) clusters of cancer cells in the primary tumor enter the circulation through an invasion-independent pathway, form local BVI and eventually migrate until they reach the site of metastasis [43]. Notably, the size of some of the BVI in this study suggests that, if circulating BVI existed in their model, they would be present in large vessels. Another model suggests that single cells or clusters of circulating tumor cells

(CTC), with or without an ECM coating and stromal cells, proliferate in the lung vasculature forming BVI at the metastatic site. Several observations support this model. Clusters of around 50 CTC were identified in tumor-bearing mice and, represent a higher metastatic potential than single CTC [45]. Moreover, a few hours after tail vein inoculation, cancer cells found in the lumen of lung vessels were already coated with ECM and platelets. These authors suggest that BVI formation occurs when cancer cells reach pulmonary arterioles but not capillaries [3]. Here, we show that stromal cells, probably platelets or Fsp1+ cells, are a source of TNC in pulmonary BVI. The prominent location of platelets deep inside the BVI (our observation) argues for an early role of platelets in BVI formation, apparently immediately after intravasation [25]. Finally, stromal cells on pulmonary BVI can migrate from the primary tumor as proposed in another model [46].

We consider the trans-differentiation of tumor cells into endothelial cells [28] as unlikely, since endothelial cells form a contiguous monolayer and are not found inside the BVI core. Also, budding from the tumor vasculature [27] may not occur as we do not see a monolayer of α SMA+ cells underneath the endothelial layer in the BVI. Upon release into the circulation by budding, only tumor cells at the periphery of the tumor cell cluster would get in contact with platelets and therefore platelets should be placed at the rim of the BVI. Yet, this is not the case, as we see platelets inside the BVI beneath the endothelial layer. On the contrary, we consider endothelialization, where endothelial cells from the vasculature wrap around circulating tumor cells [3], a likely scenario, as we observed a mostly contiguous monolayer of endothelial cells around the BVI, in the murine model and in human cancers, occurring in the primary tumor as well as in the metastatic lung.

As in the MMTV-NeuNT model also in MMTV-NeuYD mice endothelialization of BVI is frequent, yet only when VEGFA is coexpressed (MMTV-NeuYD/VEGFA) [47]. Also, VEGFA was involved in TNC-promoted lung metastasis in the 4 T1 grafting model establishing a crosstalk of TNC with endothelial cells in metastasis [21]. As VEGFA can bind to TNC, a potential combined impact on endothelial cells is likely [11]. We showed that BVI endothelial layer integrity, tumor cell survival and overall metastasis were correlated and, promoted by TNC. Thus, it is conceivable that impacting BVI endothelialization is an important mechanism how TNC promotes metastasis. Given its role in promoting the angiogenic switch and tumor angiogenesis [11,26,27,48] future research has to determine how TNC impacts BVI endothelial cell function and endothelialization. This may involve an autocrine mechanism as previously described, where TNC

induced Wnt signaling, VEGFA and a pericellular fibronectin layer in endothelial cells [11,27]. Also a paracrine mechanism may apply where TNC induces pro-angiogenic factors in tumor cells, fibroblasts or Fsp1+ cells as previously described in other tumors [21,26]. In this scenario, TNC-induced TGF β signaling could play a role in promoting survival of endothelial cells of the BVI.

Lympho-vascular invasions are frequently observed in routine analysis of many cancers, but incidence and relevance depends on the tumor type and subtype [49–52]. By using blood- and lymph-vessel markers recent analysis allowed to discriminate between LVI and BVI. Whereas LVI appeared smaller in size and in smaller vessels, many BVI were huge and present in bigger vessels (our results). Maybe physical properties such as local high shear stress in bigger vessels impact the size of BVI which has to be addressed in the future. So far there are only a dozen of retrospective studies that analyzed the impact of BVI versus LVI in cancer. BVI can be found inside and in the periphery of primary breast tumors, but apparently in breast cancer BVI are less frequent than LVI [5,49,53–55].

A few studies analyzed the relevance of tumor BVI versus LVI as a prognosis factor in breast cancer, but the results are controversial [5,53–55]. Disseminated lympho-vascular invasions are almost impossible to identify ante mortem [56]. Here our models could be highly relevant as both, the MMTV-NeuNT and the autochthonous grafting model that we had developed, present intra- and peritumoral BVI and, more importantly, disseminated BVI in the lung. Clinical trials of anti-angiogenic drugs failed to improve recurrence-free survival of breast cancer patients and lost approval by the FDA [57–59]. However, the presence of BVI/LVI was not considered as an inclusion factor. We believe that anti-angiogenic drugs can impair disseminated BVI, decrease metastasis and increase survival of breast cancer patients with BVI. Since BVI are frequent in many tumors and have an endothelial lining they may respond to anti-angiogenic drugs, which has to be addressed in the future. Indeed impacting the endothelial layer of BVI may reduce metastasis, as our results from the TNCKO mice suggest, where we observed an interrupted or missing endothelial BVI monolayer and, reduced overall metastasis in the absence of TNC. Anti-angiogenic drug treatment is already applied in patients with RCC, HCC and PNET [60] thus, likely affecting BVI. Hence, TNC expression and endothelial ensheathing of BVI in tumor biopsies could be used to stratify patients that may benefit from an anti-angiogenic drug treatment targeting the BVI endothelial coat. In contrast to BVI, we have found that LVI (here observed in MaCa and PDAC) do not exhibit an endothelial layer nor TNC expression thus likely not responding well to anti-angiogenic treatment.

In summary, our study has described the composition of metastatic vascular invasions in blood vessels, BVI, and has revealed that they are different from lymphatic vessel invasions, LVI. By using a murine metastasis model with abundant or no TNC expression, we have identified host-derived TNC as an important component of BVI and that TNC increases endothelial layering and tumor cell survival, cellular plasticity and extravasation, involving TGF- β signaling. This information may present novel prognostic and therapeutic opportunities. Finally, as relevant immune competent transplantation models are scarce, our novel autochthonous model of cancer progression providing the opportunity to engineer the host as well as the tumor cells, recapitulating the TME and metastatic traits of the stochastic genetic model could be relevant for future mechanistic research and metastasis targeting.

Material and methods

Human cancer tissue

Human cancer tissue (mammary carcinoma (MaCa), MaCa lung metastasis, renal cell carcinoma (RCC), hepatocellular carcinoma (HCC), pancreatic neuroendocrine tumor (PNET)) from two sites, the Medical University of Vienna/General Hospital Vienna/Medical University Wien (MUW) and the Hôpital Universitaire de Strasbourg Haute-pierre (HUS) was analyzed. In the MUW cohort 30 cases of histologically proven invasive MaCa with metastasis to the lung were investigated. In the HUS cohort, 35 breast cancer specimen were collected (November 2013 – October 2014) and selected according to clinical annotation of present vascular invasions. Patients underwent surgical treatment at the MUW, Department of Obstetrics and Gynecology and at the Department of Surgery/Division of Thoracic Surgery (MUW cohort), at the HUS for the pancreatic and hepatic tumors, and the Nouvel Hôpital Civil for the renal tumors (HUS cohort). In the MUW cohort, in 12 cases enough material was available to perform all IHC stainings (Table S3). Serial sections of 2 μ m were prepared and stained with antibodies specific for TNC, Factor VIII, CD31, CD34 and podoplanin by using an automated stainer (BenchMark Ultra, Roche/Ventana). Immunohistochemical staining was carried out in accordance with the manufacturer's instructions (Ventana Medical Systems). Immunohistochemical staining for platelets (CD61) was performed using the LEICA BOND III automated Immunostainer. In the HUS cohort, 35 patients with mammary carcinoma including 29 ductal invasive carcinomas and 5 lobular invasive carcinomas were

included (Table S4). In addition, tumor tissue from 7 PDAC, 9 RCC, 9 HCC and 5 PNET was selected according to clinical annotations of present vascular invasions (HUS cohort) (Table S4). Four μ m thick paraffin sections were analyzed upon staining with HE or incubation with antibodies against TNC, CD31, and podoplanin (D2–40) by using an automated stainer (BenchMark Ultra, Roche/Ventana). Immunohistochemical staining was carried out in accordance with the manufacturer's instructions (Ventana Medical Systems). Analysis of staining results was performed by two pathologists independently (FO/RK, MUW cohort of breast cancer; AO/RK MUW cohort of RCC; GA/MPC, HUS cohort of breast cancer; GA/ZS, HUS cohort of RCC, HCC, PNET) in each center. Details can be found in Table S2, S3 and S4 and results are summarized in Table S1. Ethical approval for the procedures described has been granted.

Mice

MMTV-NeuNT female mice (FVB/NCrI background) with a mutated constitutively active form of rat ErbB2 (NeuNT), expressed under control of the mouse mammary tumor virus (MMTV) regulatory region [37], were provided by Gerhard Christofori (University of Basel, Switzerland). Mice expressing NeuNT develop multifocal breast adenocarcinoma and lung metastasis; TNC $+$ / $-$ mice in the 129/Sv genetic background were generously donated by Reinhard Fässler [38]. Ten consecutive crosses with FVB/NCrI mice (Charles River) were done to homogenize the background. TNC $+$ / $-$ males were crossed with TNC $+$ / $-$ females to obtain TNC $+/+$ (WT) and TNC $-/-$ (KO) littermates; MMTV-NeuNT mice (FVB/NCrI background) were crossed with TNC $+/+$ mice to generate double-transgenic mice to obtain MMTV-NeuNT mice with a TNC $+/+$ and TNC $-/-$ genotype. All mice were housed and handled according to the guidelines of INSERM and the ethical committee of Alsace, France (CREMEAS) (Directive 2010/63/EU on the protection of animals used for scientific purposes).

Animal experiments

Tumor size was measured every 3 or 7 days with a caliper, and tumor volume was calculated using the formula $V = (a^2 * b)/2$, where b is the longest axis and a is the perpendicular axis to b. For the syngeneic mouse model, 10×10^6 NT193 cells were diluted in 50 μ l PBS and injected orthotopically into the left fourth mammary gland. Mice were euthanized at indicated time points and mammary gland tumors and lungs were processed for histological analysis and western blot. Tissue was snap frozen in liquid nitrogen or embedded in O.C.T. (Sakura Finetek) as well as in paraffin for tissue staining.

Tissue analysis

The stereological analysis of the lung metastasis (index and number) was done as published [19]. Briefly, the left lung lobe was cut transversally into 2.0 mm thick parallel pieces, giving rise to a total of five to six pieces before paraffin embedding in parallel orientation, and cutting into 7 μ m thick sections. In cases where no metastasis was found, 8 to 10 additional sections separated by 200 μ m were analyzed.

HE staining

Tissue from breast tumors and lungs were prepared and fixed overnight in 4% PFA, dehydrated in 100% ethanol for 24 h, embedded in paraffin, cut in 7 μ m thick sections, dewaxed and rehydrated with 100% Toluene (2 washes of 15 min) then incubated in 100%–70% alcohol solutions (10 min each) followed by a final staining with hematoxylin (Surgi-path) for 5 min and washing with tap water or followed by IHC. Sections were further processed with differentiation solution (1% HCl in absolute ethanol, for 7 s), followed by washing under tap water for 10 min. Sections were then incubated in eosin (Harris) for 10 s, rinsed and dehydrated in 70% - 100% alcohol baths with rapid dips in each bath before a final wash in toluene for 15 min and embedded in Eukitt solution (Sigma).

Giemsa staining

Tissue was cut in 7 μ m thick sections, dewaxed and stained with Giemsa (320310–0125, RAL) for 2 h at 37 °C, further processed in a 0.5% aqueous acetic acid solution, dehydrated and embedded with Eukitt solution.

Immunohistochemistry

Paraffin embedded tissue was rehydrated and the antigens were unmasked by boiling in 10 mM pH 6 citrate solution for 20 min. Cooled slides were washed and incubated in a peroxide solution (0.6% H₂O₂, 0.1% triton X-100 in PBS) to eliminate endogenous peroxidase activity. Non-specific binding sites were blocked with a blocking solution (5% normal goat serum in PBS) for 1 h at room temperature (RT) and then avidin/biotin receptors were blocked by using the avidin/biotin blocking kit as recommended by the manufacturer (Vector). Slides were incubated with the first antibody overnight at 4 °C in a humidified container. Next day, slides were washed and incubated for 45 min at room temperature with a secondary antibody (coupled to biotin). The detection of peroxidase was done using the Elite ABC system (VECTASTAIN) with DAB (Vector) as substrate. Finally, tissue

was stained with hematoxylin, dehydrated and embedded in Eukitt solution. Proliferation and apoptosis were quantified as events per area upon staining for Ki-67 and cleaved caspase-3, respectively.

Immunofluorescence staining

Tissue was air-dried and unspecific signals were reduced with blocking solution (5% normal goat or donkey serum in PBS) for 1 h at RT. Tissue sections were incubated with the primary antibody overnight at 4 °C in a humidified container. The following day the primary antibody was removed and tissue was incubated with a fluorescent secondary antibody for 1 h at RT. Slides were washed and incubated with DAPI (Sigma) to visualize the nuclei (10 min at RT). Excess of dye was removed and tissue was embedded with FluorSave™ Reagent (Calbiochem). Fluorescent signal was analyzed with a Zeiss Axio Imager Z2 microscope. The staining procedure (fixation, blocking, antibody dilution) and image acquisition setting (microscope, magnification, light intensity, exposure time) were kept constant per experiment and genetic conditions. Quantification of immunofluorescent microscopic images was done by the ImageJ (National Institutes of Health) software using a constant threshold. The expression of TNC was scored according to the signal extent and intensity of the mosaic picture of the whole tumor. A typical fibrillar TNC staining with the MTn12 antibody in the stroma around the tumor cells was considered as positive signal (no signal was seen with the secondary antibody alone). The extent of TNC staining was scored by the percentage of the positively stained area. The stained area in each region of interest was scored as 0 for staining <5%, as 1 for 5–25%, 2 for 25–50%, 3 for 50–75%, and 4 for >75% of the stained area. The intensity of staining was scored as 0, 1, 2 and 3 representing no staining, mild (weak but detectable above control), moderate (distinct) and intense (strong) staining, respectively. The percentage of positively stained area and intensity of staining were multiplied to produce a weighted score [61].

qPCR analysis

Total RNA was prepared using TriReagent (Life Technologies) according to the manufacturer's instructions. RNA was reverse transcribed (Multi-Scribe reverse transcriptase, Applied Biosystems) and qPCR was done on cDNA (diluted 1:5 in water) using a 7500 Real Time PCR machine (Applied Biosystems) with a SYBR green reaction mixture or Taqman reaction mixture (Applied Biosystems). Data were normalized by using a Taqman mouse *Gapdh* Endogenous Control (4333764T, Life Technology) and fold induction was calculated using the comparative Ct method (-ddCt). Primers used for qPCR are listed in Table S3.

Immunoblotting

Cell lysates were prepared in lysis buffer (25 mM Tris-HCl pH 7.6, 150 mM NaCl, 1% NP-40, 1% sodium deoxycholate, 0.1% SDS) supplemented with protease inhibitor (Roche) and Phosphatase Inhibitor Cocktail (Santa Cruz). Protein concentration was determined with a Bradford Assay (BioRad). After addition of Laemmli buffer (BioRad), 20–30 µg protein lysate was separated by SDS-PAGE in precasted 4–20% gradient gels (BioRad), transferred onto nitrocellulose membranes (BioRad) using TransBlot Turbo™ Transfer System (BioRad), blocked with 5% Blocking-Grade blocker (BioRad) in 0.1% Tween 20-PBS and incubated with the primary (overnight at 4 °C) and secondary antibodies (1 h at RT) in 1.5% Blocking-Grade Blocker in 0.1% Tween 20-PBS. Protein bands were detected with the Amersham ECL Western Blotting detection reagent (GE Healthcare) or SuperSignal™ West Femto Maximum Sensitivity Substrate (ThermoFisher).

Immunofluorescence staining of cells

Cells were fixed in 4% PFA for 10 min, permeabilized in PBS-Triton 0.1% for 10 min, incubated with the primary antibody overnight at 4 °C, secondary antibody for 1 h at RT, DAPI, embedded with FluorSave™ Reagent (Calbiochem) and analyzed with an Zeiss Axio Imager Z2 microscope.

Antibodies

The primary antibodies are shown in Table S4. Secondary antibodies were ECL horseradish peroxidase-linked (1/1000): anti-rat (NA935) and anti-rabbit (NA934V) (GE Healthcare). Secondary goat or donkey antibodies were fluorescently labeled (1/1000): anti-mouse, anti-rabbit, anti-rat, anti-guinea pig and anti-goat IgG (Jackson Laboratory).

Cell culture

NT193 cells derived from a MMTV-NeuNT primary tumor [20] were cultured in DMEM medium with 4.5 g/L glucose (GIBCO) supplemented with 10% of inactivated fetal bovine serum, penicillin (10,000 U/ml) and streptomycin (10 mg/ml). Cells were maintained at 37 °C in a humidified atmosphere of 5% CO₂.

Treatment with TGF-β and GW788388

Cells were starved in the absence of serum overnight before treatment with human recombinant TGF-β1 (100–21, PEPROTECH), recombinant TNC (purified as described [62]) or the TGF-β type I receptor inhibitor GW 788388 (Selleckchem). Cells were pretreated with the inhibitor for 45 min prior to incubation with TNC, TGF-β and platelets,

respectively. All reagents were diluted following the manufacturer's instructions.

Transduction of cells

Silencing of *Tnc* in mouse cells was done by short hairpin (sh) mediated gene expression knock down (KD). Lentiviral particles with shRNA vectors (Sigma-Aldrich) specific for *Tnc* were used. sh1, TRCN0000312137, sequence 5'-CCGGCCCG GAACTGAATATGGGATTCTCGAGAATCCCA-T ATT CAG TT C C G G G T T T T G -3'; sh2, TRCN0000312138, 5'-CCGGGCATCAACACAAC-C A G T C T A A C T C G A G T T A G A C T G G TTGTGTTGATGCTTTTG-3'. Lentiviral particles encoding a non-targeting shRNA vector were used as a control (SHC202V, Sigma-Aldrich). Transduced cells were selected with normal medium supplemented with 10 µg/ml puromycin (ThermoFisher) and the selection pressure was maintained in all in vitro experiments.

Spheroid assay

NT193 cells were seeded at 5000 cells per 100 µl together with TNC (10 µg/ml) or PBS-Tween-20 (0.01%) in 96 well plates with round bottom pre-coated with 10 µg/ml of poly-HEMA (Sigma) for 24 h to allow spheroid formation and then were embedded in OCT for further immunostaining analysis.

Wound healing assay

NT193 cells (2×10^5) were grown to confluence in 24-well plates for 24 h. Confluent cell monolayers were treated 2 h with mitomycin-C (Sigma) at 2 µg/ml to inhibit proliferation before application of a scratch wound with a pipet tip. Cell debris was removed by PBS washing before addition of serum-free medium supplemented with the indicated molecules. Images of the wounding area were acquired immediately after scratching and then in the same field after 24 h. The relative wound closure was quantified by measuring the surface of the cell-free area at the time of injury and at the end point of the experiment.

Cell death assessment with caspase 3/7 activity assay

Caspase 3/7 activity assay (Promega) was performed according to the manufacturer's instructions. Briefly, 2000 cells/well were plated overnight in 96-well plates. Cells were treated as described for the indicated time period and then cell apoptosis was induced by staurosporine (1 µg/ml, Sigma) for 24 h. To measure caspase 3/7 activity, 75 µl of caspase Glo 3/7 reagent was added to each well for 1 h with constant shaking at RT. Luminescence was measured using a TriStar² LB942 multidetection microplate reader.

Preparation of washed platelets

Blood was drawn from the abdominal aorta of adult FVB/NCr mice anesthetized intraperitoneally with a mixture of xylazine (20 mg/kg, Rompun, Bayer) and ketamine (100 mg/kg, Imalgene 1000, Merial). Platelets were washed using ACD-anticoagulated whole blood as previously described [63].

Enzyme-linked immunosorbent assay (ELISA)

Subconfluent NT193 sh2TNC cells (5×10^5) were grown on plastic (6 wells plates) for 24 h in full medium (10%FCS), serum starved (no serum) overnight, and incubated for 24 h in serum-free DMEM containing 0.01% Tween-20 (CTRL), TGF-β (10 ng/ml), TNC (10 µg/ml, 35 nM (MW 280 kDa)), TNC-FBG (10 µg/ml, 383 nM (MW 26.1 kDa)) and TNC-FnIII3-5 (10 µg/ml, 327 nM (MW 30.6 kDa)), respectively. All proteins were synthesized and purified as described [64]. Cells were separated from the conditioned medium by centrifugation and, secreted TGF-β was determined using ELISA (RnD Systems DY1679) following the manufacturer's recommendations.

Statistical analysis

The GraphPad Prism software (version 6) was used for graphical representations of data and statistical analyses to assess significance of observed differences. All parametric (unpaired Student *t*-test with Welch's correction in case of unequal variance) and non-parametric tests (Mann-Whitney) were performed in a two-tailed fashion. To compare the proportion of BVI and parenchymal metastases, Fisher's exact test or Chi-square test was used. Mean \pm SEM. *p* values <0.05 were considered as statistically significant (**p* < 0.05 ; ***p* < 0.01 ; ****p* < 0.001 ; *****p* < 0.0001).

Declaration of Competing Interest

The authors declare no competing financial interests.

Acknowledgement

We are grateful for technical support by Christiane Arnold, Fanny Steinbach, Anna Brown and the personnel of the animal facility. This work was supported by grants from Worldwide Cancer

Research/AICR (14-1070), INCa (TENPLAMET), Ligue Régional contre le Cancer CCIR Grand Est, INSERM and University Strasbourg to GO, INCa (TENPLAMET) to PM, National Natural Science Foundation of China (Grant No. 81802655) to ZS and fellowship grants from the Chinese Scholarship Council (ZS) and the Mexican scholarship program CONACYT (IVQ). KSM is supported by Arthritis Research UK.

Author contribution

ZS, IVQ and TH developed the genetic and orthotopic grafting model. ZS, IVQ, DM, AY, TH, CA, CD, WE and CS performed experiments, analyzed and interpreted the data. OL, AK, AB, MvdH and CB provided technical assistance. GA, FO, AO, MPC, CM and RK provided, analyzed and interpreted data from human cancer patients. PM supervised the platelet study. GC provided the MMTV-NeuNT mice. GC, TL, CAF and KM critically reviewed the manuscript and interpreted data. ZS, IVQ and GO conceptualized and wrote the manuscript. Grants to GO financed this study.

Appendix A. Supplementary data

Supplementary data to this article can be found online at <https://doi.org/10.1016/j.matbio.2019.07.001>.

Received 27 March 2019;
Received in revised form 30 May 2019;
Accepted 2 July 2019
Available online 6 July 2019

Keywords:
Blood vessel invasions;
Circulating tumor cells;
Tumor emboli;
Tenascin-C;
Cellular plasticity;
TGF- β signaling;
Lung metastasis;
Endothelialization;
Fsp1+ cells;
Endothelial cells

Current address: 1. Tongji Cancer Research Institute, Tongji Hospital, Tongji Medical College in Huazhong University of Science and Technology, Wuhan, Hubei, China. 2. Department of Gastrointestinal Surgery, Tongji Hospital, Tongji Medical College in Huazhong University of Science and Technology, Wuhan, Hubei, China.

2 Equal contribution.

Abbreviations used:

BVI, blood vessel invasions; CD31, cluster of differentiation 31; CD41, cluster of differentiation 41, integrin alpha chain 2b; Cl. Cas-3, cleaved caspase-3; CK8/18, cytokeratin 8/18; DAPI, 4',6-diamidino-2-phenylindole; DMEM, Dulbecco's Modified Eagle's Medium; ELISA, Enzyme-linked immunosorbent assay; EPC, endothelial progenitor cells; EMT, epithelial-to-mesenchymal transition; ERK, extracellular signal-regulated kinases; ECM, extracellular matrix; FN, fibronectin; Fsp1, fibroblast-specific protein 1; GAPDH, Glyceraldehyde 3-phosphate dehydrogenase; GW788388, 4-(4-[3-(Pyridin-2-yl)-1H-pyrazol-4-yl]pyridin-2-yl)-N-(tetrahydro-2Hpyran-4-yl) benzamide; HCC, hepatocellular carcinoma; HE, Hematoxylin and eosin; IDC NST, invasive ductal carcinoma, no special type; KD, knock down; KO, knock out; LM, laminin; LVI, lymph vessel invasions; MaCa, mammary carcinomas; Mmp9, Matrix metallopeptidase 9; MMTV-NeuNT, mouse mammary tumor virus driven NeuNT (activated rat ErbB2 homologue) transformed; NOS, not otherwise specified; NT193, MMTV-NeuNT breast tumor derived cell line; Pai-1, plasminogen activator inhibitor-1; PBS, phosphate-buffered saline; PDAC, pancreatic ductal adenocarcinomas; PNET, pancreatic neuroendocrine tumors; PyMT, polyoma middle T antigen; RAM1, reduced Arbuscular Myorrhization 1; RCC, renal cell carcinoma; Sh, short hairpin; Slug, snail family zinc finger 2; Snail, snail family zinc finger 1; STS, staurosporine; TGF- β , transforming growth factor β ; TME, tumor microenvironment; TNBC, triple negative breast cancer; TNC, tenascin-C; VEGFA, vascular endothelial growth factor A; WT, wild type; Zeb1, zinc finger E-box-binding homeobox 1; α -SMA, alpha-smooth muscle actin.

References

- [1] J.E. Talmadge, I.J. Fidler, AACR centennial series: the biology of cancer metastasis: historical perspective, *Cancer Res.* 70 (2010) 5649–5669, <https://doi.org/10.1158/0008-5472.CAN-10-1040>.
- [2] S. Gkountela, F. Castro-Giner, B.M. Szczerba, M. Vetter, J. Landin, R. Scherrer, I. Krol, M.C. Scheidmann, C. Beisel, C.U. Stirnimann, C. Kurzeder, V. Heinzelmann-Schwarz, C. Rochlitz, W.P. Weber, N. Aceto, Circulating tumor cell clustering shapes dna methylation to enable metastasis seeding, *Cell.* 176 (2019) 98–112.e14. doi:<https://doi.org/10.1016/j.cell.2018.11.046>.
- [3] K. Lapis, S. Paku, L.A. Liotta, Endothelialization of embolized tumor cells during metastasis formation, *Clin. Exp. Metastasis.* 6 (1988) 73–89.
- [4] E.A. Rakha, S. Martin, A.H.S. Lee, D. Morgan, P.D.P. Pharoah, Z. Hodi, D. MacMillan, I.O. Ellis, The prognostic significance of lymphovascular invasion in invasive breast carcinoma, *Cancer.* 118 (2012) 3670–3680, <https://doi.org/10.1002/cncr.26711>.
- [5] T. Fujii, R. Yajima, T. Hirakata, T. Miyamoto, T. Fujisawa, S. Tsutsumi, Y. Ynagita, M. Iijima, H. Kuwano, Impact of the prognostic value of vascular invasion, but not lymphatic

invasion, of the primary tumor in patients with breast cancer, *Anticancer Res.* 34 (2014) 1255–1259.

[6] I. Soerjomataram, M.W.J. Louwman, J.G. Ribot, J.A. Roukema, J.W.W. Coebergh, An overview of prognostic factors for long-term survivors of breast cancer, *Breast Cancer Res. Treat.* 107 (2008) 309–330, <https://doi.org/10.1007/s10549-007-9556-1>.

[7] M.J. Bissell, W.C. Hines, Why don't we get more cancer? A proposed role of the microenvironment in restraining cancer progression, *Nat. Med.* 17 (2011) 320–329, <https://doi.org/10.1038/nm.2328>.

[8] A.J. Minn, G.P. Gupta, P.M. Siegel, P.D. Bos, W. Shu, D.D. Giri, A. Viale, A.B. Olshen, W.L. Gerald, J. Massagué, Genes that mediate breast cancer metastasis to lung, *Nature* 436 (2005) 518–524, <https://doi.org/10.1038/nature03799>.

[9] T. Oskarsson, S. Acharya, X.H.-F. Zhang, S. Vanharanta, S.F. Tavazoie, P.G. Morris, R.J. Downey, K. Manova-Todorova, E. Brogi, J. Massagué, Breast cancer cells produce tenascin C as a metastatic niche component to colonize the lungs, *Nat. Med.* 17 (2011) 867–874, <https://doi.org/10.1038/nm.2379>.

[10] K.S. Midwood, M. Chiquet, R.P. Tucker, G. Orend, Tenascin-C at a glance, *J. Cell Sci.* 129 (2016) 4321–4327, <https://doi.org/10.1242/jcs.190546>.

[11] F. Saupe, A. Schwenger, Y. Jia, I. Gasser, C. Spenlé, B. Langlois, M. Kammerer, O. Lefebvre, R. Hlushchuk, T. Rupp, M. Marko, M. van der Heyden, G. Cremel, C. Arnold, A. Klein, P. Simon-Assmann, V. Djonov, A. Neuville-Méchine, I. Esposito, J. Slotta-Huspenina, K.-P. Janssen, O. de Wever, G. Christofori, T. Hussenet, G. Orend, Tenascin-C downregulates Wnt inhibitor Dickkopf-1, promoting tumorigenesis in a neuroendocrine tumor model, *Cell Reports*. 5 (2013) 482–492. doi:<https://doi.org/10.1016/j.celrep.2013.09.014>.

[12] J. Insua-Rodríguez, M. Pein, T. Hongu, J. Meier, A. Descot, C.M. Lowy, E. De Braekeleer, H.-P. Sinn, S. Spaich, M. Sütterlin, A. Schneeweiss, T. Oskarsson, Stress signaling in breast cancer cells induces matrix components that promote chemoresistant metastasis, *EMBO Mol Med.* 10 (2018). doi: [10.15252/emmm.201809003](https://doi.org/10.15252/emmm.201809003).

[13] J.F. Taits, G. Wirl, M. Dector, W.J. Muller, R. Fässler, Tenascin-C modulates tumor stroma and monocyte/macrophage recruitment but not tumor growth or metastasis in a mouse strain with spontaneous mammary cancer, *J. Cell Sci.* 112 (Pt 12) (1999) 1855–1864.

[14] S.F. Tavazoie, C. Alarcón, T. Oskarsson, D. Padua, Q. Wang, P.D. Bos, W.L. Gerald, J. Massagué, Endogenous human microRNAs that suppress breast cancer metastasis, *Nature*. 451 (2008) 147–152, <https://doi.org/10.1038/nature06487>.

[15] L. Bouchard, L. Lamarre, P.J. Tremblay, P. Jolicoeur, Stochastic appearance of mammary tumors in transgenic mice carrying the MMTV/c-neu oncogene, *Cell*. 57 (1989) 931–936.

[16] W.J. Muller, E. Sinn, P.K. Pattengale, R. Wallace, P. Leder, Single-step induction of mammary adenocarcinoma in transgenic mice bearing the activated c-neu oncogene, *Cell*. 54 (1988) 105–115.

[17] P.M. Siegel, W. Shu, R.D. Cardiff, W.J. Muller, J. Massagué, Transforming growth factor β signaling impairs Neu-induced mammary tumorigenesis while promoting pulmonary metastasis, *Proc. Natl. Acad. Sci.* 100 (2003) 8430–8435, <https://doi.org/10.1073/pnas.0932636100>.

[18] C. Spenlé, I. Gasser, F. Saupe, K.-P. Janssen, C. Arnold, A. Klein, M. van der Heyden, J. Mutterer, A. Neuville-Méchine, M.-P. Chenard, D. Guenot, I. Esposito, J. Slotta-Huspenina, N. Ambartsumian, P. Simon-Assmann, G. Orend, Spatial organization of the tenascin-C microenvironment in experimental and human cancer, *Cell Adhes. Migr.* 9 (2015) 4–13, <https://doi.org/10.1080/19336918.2015.1005452>.

[19] B.S. Nielsen, L.R. Lund, I.J. Christensen, M. Johnsen, P.A. Usher, L. Wulf-Andersen, T.L. Frandsen, K. Danø, H.J.G. Gundersen, A precise and efficient stereological method for determining murine lung metastasis volumes, *Am. J. Pathol.* 158 (2001) 1997–2003, [https://doi.org/10.1016/S0002-9440\(10\)64671-8](https://doi.org/10.1016/S0002-9440(10)64671-8).

[20] A. Arpel, P. Sawma, C. Spenlé, J. Fritz, L. Meyer, N. Garnier, I. Velázquez-Quesada, T. Hussenet, S. Aci-Sèche, N. Baumlin, M. Genest, D. Brasse, P. Hubert, G. Crémel, G. Orend, P. Laquerrière, D. Bagnard, Transmembrane domain targeting peptide antagonizing ErbB2/Neu inhibits breast tumor growth and metastasis, *Cell Rep.* 8 (2014) 1714–1721, <https://doi.org/10.1016/j.celrep.2014.07.044>.

[21] J.T. O'Connell, H. Sugimoto, V.G. Cooke, B.A. MacDonald, A.I. Mehta, V.S. LeBleu, R. Dewar, R.M. Rocha, R.R. Brentani, M.B. Resnick, E.G. Neilson, M. Zeisberg, R. Kalluri, VEGF-A and Tenascin-C produced by S100A4+ stromal cells are important for metastatic colonization, *Proc. Natl. Acad. Sci.* 108 (2011) 16002–16007, <https://doi.org/10.1073/pnas.1109493108>.

[22] A. Dongre, R.A. Weinberg, New insights into the mechanisms of epithelial–mesenchymal transition and implications for cancer, *Nat. Rev. Mol. Cell Biol.* 20 (2019) 69, <https://doi.org/10.1038/s41580-018-0080-4>.

[23] C.K.S. Meikle, C.A. Kelly, P. Garg, L.M. Wuescher, R.A. Ali, R.G. Worth, Cancer and thrombosis: the platelet perspective, *Frontiers in Cell and Developmental Biology*. 4 (2017). doi:<https://doi.org/10.3389/fcell.2016.00147>.

[24] P.H. Mangin, N. Receveur, V. Wurtz, T. David, C. Gachet, F. Lanza, Identification of five novel 14-3-3 isoforms interacting with the GPIb-IX complex in platelets, *J. Thromb. Haemost.* 7 (2009) 1550–1555, <https://doi.org/10.1111/j.1538-7836.2009.03530.x>.

[25] M. Labelle, S. Begum, R.O. Hynes, Direct signaling between platelets and cancer cells induces an epithelial-mesenchymal-like transition and promotes metastasis, *Cancer Cell* 20 (2011) 576–590, <https://doi.org/10.1016/j.ccr.2011.09.009>.

[26] T. Rupp, B. Langlois, M.M. Koczorowska, A. Radwanska, Z. Sun, T. Hussenet, O. Lefebvre, D. Murdamoothoo, C. Arnold, A. Klein, M.L. Biniossek, V. Hyenne, E. Naudin, I. Velazquez-Quesada, O. Schilling, E. Van Obberghen-Schilling, G. Orend, Tenascin-C orchestrates glioblastoma angiogenesis by modulation of pro- and anti-angiogenic signaling, *Cell Rep.* 17 (2016) 2607–2619, <https://doi.org/10.1016/j.celrep.2016.11.012>.

[27] A. Radwanska, D. Grall, S. Schaub, S.B. la F. Divonne, D. Ciais, S. Rekima, T. Rupp, A. Sudaka, G. Orend, E. Van Obberghen-Schilling, Counterbalancing anti-adhesive effects of Tenascin-C through fibronectin expression in endothelial cells, *Scientific Reports*. 7 (2017). doi:<https://doi.org/10.1038/s41598-017-13008-9>.

[28] K.J. Cheung, V. Padmanaban, V. Silvestri, K. Schipper, J.D. Cohen, A.N. Fairchild, M.A. Gorin, J.E. Verdone, K.J. Pienta, J.S. Bader, A.J. Ewald, Polyclonal breast cancer metastases arise from collective dissemination of keratin 14-expressing tumor cell clusters, *Proc. Natl. Acad. Sci.* 113 (2016) E854–E863, <https://doi.org/10.1073/pnas.1508541113>.

[29] Y. Zhang, R.A. Weinberg, Epithelial-to-mesenchymal transition in cancer: complexity and opportunities, *Front. Med.* 12 (2018) 361–373, <https://doi.org/10.1007/s11684-018-0656-6>.

[30] K. Nagaharu, X. Zhang, T. Yoshida, D. Katoh, N. Hanamura, Y. Kozuka, T. Ogawa, T. Shiraishi, K. Imanaka-Yoshida, Tenascin C induces epithelial-mesenchymal transition-like change accompanied by SRC activation and focal adhesion kinase phosphorylation in human breast cancer cells, *Am. J. Pathol.* 178 (2011) 754–763, <https://doi.org/10.1016/j.ajpath.2010.10.015>.

[31] J. Xu, S. Lamouille, R. Deryck, TGF- β -induced epithelial to mesenchymal transition, *Cell Res.* 19 (2009) 156–172, <https://doi.org/10.1038/cr.2009.5>.

[32] A. Singh, J. Settleman, EMT, cancer stem cells and drug resistance: an emerging axis of evil in the war on cancer, *Oncogene.* 29 (2010) 4741–4751, <https://doi.org/10.1038/onc.2010.215>.

[33] L. De Laporte, J.J. Rice, F. Tortelli, J.A. Hubbell, Tenascin C promiscuously binds growth factors via its fifth fibronectin type III-like domain, *PLoS One* 8 (2013), e62076, <https://doi.org/10.1371/journal.pone.0062076>.

[34] C. Koliopoulos, C.-Y. Lin, C.-H. Heldin, A. Moustakas, P. Heldin, Has2 natural antisense RNA and Hmga2 promote Has2 expression during TGF β -induced EMT in breast cancer, *Matrix Biol.* 80 (2019) 29–45, <https://doi.org/10.1016/j.matbio.2018.09.002>.

[35] L.A. Griggs, N.T. Hassan, R.S. Malik, B.P. Griffin, B.A. Martinez, L.W. Elmore, C.A. Lemmon, Fibronectin fibrils regulate TGF- β 1-induced epithelial-mesenchymal transition, *Matrix Biol.* 60–61 (2017) 157–175, <https://doi.org/10.1016/j.matbio.2017.01.001>.

[36] A. Pezzolo, F. Parodi, D. Marimpietri, L. Raffaghelli, C. Cocco, A. Pistorio, M. Mosconi, C. Gambini, M. Cilli, S. Deaglio, F. Malavasi, V. Pistoia, Oct-4+/Tenascin C+ neuroblastoma cells serve as progenitors of tumor-derived endothelial cells, *Cell Res.* 21 (2011) 1470–1486, <https://doi.org/10.1038/cr.2011.38>.

[37] T. Sugino, T. Yamaguchi, G. Ogura, A. Saito, T. Hashimoto, N. Hoshi, S. Yoshida, S. Goodison, T. Suzuki, Morphological evidence for an invasion-independent metastasis pathway exists in multiple human cancers, *BMC Medicine.* 2 (2004). doi:<https://doi.org/10.1186/1741-7015-2-9>.

[38] R.V. Iozzo, M.A. Gubbiotti, Extracellular matrix: the driving force of mammalian diseases, *Matrix Biol.* 71–72 (2018) 1–9, <https://doi.org/10.1016/j.matbio.2018.03.023>.

[39] N.K. Karamanos, A.D. Theocaris, T. Neill, R.V. Iozzo, Matrix modeling and remodeling: a biological interplay regulating tissue homeostasis and diseases, *Matrix Biol.* 75–76 (2019) 1–11, <https://doi.org/10.1016/j.matbio.2018.08.007>.

[40] N. Dandachi, C. Hauser-Kronberger, E. Moré, B. Wiesener, G.W. Hacker, O. Dietze, G. Wirl, Co-expression of tenascin-C and vimentin in human breast cancer cells indicates phenotypic transdifferentiation during tumour progression: correlation with histopathological parameters, hormone receptors, and oncoproteins, *J. Pathol.* 193 (2001) 181–189, [https://doi.org/10.1002/1096-9896\(2000\)9999:9999<::AID-PATH752>3.0.CO;2-V](https://doi.org/10.1002/1096-9896(2000)9999:9999<::AID-PATH752>3.0.CO;2-V).

[41] X. Shen, R.H. Kramer, Adhesion-mediated squamous cell carcinoma survival through ligand-independent activation of epidermal growth factor receptor, *Am. J. Pathol.* 165 (2004) 1315–1329, [https://doi.org/10.1016/S0002-9440\(10\)63390-1](https://doi.org/10.1016/S0002-9440(10)63390-1).

[42] Y. Katsuno, D.S. Meyer, Z. Zhang, K.M. Shokat, R.J. Akhurst, K. Miyazono, R. Deryck, Chronic TGF- β exposure drives stabilized EMT, tumor stemness, and cancer drug resistance with vulnerability to bitopic mTOR inhibition, *Sci. Signal.* 12 (2019) eaau8544. doi:<https://doi.org/10.1126/scisignal.aau8544>.

[43] T. Sugino, T. Kusakabe, N. Hoshi, T. Yamaguchi, T. Kawaguchi, S. Goodison, M. Sekimata, Y. Homma, T. Suzuki, An invasion-independent pathway of blood-borne metastasis, *Am. J. Pathol.* 160 (2002) 1973–1980.

[44] V.L.T. Ballard, A. Sharma, I. Duignan, J.M. Holm, A. Chin, R. Choi, K.A. Hajjar, S.-C. Wong, J.M. Edelberg, Vascular tenascin-C regulates cardiac endothelial phenotype and neovascularization, *FASEB J.* 20 (2006) 717–719, <https://doi.org/10.1096/fj.05-5131fje>.

[45] N. Aceto, A. Bardia, D.T. Miyamoto, M.C. Donaldson, B.S. Wittner, J.A. Spencer, M. Yu, A. Pely, A. Engstrom, H. Zhu, B.W. Brannigan, R. Kapur, S.L. Stott, T. Shioda, S. Ramaswamy, D.T. Ting, C.P. Lin, M. Toner, D.A. Haber, S. Maheswaran, Circulating tumor cell clusters are oligoclonal precursors of breast cancer metastasis, *Cell.* 158 (2014) 1110–1122, <https://doi.org/10.1016/j.cell.2014.07.013>.

[46] D.G. Duda, A.M.M.J. Duyverman, M. Kohno, M. Snuderl, E.J.A. Steller, D. Fukumura, R.K. Jain, Malignant cells facilitate lung metastasis by bringing their own soil, *Proc. Natl. Acad. Sci. U. S. A.* 107 (2010) 21677–21682, <https://doi.org/10.1073/pnas.1016234107>.

[47] R.G. Oshima, J. Esperance, V. Munoz, L. Hebbard, B. Ranscht, N. Sharan, W.J. Muller, C.A. Hauser, R.D. Cardiff, Angiogenic acceleration of Neu induced mammary tumor progression and metastasis, *Cancer Res.* 64 (2004) 169–179.

[48] B. Langlois, F. Saupe, T. Rupp, C. Arnold, M. van der Heyden, G. Orend, T. Husseinet, AngioMatrix, a signature of the tumor angiogenic switch-specific matrisome, correlates with poor prognosis for glioma and colorectal cancer patients, *Oncotarget* 5 (2014) 10529–10545.

[49] R. Lauria, F. Perrone, C. Carloni, M. De Laurentiis, A. Morabito, C. Gallo, E. Varriale, G. Pettinato, L. Panico, G. Petrella, The prognostic value of lymphatic and blood vessel invasion in operable breast cancer, *Cancer* 76 (1995) 1772–1778.

[50] N. Knijn, U.E.M. van Exsel, M.E. de Noo, I.D. Nagtegaal, The value of intramural vascular invasion in colorectal cancer - a systematic review and meta-analysis, *Histopathology.* 72 (2018) 721–728, <https://doi.org/10.1111/his.13404>.

[51] S. Okada, S. Mizuguchi, N. Izumi, H. Komatsu, M. Toda, K. Hara, T. Okuno, T. Shibata, H. Wanibuchi, N. Nishiyama, Prognostic value of the frequency of vascular invasion in stage I non-small cell lung cancer, *Gen. Thorac. Cardiovasc. Surg.* 65 (2017) 32–39, <https://doi.org/10.1007/s11748-016-0720-6>.

[52] M.R.S. Siddiqui, C. Simillis, C. Hunter, M. Chand, J. Bhoday, A. Garant, T. Vuong, G. Artho, S. Rasheed, P. Tekkis, A.-M. Abulafia, G. Brown, A meta-analysis comparing the risk of metastases in patients with rectal cancer and MRI-detected extramural vascular invasion (mrEMVI) vs mrEMVI-negative cases, *Br. J. Cancer* 116 (2017) 1513–1519, <https://doi.org/10.1038/bjc.2017.99>.

[53] T.A. Klingen, Y. Chen, I.M. Stefansson, G. Knutsvik, K. Collett, A.L. Abrahamsen, H. Aase, H. Aas, T. Aas, E. Wik, L.A. Akslen, Tumour cell invasion into blood vessels is significantly related to breast cancer subtypes and decreased survival, *J. Clin. Pathol.* 70 (2017) 313–319, <https://doi.org/10.1136/jclinpath-2016-203861>.

[54] V.F. Marinho, K. Metze, F.S. Sanches, G.F. Rocha, H. Gobbi, Lymph vascular invasion in invasive mammary carcinomas identified by the endothelial lymphatic marker D2-40 is associated with other indicators of poor prognosis,

BMC Cancer 8 (2008) 64, <https://doi.org/10.1186/1471-2407-8-64>.

[55] G.G. Van den Eynden, I. Van der Auwera, S.J. Van Laere, C.G. Colpaert, P. van Dam, L.Y. Dirix, P.B. Vermeulen, E.A. Van Marck, Distinguishing blood and lymph vessel invasion in breast cancer: a prospective immunohistochemical study, Br. J. Cancer 94 (2006) 1643–1649, <https://doi.org/10.1038/sj.bjc.6603152>.

[56] K.E. Roberts, D. Hamele-Bena, A. Saqi, C.A. Stein, R.P. Cole, Pulmonary tumor embolism: a review of the literature, Am. J. Med. 115 (2003) 228–232.

[57] N.S. Vasudev, A.R. Reynolds, Anti-angiogenic therapy for cancer: current progress, unresolved questions and future directions, Angiogenesis 17 (2014) 471–494, <https://doi.org/10.1007/s10456-014-9420-y>.

[58] V. Zambonin, A. De Toma, L. Carbognin, R. Nortilli, E. Fiorio, V. Parolin, S. Pilotto, F. Cuppone, F. Pellini, D. Lombardi, G.P. Pollini, G. Tortora, E. Bria, Clinical results of randomized trials and “real-world” data exploring the impact of Bevacizumab for breast cancer: opportunities for clinical practice and perspectives for research, Expert. Opin. Biol. Ther. 17 (2017) 497–506, <https://doi.org/10.1080/14712598.2017.1289171>.

[59] K.C. Aalders, K. Tryfonidis, E. Senkus, F. Cardoso, Anti-angiogenic treatment in breast cancer: facts, successes, failures and future perspectives, Cancer Treat. Rev. 53 (2017) 98–110, <https://doi.org/10.1016/j.ctrv.2016.12.009>.

[60] M. Rajabi, S. Mousa, The role of angiogenesis in cancer treatment, Biomedicines 5 (2017) 34, <https://doi.org/10.3390/biomedicines5020034>.

[61] M. Shi, X. He, W. Wei, J. Wang, T. Zhang, X. Shen, Tenascin-C induces resistance to apoptosis in pancreatic cancer cell through activation of ERK/NF- κ B pathway, Apoptosis. 20 (2015) 843–857, <https://doi.org/10.1007/s10495-015-1106-4>.

[62] W. Huang, R. Chiquet-Ehrismann, J.V. Moyano, A. Garcia-Pardo, G. Orend, Interference of tenascin-C with syndecan-4 binding to fibronectin blocks cell adhesion and stimulates tumor cell proliferation, Cancer Res. 61 (2001) 8586–8594.

[63] J.-P. Cazenave, P. Ohlmann, D. Cassel, A. Eckly, B. Hechler, C. Gachet, Preparation of Washed Platelet Suspensions From Human and Rodent Blood, in: Platelets and Megakaryocytes, Humana Press, New Jersey, 2004, pp. 013–028, <https://doi.org/10.1385/1-59259-782-3:013>.

[64] K. Midwood, S. Sacre, A.M. Piccinini, J. Inglis, A. Trebaul, E. Chan, S. Drexler, N. Sofat, M. Kashiwagi, G. Orend, F. Brennan, B. Foxwell, Tenascin-C is an endogenous activator of toll-like receptor 4 that is essential for maintaining inflammation in arthritic joint disease, Nat. Med. 15 (2009) 774–780, <https://doi.org/10.1038/nm.1987>.

Appendix II



OPEN ACCESS

Edited by:

Joanne Murphy-Ullrich,
University of Alabama at Birmingham,
United States

Reviewed by:

Tomer Cooks,
Ben-Gurion University of the Negev,
Israel
Michal Amit Rahat,
Technion-Israel Institute of
Technology, Israel
Andreas Faissner,
Ruhr University Bochum, Germany

***Correspondence:**

Gertraud Orend
gertraud.orend@inserm.fr
Caroline Spenlé
cspenle@unistra.fr

[†]These authors have contributed
equally to this work and share
first authorship

[‡]These authors have contributed
equally to this work and
share second authorship

Specialty section:

This article was submitted to
Inflammation,
a section of the journal
Frontiers in Immunology

Received: 30 November 2020

Accepted: 11 June 2021

Published: 05 July 2021

Citation:

Spenlé C, Loustau T, Burckel H,
Riegel G, Abou Faycal C, Li C,
Yilmaz A, Petti L, Steinbach F,
Ahowesso C, Jost C, Paul N,
Carapito R, Noël G, Anjuère F,
Salomé N and Orend G (2021) Impact
of Tenascin-C on Radiotherapy in a
Novel Syngeneic Oral Squamous Cell
Carcinoma Model With Spontaneous
Dissemination to the Lymph Nodes.
Front. Immunol. 12:636108.
doi: 10.3389/fimmu.2021.636108

Impact of Tenascin-C on Radiotherapy in a Novel Syngeneic Oral Squamous Cell Carcinoma Model With Spontaneous Dissemination to the Lymph Nodes

Caroline Spenlé^{1,2,3*†}, Thomas Loustau^{2,3,4†}, Hélène Burckel^{5‡}, Gilles Riegel^{2,3,4‡}, Chérine Abou Faycal^{2,3,4‡}, Chengbei Li^{2,3,4‡}, Alev Yilmaz^{1,2,3,4‡}, Luciana Petti⁶, Fanny Steinbach^{2,3,4}, Constance Ahowesso^{1,2,3}, Camille Jost^{1,2,3}, Nicodème Paul^{2,3,7}, Raphael Carapito^{2,3,7}, Georges Noël^{5,8}, Fabienne Anjuère⁶, Nathalie Salomé^{2,3,4} and Gertraud Orend^{1,2,3,4*}

¹ INSERM U1109-MN3T, The Microenvironmental Niche in Tumorigenesis and Targeted Therapy, Strasbourg, France

² Université de Strasbourg, Strasbourg, France, ³ Fédération de Médecine Translationnelle de Strasbourg (FMTS), Strasbourg, France, ⁴ INSERM U1109, The Tumor Microenvironment Group, Strasbourg, France, ⁵ Institut de Cancérologie de Strasbourg Europe (ICANS), UNICANCER, Paul Strauss Comprehensive Cancer Center, Radiobiology Laboratory, Université de Strasbourg, Strasbourg, France, ⁶ Université Côte d'Azur, CNRS, IPMC, Valbonne-Sophia Antipolis, France,

⁷ Platform GENOMAX, INSERM UMR_S 1109, Faculté de Médecine, Fédération Hospitalo-Universitaire OMICARE, LabEx TRANSPLANTEX, Strasbourg, France, ⁸ Institut de Cancérologie Strasbourg Europe (ICANS), UNICANCER, Department of Radiation Oncology, Strasbourg, France

Radiotherapy, the most frequent treatment of oral squamous cell carcinomas (OSCC) besides surgery is employed to kill tumor cells but, radiotherapy may also promote tumor relapse where the immune-suppressive tumor microenvironment (TME) could be instrumental. We established a novel syngeneic grafting model from a carcinogen-induced tongue tumor, OSCC13, to address the impact of radiotherapy on OSCC. This model revealed similarities with human OSCC, recapitulating carcinogen-induced mutations found in smoking associated human tongue tumors, abundant tumor infiltrating leukocytes (TIL) and, spontaneous tumor cell dissemination to the local lymph nodes. Cultured OSCC13 cells and OSCC13-derived tongue tumors were sensitive to irradiation. At the chosen dose of 2 Gy mimicking treatment of human OSCC patients not all tumor cells were killed allowing to investigate effects on the TME. By investigating expression of the extracellular matrix molecule tenascin-C (TNC), an indicator of an immune suppressive TME, we observed high local TNC expression and TIL infiltration in the irradiated tumors. In a TNC knockout host the TME appeared less immune suppressive with a tendency towards more tumor regression than in WT conditions. Altogether, our novel syngeneic tongue OSCC grafting model, sharing important features with the human OSCC disease could be relevant for future anti-cancer targeting of OSCC by radiotherapy and other therapeutic approaches.

Keywords: radiotherapy, oral squamous carcinoma, tumor microenvironment, tenascin-C, syngeneic animal model, immune suppression

INTRODUCTION

Head and neck squamous cell carcinoma (HNSCC) is the 7th most frequent cancer with a low percentage of 5-year survival (1). HNSCC in the oral cavity, lip, tongue and upper throat, coined oral squamous cell carcinoma (OSCC), can metastasize to regional lymph nodes and the lung (2). Exposure to tobacco, betel nut and alcohol represent high risk factors for developing OSCC (1, 3).

Apart from surgical removal of cancer tissue in OSCC, radiotherapy is the most common treatment (4, 5). Radiotherapy is used in 70% of cancer patients and includes high energy rays (photons, protons or charged particles) where the total dose varies between 50 and 70 Gy, with a daily fractionation of 1.8–2 Gy (5). Absorption of these rays induces DNA double strand breaks and reactive oxygen species causing a tumoricidal effect that is largely dependent on an anti-tumor immune response (6, 7). Dying tumor cells can generate neoantigens that activate the immune system involving dendritic cells (DC), macrophages and other immune subtypes (8). Radiotherapy can act as a two-edged sword by activating and inhibiting the immune defense against tumor cells, respectively (9, 10).

The extracellular matrix (ECM) molecule tenascin-C (TNC) is highly expressed in malignant tumors including HNSCC and plays multiple roles in the tumor microenvironment (TME) promoting cancer progression and metastasis (11–13). TNC promotes tumor cell survival, proliferation, invasion, formation of leaky blood vessels and lung metastasis as demonstrated in spontaneous tumor models with high TNC in comparison to engineered low TNC (14–16). Moreover, TNC forms local niches within the tumor where stromal and immune cells are enriched, regulating cell behavior (14, 15, 17). Recently, by using mice expressing or lacking TNC, we have shown that TNC orchestrates an immune-suppressive TME in the carcinogen 4-nitroquinoline-1-oxide (4NQO)-induced OSCC model (18).

In the past several OSCC tumor grafting models have been established from 4NQO-induced tongue, lip and esophageal squamous cell carcinomas that were used in drug targeting (19–23). Some of these models showed high resemblance with human papilloma virus (HPV)-negative OSCC which was recently confirmed at mutation level (24). However, in none of these models the impact of radiotherapy on the TME has been addressed.

Abbreviations: 4NQO, 4-nitroquinoline-1-oxide; AUF, arbitrary units of fluorescence; CBA, cytometry bead array; CCL21, Chemokine (C-C motif) ligand 21; CCR7, C-C chemokine receptor type 7; CXCR4, C-X-C chemokine receptor type 4; DC, dendritic cells; ECM, the extracellular matrix; EMT, epithelial-to-mesenchymal transition; FNIII, fibronectin type III; FRC, fibroblast reticular cells; H&E, hematoxylin and eosin; HNSCC, head and neck squamous cell carcinoma; HPV, human papillomavirus; IF, immunofluorescence; IFN γ , Interferon γ ; IL1 β , Interleukin 1 β ; IR, irradiated; LM, Laminin; NIR, non-irradiated; ORA, over-representation analysis; OSCC, oral squamous cell carcinomas; PE, plating efficiency; PFA, paraformaldehyde; SF, surviving fraction; TGF β , transforming growth factor beta; TIL, tumor infiltrating leukocytes; TLR4, Toll Like Receptor 4; TME, tumor microenvironment; TMT, tumor matrix tracks; TNC, tenascin-C; TNF α , tumor necrosis factors α .

Here, we established a novel syngeneic OSCC model derived from a 4NQO-induced OSCC in the tongue that showed similarities with HPV-negative HNSCC by recapitulating mutations seen in human tumors, constitutive transforming growth factor beta (TGF β) signaling, abundant TIL in TNC-rich stroma, and spontaneous tumor cell dissemination to the local lymph nodes. Most importantly, this model was sensitive to radiotherapy and revealed an impact of TNC on tumor regression. This model does allow not only to investigate tumor regression by radiotherapy but could be useful for assessing effects of radiotherapy on the TME. Finally, our model could be relevant for future anti-cancer targeting of OSCC by radiotherapy and/or other therapeutic approaches.

MATERIAL AND METHODS

Cell Culture

OSCC2 cells were established from a murine 4NQO induced tongue tumor arising in a female C57Bl/6J mouse (18) and cultured in DMEM-F12 with 4.5 g/L glucose, 10% FBS, 1% penicillin-streptomycin (Sigma, P4333), 40 μ g/ml gentamicin (Dutscher, L0012-100) and 0.4 μ g/ml hydrocortisone (Sigma, H4001). Cells were checked for the absence of mycoplasmas (once every two months, PlascoTest, Invivogen, rep-pt1). OSCC2 cells (5×10^6) were subcutaneously engrafted into the back of a C57Bl/6J mouse for 4 weeks before extraction of the tumor, treatment with collagenase as described (18) and explanting cells into cell culture dishes. After three passages *in vitro*, 5×10^6 cells were again grafted into the neck of a C57Bl/6J mouse which induced a tumor from which cells were explanted in cell culture as described, giving rise to the cell line OSCC13. For bioluminescence experiments, OSCC13 cells were infected with lentiviral particles carrying a luciferase reporter gene. In brief, lentiviral particles were established with ViraPowerTM Lentiviral Expression Systems (Invitrogen) and the plasmid pLenti-CMV-LUC (Addgene, #21474) in HEK293T cells (ATCC). OSCC13 cells were then infected with the lentiviral particles and cells stably expressing the luciferase reporter were established by selection with 10 μ g/ml of blasticidin (InvivoGen) giving rise to the OSCC13-LUC cell line.

Orthotopic Grafting of OSCC13 Cells in the Tongue and Bioluminescence Detection

Nude mice (8 weeks of age) or WT and TNCKO (C57Bl/6J) mice (bred in house) were grafted in the first third part of the tongue. In particular, 3×10^6 OSCC13 cells in 10 μ l PBS were injected using a U-100 insulin syringe (BD Micro-Fine) in C57Bl/6J mice. Some 1×10^6 cells OSCC13-LUC (luciferase expression vector expressing cells) were similarly grafted. Tumors were visible 2 weeks upon engraftment and mice were sacrificed for analysis at 3 weeks (bioluminescence experiment), 2 and 4 weeks (NIR) or 4 weeks (IR). For irradiation analysis, a 2 Gy unique dose of photons was delivered two weeks after tumor cell engraftment (3×10^6 cells). Mice were sacrificed two weeks later and tissue was analyzed by staining. For bioluminescence detection, a RediJect D-Luciferin Ultra Bioluminescent Substrate

(PerkinElmer 770505) solution at 30 mg/ml was injected intraperitoneally 7 min before imaging. Images were acquired for 5 min using a live imager (NightOwl, Berthold). All mice were housed and handled according to the guidelines of INSERM and the ethical committee of Alsace, France (CREMEAS) (Directive 2010/63/EU, 01386.02, C-67-482-033 on the protection of animals used for scientific purposes).

Immune Cell Preparation From Tumors and Cytokine Production

OSCC13 tumor tissues were cut in small pieces and then treated with a solution of collagenase IV (1 mg/ml; Sigma-Aldrich, France) and DNase (0.2 mg/ml; Roche Diagnostics, France) at 37°C for 20 min under constant shaking. Cell suspensions from the OSCC13 tongue tumors (400,000 cells/well) were stimulated with anti-CD3/CD28 dynabeads (Gibco #11452D) at a bead-to-cell ratio of 1:1 for 24 h according to the provider's instructions (Becton Dickinson). Supernatants were collected and assessed for the indicated cytokines using the CBA technology (BD Biosciences, France).

Immunostaining

For immunofluorescence staining (IF), unfixed frozen 8 µm tumor sections or cells fixed with 2% paraformaldehyde (PFA) followed by permeabilization in 0.1% TritonX-100/PBS for 10 min were directly incubated overnight with the primary antibodies (**Supplementary Table S1**). Secondary antibodies conjugated with Alexa 488, Cy3 or Cy5 were used (**Supplementary Table S1**). Dapi (Sigma D9542) was used to visualize nuclei. After embedding in FluorSave Reagent (Calbiochem, 345789), sections were examined using a Zeiss Axio Imager Z2 microscope. Pictures were taken with an AxioCam MRm (Zeiss) camera and were analyzed using the Axiovision software. Control sections were processed as mentioned above with omission of the primary antibodies. The image acquisition setting (microscope, magnification, light intensity, exposure time) was kept constant per experiment and in between experimental conditions (comparison NIR with IR tumors) or was adjusted to get the best image (all other stainings).

Real-Time Quantitative PCR

Cells were dissolved in the TRIzol reagent (Invitrogen, 12044977) for total RNA extraction. RNA quality was confirmed by optical density measurement. cDNA was synthesized from 1 µg of total RNA using random primers and Moloney murine leukemia virus reverse transcriptase (MultiScribe, Applied Biosystems, 10117254). The cDNA was used for qRT-PCR in an Mx3005P Real-Time PCR System (ThermoFisher Scientific). Reactions were carried out in duplicate for all conditions using a Sybr Green Master mix (ThermoFisher Scientific, 4344463) or Fast Taqman mix (ThermoFisher Scientific, 4444557) and expression of mouse Gapdh mRNA (Life Technology, 433764T) was used as endogenous control in the comparative cycle threshold method ($2^{-\Delta\Delta Ct}$). Primer sequences used are listed in **Supplementary Table S2**.

RNAseq Analysis

RNA from OSCC13 cells (grown for 24 h in DMEM/10% FCS, $N = 2$) was isolated using the RNeasy Mini Kit (Qiagen). For each sample, quality control was carried out and assessed with the NGS Core Tools FastQC (<http://www.bioinformatics.babraham.ac.uk/projects/fastqc/>). Sequence reads were mapped using STAR (25). The total mapped reads were finally available in a BAM (Binary Alignment Map) format for variant calling. Variant calling was performed using the ultra-sensitive variant caller VarDict (26) where only variants with a PASS status were selected. At last, the variants were annotated by the Ensembl Variant Effect Predictor tool (27). Mutation signatures were obtained using the computational framework SigProfiler (<https://www.mathworks.com/matlabcentral/fileexchange/38724-sigprofiler>). Gene mutation analyses were performed by comparing data from OSCC13 cells with that from publicly available HNSCC dataset from the TCGA consortium (28) and 4MOQ cell lines previously described (24). In addition, p53 mutation patterns observed in the characterized HNSCC samples from TCGA and OCSS13 cell lines were represented and compared using the "lolipop" mutation pattern generator (29). From the list of genes expressed by OSCC13 cells, an over-representation analysis (ORA) was performed in order to determine the gene sets statistically over-represented (**Supplementary Table S3**). Visualization of genes and GO terms was performed using Webgestalt program (30) and Gene Ontology database (31). Multiple testing Benjamini-Hochberg correction was performed and an False-discovery rate threshold was applied (FDR ≤ 0.05). The original data are available at ArrayExpress accession *E-MTAB-10614*.

Irradiation of Tumor Cells and Tumor Mice

Cells seeded in 6-well plates (Falcon, 353046) were exposed, at room temperature, to gamma irradiation, with single doses of 2, 4, 6, 8 or 10 Gy. A ^{137}Cs γ -irradiator (Biobeam GM 8000, GSM GmbH, Leipzig, Germany) was used in the Paul Strauss Center/ Institut de Cancérologie Strasbourg Europe (Strasbourg, France) at a dose rate of 2.5 Gy/min. Cells in control flasks were sham irradiated. Tumor bearing (WT and TNCKO) mice, 2 weeks after engrafting of 3×10^6 OSCC13 cells in the tongue, were irradiated under anesthesia (ketamine 100 mg/kg and xylazine 10 mg/kg) with the irradiator Biobeam GM 8000 with a single fraction of 2 Gy at dose rate of 2.5 Gy/min. The whole body of the mouse, apart from the front of the head, was protected with a lead shield to avoid radiation toxicity. Eyes were protected with a moisturizing cream. No toxic effect was seen in non-tumor bearing mice as assessed by quantification of white and red blood cells numbers, respectively.

Cell Proliferation Assay

In vitro determination of OSCC2 and OSCC13 cell growth was performed using a resazurin assay (Interchim (UP669413 Upti-blue, Montluçon, France). Cells were seeded in 96-well plates at a density of 1×10^3 cells per well in 100 µl and incubated for 24 h. Subsequently, cells were irradiated with single irradiation doses and incubated at 37°C for 1, 2, 3 or 6 days. Subsequently, 20 µl

(10% of final volume) of resazurin were added to each well and cells were incubated at 37°C for four additional hours. The fluorescence of each well was measured at 560–590 nm using a Synergy™ microplate reader (Biotek, Winooski, USA). Results were expressed in arbitrary units of fluorescence (AUF) after subtraction of the blank value (medium only). All experiments were repeated at least three times independently.

Clonogenic Survival Assay

Cells were seeded in 6-well plates (Falcon, 353046) at a density of 2×10^5 cells per well and allowed to adhere overnight in standard culture conditions (DMEM with 10% FBS). Cells were then exposed to irradiation and collected 24 h after irradiation. Cells were trypsinized and enumerated using a Countess® cell counter (Countess, Invitrogen, Carlsbad, USA). Then, cells were seeded in fresh medium and plated at two different dilutions into 6-well plates. The seeding densities used were 100 and 200 cells for the control non-irradiated condition, 200 and 400 cells after 2 Gy, 400 and 800 after 4 Gy, 750 and 1500 after 6 Gy, 1,500 and 3,000 after 8 Gy and 3,000 and 6,000 cells after 10 Gy. Thirteen days later, clones were stained using 0.05% crystal violet (Sigma-Aldrich, C0775) in a 5% ethanol solution and positive colonies containing more than 50 cells were scored. The plating efficiency (PE) and then the surviving fractions (SF) were calculated. The plating efficiency (PE) is defined as the ratio of the number of colonies formed for each condition to the number of cells seeded for each condition. Furthermore, the surviving fraction (SF) is expressed as the ratio of the plating efficiency after treatment to plating efficiency without treatment (non-irradiated control). Survival curves were plotted using surviving fractions for the different doses. Treatments were performed in triplicate and the experiments were repeated four times independently.

Statistical Analysis

For all data, Gaussian distribution was tested. When data followed a Gaussian distribution, statistical differences were analyzed by unpaired t-test (with Welch's correction in case of unequal variance) or ANOVA one-way with Tukey post-test. Otherwise, the Mann-Whitney test or a non-parametric ANOVA followed by Dunns post-test were used to verify significance of the observed differences. For clonogenic survival assay, data were compared pairwise with a Student-Newman-Keuls test. All statistical analyses were performed using the GraphPad Prism 5.02 software. Mean \pm SEM. p values <0.05 were considered as statistically significant, *p <0.05 ; **p <0.01 ; ***p <0.001 .

RESULTS

Establishment of the OSCC13 Cell Line From a 4NQO-Induced Tongue Tumor

We established a murine OSCC tumor by exposing a C57Bl/6J mouse to the carcinogen 4-nitroquinoline-1-oxide (4NQO) in the drinking water for 20 weeks as recently described (18). Then

cells were explanted giving rise to the epithelioid cell line OSCC2 as seen by phase contrast imaging and immunofluorescence (IF) staining for E-cadherin (Figure 1A). As OSCC2 cells generated tumors in the tongues of 60% of mice we sought to increase the grafting efficiency to 100% which was accomplished by a two times sub-cutaneous grafting of OSCC2 cells in the upper neck of C57Bl/6J mice. The arising OSCC13 cells were phenotypically indistinguishable from the OSCC2 cells as seen by phase contrast imaging and E-cadherin IF staining (Figure 1A). To compare the genetic differences and similarities between OSCC13 cells and human HNSCC tumors, we performed RNAseq analysis. By using SigProfiler program we compared the mutation rate in OSCC13 cells with that in tobacco smoking associated human HNSCC (32) and in 4NQO-induced tongue tumors (24). As described previously, cells extracted from 4NQO-induced tumors show remarkable similarity to human cancer cells (24). The mutational patterns induced by 4NQO and tobacco have similar higher mutation rate in translated than in untranslated regions and substitution type rates on each nucleotide. Only the T to A transition, frequently mutated in the tobacco signature is barely found in the 4NQO signature. Interestingly the OSCC13 signature presented nucleotide substitution rates recapitulating tobacco and 4NQO signatures with both high T to A and C to T substitution frequencies (Figure 1B). Investigation of mutations in 18 genes that are frequently mutated in human HPV-negative HNSCC and in the 4NQO-induced 4MOSC cells, revealed also high mutation rates in the OSCC13 cells (except for *Fat4* and *Keap1* that did not show mutations). Moreover, six other genes frequently affected in human OSCC, but not found to be altered in the 4MOSC cells, were also mutated in the OSCC13 cells (*Pik3cd*, *Fat1*, *Notch2*, *Cdh10*, *Nf1* and *Pten*) suggesting that OSCC13 cells phenocopy characteristics described for human HNSCC (Figure 1C). *TP53* encoding the tumor suppressor molecule p53 is frequently mutated in human tumors (84.8% of HPV-negative HNSCC (TGCA cohort)). We investigated hotspots of mutations in *TP53* and observed seven mutations in the DNA binding domain with four in common to HPV-negative HNSCC (Figure 1D). Next, by over-representation analysis (ORA) we investigated gene expression of the cultured OSCC13 cells. We observed several immune modulating molecules such as *Cd274*, *Ctla4* and *Irf7* to be expressed by the cultured OSCC13 cells, mimicking HNSCC, 4NQO-induced tumors and the 4MOSC1-4 cells [Supplementary Table S3 (18, 24, 33)]. Moreover, many molecules involved in the TGF β (46 genes) and Wnt signaling pathways (68 genes) were significantly expressed suggesting intrinsic activation of these pathways again recapitulating features of human HNSCC [Figure 1E and Supplementary Table S3 (34, 35)]. Altogether, we propose that the OSCC13 cells could be a relevant novel cellular model that recapitulates properties of human tobacco smoking associated HNSCC.

OSCC13 Cells Induce Tumors Upon Grafting in the Tongue of Syngeneic Mice

Grafting OSCC13 cells underneath the mucosa induced tongue tumors that were collected and characterized by tissue staining

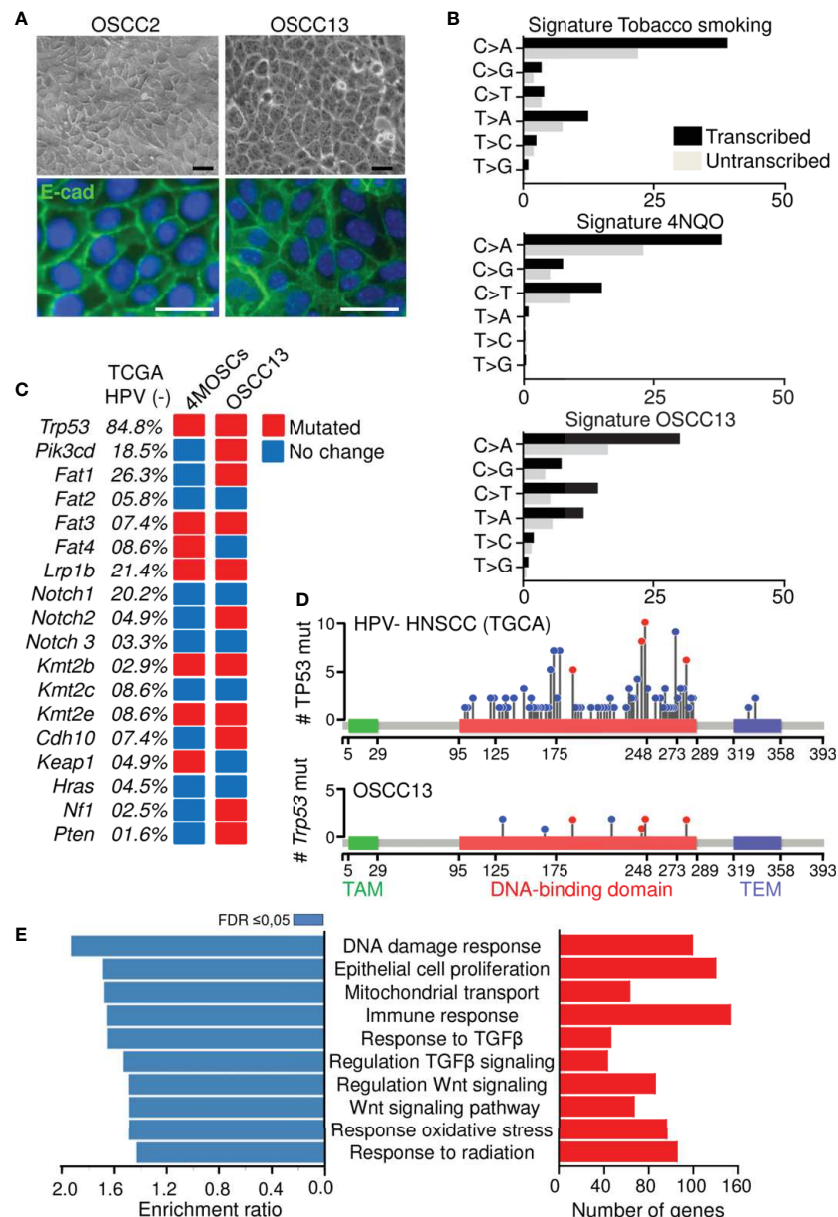


FIGURE 1 | Phenotype of a new OSCC model. **(A)** Phase contrast and IF imaging of E-cadherin in OSCC2 and OSCC13 cells. Scale bar, 25 μ m. **(B)** Percentage of somatic substitutions located in the translated or untranslated genome regions in patients with smoking-associated HNSCC (top (32)), in 4NQO-derived lesions (middle (24)); and in OSCC13 cells (bottom). **(C)** Graphical matrix representation of individual mutations in OSCC13 compared to 4MOSCs and smoking-associated HNSCC (24, 32). The most frequently observed alterations in the indicated genes of human HPV negative HNSCC (TGCA database) and the corresponding percentage of mutations in 4MOSCs and OSCC13 are shown. The presence (red) or absence (blue) of mutations are indicated for OSCC13 and the 4MOSCs-4 cells when at least two of the four cells showed the same phenotype. **(D, E)** RNA data analysis of cultured OSCC13 cells 24 h after plating. **(D)** Lollipop mutational plot of TP53 mutations in human HNSCC (HPV-negative) tumor samples from TCGA database (top) and mouse HNSCC cell line (OSCC13) (bottom). The frequency of mutations is represented by the height of the lollipop. The blue circles indicate mutations specific to human or mouse, and the red circles illustrate mutations common to human and mouse HNSCCs. TAM, Transactivation motif; TEM, Tetramerisation motif. **(E)** Over-represented gene ontology terms as determined by the Webgestalt program and Geneontology database. Bar charts show the enrichment ratio (blue) and expressed gene numbers (red) of the 10 most over-represented GO processes associated with FDR ≤ 0.05 .

with hematoxylin and eosin (H&E), and IF with antibodies against specific markers. We observed that tumors highly expressed TNC (Supplementary Figures S1A, B). Human OSCC tumors and 4NQO-induced tumors are highly

vascularized (18, 36), therefore we stained for lymphatic (LYVE1) and blood vessels (CD31). We observed a high staining of LYVE1 and CD31 around but not inside the tumors which indicates that the angiogenic switch may not

have occurred yet (Figure 2A). As the RNA seq analysis revealed constitutive TGF β signaling in the tumor cells we investigated phosphorylation of Smad3 as indicator of pathway activation. Indeed, P-Smad3 was highly abundant however mostly cytoplasmic (Figure 2B). As TGF β signaling can be activated in stromal, immune and cancer cells (34), future studies have to determine in which stromal cells this pathway is preactivated in the OSCC13 tumors. OSCC tongue tumors are mainly of epithelial origin (two over three patients) (37). We investigated the cellular properties by combined staining for CK8/18 and

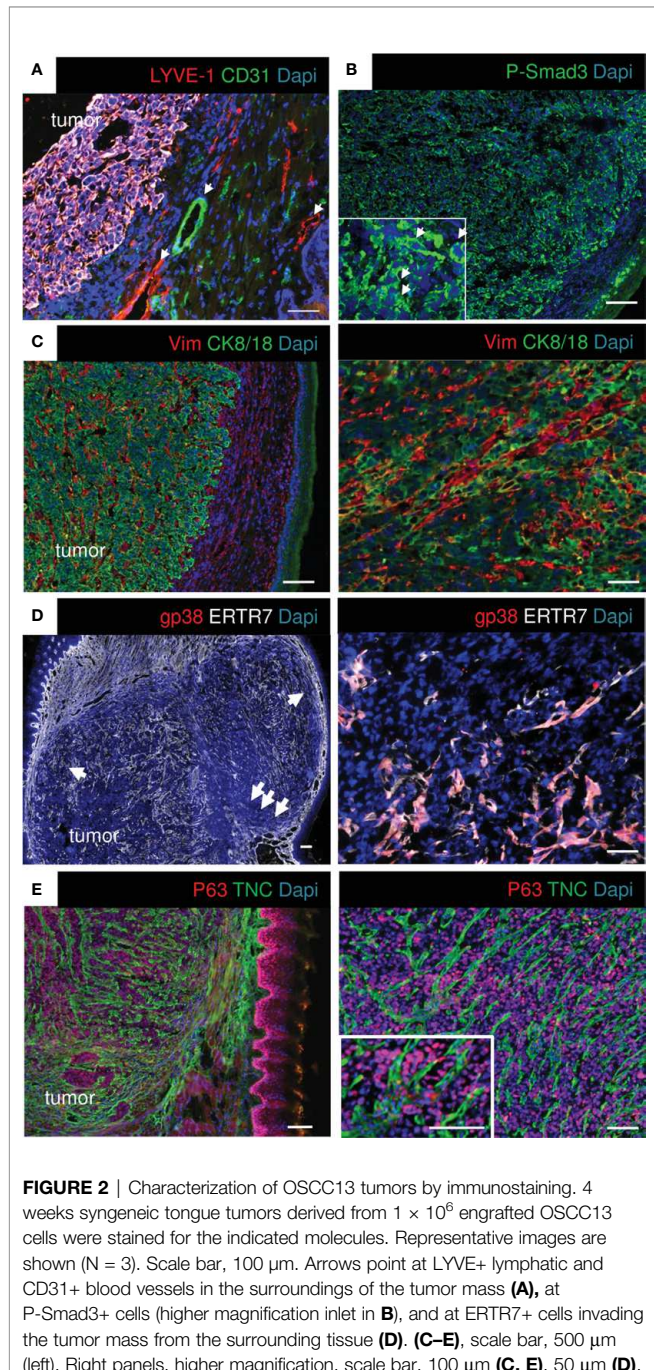


FIGURE 2 | Characterization of OSCC13 tumors by immunostaining. 4 weeks syngeneic tongue tumors derived from 1×10^6 engrafted OSCC13 cells were stained for the indicated molecules. Representative images are shown ($N = 3$). Scale bar, 100 μ m. Arrows point at LYVE+ lymphatic and CD31+ blood vessels in the surroundings of the tumor mass (A), at P-Smad3+ cells (higher magnification inset in B), and at ERTR7+ cells invading the tumor mass from the surrounding tissue (D). (C–E), scale bar, 500 μ m (left). Right panels, higher magnification, scale bar, 100 μ m (C, E), 50 μ m (D).

vimentin and noticed that the majority of cells inside the tumor mass expressed CK8/18 (Figure 2C). In addition, streaks of vimentin+ cells were seen to separate CK8/18+ tumor cell nests (Figure 2C). Vimentin+ cells likely represent carcinoma associated fibroblasts. Future studies have to reveal whether vimentin+ cells also derive from tumor cells having undergone epithelial-to-mesenchymal transition (EMT). As ERTR7+ fibroblast reticular cells (FRC) were numerous in 4NQO-induced tumors (18) we investigated their abundance by staining for gp38 and ERTR7 (and the lack of LYVE1 staining). Indeed we observed FRC to be highly abundant in the OSCC13 tumors (Figure 2D). We noticed that ERTR7+/gp38+ cells surrounded the tumors and that the ERTR7 signal showed a continuation from the tumor border into the tumor mass reminiscent of FRC migrating from outside tissue into the tumor mass. FRC are an important source of matrix as demonstrated in the 4NQO-induced tumors (18). Here, we stained for TNC and saw a similar staining pattern as for ERTR7, separating tumor cells (p63+), supportive of FRC also expressing TNC in this model (Figure 2E). TNC was arranged in fibrillar matrix alignments resembling tumor matrix tracks (TMT) like in 4NQO-induced tongue and other tumors (12, 18, 38) (Figure 2E).

Immune Suppressive TME in OSCC13 Tumors

As the RNA seq analysis showed that the cultured OSCC13 cells expressed *Cd274* we stained the OSCC13 tumors for PDL-1 and indeed found an ubiquitous expression, resembling high PDL-1 in human OSCC, 4NQO-induced OSCC and other OSCC grafted tumors [Figure 3A (24)]. Human OSCC and 4NQO-induced tumors are known to be highly invaded by tumor-infiltrating leucocytes (TIL). To address the immune status also in the OSCC13 tumors we stained for the leukocyte marker CD45+ and noticed an accumulation of leukocytes around and inside the tumors with close vicinity to TNC and laminin (LM) matrix tracks which is again similar to the 4NQO-induced OSCC [Figure 3B and Supplementary Figure S1C (18)]. Staining for CD11c+ myeloid/dendritic cells revealed localization inside the TNC-rich stroma, like in the 4NQO-induced OSCC [Figure 3C (18)]. By staining for Col12 (another prominent matrix molecule in OSCC) together with C-C chemokine receptor type 7 (CCR7) we observed a TMT-like organization of Col12 similar to the 4NQO tumors (18). Moreover, we noticed CCR7+ cells [dendritic cells, macrophages and naïve T cells (39)] invading the tumors (Figure 3D). Staining for CD206 and F4/80 revealed high colocalization of both markers inside the tumors, indicating abundance of macrophages with a M2 phenotype (Figure 3E). Finally, we assessed the potential presence of immune suppressive Treg by Foxp3 staining. Indeed, FoxP3+ cells were present in vicinity to Col12 (Figure 3F). In summary, engrafted OSCC13 cells gave rise to tumors with a TME comprising TNC, LM and Col12 matrix, abundant fibroblasts and immune cells that shared an immune suppressive phenotype with 4NQO-induced tumors and human HNSCC (18).

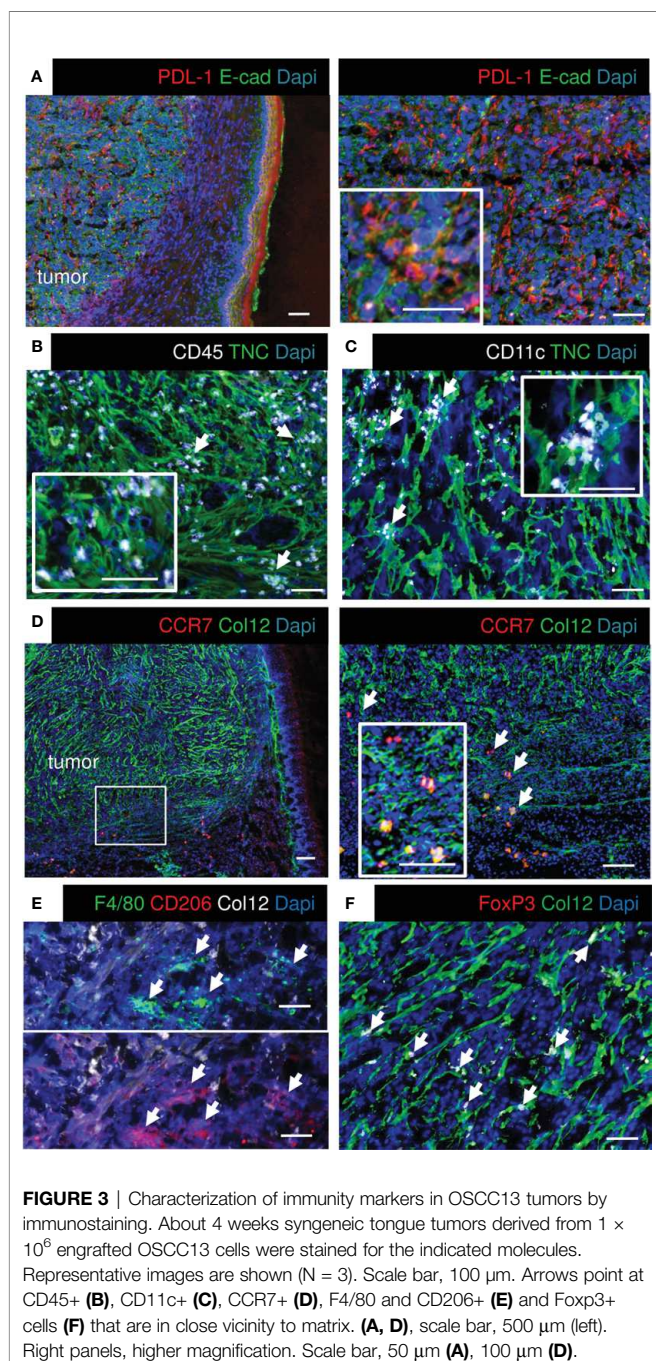


FIGURE 3 | Characterization of immunity markers in OSCC13 tumors by immunostaining. About 4 weeks syngeneic tongue tumors derived from 1×10^6 engrafted OSCC13 cells were stained for the indicated molecules. Representative images are shown ($N = 3$). Scale bar, 100 μ m. Arrows point at CD45+ (B), CD11c+ (C), CCR7+ (D), F4/80 and CD206+ (E) and Foxp3+ cells (F) that are in close vicinity to matrix. (A, D), scale bar, 500 μ m (left). Right panels, higher magnification. Scale bar, 50 μ m (A), 100 μ m (D).

OSCC13 Tumor Cells Spontaneously Disseminate and Home to the Local Lymph Nodes

As tumor cells were found in the local lymph nodes of mice with 4NQO-induced tumors (18), we wondered whether OSCC13 cells were also able to spontaneously disseminate. First, we used a bioluminescence approach to detect OSCC13 cells engineered to express luciferase and monitored luciferin in tumors and local lymph nodes upon grafting of OSCC13 cells underneath the tongue mucosa of nude mice. We saw a bioluminescence signal in the primary tumor one week after grafting that increased with

time (but was hidden at 3 weeks behind the anesthesia cap) (Figure 4A). More importantly, we also saw a small luciferin signal in the lymph nodes already one week after grafting that further increased by week 2 and was highly prominent at week 3. A strong luciferin signal was confirmed by imaging of the extracted lymph nodes demonstrating that the OSCC13 tumor cells had spontaneously homed to the lymph nodes and expanded there (Figure 4A). Next, we investigated potential lymph node metastasis in the immune competent condition by grafting OSCC13 cells into the tongue mucosa of a C57Bl/6J mouse followed by tissue staining of the lymph nodes 4 weeks after grafting. As we had seen P-Smad3 expression in OSCC13 tumors [Figure 2B (18)], we stained the lymph nodes for p63, in addition to other markers. Indeed in the lymph nodes of all investigated tumor mice (3/3) we saw numerous p63+ cells inside the lymph nodes (Figure 4B). Co-staining with TNC revealed that the p63+ tumor cells were present in association with TNC that was expressed in short fibrillar networks resembling TNC-rich reticular fibers in lymph nodes [Figure 4C (18)]. As tumor cells expressed P-Smad3 (Figure 2B) we used this marker together with CK8/18 and observed cells that were positive for both markers, further supporting the presence of OSCC13 tumor cells in the lymph nodes (Figure 4D). Next, we addressed whether tumor cells expanded in this model as seen in nude mice (Figure 4A) and used staining for the proliferation marker Ki67 in combination with CK8/18+. Indeed, we noticed CK8/18+ cells in the lymph nodes that also expressed Ki67 confirming that disseminated tumor cells could expand in the lymph nodes (Figure 4E). We wondered whether tumor cells potentially also homed to the lung in the grafting model, the second most frequent site of metastasis in the human OSCC patient (40). However, the experiment had to be discontinued after 4 weeks as the tumors had reached the ethically accepted size, thus a potential metastasis to the lung could not be addressed rigorously. Interestingly, in one tumor mouse we observed a macroscopical metastasis on the outer surface of the lung, suggesting that potentially tumor cells may also disseminate to the lung. Future studies have to address the lung metastatic potential of OSCC13 cells in more detail.

Altogether, these results strongly suggest that tumor cells from the OSCC13 engrafted tongue tumors spontaneously disseminated and homed to the local lymph nodes where some tumor cells proliferated demonstrating their metastatic potential.

Response of OSCC13 Cells and Derived Tumors to Radiotherapy

Radiotherapy cannot only kill tumor cells but also triggers inflammation and changes in the tumor bed that may counteract tumor regression (41). So far immune competent murine grafting models with a relevant TME to address the roles of radiotherapy in OSCC were not described. To investigate radiosensitivity we exposed OSCC13 cells (in comparison to OSCC2 cells) to increasing single doses of irradiation and determined subsequent tumor cell proliferation and survival in clonogenic assays. We observed a significant reduction in proliferation of OSCC13 cells 6 days after

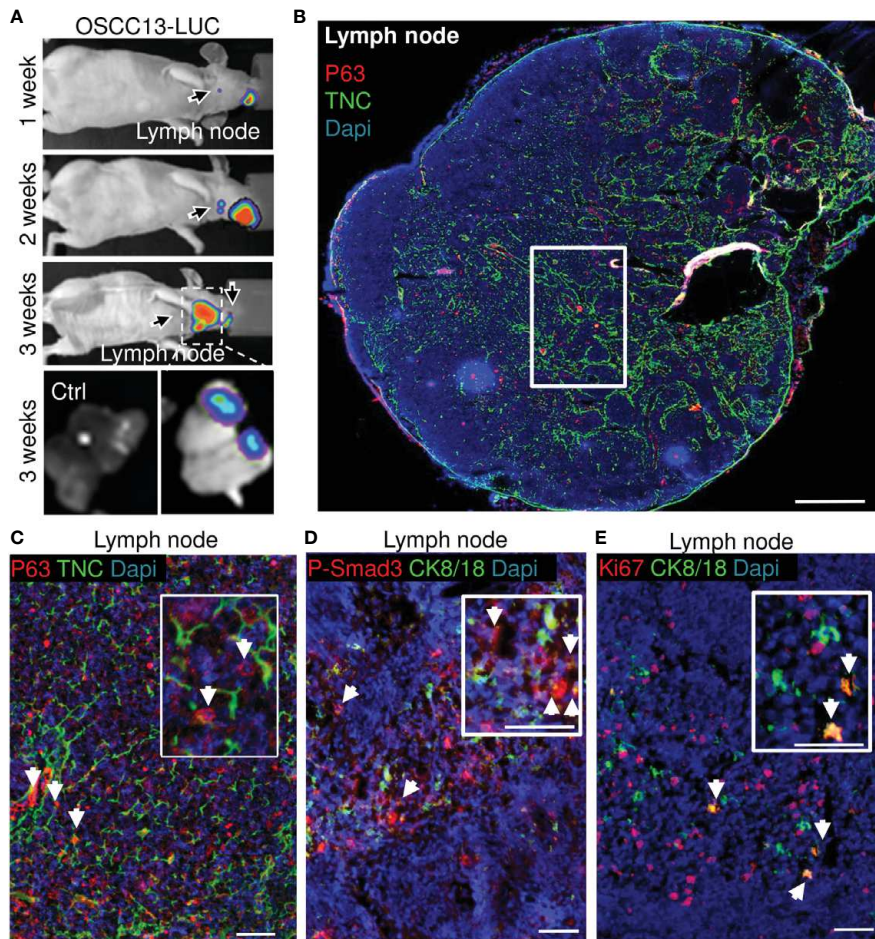


FIGURE 4 | OSCC13 tumor cells home to the local lymph nodes and expand. **(A)** Detection of luciferase expressing OSCC13 cells in the lymph node by a Nightowl imaging machine in a nude mouse and in the dissected lymph nodes. Luciferin signal in the tumor and, expanding in the lymph node from 1–3 weeks. N = 3 mice. **(B–D)**, OSCC13 cells were engrafted in a C57Bl/6J mouse. **(B)** Representative result (N = 3) of disseminated OSCC13 cells in the lymph node by p63 **(C)** and P-Smad3 **(D)** staining and proliferating CK8/18+ tumor cells by Ki67 staining **(E)**. Note tumor cells (p63+) to be placed in TNC+ matrix (inlet of **C**) and proliferation of tumor cells (CK8/18+) **(E)**, confirming tumor cell expansion in the lymph nodes presumably forming metastasis in the immune competent context like in nude mice **(A)**. N = 3 mice. Scale bar, 500 μ m **(B)** and 50 μ m **(C–E)**. Arrows point at tumor cells.

irradiation already at 2 Gy (only 68% living cells) with a pronounced dose-dependent effect up to 10 Gy, respectively rendering only 10% cells alive after exposure to 10 Gy (**Figure 5A**). In comparison, a 2 Gy irradiation dose had no effect on proliferation of OSCC2 cells 6 days post-radiotherapy (**Supplementary Figure S2**). Cell survival of OSCC13 cells at 2 Gy was already significantly reduced compared to OSCC2 cells (surviving fraction at 2 Gy (SF2) was 0.38 and 0.94, respectively for OSCC13 and OSCC2) and decreased further, down to 0.2% and 0.9% for OSCC13 and OSCC2, respectively after 10 Gy (**Figure 5B** and **Supplementary Figure S2**). This experiment revealed that OSCC13 cells were more radiosensitive than OSCC2 cells. Therefore, we used OSCC13 cells in the following grafting and irradiation experiments.

Non-tumor bearing mice were irradiated with 2 Gy before collection of blood and enumeration of white and red blood cells 2 weeks later that indicated the absence of irradiation-induced

toxicity (**Supplementary Figure S3A**). Therefore we used 2Gy to irradiate mice with OSCC13 cell (submucosal) engrafted tumors, collected the tongues 2 weeks later and investigated a potential impact of radiotherapy by tissue staining. Indeed, H&E staining revealed that a 2 Gy irradiation dose destroyed large tumor areas indicated by an altered tumor appearance and lower tumor cell density as seen by reduced H&E, p63 and DAPI staining (**Figure 5C**). We also noticed high CD45+ leukocyte abundance with different distribution patterns showing an accumulation at the tumor rim or, within the tumor center as clusters or as single cells (**Figure 5C**) and **Supplementary Figure S3B**). As TNC can be induced by radiotherapy (42) we wondered whether 2 Gy irradiation had an impact on TNC expression. Whereas, TNC appeared as a regular and homogenous fibrillar network in non-irradiated (NIR) tumors as seen before (**Figure 2**), upon

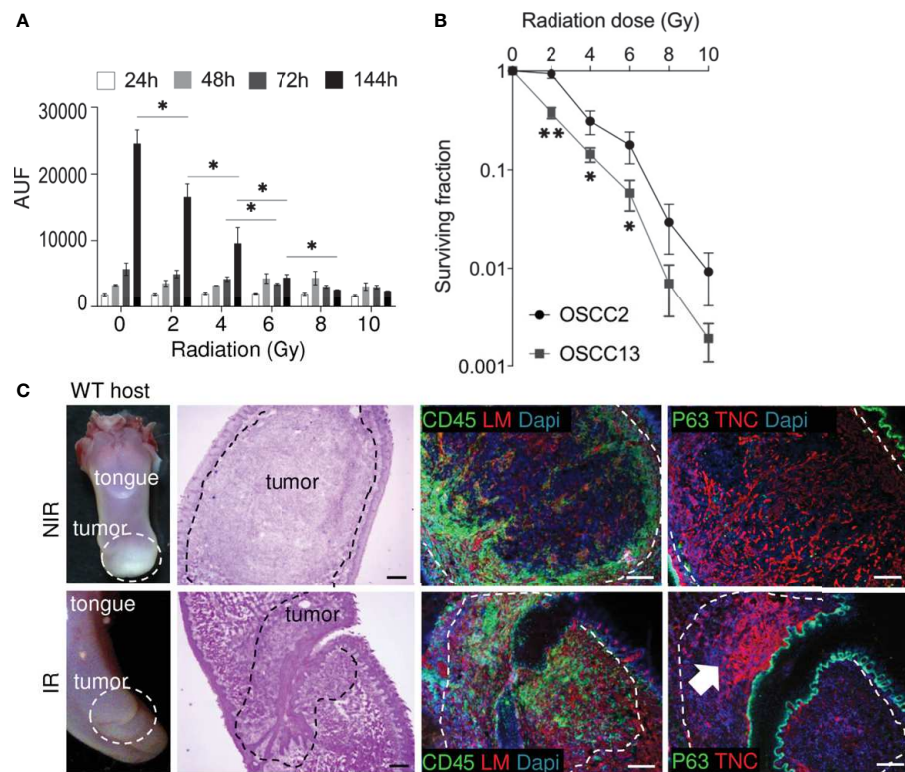


FIGURE 5 | Impact of irradiation on cultured OSCC13 cells and tumors. **(A)** OSCC13 cell proliferation upon exposure to the indicated irradiation doses after the indicated time points (hours, h) using a resazurin assay. Data are represented as mean \pm SEM of at least three independent experiments. Student–Newman–Keuls test. * $p < 0.05$. **(B)** Clonogenic survival assessment upon exposure to the indicated irradiation doses. The surviving fractions are represented. Mean \pm SD of four independent experiments. ANOVA test. ** $p < 0.001$, * $p < 0.05$. **(C)** Representative ($N = 5$) macroscopic images of H&E stained tongue tissue from OSCC13 tumors in a WT host and upon immunostaining with specific antibodies against laminin (LM, red) or TNC (red) together with CD45 (green) or p63 (green). Scale bar, 100 μ m. Arrow points at dense TNC matrix seen upon irradiation. IR, irradiated; NIR, non-irradiated.

irradiation the TNC signal was largely gone (in destroyed tissue) or appeared locally as condensed matrix together with dense nuclei. We propose that thick TNC matrix and cell dense areas represent tissue that has not been killed by irradiation (Figure 5C and Supplementary Figures S3B, C).

Impact of TNC on Immunity and Radiotherapy-Induced Tumor Regression

In a tumor TNC is mostly expressed by stromal cells, but can also be expressed by immune and tumor cells (43). We used OSCC13 tumor cell grafting into a WT or TNCKO host, respectively to address the origin of TNC. We observed no TNC in tumors of a TNCKO host indicating that tumor cells poorly express TNC. Upon irradiation with 2 Gy, TNC levels increased in the irradiated tumors both in the TNCKO and WT context, however much less in the TNCKO host suggesting that the stromal cells were the major source of TNC (Figure 6A). Apparently, 2 Gy radiotherapy also triggered some TNC expression in the tumor cells as seen by a TNC signal in the TNCKO tumors (Figure 6A). As TNC can be expressed in different isoforms, we used exon junction specific primers to

determine by qRT-PCR whether radiotherapy had an impact on the TNC isoforms expressed by the tumor cells. Indeed cultured OSCC13 cells expressed some higher molecular weight TNC isoforms 24 h after irradiation as all primers amplified the respective alternatively spliced fibronectin type III (FNIII) domains, however the short form of TNC without the extra FNIII domains was the prominent form (Figure 6B). As in tumors the large isoform of TNC is highly expressed and was shown to be associated with an inflammatory pro-tumorigenic function (44) future studies have to address the potential roles of the different forms of TNC in the irradiated tumor tissue.

Next we investigated whether TNC had an impact on immunity. Therefore we investigated the abundance of different immune subtypes by flow cytometry. We observed that CD4+ and CD8+ TIL were more abundant than NK and B cells. However, no difference between tumor genotypes was seen (Supplementary Figure S4A). Next, we lysed the tumors and triggered T cells with a mixture of CD3 and CD28 antibodies and determined expression of cytokines 24 and 72 h later, using a cytokine cytometry bead array (CBA) assay, respectively. This analysis revealed an induction at both time points and a clear difference between tumor genotypes. Stimulated T cells from

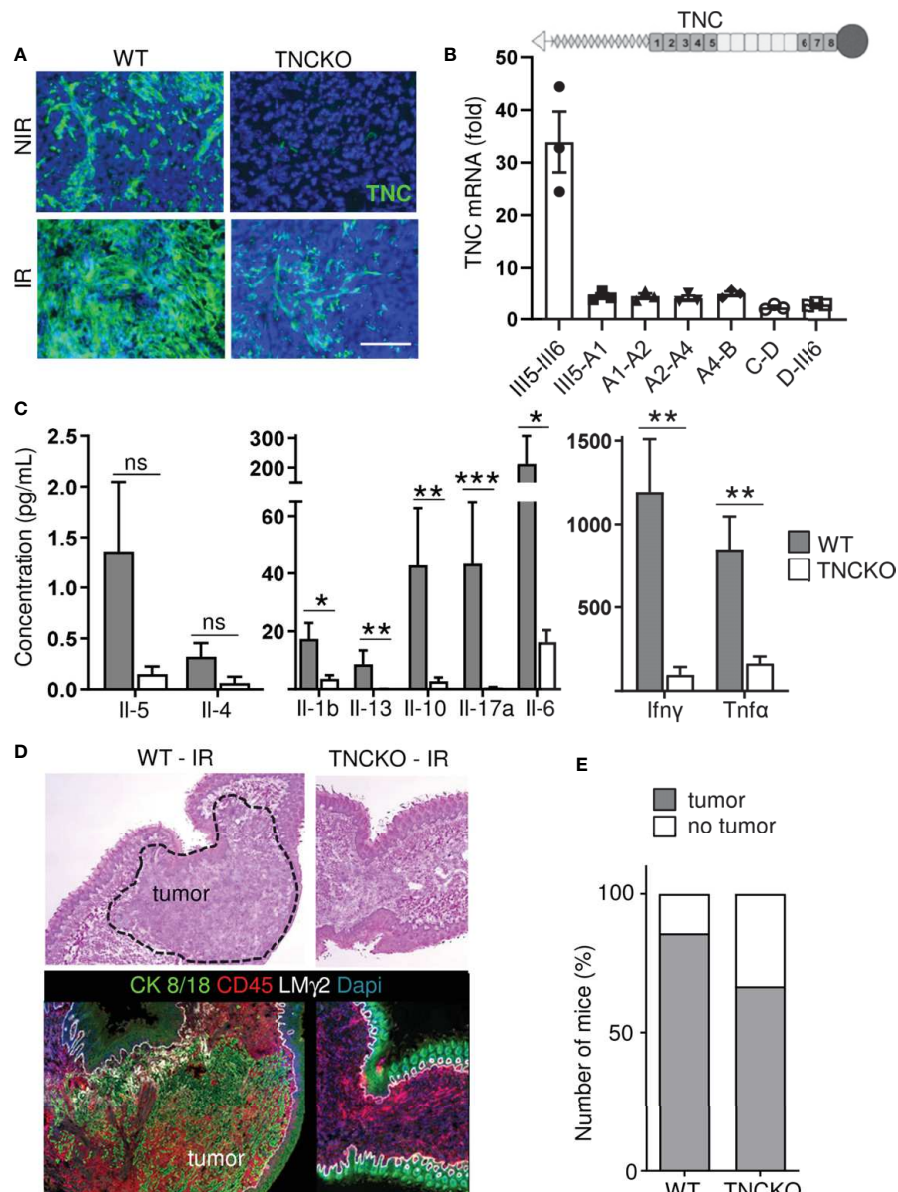


FIGURE 6 | Impact of TNC on T cell stimulation and on OSCC13 tumor abundance upon irradiation. **(A)** TNC immunostaining of non-irradiated (NIR) and irradiated (IR) tumors from WT and TNCKO mice 2 weeks upon irradiation with 2 Gy. Scale bar 100 μ m. WT, N = 6, TNCKO, N = 9. **(B)** Gene expression analysis (qRT-PCR) of different TNC FNIII domains (exon junctions) in OSCC13 cells 24 h upon 2 Gy irradiation (normalized to GAPDH). N = three experiments. The domain organization of TNC is schematically depicted on top with heptad oligomerization domain (triangle), FNIII domains (dark, constant, light, alternatively spliced) and fibrinogen globe (circle). **(C)** Expression of cytokines in T cells present in OSCC13 tumors from WT and TNCKO mice (2 weeks upon engraftment), 24 h after stimulation with CD3/CD28 beads, with a cytokine cytometry bead array (CBA) assay. Mean \pm SEM, Mann-Whitney test, *p < 0.05, **p < 0.01, ***p < 0.05. **(D)** Representative H&E and immunostaining images for CK8/18 and CD45 (N = 5) of a non-irradiated and irradiated tongue from a OSCC13 tumor bearing mouse (WT or TNCKO). **(E)** Detection of tumors (by CK8/18 signal) in irradiated WT (N = 6/7) and TNCKO mice (N = 6/9); ns, not significant. Note that whereas all engrafted mice developed tumors in both genotypes, upon irradiation there was a partial regress.

TNCKO tumors expressed less Interleukin 1 beta (IL1 β), IL10, IL17A, IL6, IFN γ and tumor necrosis factors α (TNF α) whereas no difference for IL4 nor IL5 was seen that were poorly expressed (Figure 6C and Supplementary Figure S4B). These results indicated that the TME in tumors of a TNCKO host may have a less inflammatory TME with less active T cells.

To address whether TNC impacted irradiation-induced tumor regression, we applied 2 Gy to OSCC13 tumors grown in a WT or TNCKO host. By staining for Dapi and CK8/18 we investigated the irradiated tissue and noticed that in the TNCKO host 30% of mice showed complete tumor regression which was less prominent in the WT host (14%) (Figures 6D, E). In all

other tumors we determined the tumor areas by H&E staining before and after irradiation. We noticed that tumors of both genotypes partially regressed upon irradiation but that the host genotype did not have an impact on the tumor size (measured as surface) in the given short time frame of the experiment (**Supplementary Figure S4C**).

Impact of Irradiation and TNC on CD45+ and CD206+ Immune Cell Infiltration

We compared the localization and abundance of leukocytes in OSCC13 tumors upon growth in a TNCKO host with that in a WT host by IF imaging. This showed abundant CD45+ leukocytes also in the TNCKO context within the tumors and in their direct vicinity (**Supplementary Figures S4B, D**). Upon irradiation CD45+ leukocytes also infiltrated the TNCKO tumors. In contrast to this broad infiltration in the TNCKO tumors this appeared to be more local in the WT tumors (**Supplementary Figure S4D**).

As we previously described an impact of TNC on CD206+ pro-tumoral M2 macrophages in the syngeneic NT193 breast cancer grafting model (45) we investigated the abundance and spatial distribution of CD206+ by tissue staining and subsequent quantification (**Figures 7A–D**). This experiment revealed numerous CD206+ macrophages inside the tumors and in direct tumor vicinity (**Figures 7A, B**). Whereas no difference in CD206+ macrophages was seen in WT tumors with and without irradiation TNCKO tumors showed a tendency towards less CD206+ cells after irradiation (**Figure 7C**). Determining the spatial distribution of CD206+ cells we noticed a higher inside-to-outside ratio of CD206+ macrophages in WT than TNCKO tumors. Irradiation did not impact this ratio in the given time frame (**Figure 7D**).

Altogether we have established a novel syngeneic OSCC grafting model derived from a 4NQO-induced tongue tumor that showed similarities with human OSCC by recapitulating mutations seen in human tumors, constitutive TGF β signaling, abundant TIL within TNC-rich stroma and, spontaneous tumor cell dissemination to and expansion in the local lymph nodes. Most importantly, this model was sensitive to a 2 Gy dose of irradiation and allows not only to investigate tumor cell killing by radiotherapy but may be also useful to investigate potential rebound effects where induction of TNC could function as marker for adverse responses.

DISCUSSION

Radiotherapy is the most frequent treatment of patients with OSCC apart from surgery. Although radiotherapy kills the tumor cells, tumors relapse frequently and patients manifest with secondary tumors causing high morbidity and frequent metastasis to the local lymph nodes and lung, altogether resulting in a low 5-year survival (1). Radiotherapy and immune checkpoint therapy applied in human HNSCC cancer patients are important however, they often have either low

efficiency or strong side effects (46). Therefore, novel immune competent tumor models recapitulating HNSCC-specific mutations and HNSCC-specific TME parameters are needed to better understand the targeting actions, to improve established targeting regimens and to develop novel targeting approaches.

Here we have developed a novel immune competent tongue OSCC tumor grafting model that we have investigated in detail by mutation and gene expression analysis, flow cytometry, cytokine expression analysis, extensive tissue staining and loss of function analysis. This comprehensive information on the TME and mutation phenotype has not been provided on previously published models. Mutation analysis revealed that our OSCC13 cells present mutational patterns and nucleotide substitution exchanges that recapitulate both the characteristics of tobacco- and 4NQO-induced tumor signatures. Moreover, OSCC13 cells present mutations on genes also frequently mutated in human tumors and in particular mutations in the Trp53 gene common to human HNSCC. Transcriptomic analysis of OSCC13 cells also revealed similarities in activation of signaling pathways (including TGF β) like in many human HNSCC. Altogether the mutation pattern and gene expression profile of the OSCC13 cells is more similar to human HNSCC than other published models (24).

Although we did not detect tumor vascularization presumably due to the short duration of the experiment, important events seen in 4NQO-induced tumors were recapitulated in this model such as the development of a structured stroma with abundant matrix and TIL infiltration. We noticed effects on tumor immunity that can be considered to be anti-tumorigenic (e.g. abundant infiltration of macrophages, CD11c+ myeloid/dendritic cells, CD4+ and CD8+ TIL cells) but also pro-tumorigenic (e.g. high abundance of FRC as potential source for deposited matrix, co-localization of immune subtypes with matrix (reminiscent of retention by the matrix), numerous immune suppressive CD206+ M2 macrophages and Foxp3+ T reg cells and high PDL-1). Thus, this model could be suitable to investigate immune evolution in context of radiotherapy and/or drug targeting. Moreover, the OSCC13 tumor cells spontaneously disseminated to the local lymph nodes where they expanded demonstrating a high metastatic capacity. Whereas metastatic properties of murine OSCC cells were previously documented in a nude mouse model (47) here we described tumor cell dissemination and proliferation in the lymph nodes of immune competent OSCC13 tumor mice.

As the tumor cells expressed high PDL-1 and CTLA4 the syngeneic OSCC13 grafting model may be amenable for targeting immune checkpoints in particular in combination with radiotherapy as we have shown that OSCC13 cells and tumors are radiosensitive. Whereas irradiation experiments with human OSCC cells have previously been published in immunodeficient mice (48) to our knowledge OSCC grafting models in an immune competent host have not yet been developed for radiotherapy research. In our novel model, we have shown that OSCC13 tumors partially regressed upon exposure to 2 Gy. This model is also useful to address the effects of radiotherapy on tumor immunity as tumor cells are

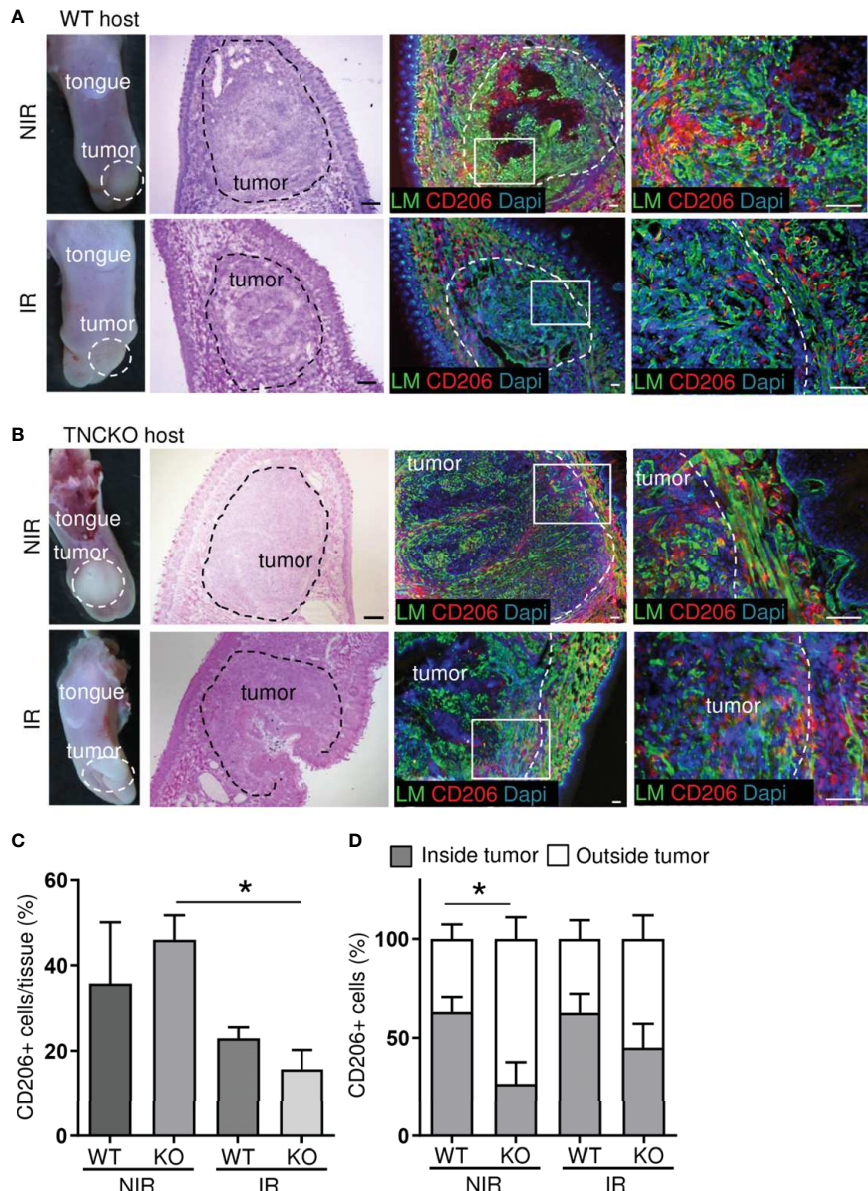


FIGURE 7 | Irradiation effects on CD206+ macrophages in OSCC13 tumors. Representative ($N = 5$) macroscopical images of H&E stained tongue tissue and immunostaining with specific antibodies against laminin (LM, green) and CD206 (red) in OSCC13 tumors from WT (A) and TNCKO mice (B). Scale bar, 100 μ m. (C) Quantification of CD206+ cells in the tongue (referenced to DAPI signal) in percentage. $N = 3$, mean \pm SEM, non-parametric ANOVA followed by Dunn's post-test, * $p < 0.05$. (D) Relative distribution of CD206+ cells inside or outside the tumor of WT and TNCKO mice in non-irradiated (NIR) and irradiated (IR) conditions, respectively. $N = 3$, mean \pm SEM, non-parametric ANOVA followed by Dunn's post-test, * $p < 0.05$. NIR, non-irradiated mice; IR, irradiated mice.

grafted in the tongues of immune competent mice. We propose that this model may be useful for a future investigation of rebound effects (potentially enhancing lymph node metastasis) as we have seen that 2 Gy upregulated TNC. As we saw an impact of radiotherapy on dense TNC matrix expression and TIL infiltration, we speculate that TNC could serve as indicator for an immune-suppressive TME enforced by irradiation, potentially promoting tumor regrowth in the future. Here, several pathways could be involved as we saw that TNC promoted conversion of macrophages into a pro-tumoral M2

phenotype involving Toll Like Receptor 4 (TLR4) and activated C-X-C chemokine receptor type 4 (CXCR4) signaling causing immobilization of CD8+ T cells in the stroma thereby inhibiting anti-tumor immunity (17, 45, 49). Moreover, TNC profoundly shaped the TME enhancing Chemokine (C-C motif) ligand 21 (CCL21)/CCR7 signaling thereby immobilizing CD11c+ myeloid cells thus impairing their function. As inhibition of TLR4, CXCR4 and CCR7 impacted anti-tumor immunity and reduced tumorigenesis (tumor numbers, growth and metastasis) (17, 18, 45), our novel OSCC13 grafting model may be suitable to

investigate these and other alternative targeting approaches in particular in combination with radiotherapy.

Altogether, we have generated a novel immune competent OSCC grafting model recapitulating important properties of human HNSCC including HNSCC-relevant mutations, an immune-suppressive TME and radiosensitivity which opens novel opportunities for future targeting the TME and in particular the matrix in conjunction with radiotherapy and perhaps immune checkpoint targeting drugs.

DATA AVAILABILITY STATEMENT

The original contributions presented in the study are included in the article/**Supplementary Material**. Further inquiries can be directed to the corresponding authors.

ETHICS STATEMENT

The animal study was reviewed and approved by CREMEAS.

AUTHOR CONTRIBUTIONS

CS, TL, HB, CL, LP, AY, GR, CJ, CA-F, CA, FS, and NP performed experiments and analyzed data. CS, TL, HB, and GO wrote the manuscript. GN, FA, and RC supervised experiments. CS and GO

REFERENCES

1. Chow LQM. Head and Neck Cancer. *New Engl J Med* (2020) 382:60–72. doi: 10.1056/NEJMra1715715
2. Argiris A, Karamouzis MV, Raben D, Ferris RL. Head and Neck Cancer. *Lancet* (2008) 371:1695–709. doi: 10.1016/S0140-6736(08)60728-X
3. Chi AC, Day TA, Neville BW. Oral Cavity and Oropharyngeal Squamous Cell Carcinoma—an Update. *CA Cancer J Clin* (2015) 65:401–21. doi: 10.3322/caac.21293
4. Castelli J, Simon A, Lafond C, Perichon N, Rigaud B, Chajon E, et al. Adaptive Radiotherapy for Head and Neck Cancer. *Acta Oncol* (2018) 57:1284–92. doi: 10.1080/0284186X.2018.1505053
5. Caudell JJ, Torres-Roca JF, Gillies RJ, Enderling H, Kim S, Rishi A, et al. The Future of Personalised Radiotherapy for Head and Neck Cancer. *Lancet Oncol* (2017) 18:e266–73. doi: 10.1016/S1470-2045(17)30252-8
6. Ray S, Cekanaviciute E, Lima IP, Sørensen BS, Costes SV. Comparing Photon and Charged Particle Therapy Using DNA Damage Biomarkers. *Int J Part Ther* (2018) 5:15–24. doi: 10.14338/IJPT-18-00018.1
7. Azzam EI, Jay-Gerin J-P, Pain D. Ionizing Radiation-Induced Metabolic Oxidative Stress and Prolonged Cell Injury. *Cancer Lett* (2012) 327:48–60. doi: 10.1016/j.canlet.2011.12.012
8. Lamberti MJ, Nigro A, Mentuccia FM, Rumie Vittar NB, Casolario V, Dal Col J. Dendritic Cells and Immunogenic Cancer Cell Death: A Combination for Improving Antitumor Immunity. *Pharmaceutics* (2020) 12:256. doi: 10.3390/pharmaceutics12030256
9. Russell JS, Brown JM. The Irradiated Tumor Microenvironment: Role of Tumor-Associated Macrophages in Vascular Recovery. *Front Physiol* (2013) 4:157. doi: 10.3389/fphys.2013.00157
10. Moeller BJ, Cao Y, Li CY, Dewhirst MW. Radiation Activates HIF-1 to Regulate Vascular Radiosensitivity in Tumors: Role of Reoxygenation, Free Radicals, and Stress Granules. *Cancer Cell* (2004) 5:429–41. doi: 10.1016/s1535-6108(04)00115-1
11. Sundquist E, Kauppila JH, Veijola J, Mroueh R, Lehenkari P, Laitinen S, et al. Tenascin-C and Fibronectin Expression Divide Early Stage Tongue Cancer Into Low- and High-Risk Groups. *Br J Cancer* (2017) 116:640–8. doi: 10.1038/bjc.2016.455
12. Midwood KS, Hussinet T, Langlois B, Orend G. Advances in Tenascin-C Biology. *Cell Mol Life Sci* (2011) 68:3175–99. doi: 10.1007/s00018-011-0783-6
13. The Extracellular Matrix and Cancer | iConcept Press, in: *The Extracellular Matrix and Cancer: Regulation of Tumor Cell Biology by Tenascin-C*. Available at: <https://www.iconceptpress.com/book/the-extracellular-matrix-and-cancer-regulation-of-tumor-cell-biology-by-tenascin-c/11000138/> (Accessed August 4, 2018).
14. Langlois B, Saupe F, Rupp T, Arnold C, van der Heyden M, Orend G, et al. AngioMatrix, a Signature of the Tumor Angiogenic Switch-Specific Matrisome, Correlates With Poor Prognosis for Glioma and Colorectal Cancer Patients. *Oncotarget* (2014) 5:10529–45. doi: 10.18632/oncotarget.2470
15. Saupe F, Schwenger A, Jia Y, Gasser I, Spenlé C, Langlois B, et al. Tenascin-C Downregulates Wnt Inhibitor Dickkopf-1, Promoting Tumorigenesis in a Neuroendocrine Tumor Model. *Cell Rep* (2013) 5:482–92. doi: 10.1016/j.celrep.2013.09.014
16. Sun Z, Velázquez-Quesada I, Murdamoothoo D, Ahowesso C, Yilmaz A, Spenlé C, et al. Tenascin-C Increases Lung Metastasis by Impacting Blood Vessel Invasions. *Matrix Biol* (2019) 83:26–47. doi: 10.1016/j.matbio.2019.07.001
17. Murdamoothoo D, Sun Z, Yilmaz A, Riegel G, Abou-Faycal C, Deligne C, et al. Tenascin-C Immobilizes Infiltrating T Lymphocytes Through CXCL12 Promoting Breast Cancer Progression. *EMBO Mol Med* (2021) n/a:e13270. doi: 10.15252/emmm.202013270
18. Spenlé C, Loustau T, Murdamoothoo D, Erne W, Beghelli-de la Forest Divonne S, Veber R, et al. Tenascin-C Orchestrates an Immune Suppressive Tumor

designed the study, analyzed data, and revised the manuscript. NS assisted the manuscript revision. All authors contributed to the article and approved the submitted version.

FUNDING

This work was supported by INCa (FITMANET, PAIR-VADS11-023) and INCa/LNCC ECMpact (AAP2017.LNCC), ANR (AngioFib), Ligue contre le cancer (CCIRGE), University Strasbourg and INSERM to GO, Aviesan ITMO cancer (Radio-3R) to GO and GN, AAP2017.LNCC (FA), MRT fellowship to AY and fellowship from the Chinese Scholarship Council to CL.

ACKNOWLEDGMENTS

We acknowledge technical support by O. Lefebvre, A. Klein, C. Arnold, the animal facility of INSERM U1109 and the Genomax facility of INSERM U1109.

SUPPLEMENTARY MATERIAL

The Supplementary Material for this article can be found online at: <https://www.frontiersin.org/articles/10.3389/fimmu.2021.636108/full#supplementary-material>

Microenvironment in Oral Squamous Cell Carcinoma. *Cancer Immunol Res* (2020) 8:1122–38. doi: 10.1158/2326-6066.CIR-20-0074

19. Czerninski R, Amornphimoltham P, Patel V, Molinolo AA, Gutkind JS. Targeting Mammalian Target of Rapamycin by Rapamycin Prevents Tumor Progression in an Oral-Specific Chemical Carcinogenesis Model. *Cancer Prev Res (Phila)* (2009) 2:27–36. doi: 10.1158/1940-6207.CAPR-08-0147

20. Vitale-Cross L, Czerninski R, Amornphimoltham P, Patel V, Molinolo AA, Gutkind JS. Chemical Carcinogenesis Models for Evaluating Molecular-Targeted Prevention and Treatment of Oral Cancer. *Cancer Prev Res (Phila)* (2009) 2:419–22. doi: 10.1158/1940-6207.CAPR-09-0058

21. Tang X-H, Urvalek AM, Osei-Sarfo K, Zhang T, Scognamiglio T, Gudas LJ. Gene Expression Profiling Signatures for the Diagnosis and Prevention of Oral Cavity Carcinogenesis-Genome-Wide Analysis Using RNA-Seq Technology. *Oncotarget* (2015) 6:24424–35. doi: 10.18632/oncotarget.4420

22. Badarni M, Prasad M, Balaban N, Zoreia J, Yegodave KM, Joshua B-Z, et al. Repression of AXL Expression by AP-1/JNK Blockage Overcomes Resistance to PI3Ka Therapy. *JCI Insight* (2019) 4. doi: 10.1172/jci.insight.125341

23. Elkabets M, Pazarentzos E, Juric D, Sheng Q, Pelossof RA, Brook S, et al. AXL Mediates Resistance to PI3K α Inhibition by Activating the EGFR/PKC/mTOR Axis in Head and Neck and Esophageal Squamous Cell Carcinomas. *Cancer Cell* (2015) 27:533–46. doi: 10.1016/j.ccr.2015.03.010

24. Wang Z, Wu VH, Allevato MM, Gilardi M, He Y, Luis Callejas-Valera J, et al. Syngeneic Animal Models of Tobacco-Associated Oral Cancer Reveal the Activity of In Situ Anti-CTLA-4. *Nat Commun* (2019) 10:5546. doi: 10.1038/s41467-019-13471-0

25. Dobin A, Davis CA, Schlesinger F, Drenkow J, Zaleski C, Jha S, et al. STAR: Ultrafast Universal RNA-seq Aligner. *Bioinformatics* (2013) 29:15–21. doi: 10.1093/bioinformatics/bts635

26. Lai Z, Markovets A, Ahdesmaki M, Chapman B, Hofmann O, McEwen R, et al. VarDict: A Novel and Versatile Variant Caller for Next-Generation Sequencing in Cancer Research. *Nucleic Acids Res* (2016) 44:e108. doi: 10.1093/nar/gkw227

27. McLaren W, Gil L, Hunt SE, Riat HS, Ritchie GRS, Thormann A, et al. The Ensembl Variant Effect Predictor. *Genome Biol* (2016) 17:122. doi: 10.1186/s13059-016-0974-4

28. Lawrence MS, Sougnez C, Lichtenstein L, Cibulskis K, Lander E, Gabriel SB, et al. Comprehensive Genomic Characterization of Head and Neck Squamous Cell Carcinomas. *Nature* (2015) 517:576–82. doi: 10.1038/nature14129

29. Jay JJ, Brouwer C. Lollipops in the Clinic: Information Dense Mutation Plots for Precision Medicine. *PLoS One* (2016) 11:e0160519. doi: 10.1371/journal.pone.0160519

30. Liao Y, Wang J, Jaehnig EJ, Shi Z, Zhang B. WebGestalt 2019: Gene Set Analysis Toolkit With Revamped UIs and Apis. *Nucleic Acids Res* (2019) 47:W199–205. doi: 10.1093/nar/gkz401

31. Harris MA, Clark J, Ireland A, Lomax J, Ashburner M, Foulger R, et al. The Gene Ontology (GO) Database and Informatics Resource. *Nucleic Acids Res* (2004) 32:D258–261. doi: 10.1093/nar/gkh036

32. Alexandrov LB, Ju YS, Haase K, Van Loo P, Martincorena I, Nik-Zainal S, et al. Mutational Signatures Associated With Tobacco Smoking in Human Cancer. *Science* (2016) 354:618–22. doi: 10.1126/science.aag0299

33. Ma H, Yang W, Zhang L, Liu S, Zhao M, Zhou G, et al. Interferon-Alpha Promotes Immunosuppression Through IFNAR1/STAT1 Signalling in Head and Neck Squamous Cell Carcinoma. *Br J Cancer* (2019) 120:317–30. doi: 10.1038/s41416-018-0352-y

34. White R, Malkoski S, Wang X-J. Tgf β Signaling in Head and Neck Squamous Cell Carcinoma. *Oncogene* (2010) 29:5437–46. doi: 10.1038/onc.2010.306

35. Paluszczak J. The Significance of the Dysregulation of Canonical Wnt Signaling in Head and Neck Squamous Cell Carcinomas. *Cells* (2020) 9:E723. doi: 10.3390/cells9030723

36. Michikawa C, Uzawa N, Kayamori K, Sonoda I, Ohyama Y, Okada N, et al. Clinical Significance of Lymphatic and Blood Vessel Invasion in Oral Tongue Squamous Cell Carcinomas. *Oral Oncol* (2012) 48:320–4. doi: 10.1016/j.oraloncology.2011.11.014

37. Kinouchi M, Izumi S, Nakashiro K, Haruyama Y, Kobashi G, Uchida D, et al. Determination of the Origin of Oral Squamous Cell Carcinoma by Microarray Analysis: Squamous Epithelium or Minor Salivary Gland? *Int J Cancer* (2018) 143:2551–60. doi: 10.1002/ijc.31811

38. Spenlé C, Gasser I, Saupe F, Janssen K-P, Arnold C, Klein A, et al. Spatial Organization of the Tenascin-C Microenvironment in Experimental and Human Cancer. *Cell Adh Migr* (2015) 9:4–13. doi: 10.1080/19336918.2015.1005452

39. Bjorkdahl O, Barber KA, Brett SJ, Daly MG, Plumpton C, Elshourbagy NA, et al. Characterization of CC-Chemokine Receptor 7 Expression on Murine T Cells in Lymphoid Tissues. *Immunology* (2003) 110:170–9. doi: 10.1046/j.1365-2567.2003.01727.x

40. Noguti J, Moura CEGD, Jesus GPPD, Silva VHPD, Hossaka TA, Oshima CTF, et al. Metastasis From Oral Cancer: An Overview. *Cancer Genomics Proteomics* (2012) 9:329–35.

41. Spenlé C, Saupe F, Midwood K, Burckel H, Noel G, Orend G. Tenascin-C: Exploitation and Collateral Damage in Cancer Management. *Cell Adh Migr* (2015) 9:141–53. doi: 10.1080/19336918.2014.1000074

42. Sugyo A, Tsuji AB, Sudo H, Takano K, Kusakabe M, Higashi T. Proof of Concept Study for Increasing Tenascin-C-Targeted Drug Delivery to Tumors Previously Subjected to Therapy: X-Irradiation Increases Tumor Uptake. *Cancers (Basel)* (2020) 12:E3652. doi: 10.3390/cancers12123652

43. Yoshida T, Akatsuka T, Imanaka-Yoshida K. Tenascin-C and Integrins in Cancer. *Cell Adh Migr* (2015) 9:96–104. doi: 10.1080/19336918.2015.1008332

44. Hancox RA, Allen MD, Holliday DL, Edwards DR, Pennington CJ, Guttry DS, et al. Tumour-Associated Tenascin-C Isoforms Promote Breast Cancer Cell Invasion and Growth by Matrix Metalloproteinase-Dependent and Independent Mechanisms. *Breast Cancer Res* (2009) 11:R24. doi: 10.1186/bcr2251

45. Deligne C, Murdamoothoo D, Gammie AN, Gschwandtner M, Erne W, Loustau T, et al. Matrix-Targeting Immunotherapy Controls Tumor Growth and Spread by Switching Macrophage Phenotype. *Cancer Immunol Res* (2020) 8:368–82. doi: 10.1158/2326-6066.CIR-19-0276

46. Qian JM, Schoenfeld JD. Radiotherapy and Immunotherapy for Head and Neck Cancer: Current Evidence and Challenges. *Front Oncol* (2021) 10:608772. doi: 10.3389/fonc.2020.608772

47. Chen Y-F, Liu C-J, Lin L-H, Chou C-H, Yeh L-Y, Lin S-C, et al. Establishing of Mouse Oral Carcinoma Cell Lines Derived From Transgenic Mice and Their Use as Syngeneic Tumorigenesis Models. *BMC Cancer* (2019) 19:281. doi: 10.1186/s12885-019-5486-7

48. Shintani S, Li C, Mihara M, Terakado N, Yano J, Nakashiro K, et al. Enhancement of Tumor Radioreponse by Combined Treatment With Gefitinib (Iressa, ZD1839), an Epidermal Growth Factor Receptor Tyrosine Kinase Inhibitor, is Accompanied by Inhibition of DNA Damage Repair and Cell Growth in Oral Cancer. *Int J Cancer* (2003) 107:1030–7. doi: 10.1002/ijc.11437

49. Murdamoothoo D, Sun Z, Yilmaz A, Deligne C, Velazquez-Quesada I, Erne W, et al. Immobilization of Infiltrating Cytotoxic T Lymphocytes by Tenascin-C and CXCL12 Enhances Lung Metastasis. *EMBO Mol Med* (2021) 13(6): e13270. doi: 10.15252/emmm.202013270

Conflict of Interest: The authors declare that the research was conducted in the absence of any commercial or financial relationships that could be construed as a potential conflict of interest.

Copyright © 2021 Spenlé, Loustau, Burckel, Riegel, Abou Faycal, Li, Yilmaz, Petti, Steinbach, Ahowesso, Jost, Paul, Carapito, Noël, Anjuère, Salomé and Orend. This is an open-access article distributed under the terms of the Creative Commons Attribution License (CC BY). The use, distribution or reproduction in other forums is permitted, provided the original author(s) and the copyright owner(s) are credited and that the original publication in this journal is cited, in accordance with accepted academic practice. No use, distribution or reproduction is permitted which does not comply with these terms.

Alev YILMAZ

Impact of Tenascin-C on anti-tumor immunity in a breast tumor progression model

Résumé

La ténascine-C (TNC) est une protéine matricielle favorisant la progression tumorale et le développement de métastases, et son expression élevée chez les patients atteints de cancer est corrélée à un mauvais pronostic. Durant ma thèse j'ai étudié l'impact de la TNC sur l'immunité anti-tumorale en utilisant le modèle murin MMTV-NeuNT et le modèle de greffe orthotopique syngénique de cellules cancéreuses mammaires NT193. Nos résultats ont montré que la TNC empêche une action efficace de la réponse anti-tumorale en séquestrant les lymphocytes T CD8+ dans les réseaux de matrice, ceci en faisant intervenir la voie de signalisation CXCL12/CXCR4. L'inhibition de CXCR4 permet l'infiltration des lymphocytes T CD8+ dans la niche tumorale et augmente le nombre de cellules cancéreuses en apoptose menant ainsi à une régression tumorale. D'autre part, l'établissement d'une nouvelle lignée de cellules tumorales mammaires nous a permis de montrer que la TNC peut également avoir un rôle opposé et favoriser le rejet des cellules tumorales dans la phase initiale du développement tumoral post greffe. Les mécanismes sous-jacents restent cependant à être élucider. Enfin, nos premiers résultats sur cette lignée cellulaire montre que la TNC induit l'expression de NKG2DL dans cette lignée suggérant ainsi que la TNC a un lien avec l'axe NKG2D/NKG2DL dont l'impact sur le développement tumoral reste à établir.

Résumé en anglais

Tenascin-C is an extracellular matrix protein promoting tumor progression and metastasis development, and its expression in cancer patients correlates with poor prognosis. During my thesis I studied the impact of TNC on anti-tumor immunity using the MMTV-NeuNT mouse model and a syngeneic orthotopic grafting model based on the NT193 breast cancer cell line. Our results showed that TNC impairs the anti-tumor immune response by sequestering CD8+ T lymphocytes in the tumor matrix tracks involving CXCL12/CXCR4 signaling. Inhibition of CXCR4 enables the infiltration of CD8+ T lymphocytes into the tumor cell nest and increases tumor cell death. Moreover, the establishment of a novel breast cancer cell line enabled us to show that TNC can also have an opposite effect inducing tumor cell rejection in the early phase of tumor development after engraftment. The underlying mechanisms remain to be elucidated. Finally, our first results show that TNC regulates NKG2DL in this new cancer cell line suggesting that TNC has a link with the NKG2D/NKG2DL whose impact on tumor development has to be further studied.